AN INVESTIGATION INTO THE USE OF CORROSION INHIBITIVE TREATMENTS FOR THE CONSERVATION OF ARCHAEOLOGICAL IRON

A thesis presented to the University of London in fulfilment of the requirements for the degree of Doctor of Philosophy

RACHEL BRONJA BRAZIL

University College London
Institute of Archaeology

September 1999

ABSTRACT

Several types of surface treatments have been evaluated for their ability to inhibit the corrosion of archaeological iron. These are, octadecyltrimethoxysilane (ODTMS), $CH_3(CH_2)_{17}Si(OCH_3)_3$, 1H,1H,2H,2H-henicosafluorododecyltrimethoxysilane (HFTMS), $C_{10}F_{21}H_4Si(OCH_3)_3$, decylamine (DCA), $C_{10}H_{21}NH_2$, octadecylamine (ODA), $C_{18}H_{37}NH_2$, and isopropyl-triisostearoyltitanate (TTS), $CH_3.CH.CH_3OTi(OCO.C_{17}H_{35})_3$. These molecules bind to corrosion product surfaces, forming hydrophobic layers.

Evaluation of treatments has been carried out using accelerated corrosion tests at elevated temperature and humidity. Assessments have also been made using electrochemical monitoring, water adsorption isotherms, Fourier transform infra-red spectroscopy (FTIR), x-ray photoelectron spectroscopy (XPS) and floatation tests. A method of producing corroded iron coupons containing the chlorine containing corrosion products akaganeite, found on archaeological iron, has been devised.

TTS was found to be the most effective treatment of those investigated. Amine treatments gave some inhibition, but were not as effective as TTS. Floatation tests showed that amines are easily hydrolysed and detached from iron oxyhydroxide surfaces and they therefore are not as effective as corrosion inhibitors. An anomaly was found in the behaviour of HFTMS which contrary to expectation actually accelerated the rate of corrosion. This has been attributed to 'pin' holes in the inhibitor coating which allows the formation of differential aeration cells, and thus accelerates corrosion. The success of the TTS treatment is attributed to the fact that each molecule contains three C_{18} hydrocarbon chains, providing a more densely packed hydrophobic surface. Further long term testing of the TTS treatment on archaeological iron is recommended.

Several forms of polyaniline were synthesised and tested as corrosion inhibitors for archaeological iron. These were found not to be effective inhibitors for corroded iron, although they have been found to be effective on clean iron surfaces. This may be because they work as anodic inhibitors and therefore need to be in contact with the metal surface.

ACKNOWLEDGEMENTS

I would like to thank my supervisor Dr John Merkel for all the help he has given me throughout the course of this work and the Institute of Archaeology for the Tylecote studentship which provided me with funding for the majority of my studies.

Thanks also go to my second supervisor Prof. David Williams for his help, advise and the use of his laboratories for a large proportion of the experimental work carried out.

I am grateful to past and present members of the Williams group for their friendship and assistance, especially Dr Ana Conde for help with electrochemistry experiments and Mrs Bernie Hutton for her assistance and patience with the XPS.

Thanks go to Kevin Reeves at the Institute of Archaeology for his help with the SEM analysis and Dr Clive Orton for his discussions on statistics.

I would also like to thank Dr N. Yoshino of the Science University of Tokyo, and Dr P. Kathirgamanathan of South Bank University for supplying reagents synthesised in their laboratories and for advice on there use.

A big thank you goes to Prof. Jack Silver for his many helpful discussions and particularly for his help in the preparation of this thesis.

Thanks also to Caroline for her friendship and big scissors and to June for her help with photocopying

Finally, I must thank my parents for their proof reading skills and for their constant love and support.

CONTENTS

CHAPTER ONE

The Corrosion and Conservation of Archaeological Iron

FIGURES

CHAPTER ONE

The Corrosion and Conservation of Archaeological Iron

CHAPTER TWO

Corrosion Inhibitors and Surface Modification

CHAPTER THREE

Coupons for Corrosion Testing

CHAPTER FOUR

Corrosion Testing

CHAPTER FIVE

Water Adsorption Isotherms, Floatation Tests and Electrochemical Monitoring

CHAPTER SIX

FTIR and XPS Surface Analysis

CHAPTER SEVEN

Assessing Polyaniline as a Corrosion Inhibiting Coating for Archaeological Iron

CHAPTER EIGHT

Discussion and Conclusions

TABLES

CHAPTER ONE

The Corrosion and Conservation of Archaeological Iron

CHAPTER TWO

Corrosion Inhibitors and Surface Modification

CHAPTER THREE

Coupons for Corrosion Testing

CHAPTER FOUR

Corrosion Testing

CHAPTER SIX

FTIR and XPS Surface Analysis

CHAPTER SEVEN

Assessing Polyaniline as a Corrosion Inhibiting Coating for Archaeological Iron

CHAPTER ONE

The Corrosion and Conservation of Archaeological Iron

1.1 INTRODUCTION

The stabilisation of archaeological iron is one of the major problems still to be resolved by conservators. Ironwork is being excavated in quantity from land and marine environments, and this must be added to the material already in collections that has not been successfully stabilised (Oddy & Bradley, 1989).

The instability of archaeological iron is largely due to post-excavation changes that occur when an object is moved from a reducing, marine or damp environment, to an oxidising dry museum environment. These changes often cause the formation of acidic solutions within corrosion product layers and this leads to the initiation of further cycles of corrosion (Turgoose, 1989). The presence of chloride ions accelerates this process which explains the greater instability of marine iron artefacts. The presence of the corrosion product β-FeOOH is associated with unstable iron, as both the cause and product of post excavation corrosion. After much debate, it is now thought that β-FeOOH is the corrosion product that contains the damaging chloride ions within its structure (Zucchi *et al*, 1977, Buchwald & Clarke, 1989, Buchwald & Koch, 1995). The catalytic effect of chloride in the corrosion process is thought to be due to its ability to penetrate and destroy passive iron oxide films and due to its ability to form intermediate soluble complexes with iron (Foley, 1970).

The conservation of archaeological iron can be divided into three stages. Firstly, the cleaning and documentation of the object, including radiography and the removal of extraneous concretions and some corrosion products to reveal the original shape of the object. The second stage is the stabilisation of the object. Active methods for the

stabilisation of archaeological iron have concentrated on methods of desalination. No one method has been found completely successful and there is therefore no one method is standard procedure within the field of conservation. Desalination procedures include methods involving washing, methods involving reduction and electrolytic techniques. No single method is capable of removing all chloride ions, and the more successful reduction methods are often now considered ethically unacceptable in the aesthetic, physical and metallurgical changes they cause in the corrosion products of objects. The third stage of conservation is the applcation of protective coatings with the aim of reducing the likelihood of further corrosion, although there is little evidence to suggest that the majority of coatings used have the desired effect (Keene, 1984).

The stabilisation of archaeological iron via passive control of storage environment has been suggested as the most appropriate method of conservation. Desiccated storage at relative humidity of under 15% using silica gel has been recommended (Turgoose, 1989) and remains the dominant approach to the conservation of archaeological iron and steel in Britain (Cronyn, 1996, 196). However, this approach is risky, especially for marine iron, where any sporadic increases in humidity will lead to corrosion cycles. As well as the risk of inefficient desiccation, a study by Suzanne Keene (1994), has also indicated that storage environment is less significant than supposed, and that active treatments are more successful. The failure of desiccation is connected to the existence of pockets of high humidity within pores of corrosion products that are retainined even after desiccation.

It has been genrally recognised that the removal of all chlorides from archaeological iron does not seem to be possible. The part played by β-FeOOH in the retention of chloride ions is the key to this problem. Chlorides are not only present in the pore solution found within corrosion products, but they are present within tunnels in the lattice structure of β-FeOOH (Kaneko & Inouye, 1974). The possibility of chloride ions being substituted for hydroxide ions in the β-FeOOH lattice has also been suggested (Rezel & Genin, 1990) After washing procedures to desalinate objects, the chloride ions retained may cause future corrosion. A maximum value of 200ppm chloride ions has been suggested as the safe limit in archaeological iron (North & Pearson, 1978).

It is bearing these problems in mind that an approach involving surface treatments has been investigated in this work. Preliminary research shows that additional surface treatments after desalination processes may help to stabilise archaeological iron (Al Ahmed, 1992). Previous research into the performance of coatings used for archaeological iron has found them to have very little effect in stabilising objects other than consolidation (Keene, 1984). In fact, it is possible that coatings may actually lead to localised corrosion and thus accelerate corrosion rates. The problem with most polymer or wax coatings is a lack of adhesion to the mineral surface below. Poor adhesion leads to blistering and flaking of the coatings, allowing new exposure to the ambient environment. New coatings are required that would better adhere to the surface of an object and would have some ability to inhibit corrosion.

An additional problem in stabilising corroded archaeological iron is the nature of the corrosion products that inevitably surround the metal core of artefacts. The surfaces of iron corrosion products are normally iron oxyhydroxides (often overlying a denser magnetite layer) and these compounds have largely hydrophilic surfaces due to the presence of free hydroxyl groups (Kaneko *et al*, 1989a). In addition to the ability of these oxyhydroxides to draw water toward the corroding metal surface, adsorption sites for other pollutants such as sulphur dioxide and nitrogen monoxide are also plentiful (Corvo *et al*, 1997, Kaneko and Inouye, 1987, Kaneko *et al*, 1977). These gases can greatly increase corrosion levels.

In this doctoral research on corrosion inhibitive treatments for archaeological iron, a variety of surface treatments have been tested. Molecules that adhere to mineral surface, but also possess hydrophobic chains were chosen, so that corrosion products would obtain chemically bonded hydrophobic surfaces and the adsorption of water and other molecules likely to cause corrosion at the metal surfaces would be prevented. The performance of several long chain aliphatic amines has been compared to that of a titanate, silane and polyfluoroalkylsilane. Treatments have been assessed by accelerated corrosion tests performed at high humidity to determine the limits of any added stability the treatments afford archaeological iron. Some relevant chemical and physical properties of the inhibitor molecules when present on corrosion product surfaces have also been tested to evaluate their performance.

The use of conducting polymer polyaniline coatings has also been tested. These new materials have recently been developed for use as corrosion inhibitors in industry. Their suitability for use in conservation has been assessed.

This research also proposes new methodologies for the testing of surface treatments for the conservation of archaeological iron. A procedure for synthesising the chloride rich β-FeOOH corrosion product on modern iron test coupons is devised. The effectiveness of treatments on objects containing corrosion products with pockets of high chloride ion concentration can therefore be assessed. The objective of using modern pre-corroded test coupons is to provide some standardization against which to compare the effects of the inhibitor treatments tested, as large amounts of archaeological material is not always available for testing new treatments.

1.2 THE CORROSION OF IRON

1.2.1 The Definition of Corrosion

Corrosion is defined as the destructive result of the reaction between a metal or metal alloy and its' environment. Metallic corrosion involves the transfer of electronic charge via an electrolyte, usually an aqueous solution or a condensed vapour phase (the only exception being charge transfer in a solid state electrolyte). It is an electrochemical process. Corrosion occurs spontaneously, and involves the oxidation of the metallic species, and an accompanying reduction reaction, taking place on the metal surface or on a surface in electrical contact with the metal.

Metallic iron and steel are unstable in the presence of moisture and oxygen. Corrosion of these materials will occur in fresh and seawater environments as well as when buried underground and exposed to the atmosphere. The corrosion reaction can be divided into two half reactions. For iron, the oxidation, or anodic reaction is:

$$Fe \rightarrow Fe^{2+} + 2e^{-} \qquad \textbf{(oxidation)}$$

The reduction, or cathodic reaction may vary depending on the environmental conditions. In aerobic environments the reduction of oxygen will occur:

$$O_2 + 2H_2O + 4e^{-} \rightarrow 4OH^{-} \qquad \textbf{(oxygen reduction in neutral or basic solution)}$$

$$O_2 + 4H^{+} + 4e^{-} \rightarrow 2H_2O \qquad \textbf{(oxygen reduction in neutral or acidic solution)}$$

However in anaerobic conditions, in acid solution, the reduction of H^{+} will occur:

$$2H^{+} + 2e^{-} \rightarrow H_2 \qquad \textbf{(hydrogen evolution)}$$

There is also the possibility that other oxidised species in solution may be reduced, such as:

$$Fe^{3+} + e^{-} \rightarrow Fe^{2+} \qquad \textbf{(metal ion reduction)}$$

During the corrosion of a metal the total rate of oxidation must equal the total rate of reduction as electron donation in the anodic reaction and electron acceptance in the cathodic reaction occur at the same rate.

The initial electrochemical reaction for the corrosion of iron produces ferrous ions, (Fe^{2+}). Ferrous hydroxide can form and precipitate from solution:

$$2Fe^{2+} + 4OH^{-} \rightarrow 2Fe(OH)_2$$

However this compound is unstable in oxygenated solution and a further oxidation can occur to make ferric (Fe^{3+}) iron hydroxide the primary corrosion product, that is, the corrosion product predominantly formed at the time the electrochemical corrosion reaction occurs:

$$2Fe(OH)_2 + H_2O + \tfrac{1}{2}O_2 \rightarrow 2Fe(OH)_3$$

Another possible reaction is the formation of iron (III) oxyhydroxides from ferric hydroxide. Recent experiments (Oelkrug *et al*, 1992) have shown that iron in an alkaline electrolyte will form δ-FeOOH in the following reaction:

$$Fe(OH)_2 \rightarrow \delta\text{-}FeOOH + e^{-} + H^{+}$$

Low carbon steel however was shown to first produce α-FeOOH as the corrosion product.

Figure 1.1 The electrochemcial reactions involved in the corrosion of iron

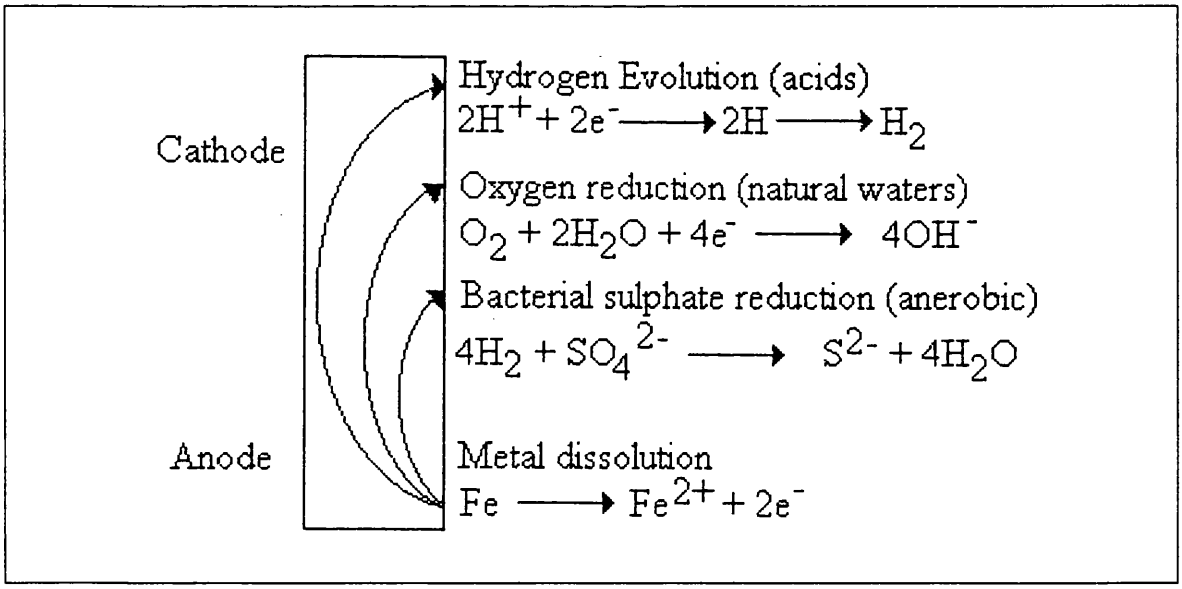

The possible reactions involving charge transfer are shown schematically in figure 1.1. Iron dissolves at the anode, liberating electrons into the bulk of the metal. These electrons migrate to a cathodic surface where they react with oxygen and water, or with hydrogen reductant species. An electrolyte is needed to transport these ions.

In sea water and other solutions with high chloride ion concentration the following reaction may occur at the anode, giving iron chloride primary corrosion products:

$$Fe^{2+} + 2Cl^{-} \rightarrow \quad FeCl_2$$

In the presence of high concentrations of other anions such as sulphates, sulphides, phosphates and carbonates there is the possibility of their corresponding ferric salts forming as primary corrosion products.

It is important to note that the corrosion products mentioned here are not necessarily the most thermodynamically stable in all environments, and therefore are not necessarily the compounds found on archaeological iron when excavated. These compounds represent the initial corrosion products stable in very localised environments.

The nature of corrosion products found on archaeological iron will later be discussed in more detail.

1.2.2 The Thermodynamics and Kinetics of the Corrosion of Iron

To understand modern theories of corrosion it is necessary to review some basic principles of thermodynamics and kinetics. Thermodynamics is the science of energy changes. The Gibbs free energy change (a measure of the chemical potential energy that a system contains) accompanying an electrochemical corrosion reaction can be calculated from:

$$\Delta G = -nFE$$

where ΔG = free energy change, n = number of electrons exchanged, F = Faraday constant, E = the potential of the electrochemical cell containing the two half cell reactions involved. This assumes standard temperature, pressure and unit activities (effective concentrations) of all solutions. To determine the potential of a system in which the reactants are not at unit activity the Nernst equation is used:

$$E = E_0 + 2.3\frac{RT}{nF} \log \frac{a_{oxid}}{a_{red}}$$

E_0 = standard cell potential (at standard temperature, pressure and unit activities), R = gas constant, T= temperature in K, and a = activities of ion species.

The change in the Gibbs free energy can be used to predict whether or not a reaction (or in this case a corrosion process) is spontaneous. In electrochemical reactions the half reaction

with the more negative standard electrode potential tends to be oxidised and the more positive will be reduced. Corrosion will not occur unless the spontaneous direction of the reaction indicates metal oxidation.

From this follows that all metal/metal ion couples with half cell potentials more negative than hydrogen will tend to be corroded in acidic solution. This is the case for all metals except copper, silver and gold which are inert to corrosion in acidic anaerobic conditions. However, in aerated solutions, even copper and silver will corrode as their half cell reactions have more negative potentials then the half cell reaction for the oxidation of oxygen.

The Gibbs free energy discussed above can be used to predict if a reaction is thermodynamically feasible, but this does not necessarily indicate that corrosion will occur as the kinetics of a reaction has not yet been considered. The kinetics of a process indicates the speed at which the reaction occurs. A reaction may be thermodynamically spontaneous but proceeds at such a slow rate that corrosion may be considered negligible. Corroding systems are not at equilibrium and therefore thermodynamics is not the only consideration. The kinetics of the system controls the rate of the corrosion.

When an electrochemical cell is 'short circuited', as is the case in a corroding system, the two half cell potentials will no longer be at their equilibrium potentials. This deviation is known as polarisation. A more formal definition of polarisation is the displacement of electrode potential resulting from a net current. The magnitude of polarisation is measured in terms of the overvoltage, η, which can be positive or negative with respect to the equilibrium potential of the electrode.

As already stated the rate of oxidation must equal the rate of reduction. Using a plot of electrode potential against reaction rate, it is possible to establish a point corresponding to the isolated electrode, i.e. when there is no net current and the rate of oxidation equals the rate of reduction. This point is known as the exchange reaction rate, and is measured in $molcm^{-2}s^{-1}$. It is more commonly expressed in terms of current density, since electrons are being exchanged, and is known as the exchange current density (i_0). The relationship

between the exchange reaction rate and the current density, can be derived from Faradays' law:

$$r_{oxid} = r_{red} = {}^{i_0}/_{nF}$$

where r_{oxid}, r_{red} = equilibrium oxid/red rate, i_0 = exchange current density. The exchange current density is therefore the rate of oxidation and reduction at equilibrium, although no net current will flow, i_0 is influenced by the ratio of oxidised and reduced species present, and by the temperature of the system. The values are calculated experimentally.

Figure 1.2 The exchange current density plotted on a potential against reaction rate graph (Fontana, 1987)

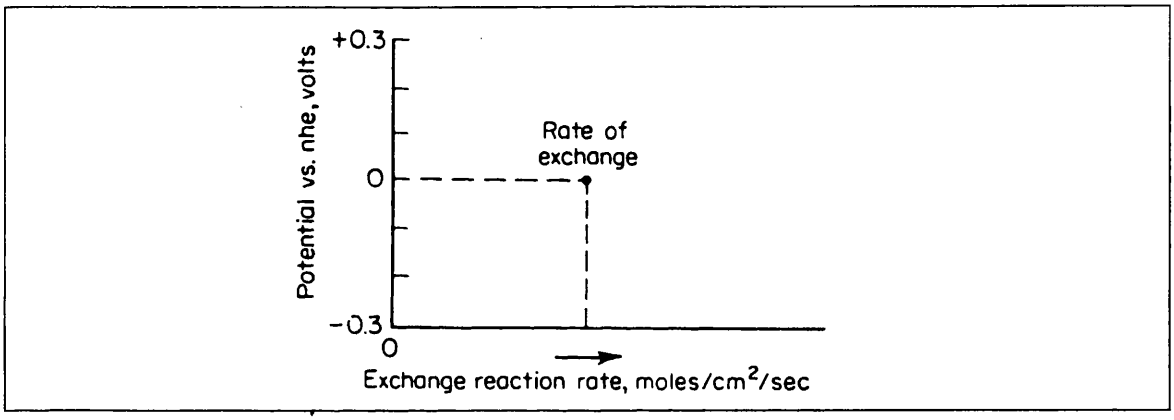

Other than by connecting two half cells together, an overvoltage can be obtained by the application of a voltage to an electrode. In this way the relationship between overvoltage and current density can be examined. The overvoltage, positive to negative can be plotted against the log current density, giving a polarisation curve. Figure 1.2 illustrates this relationship. Several shapes of the polarisation curve exist. Figure 1.3 illustrates activation polarisation. This type of polarisation curve can be characterised by an equation, the Tafel equation:

$$\eta_a = \pm \beta \log(i/i_0)$$

where β = Tafel constant, and i = rate of oxidation/reduction. In activation polarisation the corrosion mechanism is controlled by the activation step of the reaction and is limited by no other factors. This type of corrosion tends to occur in environments containing high concentrations of active species (concentrated acid solutions) or low concentrations of reducible species (salt solutions).

Figure 1.3 Activation-polarization curve of a hydrogen electrode (Fontana, 1987)

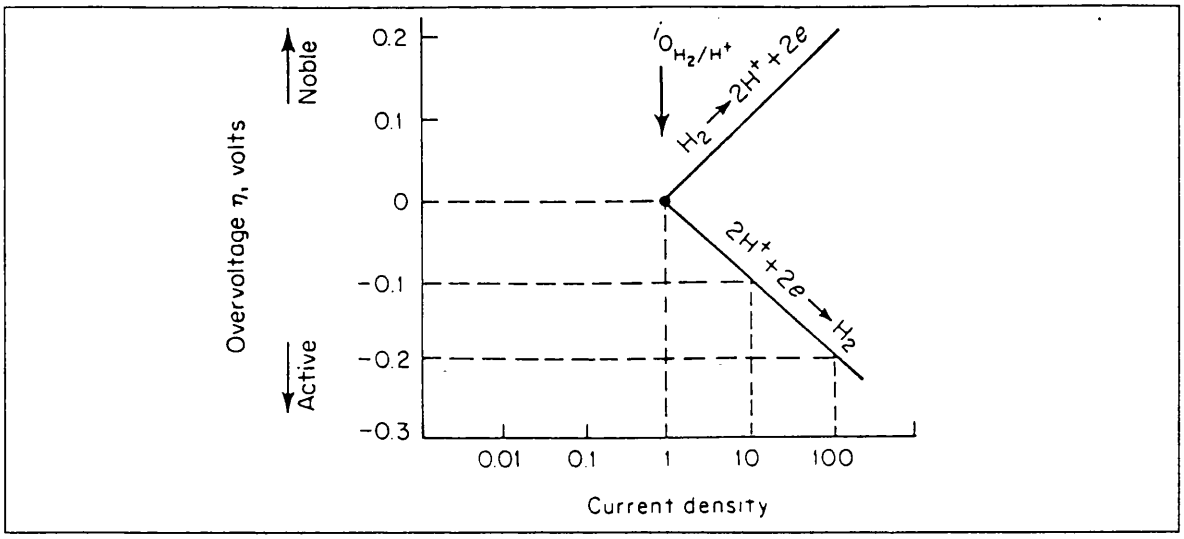

At very high reduction rates the region adjacent to the electrode surface will be depleted of reducible species. A limiting rate is reached that is determined by the speed at which ions can diffuse towards the reaction electrode surface. A limiting diffusion current density (i_L) is achieved:

$$i_L = DnFC_B/x$$

where D = diffusion coefficient of the reacting ions, C_B = concentration of reacting ions in the bulk solution, x = thickness of the diffusion layer. Concentration polarisation is usually negligible for metal dissolution. It is only important for the reducing cathodic process. The equation for concentration controlled polarisation is:

$$\eta_c = 2.3\frac{RT}{nF}\log\left(1-\frac{i}{i_L}\right)$$

Figure 1.4 illustrates the graph of concentration polarisation against log current density. Concentration polarisation does not become apparent until the net reduction current density approaches the limiting diffusion current density. The net reduction current asymptotically approaches the limiting diffusion current density. Velocity and temperature will effect the limiting diffusion current, as they increase, so will i_L.

In reality both concentration and activation polarisation occur in most corroding systems. The total polarisation can be found by summing the two components:

$$\eta_T = \eta_a + \eta_c$$

Figure 1.4 Concentration polarization curve for reduction process (Fontana, 1987)

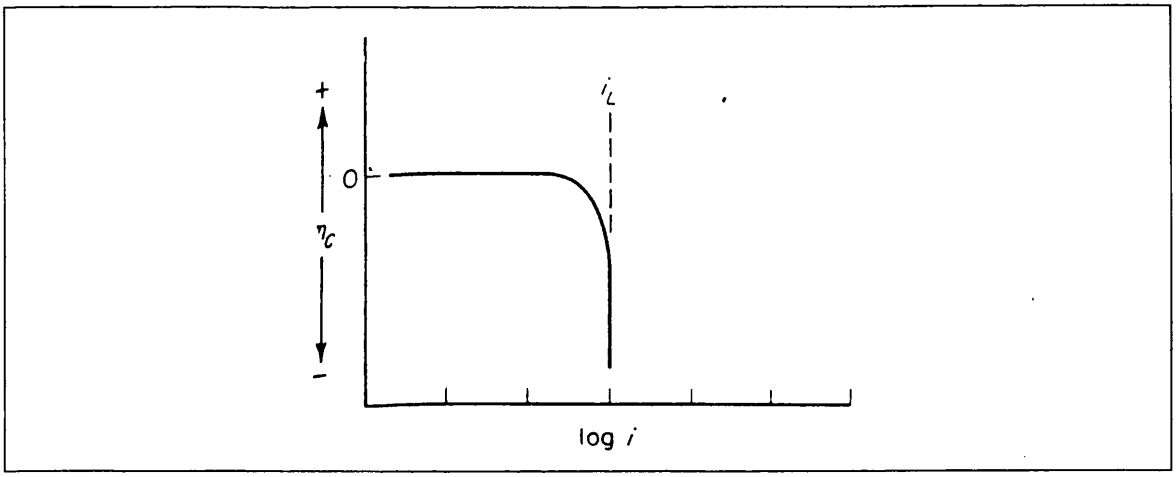

Figure 1.5 Activation and concentration polarization curve(Fontana, 1987)

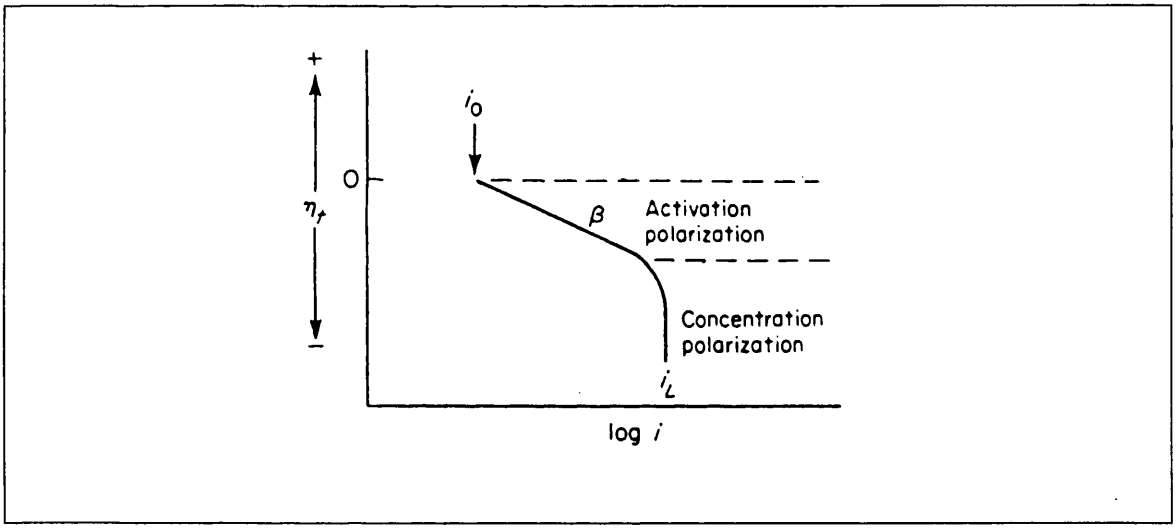

Figure 1.6 A mixed potential or Evans diagram. The resulting current and potential after 'mixing' the polarization curves of iron and hydrogen (Fontana, 1987)

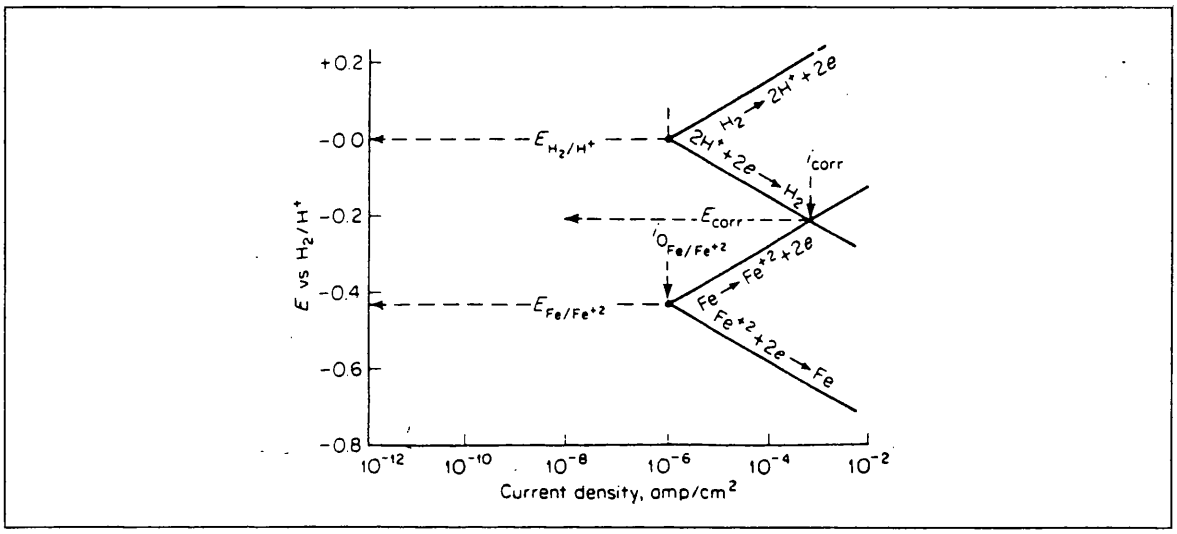

Figure 1.5 illustrates the polarisation curve obtained from this combination. During anodic dissolution $\eta_c = 0$, so:

$$\eta_{diss} = \beta \log \frac{i}{i_0}$$

During the cathodic process η_c is important so the equation changes to include this factor:

$$\eta_{red} = -\beta \log \frac{i}{i_0} + 2.3 \frac{RT}{nF} \log \frac{1 - i}{i_L}$$

This approach can be further utilised to explain spontaneous corrosion processes in the form of mixed potential theory, attributed to Wagner and Traud (1938). A mixed electrode is an electrode that is in contact with two or more redox systems. This is the case for a corroding metal. The electrochemical reactions can be represented by looking at the polarisation curves of the two redox species. An example of this is shown in figure 1.6, for the systems Fe/Fe^{2+} and H^+/H_2. These are known as Evans or mixed potential diagrams.

Figure 1.7 Metal M, in acid and Fe^{3+}, determination of E_{corr} (Fontana, 1987)

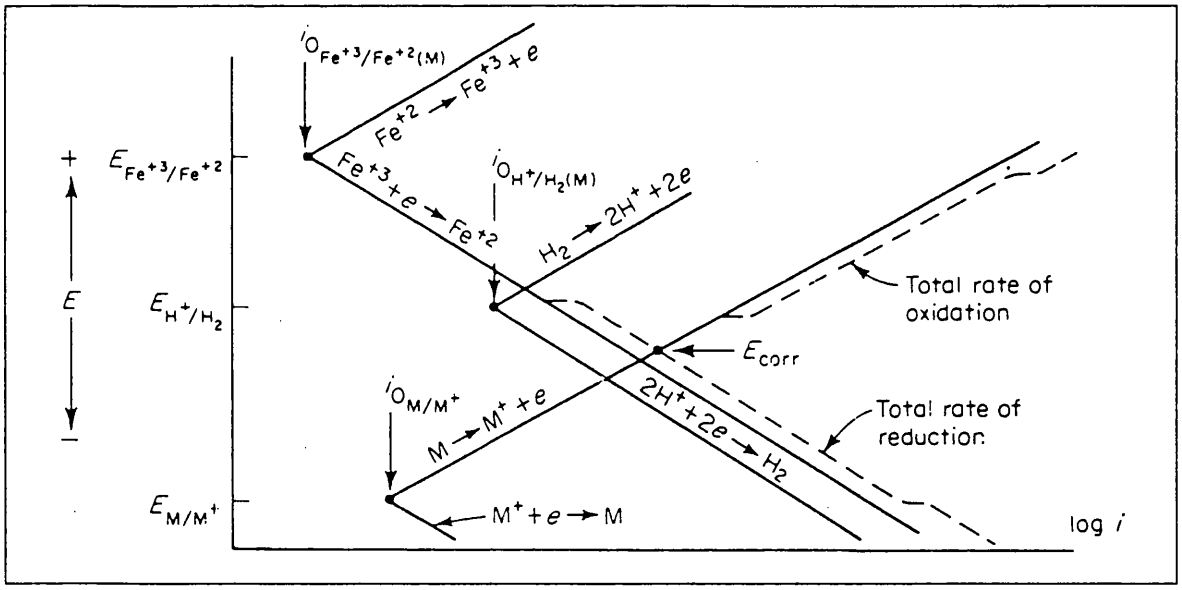

The electrode potentials show the natural potentials for each system, however as both redox systems are in electrical contact it is impossible for them to be at different potentials. The point where the two polarisation curves cross represents the point at which the rate of oxidation equals the rate of reduction. The potential at this point is the mixed or corrosion potential (E_{corr}) of the corroding system. The current density at this point is the corrosion current density (i_{corr}) and is an indication of the rate of a corrosion reaction.

Any additional redox species will also be 'mixed' to give a final corrosion current and potential. For example the addition of ferric Fe^{3+} salts to the corroding system above will increase the corrosion rate as more reducible species will be present. Fig 1.7 illustrates this process. Note that although the corrosion rate has increased, indicated by an increase in the corrosion current density, the hydrogen evolution rate decreases.

1.2.3 Passivity

Passivity is defined as the loss of chemical reactivity under certain environmental conditions. Metals in a passive state have very slow corrosion rates. The reduction in corrosion rate from an active to a passive metal can be as much as 10^6 Acm^{-1}.

Figure 1.8 Anodic dissolution behaviour of an active-passive metal (Fontana, 1987)

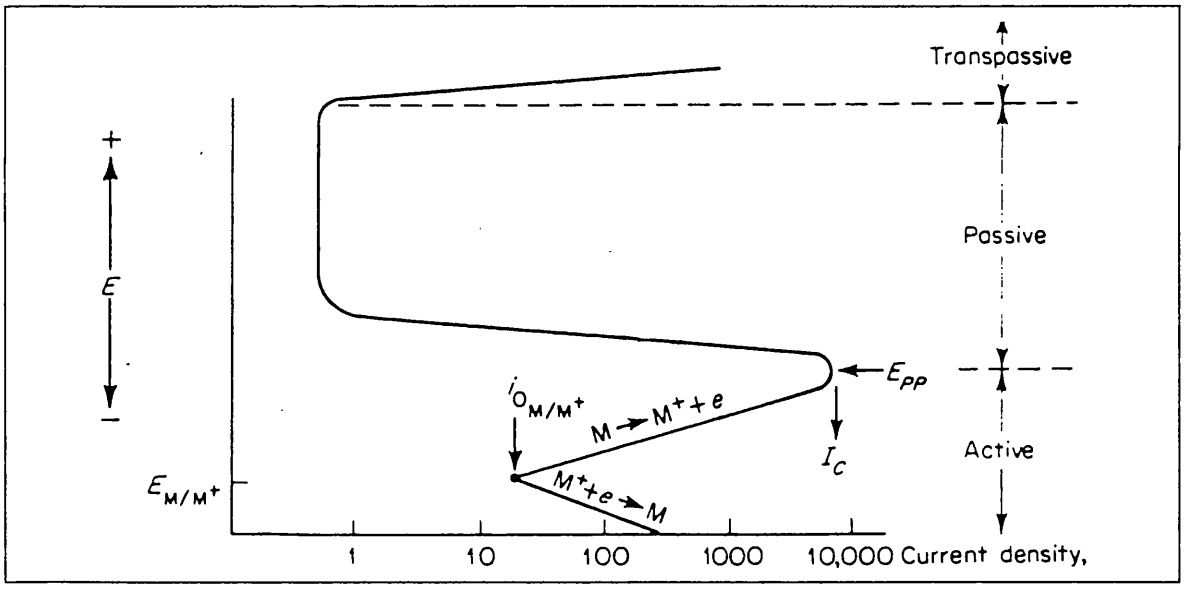

Passivity results from the formation of a surface film roughly 30Å or less. Iron demonstrates an active-passive transition. Figure 1.8 illustrates this behaviour. Initially the polarisation curve is similar to nonpassivating metals and shows 'Tafel behaviour' (active phase). But at higher potentials the dissolution rate drops and becomes independent of the applied potential (passive phase). At very high potentials the passive layer breaks down and the corrosion rate again increases (transpassive phase).The potential at which the metal changes from active to passive is known as the primary passive potential (E_{pp}).

The effect of passivation on corrosion rates can be seen by examining the mixed potential diagram for iron with differing cathodic polarisation curves (the position of the curve will depend on the solution that the iron is in. Figure 1.9 illustrates the case for three different cathodic polarisation curves, and the corrosion currents that could result. These are:

A - In this case the metal is active and high corrosion rates will be achieved. No passivation can occur.

B, C, D - C is electrically unstable so will not exist. B and D represent the active and passive states , both possible in this case. An example of this type is iron in dilute nitric acid. The metal is passive at point D unless the surface is scratched, in which case it reacts vigorously as it switches to point B in the active region.

E - In this case the metal is passive and will have a very low rate of corrosion.

Figure 1.9 Active-passive metal in corrosive conditions (Fontana, 1987)

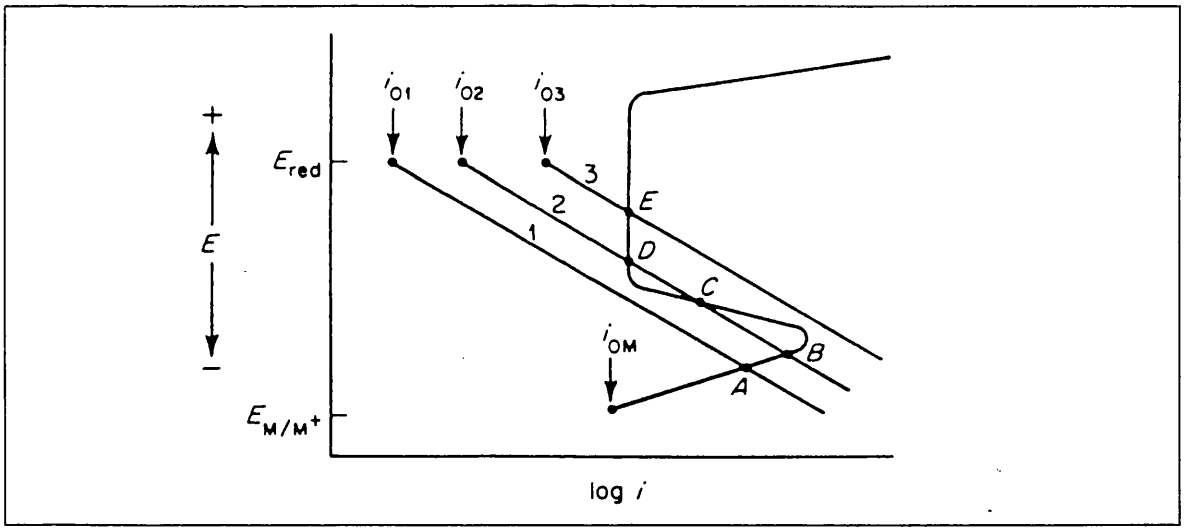

Passivity is also related to pH as well at potential. Potential v's pH plots are known as Pourbaix diagrams, after Dr. M. Pourbaix who first suggested there use (Pourbaix, 1966). The Pourbaix diagram for iron is illustrated in figure 1.10. The diagram is constructed from calculations based on the Nernst equation and solubility data for the iron compounds formed. It is possible to delineate areas in which Fe, $Fe(OH)_2$, $Fe(OH)_3$, Fe^{2+},and Fe^{3+}, are thermodynamically stable. The diagram can be used to predict the environmental changes that will prevent or reduce corrosive attack. The accompanying diagram in figure 1.10 illustrates the immune, passive and active areas. Pourbaix diagrams give no further information on the rate of corrosion when it does take place.

Pourbaix diagrams are of relevance to the discussion of conservation of archaeological iron. The nature of burial environments and the corrosion product layers that form around corroding iron can lead to localised areas of low pH. We can see from the iron Pourbaix diagram that in these conditions iron is active and corrosion will occur. However they must be used with some caution as the systems present in the corrosion of archaeological iron contain a variety of different species, such as chloride or sulphate ions, and therefore the Pourbaix diagrams become considerably more complex. It is also important to remember that Pourbaix diagrams describe only the equilibrium thermodynamic conditions which may not have been reached.

Figure 1.10 Simplified Pourbaix diagrams for the Fe-H_2O system

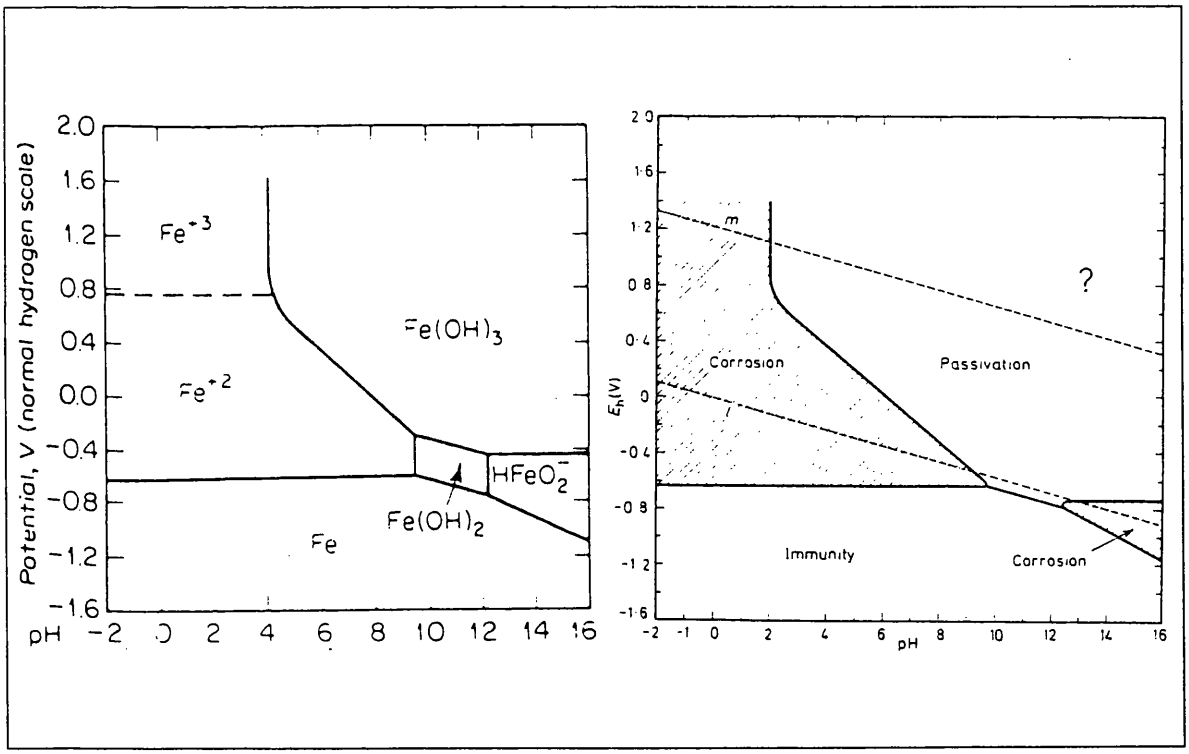

1.3. CLASSIFICATION OF CORROSION

Corrosion can be classified in many different ways. One approach is to divide corrosion into wet and dry. Another classification is low and high temperature corrosion. Corrosion can be classified by the corrosive media, for example atmospheric, soil, or marine or freshwater corrosion. Corrosion can also be categorised into further groupings by the differing mechanisms or the differing physical effects of the corrosion. Uniform corrosion accounts for the greatest losses but other forms exhibit characteristic localised effects. The list offered here is not exhaustive but covers the main types of corrosion relevant to excavated artefacts. In many corroding systems several types of corrosion can occur. Changes in burial environment of archaeological metals can lead to changes in the type of corrosion occuring and possibly lead to cyclic or periodic corrosion

1.3.1 Uniform Corrosion

This is the usually expected mode of corrosion. When an object is exposed in its entirety to the corrosive environment, dissolution of the metal occurs over the entire exposed surface. The rate of this type of corrosion can be measured in mm or cm per year, relating to the depth of metal that has dissolved. The dissolution of metal from the surface of an object causes a coating of corrosion products to form. Uniform corrosion proceeds until there is no metal core remaining inside the corrosion products. The corrosion product layers surrounding the metal core become bulky and volumous and the shape of the object can become obscured due to the differences in the relative volume of iron and its corrosion products. The molecular volume of iron oxyhydroxide relative to iron is 4.28 for example.

1.3.2 Galvanic Corrosion

Mixed potential theory can be used to explain galvanic coupling. Figure 1.11 shows the Evans diagram for such a situation. Metal M has a relatively noble corrosion potential, and a low corrosion current density, $i_{corr(M)}$, whilst metal N corrodes at a higher rate, $i_{corr(N)}$. The resultant mixed potential of the system occurs at the point where the total oxidation rate is equal to the total reduction rate. So metal M has a decreased corrosion rate $i_{corr(\underline{M}\text{-}N)}$, whilst metal N has an increased rate $i_{corr(M\text{-}\underline{N})}$. The more reactive metal therefore will corrode at the expense of the other. The relative areas of the two coupled metals will also

influence galvanic behaviour. A galvanic couple of two metal will increase the rate of corrosion of the more active metal. The corrosion decreases at points further from the junction of the two metals due to higher resistance through a longer electrolyte path. The electrolyte conductivity thus confines the current to a small surface area near the junction.

Figure 1.11 Galvanic couple between two corroding metals (Fontana, 1987)

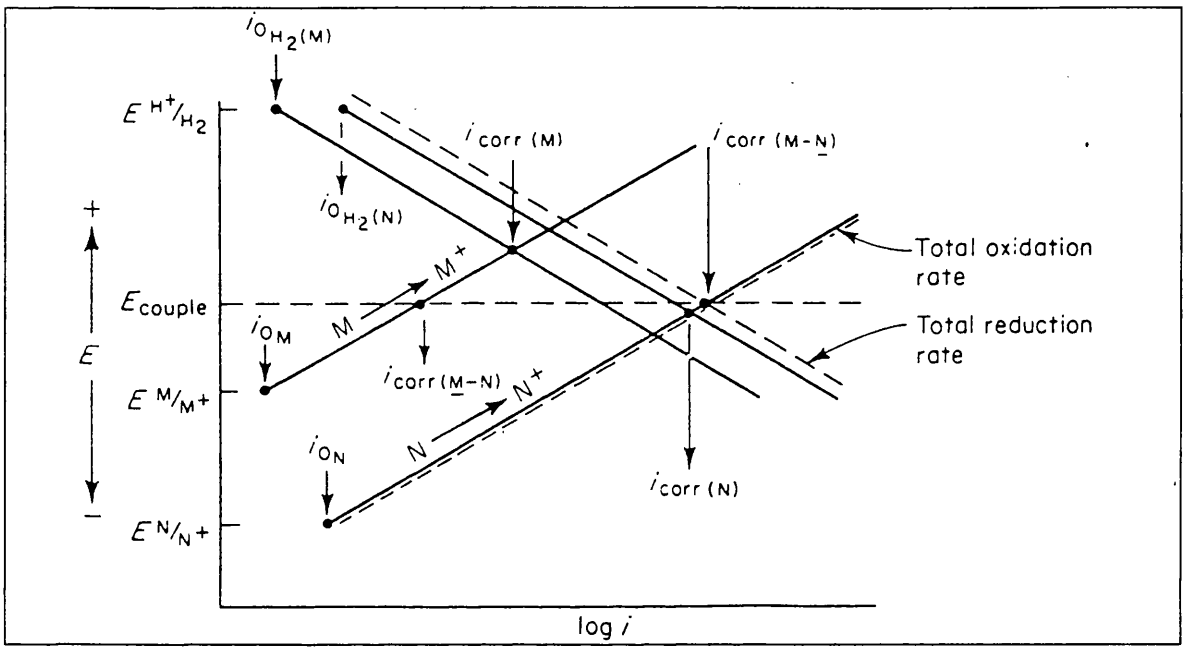

Galvanic coupling often occurs with archaeological objects. As each metal is in contact with oxidants such as H^+ and O_2 the rate of the cathodic reaction increases (i.e. the rate of electron consumption increases). and the rate of metal dissolution will increase. But the dissolution will occur at the less noble metal. This would mean that if copper were coupled to iron, the iron would corrode preferentially.

1.3.3 Crevice Corrosion

A crevice created by contact with another adjoining piece of the same metal or a different material will cause increased localised corrosion. The corrosion may be caused by the retention of water within the crevice while outer surfaces can drain better. A crevice shields part of the surface and enhances the formation of differential aeration and chloride concentration cells. The accepted mechanism for crevice corrosion can be described as follows (Rosenfeld *et al*, 1964). Corrosion consumes dissolved oxygen within a crevice

and this will cause an increase in the metal ion concentration which causes highly mobile negative ions such as Cl^- to be drawn in, to counterbalance the charge. OH^- also migrate towards the crevice, but as they are less mobile than Cl^-, this occurs at a far slower rate (Fontana, 1987). A concentrated acid chloride solution forms within the crevice:

$$Fe^{2+}_{(aq)} + 2H_2O(l) + 2Cl^-_{(aq)} \rightarrow Fe(OH)_{2(s)} + 2HCl_{(aq)}$$

As the oxygen is used up no cathodic reaction can occur in this region and so a localised anode is formed coupled to a large surface area cathode on the surrounding surfaces. The crevice grows as more chloride is attracted to the crevice promoting further acid hydrolysis. The rate of oxygen reduction on the other surfaces also increases, and these areas become cathodic so no metal dissolution occurs. These surfaces are thus protected at the expense of the crevice. The reaction becomes autocatalytic once it is initiated, although it may take some time for initiation to occur in a crevice.

1.3.4 Pitting Corrosion

Localised attack on an otherwise resistant surface is classified as pitting corrosion and leads to the formation of deep pits or holes, usually of small diameter. Pitting shares the same mechanism as crevice corrosion. The pit itself becomes a crevice, restricting transport between the bulk solution and the acid chloride pit anode. The actual mechanism of pit initiation is not well understood. It is thought that areas of a metal with high concentrations of Cl^- bound to the surface may be formed, (due to temporary anodic points on the surface) causing a low pH microenvironment (Evans, 1951). Beneath these islands, hydrolysis occurs from cation corrosion products producing HCl. Other anions such as sulphate and nitrate may also be involved in the hydrolysis, but the high mobility of Cl^- make them more aggressive in both pitting and crevice corrosion. Pit initiation often occurs preferentially at sulphide inclusions within the metal microstructure, perhaps due to the creation of microcrevices when these inclusions are dissolved away (Jones, 1992). During initiation or early growth of a pit, conditions are unstable. The local high concentrations of hydrogen and chloride ions may be swept away by random convection currents making some new pits inactive. It is only when a protective cavity has formed that pit growth accelerates and becomes autocatalytic. Pits tend to grow in the direction of gravity on the upper surfaces of metals.

1.3.5 Intergranular Corrosion

Reactive impurities may segregate to, and passivating impurities be depleted from, the grain boundaries of a metal. Grain boundaries are therefore often more susceptible to corrosion than other areas. This is also common for alloy systems.

1.3.6 Microbiologically Induced Corrosion

Microbiologically induced corrosion often occurs in nearly neutral aqueous conditions. Saturated, deaerated soils often show relatively high corrosion rates due to anaerobic bacteria, the most notorious being sulphate reducing bacteria (SRB- *D. desulfuricans*). These bacteria reduce sulphate to sulphide:

$$SO_4^{2-} + 4H_2 \rightarrow \quad S^{2-} + 4H_2O$$

The source of hydrogen can be derived from cellulose, sugars or other organic matter present in soils. These bacteria can be found in greatest numbers in wet clay, boggy soils and marshes. The presence of the sulphide ion will have a marked effect on the corrosion process. Sulphide ions will tend to accelerate the anodic metal dissolution and therefore increase the corrosion rate. The corrosion product that is commonly found in the presence of SRB is iron sulphide. A sulphate corrosion product known as Green Rust II has also been suggested as a corrosion product of microbially induced corrosion (Refait *et al*, 1997).

Corrosion can also be accelerated by aerobic bacteria such as thiobaccillus thiooxidans that are capable of oxidising sulphur and other sulphur containing compounds to sulphuric acid:

$$2S + 3O_2 + 2H_2O \quad \rightarrow \quad 2H_2SO_4$$

They can often be found in low pH environments and via the above reaction can create extremely corrosive conditions. In changing soil conditions, such as seasonal changes from wet to dry soils (from anaerobic to aerobic environments), these two types of bacteria often also exist in seasonal cycles. This cyclic effect may cause extensive corrosion damage.

1.3.7 Atmospheric Corrosion

It has already been stated that an electrolyte is need for corrosion to take place. However corrosion does not occur only in aqueous solution but also in the atmosphere. This is due to thin moisture films that form on surfaces above a certain critical relative humidity. Below this humidity level the atmospheric corrosion rate will be negligible. Experimental work has found the critical relative humidity to be between 30% - 40% for iron.

Atmospheric corrosion will be accelerated by pollutants such as sulphur and nitrogen compounds. Corrosion near seawater will also be greater due to sodium chloride contamination. In polluted atmospheres the critical relative humidity may fall. Iron objects contaminated with chlorides and sulphates may start to corrode at a relative humidity as low as 20%(Turgoose, 1982).

1.3.8 Marine Corrosion

Seawater contains 3.4% sodium chloride and has a pH of between 6.5 to 9.5. This makes it a good electrolyte and therefore facilitates corrosion. Corrosion proceeds with the formation of a biofilm (known as biofouling). An increased local concentration of chloride ions builds up in this region, up to three times that of the surrounding environment, with a pH of less than 6.5 (the metal itself when corroding will have a pH of 4.8 (North & MacLeod, 1987, 74). The high concentration of chloride ions has a great effect on the corrosion products produced. Calcineous concretions surrounding the inner corrosion products are another feature of marine corrosion.

The rate of marine corrosion will vary depending on several factors such as the amount of dissolved oxygen, the pH, the temperature and turbulence of the water. The corrosion rate is often controlled by the amount of dissolved oxygen, as oxygen reduction is the main cathodic reaction. The oxygen content in the upper layers of the ocean (where most shipwrecks are located, and hence archaeological marine iron is found) is dependent on the biological activity and rate of mixing with surface water layers. Low oxygen levels are often found in esturine and polluted waters, underneath marine concretions and below the seabed. In these cases there is the possibility of corrosion via sulphate reducing bacteria

(North & MacLeod, 1987, 74). Higher temperatures would be expected to increase the rate of corrosion, however opposite effects can be found, due to an increased growth rate of biological organisms that produce protective concretions on the corroding iron. Water turbulence is also seen to speed up corrosion as the water action prevents the formation of protective oxide concretions (North & MacLeod, 1987, 75).

1.4 THE CORROSION OF ARCHAEOLOGICAL IRON

1.4.1 Corrosion of Archaeological Iron in Differing Environments

The complex environments in which archaeological iron is often found, make the prediction of the type of corrosion products occurring complicated. A greater variety of corrosion products have been reported than those expected from laboratory experiments. Obviously burial conditions will affect the stability of corrosion products. The Pourbaix diagram for iron indicates the conditions for which specific products will predominate. Due to the long time scales involved in archaeological corrosion, changes in corrosion products may occur and therefore the most stable phases of corrosion products are expected. The thermodynamically stable state may not have yet been reached and therefore other corrosion products are possible. Corrosion products often occur in layers, with more oxidised products nearer the surface. Table 1.1 gives a list of the many corrosion products reported in the literature to have been found on archaeological iron.

Table 1.1 Corrosion products found on archaeological iron

Amorphous FeOOH	(Gilberg & Seely, 1981)
α–FeOOH	(Gilberg & Seely, 1981)
β–FeOOH	(Zucchi et al, 1977)
γ–FeOOH	(Gilberg & Seely, 1981)
α–Fe_2O_3	(Argo, 1981)
Fe_3O_4	(Argo, 1881)
$FeCl_3$	(Nosek, 1987)
$FeCl_2$	(Nosek, 1987)
$FeCO_3$	(North, 1976)
FeOCl	(North, 1976)
$Fe(II)_{1.95}Fe(III)_{2.55}(O,OH,Cl)_9$(Green Rust)	(Gilberg & Seely, 1981)
FeS	(Gilberg & Seely, 1981)
$FeSO_4.4H_2O$	(Knight, 1982)
$FePO_4$	(Sanchez del Junco *et al*, 1992)

1.4.1.1 Corrosion products formed on buried objects

Considering the O_2-Fe-H_2O Pourbaix diagram, in the absence of other anions the only stable corrosion products in aerobic conditions is α–FeOOH, also known as the mineral goethite, and Fe_3O_4, magnetite. These are indeed the corrosion products most commonly found on archaeological iron. A layer of black magnetite usually underlies the red-brown geothite as magnetite is stable in less aerated (equivalent to lower potential) environments. It has been argued that the original surface of an object is preserved in the corrosion products of lower oxidation state (the magnetite layer) as the initial corrosion products formed on the surface sufficiently restrict the diffusion of oxygen to prevent formation of more oxidised corrosion product below the original surface (Turgoose, 1989, 30).Although it is often possible to identify the original surface, the situation is rarely as straight forward as the above explanation would suggest.

In acidic environments the solubility of Fe^{2+} increases with respect to it's hydroxide as is shown by the Pourbaix diagram. In the presence of other anions with insoluble iron (II) compounds, ferric corrosion products are found. Examples of such compounds are vivianite $Fe_3(PO_4)_2.8H_2O$, and siderite, $FeCO_3$. These compounds are often found under more reducing conditions, mixed into the magnetite layer (Turgoose, 1982, 1).

Microbiologically induced corrosion in anaerobic environments has been suggested by the presence of iron sulphide, in corrosion products (Sanchez del Junco *et al*, 1992). Although this is a possibility, their presence does not necessarily indicate the actual corrosion is caused microbiologically, it only indicates the presence of sulphate reducing bacteria. Turgoose suggests that the SRB may be using hydrogen produced from the corrosion reaction as a reductant and the S^{2-} produced will then react with any Fe^{2+} ions present producing FeS (Turgoose, 1985b, 14).

The only stable ferric compound is geothite, α–FeOOH, and Fe(III) compounds of other anions are never found. Other oxyhydroxide phases, such as lepidocrocite, γ-FeOOH are often found. The other forms of FeOOH, will convert to the most stable α–phase in aqueous solution over a period of a few years and so the β, γ or δ oxyhydroxide phases that have been reported to be present in archaeological corrosion products are most likely

the result of post excavation oxidation of ferrous compounds. The β-FeOOH is often found on marine iron and is associated with unstable, high chloride containing archaeological iron. Often FeOOH found in corrosion products is amorphous and it's exact phase can not be identified.

1.4.1.2 Marine corrosion products

The corrosion of iron in marine environments can be seen as the extreme case. The high concentration of chloride ions has a great effect on the rate of corrosion and the corrosion products formed. Objects, both buried in the seabed and exposed to the seawater, corrode in a distinctive way. Marine corrosion can be divided into four distinct phases, as elucidated by North (1982).

1 - Initial Immersion:

This is the corrosion occurring in the period before complete coverage of the metallic iron surface by corrosion products. This can take 1-3 years. The cathodic production of hydrogen has been suggested (North, 1982) as the primary cathodic reaction occurring in marine corrosion. Hydrogen and methane gases have been reported to be present in corrosion products (Macleod, 1988). Other evidence suggest that oxygen reduction occurs more widely (Turgoose, 1985a). The iron surface is colonised by marine organisms (biofouling) such as Coralline algae (North, 1976). A layer of skeletal material, mostly calcium carbonate will soon build up. This then traps and encapsulates sand particles and other debris and forms a layer of low porosity (North & MacLeod, 1987).

2 - Corrosion and Concretion

In this stage residual iron is still present at the core of the corroding object, however much of the original volume of the object is occupied by corrosion products. Volumous calcium carbonate concretions have formed around the corroded object. (Turgoose, 1985). By this stage in the corrosion process the anodic and cathodic reactions will be separated. The anodic reaction must occur at the metal surface but the cathodic reaction occurs some distance from the metal, often in the magnetite layer where there is sufficient oxygen.

3 - Equilibrium State

When all the metallic iron has corroded the system starts to return to a state of equilibrium. During corrosion the microenvironment has a low pH (4.8) and potential. This starts to return to the conditions found in the surrounding environment (pH of about 7 to 8). Chloride ions trapped in the pore solution will also be released as they are no longer attracted to the corroding surface. As the iron and chloride rich acidic solution diffuses out, impurities from the inner corrosion product such as sulphates, phosphates and group 1 and 2 metals are dissolved in the solution and deposited in the outer corrosion layers. The ferrous ions present in solution, exchange with the calcium forming iron carbonate. The H^+ ions also reacts with calcium carbonate to form calcium hydrogen carbonate, and this increases the pH of the solution and causes ferric and ferrous compounds to precipitate out. The inner parts of the concretions thus become iron carbonate, cemented together by ferrous and ferric oxide, oxyhydroxide and hydroxychlorides. An outer layer of the concretion still remains that consists of calcium carbonates but contains 2% iron and some inorganic calcium carbonate precipitated from the inner zone.

Iron buried beneath the seabed undergoes very similar processes. Marine growth is negligible but calcium carbonate concretions build up from shell fragments and coral. Buried concretions are more likely to have iron corrosion products in lower oxidation states and more magnetite (Fe_3O_4) (North and MacLeod, 1987, 78).

4 - Post Excavation Changes

Post excavation changes are what makes the stabilisation of iron such a difficult problem. This crucial issue will be discussed in detail in section 1.5. Corrosion products such as iron oxides and oxyhydroxides and ferrous chloride have already been mentioned as being found on marine iron. The presence of FeOCl has been suggested (North & Pearson, 1975, 1977) as the main chloride containing corrosion product in marine iron. However this has not been confirmed by other studies (Argo, 1981, Turgoose, 1989) and its formation would not seem feasible for the given thermodynamic conditions.

Rather, the formation of basic ferrous chlorides has been suggested as the most likely marine iron corrosion product (North, 1982). These are stable under the more reducing

conditions that often exist under the thick concretions of marine iron. α-$Fe(OH)_2.FeCl_2$, β-$Fe(OH)_2.FeCl_2$, and γ-$3Fe(OH)_2.FeCl_2$, may form via the following reaction:

$$2Fe + 2H_2O + 2Cl^- \rightarrow (FeCl_2.Fe(OH)_2) + 2H^+ + 4e^-$$

Although actual detection of these compounds is difficult due to the changes that occur as soon as corroding marine iron is exposed to an oxygenating environment, their presence has been inferred by the detection of other compounds such as green rust which are known to be the products of the decomposition of basic ferrous chlorides.

1.4.2 The Corrosion of Different Metallurgical Microstructures

Turgoose has stated that whether an object is made of wrought iron, carbon steel or cast iron makes very little difference in terms of the nature of the corrosion process (Turgoose, 1989). This may be true when examining the chemical composition of corrosion products, however the physical structures of corroded wrought and cast iron differ considerably and this in turn leads to different considerations in their conservation.

Wrought iron is produced from a bloom - a spongy mixture of iron and slag ($2FeO.SiO_2$) which is the result of direct smelting. The bloom is forged at high temperatures to weld together the iron and expel the slag, although 'stringers' of slag often remain in wrought iron objects. Wrought iron was also produced by decarburising cast iron in an oxygenating environment. This process was carried out in China where the wrougt iron produced was known as 'ripe iron'. The indirect production of cast iron was a method later used in the West (Wertime & Muhly, 1980), and from the sixteen century the majority of wrought iron and steel was made by the indirect smelting of cast iron produced in blast furnaces (Rostoker & Bronson, 1990). Wrought iron contains iron in several phases. Ferrite is a body centred cubic phase of iron, and this is often accompanied with regions of iron carbide known as cementite, an orthorhombic phase. An average of 0.1% carbon, distributed heterogeneously is common in archaeological wrought iron (Cronyn, 1990, 176) Ferrite and cementite can occur as the eutectoid pearlite, which contains lamellae of ferrite and cementite. Early wrought iron has a very inhomogenious structure and often contains phosphorus and arsenic.

Steel is produced when wrought iron undergoes carburisation - that is, when it is heated to 900°C in a reducing environment and then cooled rapidly (quenching). This process increases the amount of carbon present in the metal to above 0.3% and also produces a new non equilibrium phase known as martensite which gives steel its strength. Often wrought iron undergoes secondary carburisation, with just the outer surface carburised. This can be done to produce a hard steel edge for a knife or sword for example, whilst the inner composition is that of wrought iron. Steel was also welded into the cutting edges of tools.

If wrought iron is left for a sufficient time it may corrode to leave corrosion products around a central void where the iron object has totally dissolved away. This is often seen in the corrosion of small wrought iron objects from marine environments. These objects can totally corrode away within 100 years (Cronyn, 1999, 185). Different areas of objects tend to corrode at different rates due to the compositional inhomogeneity of layered wrought iron and the presence of slag inclusions. The most rapid corrosion occurs in the metal adjacent to slag inclusions (North and Pearson, 1975), probably due to the slag providing a pathway for water and chlorides to penetrate into the metal. Corroded wrought iron has a distinctive 'wood grain' appearance, the grains often indicating the direction in which the object was forged.

The metallurgical structure of the original metal can sometimes be detected in wrought iron corrosion products. Remnant structures can be found. These are complete grains or aggregates of grains surviving intact although surrounded by corrosion products and isolated from any remaining iron core. Brian Scott explains the existence of these structures using a comparison to the erosion of a geological coastline. The corrosion of weaker grains leads to the formation of a bay, then a peninsula and finally an island (Scott, 1989, 10). These remnant structures are often created by pitting corrosion. Slag inclusions also often exist as remnant structures.

Fossil or ghost structures are areas of a corroded object where the grain structure of the original metal has been preserved by corrosion products, although none of the metal remains. Partial replacement structures are also found. These occurs when one phase such as the ferrite phase has corroded and been replaced by oxide, whilst another phase, for

example the pearlite phase, has survived. The phases that are more resistant to corrosion are obviously the ones more likely to survive and for this reason cementite and other phases containing iron carbide are more often found in partial replacement structures.

There is no simple model for the occurrence and distribution of remnant or fossil structures, and it must be remembered that differentials in the volumes of the original metal and the oxide that has replaced it means that deformations must occur and replacement structures can not be assumed to be identical to original structures. Remnant structures are thought to occur by chemoepitaxy. This is defined as a process leading to the growth of crystalline, regularly orientated reaction layers on a material resulting from a chemical reaction between the initial substance and any other substance. The new corrosion products form epitaxially; the crystal growth occurs with a regular orientation, in this case with the orientation of the metal grains being replaced, thus preserving the structural orientation of the original metal (Scott, 1991).

Evidence of organic materials such as wood or leather that were once in contact with wrought iron or steel objects can often be detected in corrosion products. Pseudomorphic replacement of organic materials by corrosion products can occur. The exact mechanism is still unknown, but it has been suggested that the surfaces of organic fibres promote the nucleation of iron oxides from pore solutions in the corrosion environment. The fibres then decay leaving cast-like corrosion product structures (Turgoose, 1989, 31).

Cast iron, a 13th century innovation in the west, although produced as early as the second century BC in China (Scott, 1991, 37) exists in two forms, white and grey and contains 2-5% carbon. White cast iron is more common in early artefacts but large objects and those produced post 18th century are usually grey cast iron (Tylecote & Black, 1980, 88). Grey cast iron contains flakes of black graphite, phosphorus and silicon. The iron phases present are ferrite, pearlite, and a eutectic comprising cementite and austenite (a phase of iron and iron carbide). White cast iron has a similar carbon composition but it contains cementite (iron carbide) rather than graphite flakes and has a much reduced silicon level. Cast iron is brittle but has compressive strength. It was widely used in the production of cannon and cannon balls

When grey cast iron corrodes it is much more likely to keep its shape than wrought iron. In fact it almost always remains solid even though totally corroded and encased within concretions. Corrosion occurs in three phases, first the pearlite, starting with the ferrite, then the cementite part disintegrates leaving the graphite flakes in the case of grey cast iron. Secondly the ledeburite is attacked, leaving only cementite needles. Finally the cementite needles are corroded. The object will consists of a matrix of corrosion products cemented together by small residual flakes of lustrous graphite and possibly cementite needles. This is known as graphitic corrosion or graphitisation and occurs as the graphite flakes have become the cathodic sites in an iron/carbon galvanic corrosion cell. The same process occurs for white cast iron however the cementite phase becomes cathodic and is thus the last phase to corrode in the graphitised structure. When cementite does corrode it is possible that hydrocarbons are formed. Vacuum distillation of some corroded cast iron produced an oily mixture of alkenes ranging from C_6 to C_{14} (MacLeod, 1981, 295).

Graphite is immune to corrosion and so remains to retain the original shape. The surface of corroded cast iron under the concretions can often become soft, however it is often still possible to read inscriptions and embossings on corroded cast iron surfaces after several centuries. The graphitised layer is very fragile and on excavation may rapidly disintegrate if not treated in the correct manner (North & Pearson, 1975).

1.4.3 Pore Solutions Found in Corrosion Products

As corrosion proceeds and an object becomes covered in a corrosion product layer, the anodic and cathodic parts of the corrosion reaction become separated. The anodic reaction occurs at the metal surface. The electrons liberated will then migrate through the magnetite layer to the magnetite surface where the cathodic reduction of oxygen can occur. The formation of positively charged Fe^{2+} ions at the metal surface requires negatively charged anions to counterbalance the electric charge. Therefore chloride, being the most mobile and often the most plentiful anion will migrate to the metal surface. This causes a chloride ion concentration gradient in the magnetite layer with the highest concentration at the metal surface. A solution with a high chloride concentration will thus form in the pores of the corrosion layer. The $FeCl_2$, ferric chloride solution becomes highly acidic due to

hydrolysis. A chloride solution with a concentration of 1-1.5M has been noted (Walker, 1996). In soils with high sulphate concentrations a sulphate pore solution will form in a similar way (Turgoose 1989).

1.4.4 Post Excavation Changes in Corrosion Products and the Instability of Archaeological Iron Objects

On excavation from terrestrial or marine sites, iron artefacts undergo rapid changes in environmental conditions. A decrease in the relative humidity and an increase in the oxygen concentration will almost always occur, causing objects to dry out and oxidise. This may lead to changes in the nature of the corrosion products and these changes can lead to further instability and corrosion. Objects transferred to drier environments will experience a decrease in the relative humidity. This will cause the pore solution to dry out and can result in the formation of solid ferrous chloride, $FeCl_2$ or in sulphate rich pore solutions ferrous sulphate, $FeSO_4$ (Turgoose, 1989).

It is also likely that any ferrous ions (Fe^{2+}) present will be oxidised to ferric (Fe^{3+}) compounds on excavation. Several different products can result from such oxidation depending on the pH of the environment to which the object is removed. The oxidation reactions that occur are complicated and often involve intermediate compounds (Bernal *et al*, 1959, Kiyama *et al*, 1969, Takada, 1969). A reaction scheme has been devised for the transformations that occur to ferrous hydroxide in basic (Misawa *et al*, 1971) and acidic (Misawa *et al*, 1974) conditions on aerial oxidation. This is illustrated in figure 1.12. In both cases an amorphous ferric oxyhydroxide is formed that will convert to the stable α–FeOOH in time or through wet/dry cycling (Maeda *et al*, 1992). In acidic conditions the reactions proceed via an intermediate product known as green rust.

Figure 1.12 Changes occuring in excavated corrosion products

Under Basic Conditions

$Fe(OH)_2 \rightarrow Fe(OH)_3 \rightarrow$ amorphous $FeO_x(OH)_{3-2x} \rightarrow$ α-FeOOH

Under Acidic Conditions

$Fe^{2+} \rightarrow$ Green Rust $\rightarrow$ amorphous FeOOH $\rightarrow$ α-FeOOH

In marine iron it is thought that the initial major primary chloride containing corrosion product formed is basic ferrous hydroxychlorides. Oxidation of these compounds can lead to a variety of corrosion products (Misawa, 1971, 1974). A scheme of the reactions and the conditions in which they occur is shown in figure 1.13. All these oxidation reactions proceed via the formation of green rust I, which is formed during the aerial oxidation of ferrous chloride solutions, or the solid state oxidation of ferrous hydroxide (Misawa *et al*, 1969, 1974). When mixed with other corrosion products this often looks a light green/brown colour. This intermediate has been identified as a mixed Fe^{2+}/Fe^{3+} compound (Yoshioka, 1949). Early research gave its typical composition as $Fe(II)_{1.95}Fe(III)_{2.55}(O,OH,Cl)_9$ (Keller, 1948). Later work (Refait & Genin, 1993) gives its formula as $3Fe(OH)_2.Fe(OH)_2Cl.nH_2O$ or $Fe_4(OH)_8Cl.nH_2O$. Its formation is as follows:

$$7Fe(OH)_2 + Fe^{2+} + 2Cl^- + \tfrac{1}{2}O_2 + (2n + 1)H_2O \rightarrow 2[3Fe(OH)_2.Fe(OH)_2Cl.nH_2O]$$

Green rust is unstable to aerial oxidation. and will decompose as shown in the following equation:

$$3Fe(OH)_2.Fe(OH)_2Cl \rightarrow 4FeOOH + 3e^- + Cl^- + 4H^+$$

The exact phase of the oxyhydroxide formed will depend on the environment the reaction occurs in, as shown in figure 1.13. Green rust is sometimes found on iron stored in sodium hydroxide solution (North, 1982).

Green rust I is found to form in the presence of chloride ions, but an analogous corrosion product exists in sulphate ion solutions, known as green rust II. Iron sulphates will oxidise via green rust II to give the same iron oxyhydroxide products. This is often found on objects from anearobic burial environments, where microbially induced corrosion occurs via sulphate reducing bacteria (Genin *et al*, 1998a). It is thought to form via a sulphite compound Green Rust II (SO_3^{2-}) which then oxidises to Green Rust II (SO_4^{2-}) (Simon *et al*, 1998). Recent work has also characterised a carbonate form of green rust (Genin *et al*, 1998b). Other ferrous salts present on excavation may oxidise. Ferrous sulphide, FeS reacts with oxygen to form jarosite, $NaFe_3(SO_4)_2(OH)_6$, and ferrous carbonate (Siderite), $FeCO_3$, oxidises and becomes α or γ-iron oxyhydroxide.

Figure 1.13 The oxidation of basic ferrous hydroxides in a variety of conditions

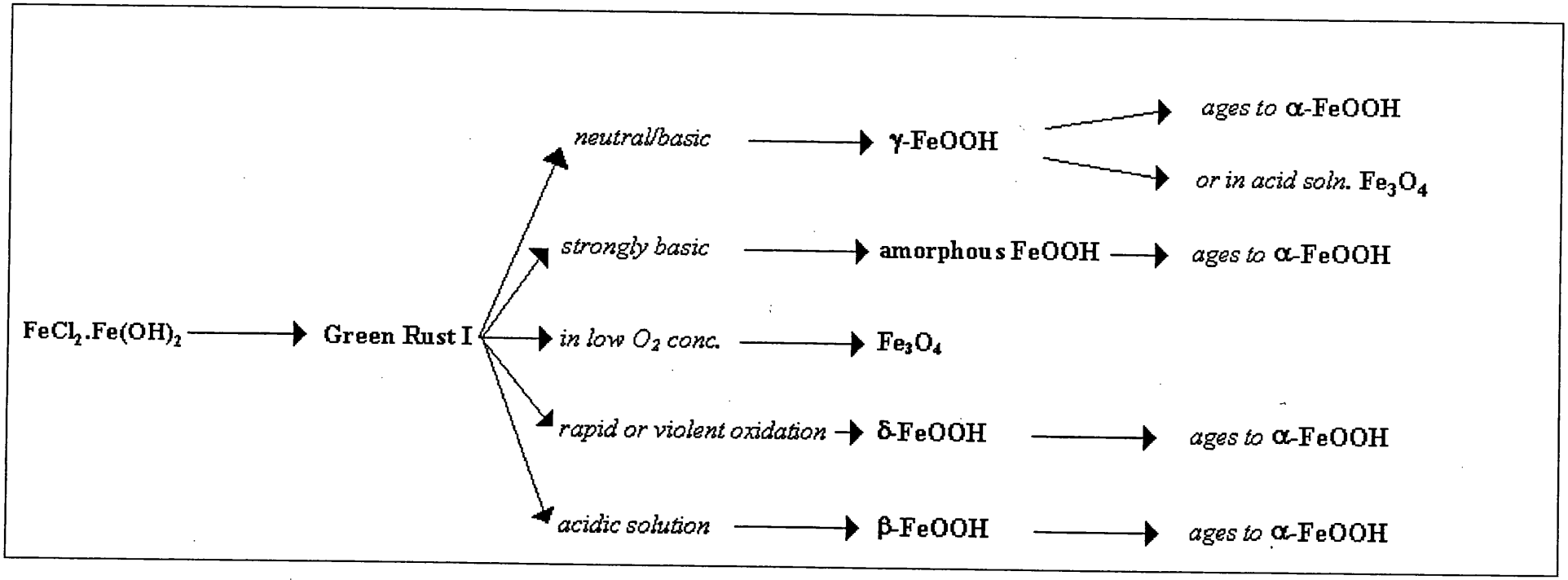

The β phase of iron oxyhydroxide is commonly found as a corrosion product in acidic, chloride rich environments. It is formed by the hydrolysis of ferric chloride solutions but also from the oxidation of β-$Fe_2(OH)_3Cl$ which precipitates from slightly acidic ferrous chloride solutions at room temperature (Misawa *et al*, 1974). β-$Fe_2(OH)_3Cl$, hibbingite, is a newly discovered naturally occurring mineral (Springer, 1989, Saini-Eidukat *et al*, 1994). It is also a likely intermediate in the mechanism for the formation of β-FeOOH in corroding systems as it has been shown to be a precursor species to green rust (Misawa, 1969).

The reaction mechanism for the formation of β-FeOOH has been discussed in detail by Refait and Genin. Ferrous hydroxychlorides formed initially after the dissolution of a metal, will oxidise to β-$Fe_2(OH)_3Cl$, a product with more chloride ions. This occurs via a metastable phase that has not yet been analysed but exists for only 15 minutes (Refait & Genin, 1997). The β-$Fe_2(OH)_3Cl$ is then oxidised to green rust 1, GR1(Cl^-), $Fe^{II}_3Fe^{III}(OH)_8Cl.nH_2O$, which contains less chloride ions than its parent compound. When the chloride concentration in the solution is high Green rust 1 will then oxidise to another species that Refait and Genin call GR1(Cl^-)*, with the formula $Fe^{II}_{3-x}Fe^{III}_{1+x}(OH)_8Cl_{1+x}$ as shown in the equation (Refait & Genin, 1997):

$$Fe^{II}_3Fe^{III}(OH)_8Cl.nH_2O + xCl^- \rightarrow Fe^{II}_{3-x}Fe^{III}_{1+x}(OH)_8Cl_{1+x} + xe^-$$

It is this precursor species that β-FeOOH forms from in solutions of high chloride concentration and low pH - the localised condition in which marine corrosion often occurs.

So far only post-excavation changes involving already existing corrosion products have been considered But does further corrosion of any remaining metallic core occur when an object is removed from its burial environment? It seems that active corrosion does accompany post-excavation changes, especially in the case of high chloride marine iron exposed to dry, oxidising environments, and it is this that causes objects to collapse and disintegrate.

It has been observed that badly deteriorating objects tend to produce a reddish brown powder in cracks that occur in the existing corrosion products. This has been found to be β–FeOOH, the mineral akaganeite (Zucchi *et al*, 1977), or, as it's formula can also be

given, $ClFe_8O_7(OH)_9$ (Ishikawa & Inouye, 1975). This new corrosion product may be accompanied by a yellow liquid or 'sweat' identified by Knight as a ferric chloride solution (Knight, 1982, 50), but by Turgoose as a solution of Fe^{2+}, Fe^{3+} ions, counterbalanced by Cl^-. The yellow colour is assigned to a thin skin of β–FeOOH forming on the surface of the droplets. The solution has a pH as low as 1(Turgoose, 1982).

An explanation for these observations is that the production of β–FeOOH occurs by the oxidation of Fe^{2+} ions

(In the presence of Cl^-)

$$4Fe^{2+} + O_2 + 6H_2O \rightarrow 4\beta\text{–}FeOOH + 8H^+$$

The Fe^{2+} ions taking part in the reaction may be from the already existing pore solution within the corrosion products that are present before excavation. It seems unlikely however that enough exists to account for the effect seen, and therefore it is more likely that the production of β–FeOOH indicates the instability of the metal and further corrosion occurring.

The ferrous ions produced by the corroding metal core diffuse away from the metal surface and when they meet oxygen diffusing inwards from the atmosphere the above reaction takes place. The solid β–FeOOH formed produces local stresses, causing fractures and cracking of the existing corrosion products. As this internal corrosion proceeds the fracturing also increases and will lead to the eventual break up of the object as illustrated in figure 1.14. The H^+ ions formed in the reaction are the cause of the low pH solution formed. At the lowered pH, iron oxyhydroxide is more soluble and therefore some of the corrosion products dissolve forming a solution of ferric and ferrous ions, the yellow sweat. It is also possible that in these conditions further magnetite will dissolve assisting the disintegration of the object (Turgoose, 1982).

The presence of chloride ions is key to the formation of β-FeOOH and the accompanying disintegration process. Chloride ions participate in the production of the β–FeOOH lattice which is more stable with chloride ions adsorbed within its structure. It is no coincidence that the corrosion products surrounding iron corroded in chloride rich environment (such

as seawater) can contain as much as 80% β-FeOOH (Refait *et al*, 1992, 998) and as expected it is these objects that suffer the worst deterioration.

With no intervention from conservators to reduce chloride levels in corrosion products, deterioration will constantly continue. The β-FeOOH is not a stable corrosion product and in time breaks down forming α-FeOOH and releasing chlorides into the pore solution of the corroding metal. These chloride ions will cause acid hydrolysis of iron salts and the resulting drop in pH will facilitate further corrosion. More β-FeOOH is produced which in time, also decomposes and releases chloride ions. Thus an autocatalytic cycle is set up which will end only when no further iron remains to be corroded.

Figure 1.14 The disintegration of iron artefacts containing chloride ions

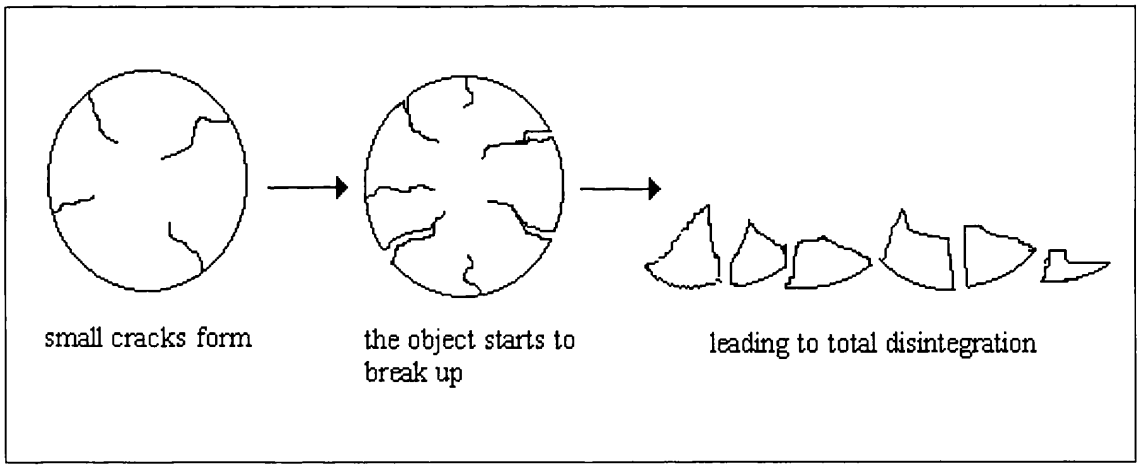

It has also been suggested that chlorides facilitate post excavation corrosion by reducing the relative humidity necessary for corrosion to occur. For corrosion, an aqueous phase is necessary. When in contact with metallic iron the following equilibrium occurs at a relative humidity of 18% (Turgoose, 1989):

$$FeCl_2.4H_2O \rightarrow FeCl_2.2H_2O + 2H_2O$$

Thus, water being released from the iron chloride structure, it is available to act as an electrolyte and facilitate corrosion. A relative humidity of less than 10% has been found to be necessary to prevent this occurring and stabilise iron in the presence of chloride ions (North, 1982).

Only artefacts with metallic cores inside the corrosion product layers would be expected to be unstable and undergo damaging changes in the manner described above. In fact this has been found to be largely true. Research relating the density of objects to their stability has shown object with weight to volume ratios of less than 2.9 are totally mineralised, contain little chloride and are stable at high relative humidity, whilst ironwork with weight to volume ratios of more than 3.1 retain some metal at their cores, have higher chloride content (up to 5000ppm) and are likely to be unstable in conditions favouring corrosion (Watkinson, 1982b).

It is interesting to note that a similar deterioration mechanism has been found to occur with iron meteorites, which contain a lot of highly reduced material and so are unstable (Golden *et al*, 1995). Buchwald *et al* have identified chloride containing akaganeite (β-FeOOH) as the key to the corrosion of meteoric iron as well as ancient corroded iron. They have also identified another chlorine containing corrosion product, the greenish hibbingite, β-$Fe_2(OH)_3Cl$ that is often associated with akaganeite and is found on meteorites and ancient corroded iron (Buchwald & Clarke, 1989, Buchwald & Koch, 1995).

1.5 PROPERTIES OF IRON OXYHYDROXIDES

1.5.1 Iron Oxyhydroxides and Iron Instability

The instability of some excavated iron objects, especially those from a marine environment has been discussed in section 1.4. Further corrosion on exposure to air can lead to the production of β–FeOOH. .Its presence is a strong indication that corrosion is actively proceeding and an object is unstable. But why do excavated objects become unstable in atmospheres in which it might be assumed that iron would be stable? A critical relative humidity of 60% has been quoted for perfectly clean iron and pure water (Scully, 1975), but some archaeological iron objects have been found to corrode at a much lower critical relative humidity. Even after attempts by conservators to stabilise iron objects, further corrosion often occurs.

This question can be answered in part by considering the structure and properties of iron oxyhydroxides, and particularly β–FeOOH. FeOOH is the main constituents of corroded surfaces. α– and γ–FeOOH are found on objects excavated from land, whilst more β–FeOOH is found on objects buried in marine environments, either formed in-situ or on excavation as described in section 1.4. A recent study has shown that up to 80% of the corrosion products on objects from high chloride environments was β-FeOOH (Refait *et al*, 1992). The properties of iron oxyhydroxides are such that further corrosion will be assisted. The surface activities of FeOOH causes adsorption of corrosive agents such as water, chlorides and oxides of sulphur and nitrogen. The electrical conductivity of the oxyhydroxide crystals will also facilitate the corrosion process.

1.5.2 The Structure of β–FeOOH and its' Influence on the Stability of Corroded Iron Objects

1.5.2.1 The crystal structure of akaganeite (β–FeOOH)

Various differing accounts of the crystal structure of β-FeOOH are to be found in the literature, spanning back to initial crystallographic research in 1960. β–FeOOH was found

to have a hollandite ($BaMn_8O_{16}$) or α–MnO_2 structure, a body centred tetragonal unit cell and space group I 4/m, with lattice parameters a = b = 10.48 ± 0.01Å, c = 3.023 ± 0.005Å (Mackay, 1960). The lattice as described by Mackay is illustrated in figure 1.15. Each unit cell contains 8 Fe atoms, and 16 O, and 16 OH. The iron is situated at the centre of an octahedron with oxide and hydroxide ions at the corners.

β-FeOOH is found only to form in the presence of chloride ions (or fluoride ions but this is less common (Ohyabu & Ujihira, 1981)). It is thought that chloride ions play a catalytic role in its formation, which starts with iron/chloride polynuclear species. Chloride ions are then exchanged for hydroxide ions as the species coagulate into colloidal particles. It is unlikely that all the chloride ions are removed which accounts for the presence of chloride ions in the lattice (Dousma *et al*, 1978). The non-stoichiometric chloride ions that are contained within the structure (Mackay detected up to 8%) were postulated to be in the positions that the Ba^{2+} ions take in hollandite, that is, at the centre of the tunnels formed when the octahedrons described above link together. These small 5Å tunnels or micropores in the β–FeOOH structure run parallel to the c-axis. They were thought also to contain water molecules and are important to the properties of the oxyhydroxide.

The crystal structure of β–FeOOH has been described as "cigar shaped" (Paterson & Tait, 1971), 1000 - 5000Å long and 400 - 600Å wide, with square or circular cross sections (Galbraith *et al*, 1979). The crystals are elongated along the c-axis. In electron microscope studies Watson *et al* described these crystals as bundles of rods (Watson *et al*, 1962), each rod being hollow with pores of inner diameter 28.4Å (Gallagher & Phillips, 1969). An illustration of this structure is given in figure 1.16. Further work has called this crystal structure into question. Galbraith *et al* have suggested that the large 30Å pores thought to exist in β-FeOOH crystals were in fact just the effect of the radiation from the electron microscope. This caused decomposition of the oxyhydroxide to γ-Fe_2O_3, leading to striations in the crystals that were wrongly interpreted as pores (Galbraith *et al*, 1979). Support for this idea was given from nitrogen absorption isotherm data collect by Conzalez-Galbet *et al*. They interpreted the pores seen on the electron microscope as interparticular pores and not tunnels within the crystals (Conzalez-Galbet et, 1981).

Figure 1.15 The β-FeOOH lattice shown in projection (Mackay, 1960) and the crystal structure (Ishikawa et al, 1986)

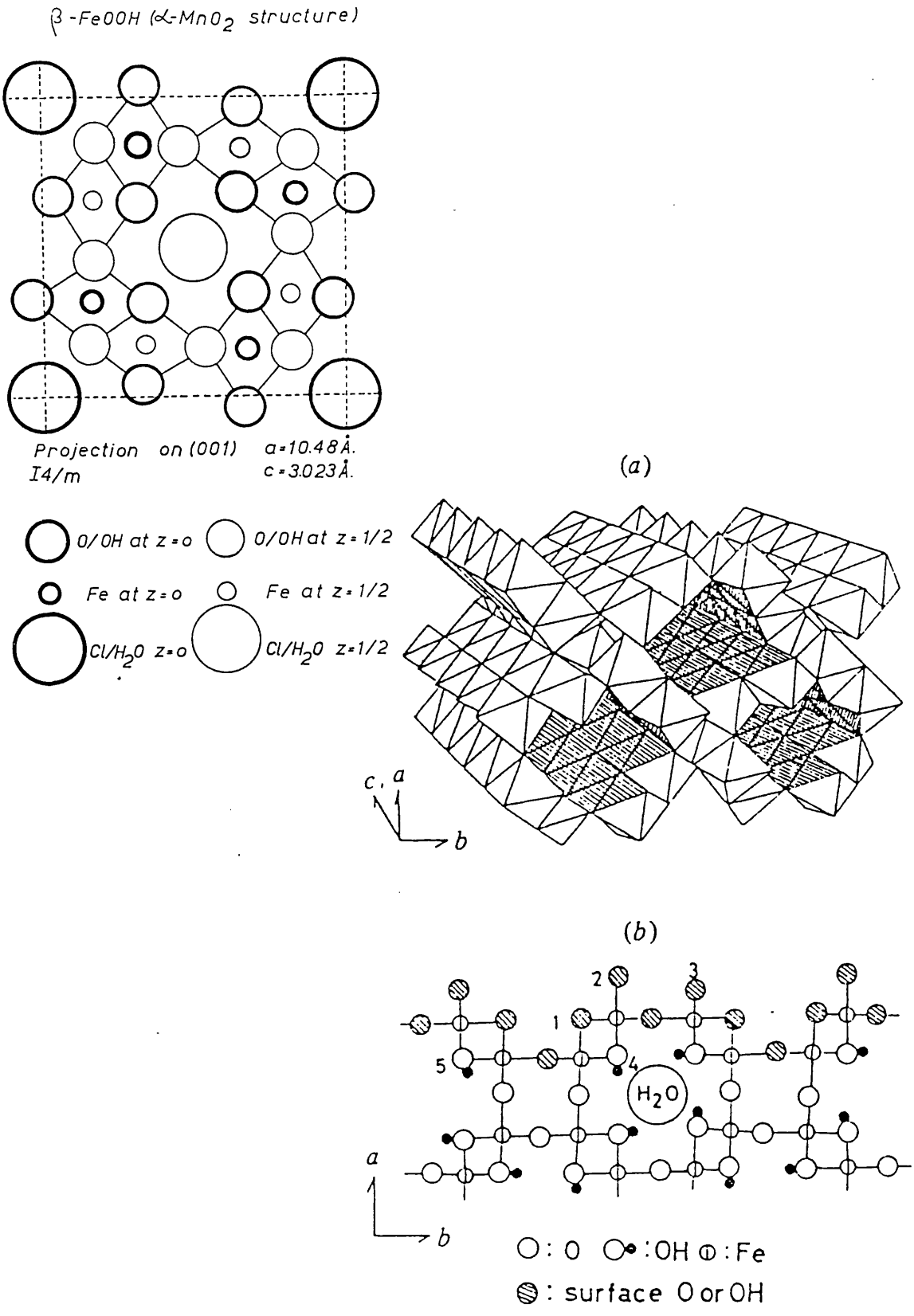

Figure 1.16 Atomic 'superstructure' suggested for β-FeOOH, showing tunnels in the 'cigar' shaped crystal structure and smaller tunnels within the unit cell (Gallagher, 1970)

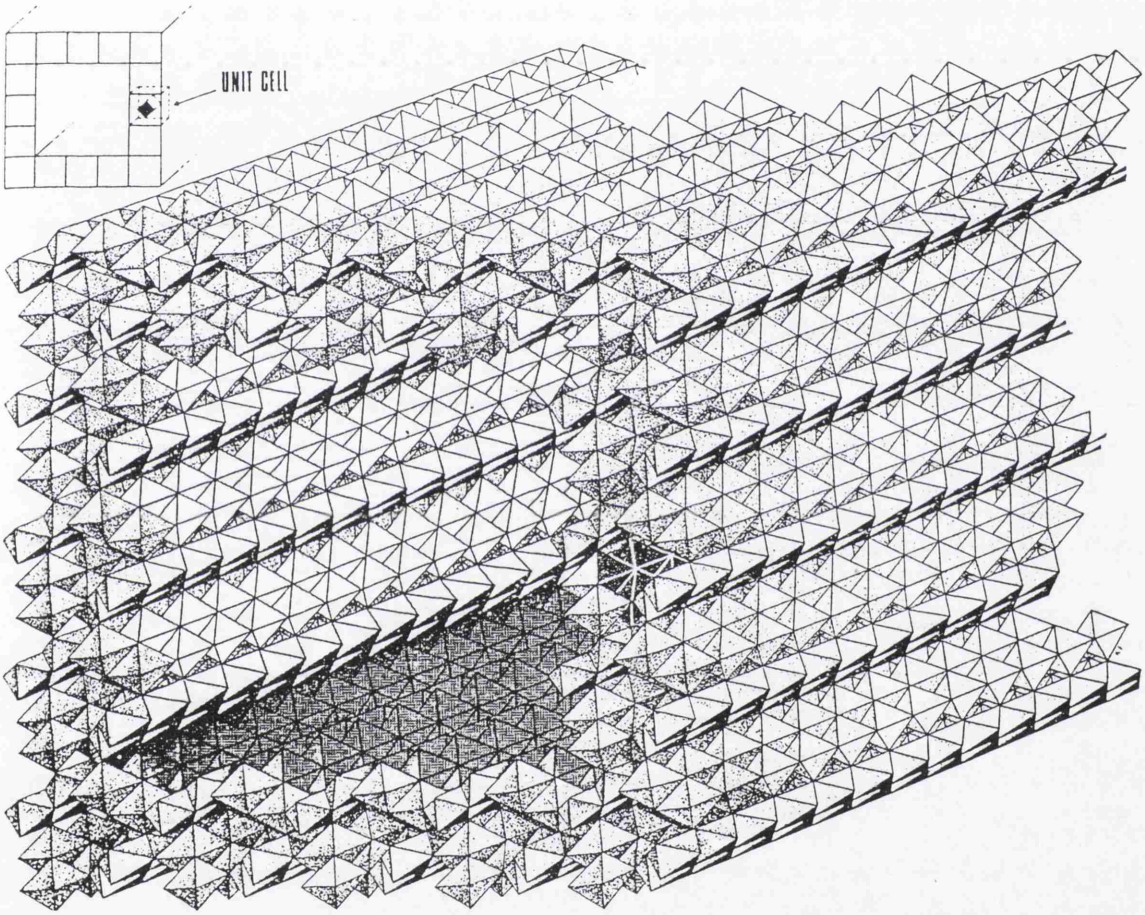

By 1985 further evidence in support of the original structure was presented. Holm believed that the large pores did exist and were stabilised by water molecules. When the compound was dehydrated, as would be the case for examination under an electron microscope, these structures collapsed. However in his experiments, samples were not dehydrated but stabilised first in an agar medium thus preserving the crystal structure. He observed these 'somatoids' as tubes in a solid matrix rather than bundles of hollow rods. His crystals had sides of 800Å with 30Å tunnels (Holm, 1985).

More problems with the actual lattice structure of akaganeite have arisen since the initial structure was assigned by Mackay. A study in 1981 of β-FeOOH formed with chloride or fluoride ions, suggested that these ions occupy the oxide/hydroxide positions (see figure 1.15). Evidence of a two step desorption of fluoride ions, but a one step desorption of chloride ions, suggests that chloride ions can occupy only one of the two different oxide/hydroxide sites, whilst fluoride can occupy either (Ohyabu and Ujihira, 1981). XRD and Mössbauer spectroscopic data were interpreted by Rezel and Genin, in 1990, to demonstrate that chloride ions could not be positioned in the small 4Å tunnels but were in fact substituted in the positions assigned to hydroxide/oxide ions (Rezel & Genin, 1990). They concluded that at least two different iron sites existed and that if the chloride ions were in tunnel sites only one type of iron site would exist. Therefore the chloride ions must be substituted for one of the hydroxide/oxide sites and not in the hollandite tunnels. Another explanation for the two iron sites was given by Childs *et al* in 1980. They believe that the sites arise from the inclusion in the lattice of extra protons to balance the charge on the chloride ions in the tunnels. This would create two types of octahedra $FeO_3(OH)_3$ and $Fe_2(OH)_4$ (Childs *et al*, 1980).

However, a refinement of the powder XRD data by the Rietveld method (Iterative method), for akaganeite formed as a corrosion product on an iron meteorite, reported in 1991, confirmed the original hollandite structure with chloride ions in the small tunnels (Post and Buchwald, 1991). Some of the iron is substituted by nickel in this form of akaganeite. The space group was found to be Monoclinic, with space group I2/m, rather than tetragonal. This would account for the different iron sites found by Rezel and Genin, as the monoclinic unit cell has iron atoms in two structurally different environments (see fig 1.17). A chloride-chloride distance of 3.03Å was calculated, which is less than the 3.3 -

3.4Å that they expected. However the chloride-chloride distance was accounted for by a slight displacement of the chloride ions from the tunnel sites (Post & Buchwald,1991). It is also worth noting that little or no water was found to be present in the small tunnel sites (Post & Buchwald, 1991).

Figure 1.17 Structure of akaganeite with the substitution of Cl^- ions for OH^- ions, showing the iron sites A1, A2, A3.

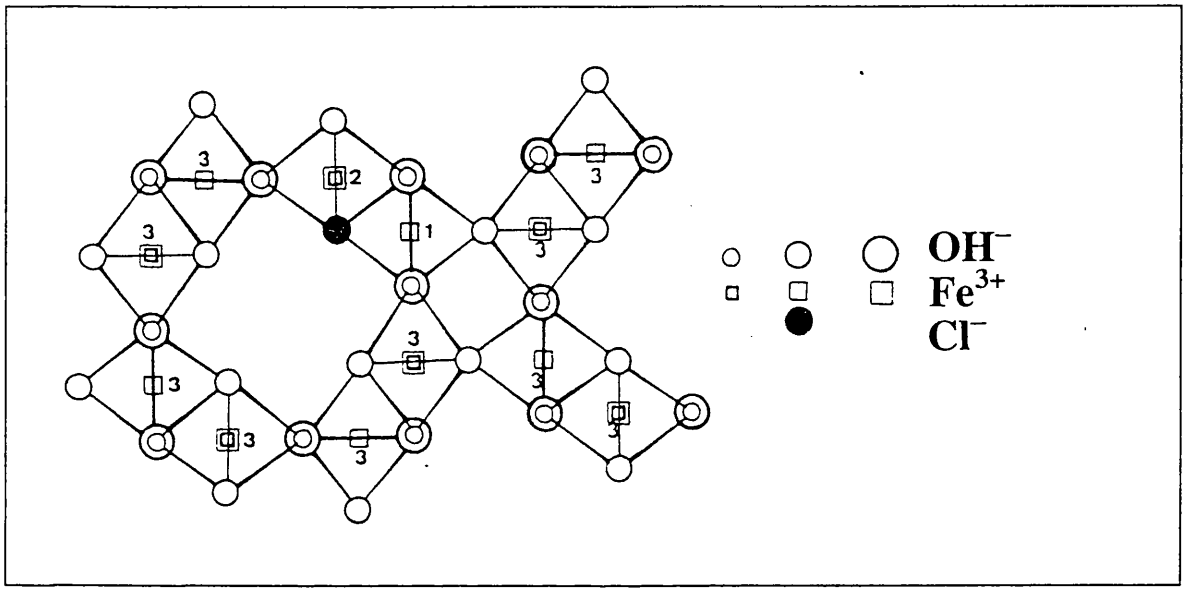

There does not seem to be any conclusive body of opinion on which structure is more accurate at the present time. There seems to be no conclusive evidence for the existence of the large 30Å pores, however their existence can not be ruled out all together.

1.5.2.2 Chloride ions in β–FeOOH.

β–FeOOH as a corrosion product normally forms with a chloride content of between 20-30% by weight (Feitnecht, 1950). Even after washing with water a residual chloride content of 8-10% has been reported (Kaneko & Inouye, 1974), indicating that some of the chloride ions present are more strongly bound to the β–FeOOH lattice. From the structural evidence already presented it seems likely that chlorides exist in lattice oxide/hydroxide sites as well as in some of the hollandite tunnel sites . This would fit with the evidence on the mechanism by which akaganeite is formed (Dousma *et al*, 1978). As iron/chloride polynuclear species are involved in the preliminary stages of the structures formation some chloride ions will remain in lattice sites in the final crystal structure. However the chlorides

that are expelled and replaced by oxide/hydroxide ions, may become trapped in the hollandite tunnels as the lattice forms around them.

When discussing chlorides present in β-FeOOH as a corrosion product we can consider them in two ways, those that are 'soluble', that is, can be washed out of the corrosion product, and those that are 'insoluble', meaning those that can not be removed by washing and will not be removed unless the β-FeOOH lattice breaks down. The positions of these two types of chlorides within the corrosion products can be classified as follows:

Soluble chlorides - chlorides in the aqueous pore solution surrounding β–FeOOH, physisorped onto the oxyhydroxide surfaces or in the large 30Å tunnel if we are to accept their existence.

Insoluble chlorides - chlorides chemisorbed onto surfaces and trapped within the 5Å tunnels of the β–FeOOH crystal lattice. If we are to accept the Rezel and Genin interpretation of the akaganeite structure these chlorides would be the ones that are part of the β-FeOOH lattice, in sites normally occupied by hydroxide ions (Rezel & Genin, 1990).

Chemical and crystallographic studies have shown the true formula of synthetic β–FeOOH to be a mixture of $(OH)_2Fe_8(O,OH)_{16}$ and $Cl_2Fe_8(O,OH)_{16}$ crystals (Keller, 1970). These insoluble chlorides are likely to be the cause of instability in excavated iron even after conservation treatments. Conservators can remove the soluble chlorides by washing (North & Pearson, 1978, Scott & Seely, 1987, Aoki *et al*, 1989), however the chlorides bound within the tunnels can not be removed in this way. Problems then occur with the decomposition of β–FeOOH in time. β–FeOOH is relatively unstable - it can exist for between several months and twenty five years (Evans, 1969). But when β–FeOOH converts to α–FeOOH it releases the previously insoluble chloride ions:

$$\beta\text{–FeO(OH,Cl)} + H_2O \rightarrow \alpha\text{–FeO(OH)} + HCl$$

This release of chloride into the pore solution of the corrosion products causes fresh corrosion, even at low relative humidity. The chloride ion combines with any ferrous ions present causing hydrolysis and therefore decreases the pH of the pore solution. This facilitates further cycles of corrosion and thus previously stable objects can start to re-corrode until completely mineralised.

1.5.3 The Influence of the Structure and Surfaces of FeOOH Crystals on the Stability of Iron Objects

1.5.3.1 Crystal structure of geothite (α-FeOOH)

Geothite crystals have an orthorhombic unit cell, with lattice parameters a = 4.60Å, b = 10.0Å and c = 3.03Å. The structure has tunnels parallel to the c-axis containing two rows of $[O\text{-}H\text{-}H]^{3-}$, hydrogen bonded groups. The ferric ions are at the centre of oxygen octahedra, each oxygen being shared by three octahedra (Oosterhout, 1960). Two morphologies of α-FeOOH crystals have been found (Cornell, 1983, Atlanson, 1968), acicular and twin crystals. Acicular crystals are needle-like and elongated in the c-axis direction, whilst twin crystals exist in varying forms including six armed stars. The crystal lattice is illustrated in figure 1.18.

1.5.3.2 Crystal Structure of lepidocrocite (γ-FeOOH)

The crystal structure of the γ phase of iron oxyhydroxide is orthorhombic, with lattice parameters a = 3.87Å, b = 12.51Å, and c = 3.06Å (Ewing, 1935). The structure consists of iron centred oxygen octahedron iron-oxygen bonds of about 2.00Å, and an oxygen-oxygen distance of 2.70Å. Figure 1.19 illustrates the layered nature of the structure. The hydroxyl groups on the outer surfaces hydrogen bond, to hold the layers together. The lattice can be described as octahedra, sharing edges in such a way that the oxygen atoms near the middle of the layers are distorted, and therefore compressed on the interior of the layers.

Figure 1.18 Crystal structure of α-FeOOH (Ishikawa et al, 1986)

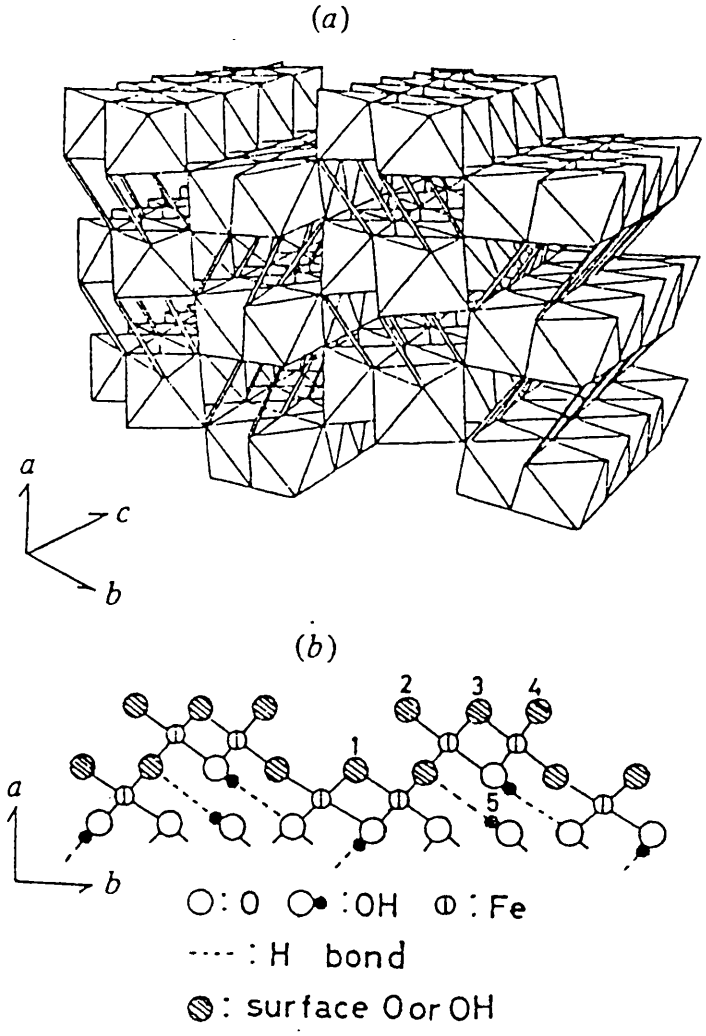

Figure 1.19 Crystal structure of γ-FeOOH (Ishikawa et al, 1986)

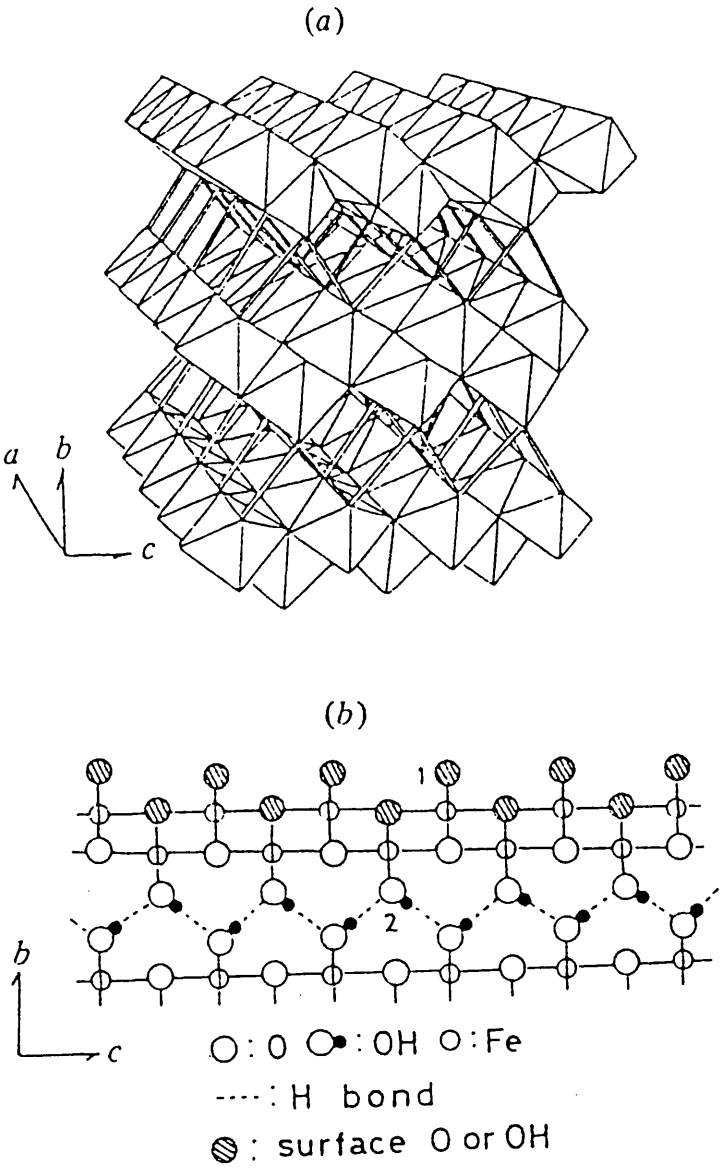

1.5.3.3 Colloidal iron oxyhydroxide crystals in corrosion products

FeOOH in corrosion products often gives diffuse X-ray diffraction peaks. This is indicative of small crystals - less than 500Å in size. The small crystals are aggregated with other iron oxides such as magnetite and amorphous oxyhydroxides (Inoue *et al*, 1986). These aggregates have macropores (>500Å), mesopores (20-500Å) and micropores (<20Å) (Naono & Fujiwara, 1980, Naono & Nakai, 1989). They can therefore be regarded as colloids (Kaneko, 1989a) combined to each other by non-chemical bonding, with large surface areas. Hence particular attention should be paid to the surface chemistry of the FeOOH crystals.

1.5.3.4 Surface structure of iron oxyhydroxides

Each crystal structure of FeOOH has a predominant crystal face. For α-FeOOH it is the bc plane, for β-FeOOH the bc and ac planes and for γ-FeOOH the ac plane. The predominant crystal faces occupy more than 95% of the total surface area (Cornell, 1983) and therefore the surface structure of the oxyhydroxides can be approximated by the structure of the predominant crystal face. The properties and reactivity of all phases of FeOOH are governed by those of the predominant crystal face, and in particular the local geometry of oxide and hydroxide ions on the surface (Ishikawa *et al*, 1986, Matsumoto & Kaneko, 1989).

The surfaces have arrays of oxygen and hydroxyl ions. α-FeOOH has two kinds of hydroxyl ions, those inside and those outside the grooves along the c-axis of the lattice. β-FeOOH has hydroxyl groups situated in two kinds of concaves, narrow and wide ones, however the tunnels parallel to the c-axis make up an inner surface amounting to 70% of the outer surface area. The γ-FeOOH structure includes surface hydroxyls at ridges parallel to the c-axis, with oxygen atoms placed beneath shallow valleys. The hydroxyl groups are shown on fig 1.20.

Figure 1.20 Crystal shapes and structures of FeOOH crystals. Solid circles denote surface hydroxyls on the predominant faces (Kaneko, 1989a)

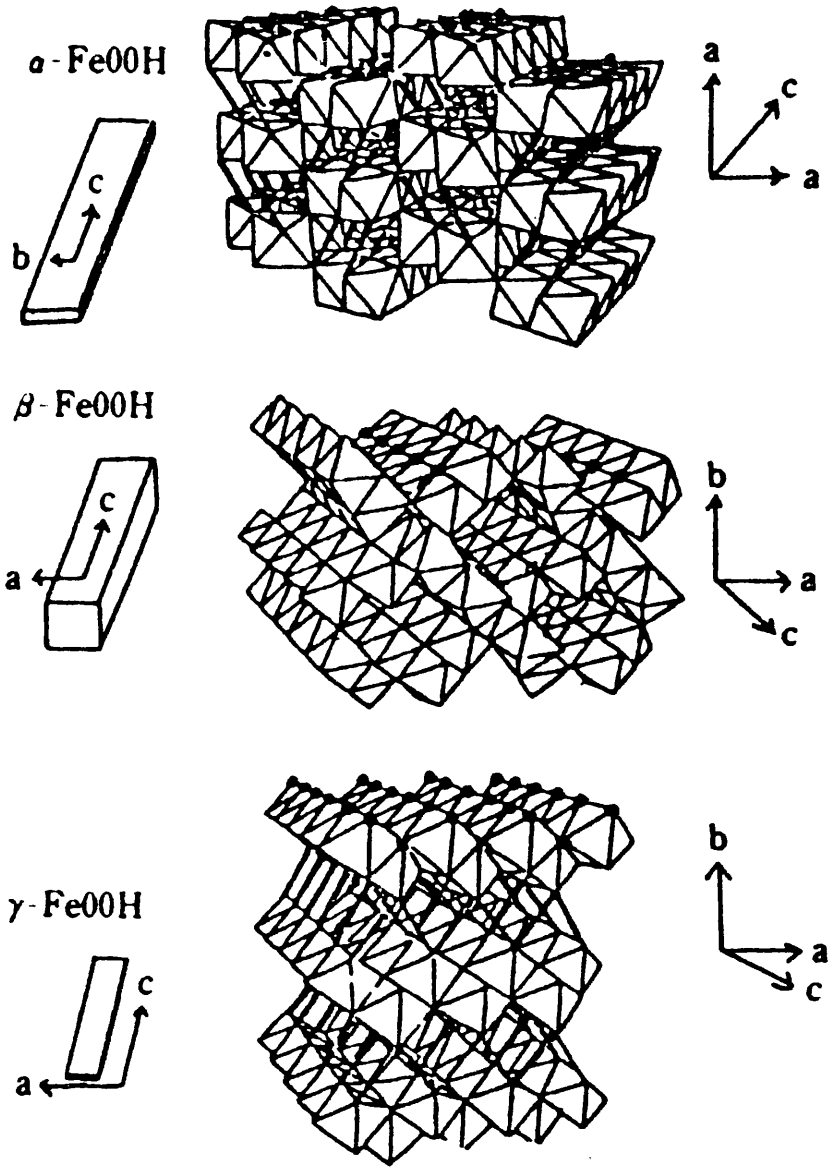

1.5.4 Ion Exchange Properties

Corrosive ions such as chlorides and sulphates, when present in aqueous solution, will be adsorbed onto the surfaces of iron oxyhydroxides. This highly absorptive nature and the large specific surface area, leads to the promotion of corrosion of any metal within iron oxyhydroxide corrosion products. The study of adsorption properties of corrosion products is therefore essential to any study of corrosion prevention (Batrakov *et al*, 1994).

α-FeOOH and γ-FeOOH are pseudo amphoteric, exhibiting anion exchange in acid and cation exchange in basic solution (Atkinson, 1968). Cationic uptake occurs by the following mechanism. In the presence of excess base the surface OH groups are deprotonated. An excess negative charge therefore builds up on the surface and is counterbalanced by the uptake of an equivalent counter cation (Paterson and Rahman, 1984). Barred species represent atoms bound to the oxyhydroxide matrix.

$$\overline{\mathbf{FeOOH}} + \mathbf{X^+}_{(aq)} \Leftrightarrow \overline{\mathbf{FeOO^-}} + \mathbf{X^+} + \mathbf{H_2O}$$

A ligand exchange of hydroxyl for water has also been proposed as an initial step (Paterson and Rahman, 1984):

$$\overline{\mathbf{Fe-OH_2}} + \mathbf{X^+}_{(aq)} + \mathbf{OH^-}_{(aq)} \Leftrightarrow \overline{\mathbf{Fe-OH^-}} + \overline{\mathbf{X^+}} + \mathbf{H_2O}$$

By the uptake of cations the equilibrium will be displaced increasing the cation capacity of the aqueous solution and removing OH^- ions will reduce the pH and thus facilitate further corrosion.

Anions such as chloride and sulphate have a strong affinity to the α-FeOOH surface. Sulphate ions are assumed to be absorbed by ligand exchange with two hydroxyl groups creating a bridging binuclear complex $FeOS(O_2)OFe$ (Parfitt & Smart, 1977):

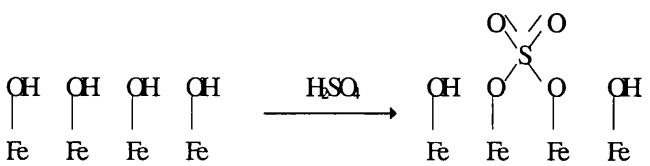

It has been suggested that other anions containing residual hydroxyl groups, (such as inorganic molecules with un-ionized acid groups or organic molecules with hydroxyl functionality), may be adsorbed on the oxyhydroxide surface by a mechanism involving hydrogen bonding to surface oxide ions (Morrison, 1984).

α and γ-FeOOH can absorb 100-200 μmole/gram of chloride at pH 6.5-7.5 (Yates *et al*, 1975). Cl^- are absorbed by two mechanisms, ligand exchange with surface hydroxyls or adsorption through electrostatic forces (which account for a high percentage of the total chloride ions adsorbed). A pore protonation mechanism was suggested (Paterson & Rahman, 1984).

$$\overline{FeOOH} + H^+_{(aq)} + Cl^-_{(aq)} \Leftrightarrow \overline{FeOOH_2^+} + \overline{Cl^-}$$

The first step is the protonation of an existing hydroxyl group on the crystal surface, followed by Cl^- uptake as counter ion. Maximum adsorption of chloride occurs at low pH.

β-FeOOH shows different behaviour - it has a selective anionic exchange capacity in acidic media but no cationic exchange properties (Kanungo, 1994). Studies have shown that OH^- ions on the β-FeOOH surface are not hydrogen bonded to other oxygen atoms present, due to the atomic orbital arrangements (Gallagher & Phillips, 1969). This therefore leads to an unusually reactive surface. Anion exchange in β-FeOOH is governed by the solution pH, the anion concentration and the anion size. β-FeOOH can therefore selectively uptake Cl^- and F^- into the hollandite tunnels but excludes larger species such as I^- and Br^- (Paterson & Smith, 1988). A "pore protonation mechanism" has been proposed for anion uptake (Paterson & Rahman, 1983). A positive site is created on the crystal pore or tunnel walls by protonation of a hydroxyl group:

$$\overline{FeOOH} + \overline{H^+} \Leftrightarrow \overline{FeO(OH_2)^+}$$

The bars represent species within the hollandite 5Å tunnels rather than just species absorbed on the external surface as described for the α and γ-FeOOH adsorption mechanisms. The pore protons are in equilibrium with those in the external solution:

$$\overline{H^+} \Leftrightarrow H^+$$

A counter anion must also enter the pore to balance the charge:

$$\overline{X^-} \Leftrightarrow X^-$$

β-FeOOH tunnels will only allow small ions such as Cl^- and F^- to enter (Ellis, 1976). So the result is the uptake of HCl (or HF) giving overall:

$$FeOOH + H^+ + X^- \Leftrightarrow FeO(OH_2)^+ X^-$$

These ion exchange properties allow the adsorption of corrosive ions onto corrosion products. Their presence will hinder the stabilisation of archaeological iron artefacts.

1.5.5 Adsorption Properties of FeOOH in Atmospheric Environments

The water adsorption properties of corrosion products determines the possibility of the presence of what has been called 'superficial wetness' (Corvo *et al*, 1997), This means the presence of an adsorbed water layer which will occur at the critical relative humidity and will allow further corrosion. Vapours and gases such as H_2O, SO_2 and nitrogen oxides also have an affinity to iron oxyhydroxide surfaces. They can be bound by chemical bonds - chemisorption, or held with weaker (although longer range) Van der Waals interactions - physisorption. The adsorption of these gases will accelerate the corrosion process.

NO chemisorbs onto the FeOOH surface. Electron transfer from the FeOOH to the NO molecules occurs. The NO adsorbs onto the oxygen atom of the α and β-FeOOH phases and the hydroxyl ions of γ-FeOOH (Kaneko & Inouye, 1987). Oxygen vacancies in the lattice also create sites for NO adsorption in α and β-FeOOH (Kaneko & Inouye, 1976). NO can also bind within the open tunnels in β-FeOOH.

SO_2 is also chemisorped onto FeOOH crystals (Kaneko *et al*, 1977) with electron transfer from the surface to the SO_2 molecules for the α and β phases but from the OH group for the γ-FeOOH phase (The hydroxide proton will hop onto the adjacent hydroxyl making OH_2 as the SO_2 adsorbs onto the oxygen). Adsorption of SO_2 (as well as NO) at oxygen vacancies also occurs and is often stronger at these sites (Kaneko & Inouye, 1984). Electron donation leads to the formation of SO_2^- or ($O\text{-}SO_2$). This then reacts with surface oxygen creating SO_3^{2-}. Infra-red studies have shown a gradual transformation from SO_2 to SO_3^{2-} and SO_4^{2-} (Matsumoto & Kaneko, 1989) creating H_2SO_4 on reaction with water. The presence of sulphuric acid will greatly accelerate corrosion.

Water vapour also exhibits an affinity for FeOOH surfaces (Clarke & Hall, 1991). Iron oxyhyroxides can be classed as a hydroscopic material. Water molecules can be chemisorped onto the surface by a dissociate mechanism, forming two hydroxyl groups, the OH^- adsorbed onto the surface ferric ions whilst the H^+ forms a second hydroxyl group with an adjacent O^{2-} ion. This process will enhance the electrical conductivity of FeOOH, as the water donates an electron to the ferric ion (Kaneko & Inouye, 1979). Further layers of physisorped water are also present on FeOOH surfaces. The first phisisorped layer is localised by hydrogen bonding (Zettlemoyer *et al*, 1966) becoming immobile. The primary physisorption sites for α and γ-FeOOH are hydroxyl groups whereas those on β-FeOOH are surface hydroxyl groups and tunnel sites. On α-FeOOH two types of hydroxyl group exist. A mechanism in which a water molecule is adsorbed onto each with a third water in a position between the two has been suggested (Kaneko *et al*, 1975). γ-FeOOH has only one type of surface hydroxyl so that each water molecule is localised between two of these giving 50% coverage. On β-FeOOH water molecules are absorbed into vacant tunnel sites. After the tunnels are filled up water is bound to two hydroxyl groups on the outer surface (Kaneko & Inouye, 1979). Subsequent physisorbed water layers are also present. These are mobile. The first 2-3 layers form 'ice-like' structures. Further layers have a more dissociated 'liquid-like' structure (Kaneko & Inouye, 1979).

CO_2 is also strongly adsorbed on moist FeOOH surfaces (Lumsdon & Evans, 1993). It adsorbs on oxide sites of α-FeOOH in the channels or grooves on the crystal surface:

$\equiv Fe\text{-}OH_2 + CO_2 \rightarrow \equiv Fe\text{-}O\text{-}CO_2^{2-} + 2H^+$ or $\equiv Fe\text{-}OH_2 + CO_2 \rightarrow \equiv Fe\text{-}OH_2H^- + H^+$

The adsorption of gases onto iron oxyhydroxide will mean that a constant supply of corrosive species will be present within the corrosion products if stored in polluted environments, even after initial conservation treatments.

1.5.6 Electrical Properties of Iron Oxyhydroxides

In the corrosion processes taking place on iron artefacts the cathode and anode are often spatially separated. Electrical current will therefore need to flow between the two. For this reason the electrical conductivity of corrosion products is of significance. The three phases of FeOOH are all found to be semiconducting (Kaneko & Inouye, 1973). Their electrical

conductivity increases steeply with temperature (Kaneko & Inouye, 1976). The alternating current electrical conductivity was found to be frequency dependent, increasing with frequency (Kaneko & Inouye, 1974). This was attributed to an "electron hopping" process occurring between Fe^{2+} and Fe^{3+} species in the FeOOH lattice.

Most FeOOH is non-stoichiometric. It's formula could be written $Fe^{2+}_{3\delta}Fe^{3+}_{1-2\delta}OOH$, where $\delta << 1$ (0.1-1% Fe^{2+} is present). Fe^{2+} ions have 6 d electrons whilst Fe^{3+} have only 5. The 6th d electron in the ferrous ion is able to hop into the d shell of the Fe^{3+} if the two are adjacent. The iron in the oxyhydroxide can be considered to be surrounded by octahedral ligands as the d-electrons are localised due to distortions of the lattice. The Fe-Fe distance is about 3Å. The d shells are therefore split into t_{2g} and e_g energy levels. The t_{2g} orbitals will have a small contribution from the oxygen 2p orbital and the t_{2g} will have a small contribution from the oxygen sp hybridised orbitals (Ballhausen & Gray, 1965). A slight overlapping of the Fe^{2+} and Fe^{3+} t_{2g} orbitals allow electron hopping to occur. The spin state must remain the same before and after hopping (Yamashika, 1960).

Figure 1.21 Electron configuration of d electrons hopping from Fe^{2+} to Fe^{3+}

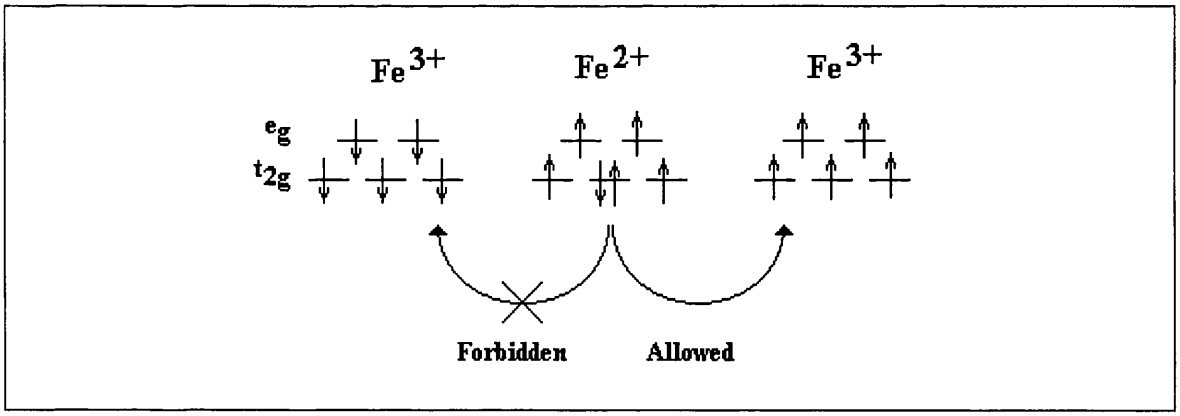

The electron hopping provides a pathway for electrical charge and explains the semiconducting properties of FeOOH (and Fe_3O_4, magnetite, which is a mixed Fe^{2+}/Fe^{3+} oxide). The electrical conductivity of iron oxyhydroxide means that rather than being an insulating layer, the oxide allows the corrosion process to continue (although obviously at a reduced rate as compared to bare, uncorroded iron). The introduction of dopants into the oxides, such as Cu^{2+} ions (which may be present in archaeological iron or the burial environment) will enhance the conductivity further (Kaneko *et al*, 1989b).

1.6 DESALINATION AND CONSERVATION OF ARCHAEOLOGICAL IRON

1.6.1 Introduction

It is possible to prevent the occurrence of the post-excavation changes to some degree. If stabilising desalination treatments are carried out immediately after excavation, then further corrosion may be avoided. If the production of the β-FeOOH phase can be stopped, the formation of the damaging catalytic corrosion cycles can be prevented. It is obviously not always possible to perform desalination treatments on-site, and so methods of 'passive' conservation must be employed. These pertain to storage and environmental control. Cronyn states that "until shown otherwise, if must be assumed that all excavated ironwork is unstable" (Cronyn, 1990, 198) and so post excavation changes must be prevented by considering the environment of storage.

Desiccation is the main method used for iron from land sites. This is usually carried out using silica gel, but dehumidifiers are also used. A relative humidity of under 20% has been quoted as a safe storage environment (Turgoose, 1982) however this is lower than the relative humidity often employed for dessicated storgae. Desiccation using solvents or freezing has also been suggested. Objects have also been stored wet in sealed containers to reduce oxygen supplies. Repackaging in soil to replicate the original burial environment has been suggested (Knight, 1982, 50). Turgoose favoured wet anoxic storage (Turgoose, 1982). Storage in sodium hydroxide is widely used, but it is debatable as to whether this can be described as a passive treatment as changes in the corrosion products do occur (Hjelm-Hansen *et al*, 1993). It can be seen that there is little overall agreement as to the best course of action. The main themes are however the removal of water and oxygen to prevent further corrosion. Storage in an inert nitrogen environment would be ideal but is considered too expensive to maintain.

It is even more essential to stabilise the more problematic marine iron immediately. Concretions should be removed and desalination carried out as soon as possible. However wet storage in the presence of corrosion inhibitors is the favoured passive conservation treatment. Alkaline potassium chromate solutions are successful as they help a passive iron

oxide film form on the remaining metal surface. Its toxicity makes its use unpopular however. Sodium hydroxide solution (pH 10-13) has been used to provide a passivating storage environment (Pearson, 1977).

Active conservation techniques are necessary so that objects can be removed from storage for study, radiography or display. Even if the above precautions are followed, when removed from storage environments, objects can become unstable once more (if they ever were stable). We must also consider the vast archive of material previously treated with unsuccessful conservation treatments. These objects often start to disintegrate after relatively short times, producing the β-FeOOH characteristic of chloride containing corrosion products.

The first stage in the conservation process of iron is often radiography followed by the investigative cleaning of an object. This is a time consuming task. Investigative cleaning is usually carried out using small tools or air abrasion. Objects are continously examined during the cleaning process to try and find the original surface or shape of the artefact or identify evidence preserved in corrosion products. The original surface is often well preserved for cast iron, however the situation is rarely as straightforward for extensively corroded wrought iron. The original surface may sometimes be found due to the presence of inlays or evidence of plating, however pitting corrosion means that the original surface will always be disorted to some extent. It is sometimes argued that differences in the colour and density of corrosion product layers can be used to identify the original surface. The boundary between the inner denser corrosion products and outer bulky layer that incorporate grains of sand and other extraneous materials may be the original surface, although it is not confirmed if this is related to a change in the chemical nature of the corrosion products (Cronyn, 1996).

North and Pearson have defined the ideal conservation method as one that "should be able to preserve...the shape and surface markings, the chemical composition of the metal and the metallurgical structure of the metal...and in addition should do so quickly, simply and cheaply." (North & Pearson, 1975).

In the field of archaeological conservation not only the technical practicalities, but also the ethics of conservation must be considered. The two main principles when selecting a conservation treatment are the reversibility of a procedure, and the minimum intervention necessary to stabilise the object. Cronyn points out, "it is realised that no treatment is in the strictest sense 'reversible' but the most important criterion is that the conservator should interfere minimally with the true nature of an artefact" (Cronyn, 1990, 9).

The reversibility of a treatment is crucial so that it may be removed if later found to be damaging. Obviously this may not always be possible, but it should always be a consideration. The ethic of minimum intervention allows for necessary treatments to be performed, so that objects do not disintegrate, whilst trying to interfere as little as possible with any archaeological (including archaeometallurgical) evidence.

1.6.2 Methods Involving Washing

The removal of corrosive chloride anions is the key to all active conservation treatments that aim to stabilise archaeological iron. In comparative studies it has been found that the most effective treatments are those that remove the greatest quantity of chloride (Keene, 1994, 259). The most widely used method is to wash the object in the hope that the chlorides will dissolve out into the wash solution. The rate of chloride removal is a diffusion controlled process (North & Pearson, 1978). In most cases the amount of chloride in the wash solution will be monitored using silver nitrate titration or conductivity measurements. The wash solutions are regularly changed and the washing process is continued until no further chloride ions can be removed. A variety of solvents and methodologies have been used, some of which will be discussed in this section.

1.6.2.1 Washing in aqueous media

Washing in hot distilled water was the standard method for desalination of archaeological iron in the past (Plenderleith & Werner, 1971). Lengthy washing is necessary to remove the maximum amount of chloride ions possible (Eichhorn, 1975). There can be problems with aqueous immersion in oxygenated environments for long periods of time however, as this provides the perfect environment for further corrosion of the object. Only 'soluble'

chlorides will be removed by this method. Chloride ions remain in corrosion products and can cause further corrosion at a later stage. The boiling of objects has also been questioned in terms of the effect of the high temperature on metallurgical structures. It was found that slight changes in the grain size and hardness of martensitic steel did occur when boiled for 20 hours (Ehrenreich, 1987).

1.6.2.2 Soxhlet apparatus

This variation on aqueous washing has been suggested for fragile iron objects that might disintegrate if stronger chemical reducing solutions were used (Scott & Seely, 1987). The main advantage over normal hot washing with distilled water is that the system is completely enclosed. Air in the system is replaced with an inert gas such as nitrogen so oxidation can not occur whilst corrosive anions are washed away. This minimises the danger of further corrosion. Figure 1.22 illustrates the Soxhlet apparatus.

Distilled water heated in the flask, vaporises rising upwards until contact with the reflux condenser causes it to condense and fall back into the soxhlet container, where the iron objects are placed. When the freshly distilled water reaches the level of the siphon, the water returns to the flask, and then is reboiled starting a second cycle. In this way the apparatus can be left to run for several hours unattended. A cycle can take 3 hours with a 2 litre soxhlet container and 5 litre flask. 10 to 15 washing cycles are needed for removal of most of the water soluble chlorides. Small samples of wash water can be removed using the stopcock to monitor the chloride concentration. Washing with the soxhlet apparatus can be used as a treatment on its own, or along with other treatments such as alkaline reduction. 50%-80% of chlorides can be removed using this method, but even with prolonged treatment all the chlorides are not removed (Aoki *et al*, 1989)

1.6.2.3 Other aqueous washing treatments

Other aqueous treatments have been used in the conservation of archaeological iron. Desalination using dilute sodium sesquicarbonate was undertaken as far back as 1921 (Scott, 1921) but more recent trials have found it to have a low success rate and it is therefore rarely used (Oddy, 1987, 155).

Figure 1.22 Soxhlet apparatus used for washing iron under nitrogen (Scott & Seely, 1987)

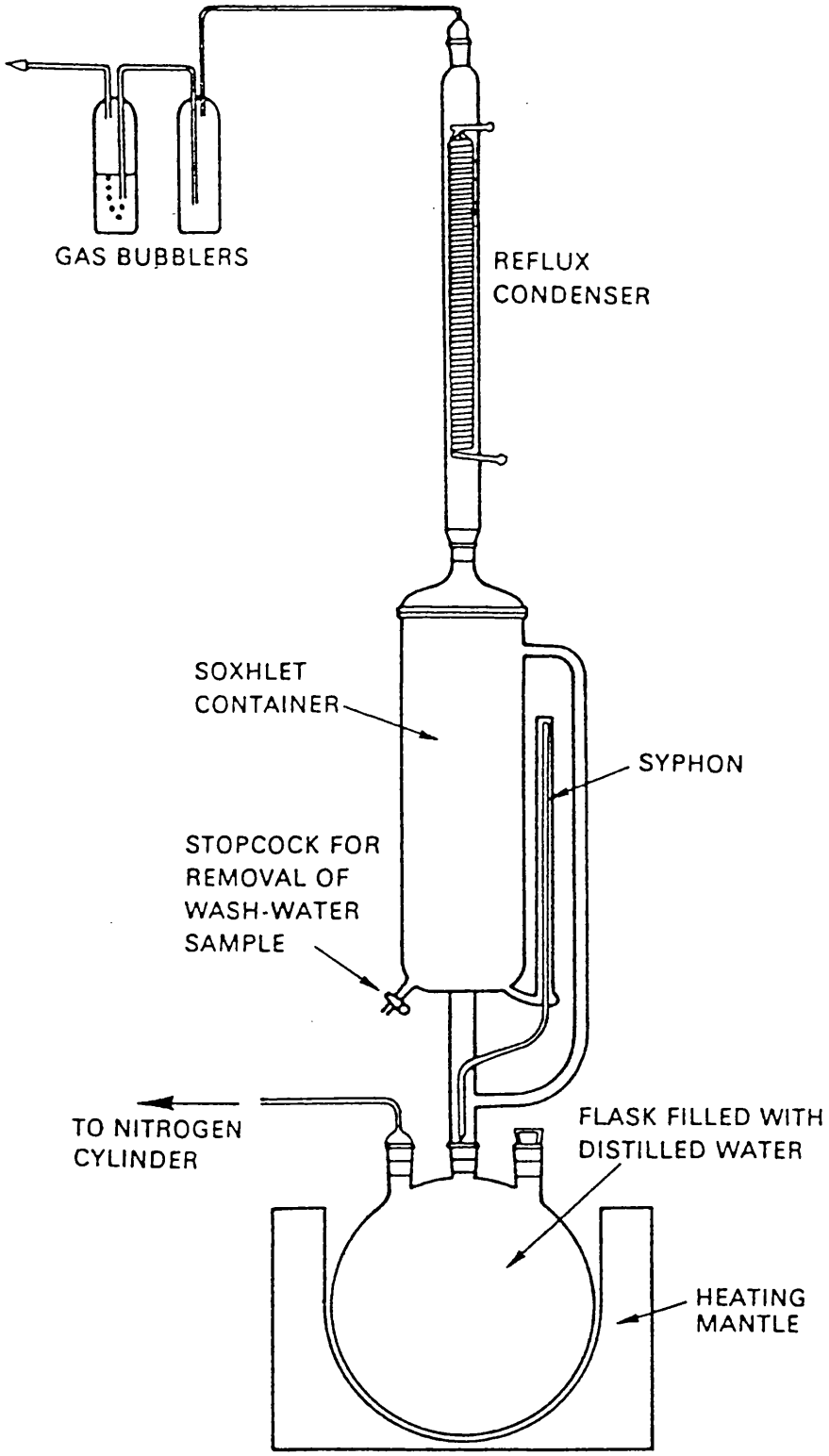

A treatment using an aqueous solution of ethylene diamine was devised by Argo (Argo, 1992). The iron was suspended over boiling aqueous 20% ethylene diamine, the solution being changed daily, or immersed in 5% ethylene diamine solution heated to 50°C during the day and cooled overnight. Finally the iron was washed with hot deionised water to remove any excess ethylene diamine. In tests the treatment was found to be relatively successful with only 3.5% of those treated being unstable (Selwyn & Logan, 1993).

The most common aqueous solution used for treatment and storage of iron artefacts is sodium hydroxide (Rinuy & Schweizer, 1982). In the basic hydroxide medium iron is passive (this can be seen from the Pourbaix diagram in fig 1.10). It is therefore hoped that in sodium hydroxide solution the iron will not corrode any further. It is thought that some OH^- ions will exchange with chloride ions within corrosion products pores and therefore facilitate desalination.

The effectiveness of any desalination method is partly due to the fact that corrosion is not occurring during washing and therefore chloride ions are not being attracted to the anodic surface and can be released (North & Pearson, 1978). The effectiveness of sodium hydroxide in this respect has been questioned (Turgoose, 1985a, 1982). The inhibitive properties of sodium hydroxide require the iron to be clean thus allowing a 'passive film' to form. Inhibition will only occur when OH^- ions have had time to diffuse to the metal surface and so further corrosion may occur until this time. Electrochemical measurements have shown the development of protection with time in sodium hydroxide solution (Hjelm-Hansen *et al*, 1993). The high pH will also affect the stability of existing corrosion products. They often oxidise to green rust in basic solution (North, 1982). These changes may however actually help in the desalination process. The changes result in porosity within the corrosion layers and this will facilitate the diffusion of chlorides (Hjelm-Hansen *et al*, 1993).

1.6.2.4 Non aqueous washing

Aqueous washing media have the problem of encouraging further corrosion when used for prolonged times. Therefore water free solvents have been experimented with. Gilberg & Seely used liquid anhydrous ammonia followed by washing with water in an inert atmosphere soxhlet apparatus (Gilberg & Seely, 1982a). The procedure must be carried

out at -33°C or at room temperature but increased pressure (300 atmospheres). It was suggested that this method removed chlorides by breaking down corrosion products and forming ammonium chloride which was then washed out of the corrosion products. Although no chloride ions were detected in the outer corrosion layers recorrosion did occur in some cases, indicating that chlorides were still present in the inner corrosion layers (Gilbert and Seely, 1982a). Duncan experimented with the use of ethylene oxide under vacuum. Chlorides would be converted into ethylene chlorohydrin which will vaporise and be removed under vacuum.

$$CH_2OCH_2 + Cl^- + H^+ \rightarrow CH_2ClCH_2OH$$

This method removed 33% of chlorides (Duncan, 1986). Anhydrous methanol was used in a soxhlet extractor (Bleck, 1978) giving a high rate of chloride removal but was less efficient than aqueous treatments. The problem with all these methods is the toxicity of the solutions used making the treatments unattractive and impractical for many conservation laboratories.

Washing with lithium hydroxide in alcoholic solution has also been tested as a desalination method. It was first proposed by Bresle (1974) and used on archaeological iron work by Fabech & Trier (1978). As with sodium hydroxide, the treatment attempts to exchange Cl^- ions in the corrosion products for OH^- and then wash out the lithium chloride produced:

$$LiOH + Cl^- \rightarrow LiCl + OH^-$$

In addition excess lithium hydroxide could react with atmospheric carbon dioxide to produce a $FeCO_3$ protective layer on the iron work surface. However in recent experimental work this treatment has been found to be ineffective. Less chloride ions were removed than with aqueous washing or sodium hydroxide treatments (Rinuy & Schweizer, 1982, Watkinson, 1979). The oxide film was found to break down leading to pitting corrosion (Watkinson, 1982a).

1.6.2.5 Fluoride treatment

All the washing methods described so far will remove only 'soluble' chlorides and not the 8-10% 'insoluble' chlorides in the iron oxyhydroxides and in particular in the hollandite tunnels in the β-FeOOH lattice. A new technique recently tested has attempted to release these chlorides. Work carried out by Al Ahmed uses fluoride ions to exchange with the

'insoluble' chlorides within the β-FeOOH structure. The objects were washed using soxhlet extraction until the soluble chlorides were removed and then immersed in a 1N sodium fluoride solution (adjusted to pH 4.5-5.5 with 1% HF) to extract further chlorides (Al Ahmed, 1992). The method was found to be more successful than sodium hydroxide treatments. However accelerated corrosion tests showed that under extreme conditions the fluoride treated objects still became unstable again (Al Ahmed, 1992).

There are two main problems with this approach to the conservation of archaeological iron. Firstly it assumes that the 'insoluble' chlorides present in β-FeOOH corrosion products are chemisorped to the surface or in tunnel sites, and can be exchanged for OH^- or F^-. From recent discussions on the β-FeOOH structure presented in section 1.5.1.1 it can be seen that it is in no way clear, that all, or even some of the chloride ions are in these tunnel sites. It seems likely that a significant proportion of the 'insoluble' chloride ions that can not be removed by washing with water are part of the β-FeOOH lattices and can only be removed by the actual decomposition of the crystal lattice.

Secondly, even if we assume that chlorides exist in tunnel sites, it seems unlikely that it will be possible for ion exchange to occur in any sites but those that exist on the β-FeOOH crystal surfaces. The hollandite tunnels are extremely small (about 5Å) and should really be seen as alternative sites for atoms within the crystal lattice, rather than as open tunnels through which atoms can freely move. For chloride ions to diffuse out of tunnel sites and other anions to exchange in to tunnel sites, they would have to be able to pass each other. The size of the tunnels simply does not give room for this to occur. In addition to this, these solid state diffusion processes within crystal structure are extremely slow.

The colloidal nature of iron corrosion products means that a large surface area exists. We know that this will facilitate ion exchange at accessible surface sites. Ion exchange at these sites alone probably accounts for the Cl^- found to have been released from β-FeOOH when treated with sodium fluoride (Al Ahmed, 1992). Within the β-FeOOH crystals however chlorides still remain in 'tunnel' or lattice sites, and it is these that will continue to make objects unstable.

1.6.3 Reduction Methods

Part of the problem in unstable iron objects is the presence of highly hydroscopic iron oxyhydroxides. In reduction treatments the aim is to convert these to less harmful magnetite or to totally reduce them to metal iron thus releasing chloride ions. Any reduction will be accompanied by a reduction in the volume of the corrosion products and this will cause voids and porosity. The newly porous structure will help in the removal of chloride ions but may also lead to unacceptable cracking and fragmentation of the corrosion layers.

1.6.3.1 Electrolytic reduction

In this method the iron object is part of an electrolytic cell. The circuit is arranged so that the corroded iron is the cathode. Two stainless steel anodes are used either side of the object. A dc supply of 5-10 V and 60mamps has been used with aqueous electrolyte (Wihr, 1975). Distilled water or sodium hydroxide electrolytes are commonly used (Carpenter & MacLeod, 1993). A sodium carbonate electrolyte has also been used (Keene & Orton, 1985) . The wash solution is changed every day initially. The chloride anions will be attracted to the anode and diffuse out of the corrosion products. The reduction of oxyhydroxide corrosion products will also occur and the conversion to magnetite or iron will help in the release of chlorides:

$$3FeOOH + e^- \rightarrow \quad Fe_3O_4 + OH^- + H_2O$$

$$FeOOH + e^- \rightarrow \quad Fe + OH^- + H_2O$$

Success in this treatment has been reported with treatment times of 18 months (Oddy, 1987, 156), but it can take up to 5 years for large objects (Carpenter & MacLeod, 1993, 763) It has also been reported that considerable quantities of Cl^- is left in the object (Wihr, 1975). The treatment leaves a deeply etched metal surface which may encourage further corrosion (Keene & Orton, 1985). Recently published research, carried out on samples made to simulate archaeological iron, found electrolysis in sodium hydroxide together with ultrasonic agitation, more successful than washing alone, even at elevated temperatures (Walker, 1996).

A major problem with this method is the electrolysis of water, forming hydrogen:

$$H_2O + e^- \rightarrow \frac{1}{2}H_2 + OH^-$$

This can cause damage to the graphitised surface layers of cast iron and to fragile wrought iron objects. The object may also become pyrophoretic and produce steam (Plendeleith & Werner, 1971). A loss of shape and of the original surface of the object treated is also disadvantageous. There is also a problem with composite objects as any organic material included within corrosion products may be damaged. Welded joins may also suffer damage from electrolytic reduction .

Another less used variation on electrolytic reduction is galvanic cleaning. This method is outlined by Hamilton and was used in the Texas archaeological research laboratory. Rather than being part of an electrolytic cell, the object is made part of a galvanic cell by connecting it to an anodic metal such as aluminium or zinc, in sodium carbonate or hydroxide solution (Hamilton, 1976). No comparative results were given so it is difficult to compare this arrangement to the more usual method.

1.6.3.2 Alkaline sulphite treatment

The alkaline sulphite treatment uses a chemical means of reduction. It was developed in 1975 to treat marine cast iron (North & Pearson, 1975). Objects are immersed in a solution of sodium hydroxide and sodium sulphite in a sealed container for three months. The sodium sulphite is oxidised producing electrons:

$$SO_3^{2-} + 4OH^- \rightarrow SO_4^{2-} + 2H_2O + 4e^-$$

The electrons can then go on to reduce corrosion products. Any excess sulphite is reacted with barium hydroxide after the treatment.

Some experimentation with the method has shown great success (Rinuy & Schweizer, 1982). However the mechanism by which the reduction occurs has been questioned by Gilberg & Seely (1982b). Magnetite does not seem to be produced as a direct reduction of FeOOH but as a result of a number of reactions involving the formation of $Fe(OH)_2$ under anaerobic and high pH conditions.

In further studies alkaline sulphide was found to stabilise 99.8% of artefacts treated with the procedure, compared to 19% stable with no treatment (Selwyn & Logan, 1993) but its use was discontinued due to the damage it caused to objects. Wrought iron nails became 'mushy' and many artefacts needed consolidation due to breaking during and after the treatment. Better survival was observed in objects with a significant iron core and light corrosion layers (Selwyn & Logan, 1993). As with other reduction method, the destruction of the objects original surface is a problem.

1.6.3.3 Hydrogen reduction method

A third reduction method is to use an elevated temperature in a hydrogen and nitrogen atmosphere. Temperatures ranging from 600 to 1000°C have been used to reduce the iron oxyhydroxides and volatilize the destructive chlorides to HCl and $FeCl_3$ (Arrhenius, 1975, Barker *et al*, 1982).

The main problem with this method is the effect that heating has on metallurgical structure. It is obviously advantageous that the original microstructure be retained for investigation into production methods. Section 1.4.2 describes the various surviving structure that may still be found, even within corrosion products. However even more evidence can be gleaned from remaining metal cores. Research has shown that heating at above 400°C creates detectable changes in all but wrought iron (North *et al*, 1976), meaning that previous differences in steel microstructures are obscured giving a uniform structure of large cementite globules in a ferritic matrix (Archer & Barker, 1987). Tylecote and Black (1980) therefore conclude that hydrogen reduction should only be used for objects where the composition and metallographic structure is accurately known. The method has the other disadvantages of reduction - the risk of cracking and the loss of surface markings and shape. There is an added problem that some objects have been observed to become pyrophoric due to the hydrogen (North & Owens, 1981).

1.6.3.4 Low pressure plasma treatment

Plasma treatments were first suggested for use in conservation in 1979 (Daniels *et al*, 1979). A treatment for removing silver tarnish and conserving early "Daguereotype" photographic plates was published in 1981 (Daniels, 1981). The method worked satisfactorily for the thin corrosion layers found on these types of materials.

The method was developed for use in iron conservation at the University of Zurich (Patscheider & Veprek, 1986). It involves the use of a high frequency plasma to reduce iron corrosion products. A potential difference applied across a gas at low pressure produces a glow discharge. When a high frequency electric field is applied a plasma - a gaseous mixture of ions and electrons, is formed. A diagram of the apparatus used is shown in figure 1.23 (Veprek, 1989). The iron object is placed in the discharge tube to which an hydrogen pressure of 0.3-2 torr (with a flow rate of several tens of standard cubic centimetres per minute) is applied. A mixture of hydrogen and argon or neon, or hydrogen and methane can also be used. A glow discharge is produced at 50Hz, 300-400V, 50mA AC. Temperatures of 280-300°C are needed and treatment is carried out for two hour periods (Veprek, 1989). The plasma effects a partial reduction of surface magnetite which becomes brittle and can be removed if required. A post-plasma treatment of hydrogen, methane and nitrogen 1:1:2 mixture, for 15-20 hours, will help to passivate the surface by forming a compact carbonitride layer (Veprek *et al*, 1987, Veprek, 1989).

The method was found to reduce chloride contents of objects to levels at which the objects were stable. Corrosion tests have shown most objects to be stabilised, although 1-2% of objects recorroded (Veprek *et al*, 1987). An added advantage was found to be that for thin corrosion layers the treatment allows the original metal surface details to be uncovered (Patscheider & Veprek, 1986, Veprek, 1989).

Experimentation with DC plasmas was found unsuccessful in removing chlorides (Aoki, 1989). It was found to be a beneficial procedure when accompanied by soxhlet washing, removing about 80% of soluble chlorides whilst soxhlet washing alone removed only 50%. Further work with the DC. mode hydrogen plasma treatment has been more successful (Sjøgren & Buchwald, 1991). A corroded iron object was made the cathode with two perforated aluminium plate anodes either side. 300-500V were applied with a hydrogen flow rate of 40ml per minute at 0.6-1mb pressure. Temperatures of 100-120°C were recorded. Severely encrusted artefacts were immersed in sodium hydroxide solution before the plasma treatment Objects treated in this way were stabilised with all but less than 0.1% chlorides removed. No changes in metallographic structures were recorded and again surface markings were uncovered The lower temperature of this treatment is preferable to the ac. hydrogen plasma treatment, although it has been reported that temperatures of 300-

500°C and several days of treatment are neccessary to remove all chlorides (Oswald, 1997).

Figure 1.23 Apparatus developed for plasma treatment of archaeological artefacts (Veprek, 1989).

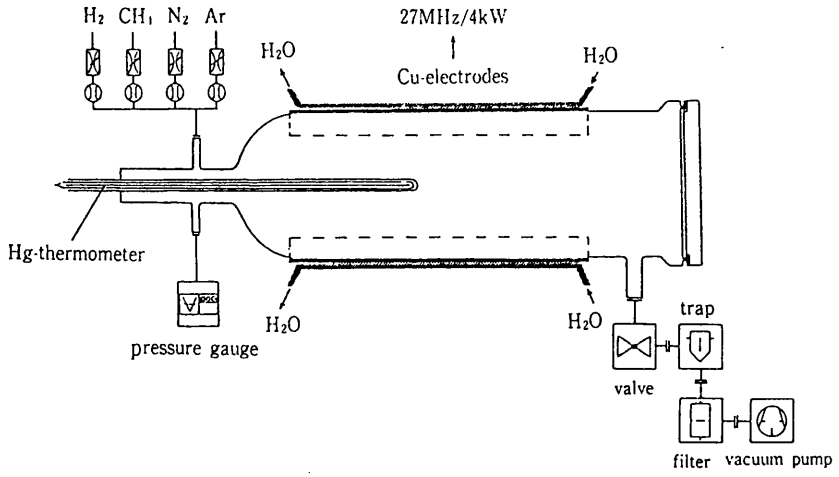

Problems are still encountered with this method. Only objects with existing metal cores are safe to treat (Veprek, 1989, 89) and an unattractive grey and fractured surface may form. It has been suggested that the grey colour can be removed after the treatment by a brief exposure to a humid environment to grow a thin, but stable corrosion layer (Sjøgren & Buchwald, 1991, 170). It also seems that chlorides are only removed from the outermost rust layers, where they are in the gas phase and so the treatment is only suitable for objects with thin corrosion layers (Oswald, 1997). The cracking and fracturing of corrosion product layers due to the volume contraction that occurs on reduction is a serious drawback (Patscheider & Veprek, 1986)

The treatment may be promising in its ability to stabilise iron, but the initial capital outlay and expertise needed to run a plasma unit, means it is a treatment available only to very large museums and conservation units and a simple and cheap strategy in the stabilisation of iron is still needed. As with all reduction methods the problem of shrinkage and cracking of oxide layers is present. However the method does have the advantage of

allowing large quantities of material to be conserved quickly. In Zurich 10,000 object were conserved within about six weeks of work (Veprek *et al*, 1987, 2404).

1.6.4 Electrolytic methods

Electrolytic desalination uses the application of electrical potential to facilitate the removal of chlorides from corrosion products. This varies slightly from electrolytic reduction methods, whereby the aim is to reduce corrosion products. Several circuit arrangements have been used. The temperature, solvent and applied potential will effect the efficiency of the process. Often electrolytic methods are used along with other treatments.

1.6.4.1 Cathodic desalination or electrolysis

This method has been discussed in section 1.6.3.1 as it employs electrical current to facilitate reduction. The treatment has been employed in combination with ionophoresis in cycles to remove further chlorides (Wihr, 1975).

1.6.4.2 Ionophoresis

In ionophoresis the object is not directly part of the electrical circuit. Two stainless steel plates are connected up as anode and cathode and the iron artefacts are hung between the electrodes. A temperature of 35-40°C is used and this arrangement increases the rate of desalination. A volume ratio of iron to electrolyte in the bath, of 1:10 is used and a voltage of 10V dc. applied. Electrolytes including sodium benzoate have been used (Keene & Orton, 1985). The process can take many months and is carried out until no further Cl^- can be removed. This method is less damaging than electrolysis but does not seem to remove as many Cl^-, when used on it's own (Wihr, 1975). Like electrolysis all chlorides can never be removed with this method. The use of aqueous solutions can also lead to further corrosion during the treatment, and it is not generally regarded as a successful method.

1.6.5 Protective Coatings Used in the Conservation of Iron

In the 19th century it was believed that iron objects removed from harmful soils could be stabilised if properly dried and a protective coating applied. Much effort went into the

search for an ideal coating. Even as late as the 1960's waxes were used on objects which had not been desalinated (Organ and Shorer, 1962-63). Harmful and aggressive coatings were sometimes applied in thick layers and these old coating are often difficult to dissolve and can not now be removed because the object itself is in such a state of deterioration that it would collapse without the physical support of the coating. (Jakobsen, 1988)

Today it is recognised that coating alone will not stabilise excavated iron. However, after cleaning and desalination it is common practice in conservation to use a coating to protect and consolidate the iron object. An example of the type of treatments used is given by North & Pearson (1975, 177). Wrought iron is suggested to be treated with a zinc phosphate based anti-corrosion clear primer (KEPHOS by Dulux paints), followed by 6 coats of clear matt polymethyl methacrylate (acrylic laquer). For cast iron the suggestion is impregnation with micro-crystalline wax by submerging the object in a wax bath at approximately 120°C. Table 1.2 lists the coatings commonly used in conservation.

Table 1.2 Coatings used in the conservation of ironwork.

Polyvinyl acetate (PVAc)
Cellulose Lacquer (Ercalene)
Microcrystalline or parafin wax
Epoxy resins (Araldite AY 903/HY 951)
Acrylic resin (Ethylmethacrylate; Paraloid B72, Methylacrylate copolymer; Acryloid B72)

Research into the effectiveness of these treatments has been undertaken by Susan Keene (Keene, 1984). Given that most treatments are designed for industrial coatings for bare metal it seems logical to question their adhesion to unprepared corroded surfaces. Most of the coatings used do not adhere particularly well to metals in the first place, and it will rarely be possible to prepare a perfectly clean metal surface in archaeological conservation.

The impermeability and continuity of the films is also questionable. None of the coatings are impermeable to oxygen and water vapour (excluding waxes). Commercial coatings rely on film thickness to stop moisture penetration, but conservators like to apply only a thin

transparent layer for aesthetic reasons. Problems also can arise from incomplete coatings. When a coating is applied to an uneven object as a liquid, surface tension will pull the liquid film into a curve, meaning that it will be thinner on peaks and edges of the objects surface (Newey *et al*, 1996, 117). There may even be gaps in the coating. This not only lessens the protective nature of the coating, but can even accelerate corrosion by creating differentially aerated cells and causing crevice corrosion

Experiments on three main groups of coatings, PVAc's, Waxes and Epoxy resins have shown these doubts to be upheld. Waxes and PVAc coatings gave no extra protection compared to the uncoated control groups. In Keenes' study better survival rate was found for objects treated with epoxy resins. This observation however may just be due to the consolidating effect of the resin, hiding corrosion within the object that would otherwise cause collapse. It is also likely that objects treated with the epoxy resin in this trial were the objects needing consolidation that consisted mainly of corrosion products and thus would be less susceptible to corrosion in the first place (Keene, 1984). However, even if it can be established that epoxy resins do work better than other coatings, they are not favoured by conservators as their application is irreversible. Even when the epoxy resin is softened by solvents it can never be completely removed from pores within an object

Although it seems coatings are ineffective in protecting iron objects they still have a role as consolidants, helping to prevent disintegration of objects and giving additional mechanical strength. The use of Paraloid B72 with the addition of Dichon corrosion inhibitor is favoured by Keene (Keene, 1984, 106) but there is no evidence to suggest that the addition of corrosion inhibitors to coatings has any significant effect.

1.6.6 Conclusions

Research into the conservation of iron has focused mainly on desalination methods, as the presence of chlorides have been perceived to be the main problem in stabilising archaeological iron. Reduction to a level of chloride ions of 0.1% in corrosion products has been found to stabilise some objects in normal indoor conditions (Sjogren & Buchwald, 1991), however this may not always be the case, and objects can recorrode

even after desalination procedures. There still seems to be no one universally accepted conservation method, although most of the high temperature techniques have now been discontinued due to the unacceptable damage they do to metallurgical structures. All methods seem to have some disadvantages and often different treatments need to be selected for materials from different sites.

Instability and the subsequent recorrosion of archaeological iron, (in particular iron excavated from marine sites) after conservation treatment, is still a major problem for conservators. It seems that the desalination treatments presently available can not remove all the chloride ions present in corrosion products. This is partly because when the metal is actively corroding, chlorides must be present to balance the anion charge and so can not be washed out (Turgoose, 1989). It is also because chlorides are actually part of the corrosion products, and are trapped in structural positions in the β-FeOOH lattice. They can not be removed without the destruction of these corrosion products.

So we have to accept that it may never be possible to remove all of the chloride ions present in the corrosion products of archaeological iron objects. Desalination and coating objects does not seem to be enough to stop recorrosion in many cases. We need to investigate other complementary conservation techniques. The approach this work has taken is to consider the use of corrosion inhibiting surface treatments.

CHAPTER TWO

Corrosion Inhibitors and Surface Modification

2.1 INTRODUCTION

From the review given in the last chapter, it can be seen that research into methods for the conservation of archaeological iron, especially marine iron, has concentrated on the removal of chloride ions and finding increasingly more efficient desalination processes. The efficiency of a desalination method can be seen as a measure of the total proportion of chloride ions that can be removed, coupled with the length of time taken for this to be achieved.

If the discussion and debate on the structure of the chloride containing corrosion product β-FeOOH is considered, it becomes clear that at least some of the chloride ions present are structurally bound within the corrosion products (Rezel & Genin, 1990), and can not be removed by any washing procedure. The only method by which this structurally bound chloride can be removed is by the destruction of the iron oxyhydroxide corrosion product. Reductive methods will achieve this, but can leave the corrosion layers disfigured. These sorts of methods are ethically questionable in that the changes they cause do not really fit the concept of minimum intervention.

If it is accepted that after washing has been carried out, an object may still be susceptible to corrosion, additional conservation methods must be sought. A possible route is to use corrosion inhibiting chemicals to treat the surfaces of objects.

2.2 THE DEFINITION AND THEORY OF CORROSION INHIBITORS

Corrosion inhibitors are substances that decrease the rate of corrosion of a metal. Corrosion inhibition can be more formerly defined as "the reduction in the oxidation rate of the metal by the addition of a chemical compound to the system" (Sastri, 1998, 25). Corrosion inhibitors can be seen as retarding catalysts (Fontana, 1987), as they are used at low concentrations and are specific to a particular metal, environment, temperature, pH and concentration range. A critical concentration exists for inhibitors above which the addition of more inhibitor will not increase the corrosion inhibiton. Theories as to how some inhibitors work are still under discussion with research being carried out by chemists and engineers. This uncertainty means that inhibitors are often chosen by empirical testing rather than any reasoned theory. Two or more inhibitors added together can often be more successful than a single substance (this is known as the synergistic effect). All this results in the exact ingredients of industrial corrosion inhibitors, being held as protected information by chemical companies (Sastri, 1998).

The mechanism of corrosion inhibitors can be described in terms of mixed potential theory, inhibitors being classed as anodic, cathodic or mixed (anodic and cathodic) (Evans, 1960). However this scheme does not take all factors into account and is inadequate to explain some phenomenon (Skerry, 1985). Other models have been suggested to explain and classify inhibitor types such as their buffering action (Hoar, 1937), adsorption effect (Brasher, 1962) or precipitation reactions (Lumsden *et al*, 1978) but again these theories will not explain all inhibitor action. It has been suggested that "inhibitor mechanisms, irrespective of the amount adsorbed by the surface, work by changing the electrophysical properties of surface atoms by the donor-acceptor inhibitor/metal reaction, rather than in screening the metal surface from the corrosive environment" (Rozenfield, 1981, 377). Evidence has also been found that many inhibitors become effective through interaction with corrosion products as they form, to produce a new more effective protective layer, rather than just absorption on the metal surface. Corrosion inhibitors have thus begun to be classified as interface or interphase inhibitors.

2.2.1 Classification of Corrosion Inhibitors

It is useful to try and classify inhibitors and explain the differences in their proposed modes of operation. Due to the incomplete understanding inhibitor classification can seem somewhat random, grouping inhibitors in terms of their mode of use as well as in terms of their assumed inhibition mechanism. Convenient classifications of inhibitors are anodic inhibitors, cathodic inhibitors, mixed inhibitors, adsorption/organic inhibitors and vapour phase inhibitors. More recently inhibitors have been classified as hard or soft. Further details of these groups will be discussed below.

2.2.1.1 Anodic inhibitors

Anodic inhibitors are so named as they work by inhibiting the anodic dissolution of metals. They are normally anions which are in contact with the metal surface and cause the reduction of the anodic area by the formation of insoluble compounds or passive films. They can be further divided into oxidising and non-oxidising inhibitors.

Oxidising inhibitors such as chromates, [CrO_4^{2-}] and nitrites, [NO_2^-] can work without the presence of oxygen. Both these inhibitors work on iron by producing a stable γ-Fe_2O_3 film which in the case of chromate also contains Cr_2O_3. The production of hydroxide ions will also increase the local pH and help prevent the development of anodic sites.

$$2Fe + NaNO_2 + 2H_2O \rightarrow Fe_2O_3 + NaOH + NH_3$$

$$2Fe + 2Na_2CrO_4 + 2H_2O \rightarrow Fe_2O_3 + Cr_2O_3 + 4NaOH$$

The effect of the inhibitor can be illustrated on a potential-current diagram. Figure 2.1a illustrates how an oxidising inhibitor will change the anodic potential and therefore move the corrosion current into the passive region. The main problem with these inhibitors is that if present in insufficient concentrations not all of the anodic surface is passivated leading to pitting and an increase in the corrosion rate. For this reason these inhibitors are often known as 'dangerous'.

Non-oxidising inhibitors such as phosphates, [PO_4^{3-}], and silicates, [SiO_3^{2-}] and hydroxide ions, OH^-, require the presence of oxygen to inhibit. The inhibitors precipitate salts containing the corroding metal's ions in areas where the metals own passive oxide layer

has broken down. These are more protective than the original passive layer. Figure 2.1b illustrates the effect on the anodic current resulting in a decrease in corrosion current.

Figure 2.1 Evans diagrams illustrating the mechanism of inhibitor action (adapted from Skerry, 1985)

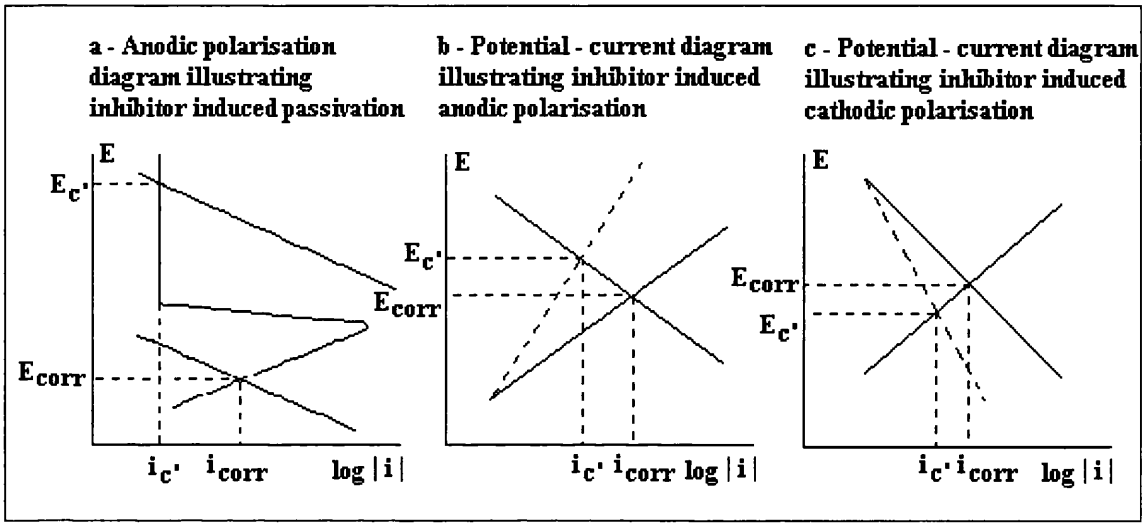

2.2.1.2 Cathodic inhibitors

Cathodic inhibitors work by controlling the cathodic reaction, which in aerated solution is the reduction of oxygen. Several types of cathodic inhibitors also exist. Scavengers remove dissolved oxygen from solution, therefore preventing its contact with the metal surface. Sodium sulphite and hydrazine both work in this way, although an enclosed system is necessary so the oxygen that is depleted is not replaced.

$$2Na_2SO_3 + O_{2(aq)} \rightarrow 2Na_2SO_4$$

$$N_2H_4 + O_2 \rightarrow N_2 + 2H_2$$

True cathodic inhibitors are ions such as zinc, calcium, magnesium, manganese and nickel. These form surface films of insoluble hydroxides at cathodic sites. These are poor conductors and therefore do not allow the cathodic oxygen reduction reaction to occur. Even if the film becomes flawed or damaged, more hydroxide is produced and the site will be self-healing. For this reason these types of inhibitors are known as 'safe'. They do not need to totally cover or even reach the anodic metal surface as long as they can reduce the cathodic surface. Figure 2.1c illustrates the process of cathodic inhibition on a potential-current diagram.

2.2.1.3 Mixed corrosion inhibitors

Many of the most successful corrosion inhibitors are classified as mixed inhibitors - meaning they inhibit the cathodic and anodic reactions. Common examples are zinc chromate and potassium dichromate. The cations act as cathodic inhibitors whilst the anions are anodic inhibitors. Some polyphosphates and silicates are also mixed corrosion inhibitors and many organic inhibitors that will be discussed as adsorption inhibitors are mixed.

2.2.1.4 Adsorption inhibitors/organic inhibitors

Organic molecules can be adsorbed onto metal surfaces and in this way act as corrosion inhibitors. Physisorption and chemisorption occur, bonding the molecule to the surface, physically restricting diffusion of metal ions, and preventing oxygen or moisture from coming into contact with the metal surface. Most organic inhibitors contain nitrogen or sulphur as these atoms have lone pairs, from where electronic interactions with a metal surface can occur. Amines and thiols, both aromatic and aliphatic, are good inhibitors. Inhibitors are often aromatic or compounds with delocalised electrons or multiple bonds, so that mesomeric or inductive effects can facilitate the adsorption process. An increase in electron availability has been found to increase the inhibition of corrosion, so for example 2-methylpyridine is a better inhibitor than pyridine (Skerry, 1985, 11). The electron charge must however be accessible to the metal surface and so steric factors play a part. As molecules become very large and bulky their inhibiting properties will be reduced.

2.2.1.5 Vapour phase inhibitors

Volatile organic molecules that typically have vapour pressures ranging from 10^{-2} to 10^{-7} mmHg (Skerry, 1985) enable inhibitors to reach inaccessible crevices and gaps in objects. Examples of vapour phase inhibitors are dibenzylamine nitrite and dicyclohexylamine chromate (Knack & Brooks, 1973). These types of inhibitors are thought to work by forming adsorbed molecular films as with organic inhibitors. As the molecules are volatile they will be able to reach the anodic metal surface underneath corrosion products and therefore they are easily applied.

Some problems with vapour phase inhibitors arose in that they did not offer protection to both ferrous and non-ferrous metals (Pourbaix, 1977, 223), however, newer inhibitors such as dinitrobenzoates have been found to do so (Rozenfield, 1981). Problems can also occur with discolouration of objects. A sealed environment is needed so the inhibitor does not escape making them most useful for packaged materials and sealed machinery.

2.2.1.6 Hard and soft Inhibitors

A more recent classification of corrosion inhibitors has been based on the hard and soft acid/base theory (Pearson, 1968). This classification helps to explain why some inhibitors work better on some metals. The labels hard and soft refer to the polarisability of atoms. Hard acids and bases are defined as atoms that have small atomic radii, high effective nuclear charges, low electronic charges and are easily oxidisable. Soft acids and bases have the opposite attributes. A borderline category is also allowed for. The acid/base theory states that hard acids react preferentially with hard bases and soft acids react preferentially with soft bases.

Following on from this, Sastri (1998) has described inhibitors as hard or soft. Neutral metals are classed as soft acids and so will react preferentially with soft bases such as sulphur containing compounds. These are therefore classed as soft inhibitors. This theory explains why in some circumstances sulphur compounds work as better inhibitors than nitrogen compounds which are classed as borderline inhibitors (Sastri *et al*, 1990).

2.3 The Use of Corrosion Inhibitors in the Conservation of Iron

With the exception of the use of BTA for copper alloys, it seems that corrosion inhibitors have perhaps not been utilised to a great enough extent in conservation. In the case of archaeological iron, very little experimental work has been carried out into their effectiveness. Some general reviews of their use in conservation can be found in Fenn & Foley, 1975, Foley, 1977, Stambolov, 1978, and Walker, 1982. The most widely used inhibitor is benzotriazole (BTA) which is used on copper and copper alloys. BTA has the ability to form compounds with copper in both Cu(I) and Cu(II) oxidation states and can therefore form a very stable passive film (Brinch Madsen, 1985, 19).

The problem with industrial corrosion inhibitors is that they are designed for use on clean metal surfaces and not on the oxide layers that inevitably exist on archaeological objects. Their ability to stabilise archaeological artefacts can therefore not be assumed (Turgoose, 1985a, 13). As already discussed anodic inhibitors need to be in contact with the anodic metal surface. But this will not always be possible with corroded objects, making anodic inhibitors such as hydroxide, chromate or nitrite ions ineffective. In the time it takes for the inhibitor ions to diffuse to the surface further corrosion can take place. The high chloride concentrations and low pH of the metal surface will also make it difficult to pacify using anodic inhibitors (Turgoose, 1985, 15).

Cathodic inhibitors are likely to be more successful as they block diffusion of oxygen to the cathodic surface. In the case of archaeological objects covered in corrosion products, the cathodic reaction is unlikely to occur at the metal surface, but somewhere within the corrosion product layers. These sites may be accessible to the inhibitor molecules. Turgoose has suggested that if an effective cathodic inhibitor could be found for archaeological iron, the disadvantages of many existing conservation method could be removed and the stabilisation of antiquities greatly facilitated (Turgoose, 1982, 100).

Organic inhibitors are often used in the acid stripping of metals, to remove unwanted concretions or corrosion products. Examples of such inhibitors used are thiourea (Desai, 1963), substituted benzotriazoles and tolytriazoles (Eldkaer, 1976), and derivatives of

thioglycolic acid and 3-mercaptopropionic acid (Carroll, 1975). In aqueous solution tannins (Coulson, 1960), salicylates (Shreir, 1964), aliphatic amines, alcohols, aldehydes and quinolines (Argo, 1992) have all been noted to inhibit corrosion.

Tannins were once widely used as an inhibitive pre-treatment (Ross & Francis, 1978). Tannins are complex mixtures of polyhydric phenols that occur naturally. They complex with iron, in metallic or oxide form and produce iron tannates. Oxygen must be present for this process to occur. A dense black insoluble layer is formed on an objects surface when treated with tanins which has made their use less popular in recent years (Turner, 1985).

Vapour phase inhibitors may also be useful, especially in sealed display units in museums. Their volatility would mean the inhibitor could reach the metal surface to be protected. The most commonly used vapour phase inhibitors in conservation are dicyclohexylammonium nitrite, commercially known as VPI. and dicyclohexylammonium carbonate, commercially known as CHC. Vapour phase inhibitors are not permanently adsorbed, making their use totally reversible. It is not clear how effectively they work on corroded surfaces and some research indicates that with a high chloride content within corrosion products, they may actually accelerate corrosion (Scheifler, 1985, 40). It is also important to note that they can not be used along with silica gel, as the silica will absorb the inhibitor molecules.

2.4 SURFACE MODIFICATION

2.4.1 A New Approach to Corrosion Inhibition of Archaeological Iron

We have already discussed that major problems are involved when trying to use industrially formulated corrosion inhibitors on archaeological objects. The main problem is the fact that we are not dealing with perfectly clean, flat metallic surfaces. With these problems in mind it was decided to consider corrosion inhibition from a slightly different angle. Research into surface modification of oxides has been carried out for many years. This research has been applied to many problems other than corrosion inhibition, but surface modification techniques have been considered applicable to the problems of conservation of archaeological iron. Treatments that modify the oxide surfaces of a corroded object are not corrosion inhibitors in the traditional sense, however, if an inhibitor is defined as any substance that decreases the rate of corrosion of a metal (Sastri, 1998, 25), then they can be considered corrosion inhibitors.

The hydrophilic surfaces properties of iron corrosion products have been disscused. They adsorb water and other pollutants such as sulphur dioxide and nitrogen oxide. If a treatment could change the nature of the surface, blocking the hydroxyl adsorption sites by introducing a hydrophobic layer, this would act as a barrier to corrosion and help stabilise the object. This technique for the stabilisation of archaeological iron was suggested as far back as 1979 by Stambolov, who proposed the use of methyltriethoxysilane, $CH_3Si(OC_2H_5)_3$, as a water-repelling treatment (Stambolov, 1979). This method has been tested widely as a method for conserving stone (Moncrieff, 1976, Weber, 1975).

Research into treatments on iron oxyhydroxide surfaces have been carried out by Micale and co-workers (1985), using hexamethyldisilazane (HMDS) and methanol The silane reacts with the proton of surface hydroxyls:

$$2FeOOH + (CH_3)_3Si.NH.Si(CH_3)_3 \rightarrow NH_3 + 2FeOOSi(CH_3)_3$$

adsorbing 1.5 silane groups per 100Å^2 of α-Fe2O3 and 2.5 groups per 100Å^2 of γ-FeOOH. If a size of 40Å^2 is assumed for each silane then 2.5 groups per 100Å^2 represents close packing. HMDS has been shown to have a measurable effect in decreasing the surface hydrophilicity of iron oxyhydroxides.

A more efficient hydrophobing treatment was found to be exposing the oxide surface to methanol at 400°C and subsequently cooling to room temperature in the presence of methanol. The following adsorption occurs:

$$CH_3OH + FeOOH \rightarrow FeOOCH_3 + H_2O$$

A reduction from 7.8 hydroxyl groups per 100Å^2 to 0.6 groups per 100Å^2 on α-Fe_2O_3 was recorded showing that the smaller size of methanol makes it able to affect greater surface coverage and therefore produce a more hydrophobic layer.

Titanates have also been used to modify the surfaces of iron oxyhydroxides (Inoue *et al*, 1986). Their anticorrsive and interfacial adhesive properties are well attested to (Monte & Sugerman, 1988a, 1988b). One of the titanates experimented with was isopropyltriisostearoyltitanate (TTS) which reacts as follows:

$$FeOOH + [CH(CH_3)_2OTi(OCOC_{17}H_{35})_3] \rightarrow FeOTi(O\text{-}CO\text{-}C_{17}H_{35})_3 + 2(CH_3)_2CHOH$$

The amount of water adsorption on FeOOH crystals decreases significantly with the TTS treatment (Kaneko, 1989a). The contact angle, (a scale indicating the cohesive properties of a liquid to a solid, with $\theta = 0$ indicating the liquid wetting the surface perfectly) increased from 4° to 92° on the treatment of FeOOH with TTS (Anraku *et al*, 1983).

2.4.2 The Surface Modification of Archaeological Iron

To find a surface modification treatment that would be useful in the conservation of archaeological iron, we must consider the properties that would be required. We need to consider the physical and chemical properties that allow a treatment to be successful in inhibiting corrosion. We must also consider the factors that are particular to conservation, such as practical and ethical considerations. Two lists pertaining to the physicochemical requirements for a surface modification treatment, and the requirements specific to archaeological conservation have been devised as follows:

Physicochemcial properties required:

1. The molecules used to modify the surface of an archaeological object must form bonds with iron and iron corrosion products.

2. The molecules must have a hydrophobic part, that will act as a barrier to the adsorption of water and water vapour.
3. The molecules should be able to close pack so that the hydrophobic barrier exists over the whole surface of the treated object
4. The molecules should be able to cross-link with each other to help stabilise the molecular layer, and prevent gaps or holes.
5. The treatment when applied should routinely reduce or stop corrosion of archaeological iron objects, and preferably work for a long time scale.

Properties required for archaeological conservation:

1. The treatment should be colourless, and not change the visible appearance of the object in any way.
2. The treatment should be reversible, that is, should be able to be removed from the object without damaging the object.
3. The treatment should be able to be applied at low temperatures so that no changes associated with heating can occur to the object.
4. The treatment should be able to be easily applied by a conservator.
5. The treatment should not cause any damage to other archaeological material that may be integrally connected to an iron object.
6. The treatment should not be toxic or cause any ill affects to the conservator, or other personnel who may have to handle the object after storage.
7. The treatment should be inexpensive.

In choosing a surface treatment these factors were kept in mind. It is not always possible to satisfy all of them. Obviously of primary importance is the success of any treatment in preventing the further corrosion of a treated object on a long term basis. This however must be seen in the context of the aims of any conservation process. Conservation not only aims to prevent disintegration of excavated objects but also to increase our understanding of the original artefact and facilitate future study and display. For these reasons a conservation procedure must not alter the fundamental nature of an object or destroy any evidence useful to archaeologists. The treatments chosen to test in this work were organo-silanes, polyfluoroalkyl-silanes, organo-titanates and long chain aliphatic amines. These will be disscussed in more detail in this chapter.

2.4.3 Hydrophobicity and Hydrophobic Surfaces

The terms hydrophobic and hydrophilic are used to describe the tendency of a surface to become wetted by an aqueous solution (Shaw, 1966). A hydrophobic surface is one that is unable to bind to water molecules via ionic or hydrogen bonds. It is the nature of the functional groups at a surface that will govern the hydrophilic or phobic properties of a surface. By changing the chemical nature of a surface, this property can be changed, for example, a glass surface is hydrophilic, but when coated with wax it becomes hydrophobic. Hydrophobic molecules tend to be non-polar molecules such as alkanes, hydrocarbons and fluorocarbons. It is possible to have molecules that possess hydrophobic ends and hydrophilic ends.

To explain hydrophobicity we need to consider the strong inclination of water to form hydrogen bonds. Each water molecule can form four hydrogen bonding interactions and so hydrogen bonds play a prominent role in the structure of water. Water is a polar molecule, meaning that it has a dipole moment, with a negative charge on the oxygen and positive charge on the hydrogen atoms. In the liquid phase, water tends to retain its ice-like tetrahedral structure, although it is disordered and labile.

Hydrophobicity tends to occur when water interacts with non-polar molecules or functional groups, incapable of forming hydrogen bonds. This causes a disruption of the random network of hydrogen bonds occurring in water and is therefore unfavourable. Hydrophobic molecules tend to increase the ordering of water molecules surrounding them. The water molecules form highly ordered arrangements known as clathrate cage structures, and these are entropically very unfavourable (Israelachvili, 1991). It is for this reason that non polar groups such as hydrocarbons are sparingly soluble in water. Hydrocarbons have a highly unfavourable free energy of solution that is mainly due to entropic considerations. This is known as the hydrophobic effect (Kauzmann, 1959, Tanford, 1980), and explains why surfaces covered with hydrocarbon or other non-polar functional groups are not easily wetted by water. When water comes into contact with such surfaces it forms into small droplets.

2.5 ORGANO-SILANE COUPLING AGENTS

2.5.1 Introduction

Silane coupling agents are organofunctional monomeric silicon compounds. They have been widely used to modify the surface properties of inorganic oxides such as silica and iron oxides (Hertl, 1968). They are used to bridge organic and inorganic composite materials such as fibre glass reinforced plastics and resin coated and painted metals (Kass, 1971, Lee, 1987). Coupling agents are materials that improve the chemical resistance of the bonding across an interface (Plueddemann, 1982, 29). The addition of silane coupling agents to the interface improves the mechanical and electrical properties of composite materials. Organic silanes improve the adhesion between filler and polymer matrix and are especially useful in the presence of water or high humidity. Silane coupling agents are also used to prepare chemically modified oxide surfaces for use as separation media in various chromatographic and electrophoretic methods. They are used in gas purification systems and to produce chiral and liquid crystal surfaces (Pesek and Matyska, 1997).

2.5.2 Chemical Structure and Reactivity of Silane Coupling Agents

A general formula for silane coupling agents can be given as $YSiX_3$, where X is a hydrolysable group bonded to silicon. X is commonly a chloride, alkoxy or acetoxy group. The X group is the part of the silane coupling agent that is responsible for the interaction with the oxide surface. Silane coupling agents will react with water to produce silanols.

$$YSiX3 + H_2O \longrightarrow YSi(OH)_3 + 3HX$$

Y can be a variety of organic functional groups. It is this part of the molecule that gives the desirable properties to the new surface such as hydrophobicity. Y may be $-CH_3$, $-CH.CH_2$, –γ-methacytoxypropyl, –γ-aminopropyl, or –γ-glycidoxypropyl.

Silane coupling agents can further be divided into two varieties. Those with formulas $YSIR_2X$, have only one hydrolisable group, X, attached to the silicon. These are known as monomeric silanes as there is only a single point of attachment to the oxide surface. A metal-oxygen-silicon interaction can then be formed which is thermodynamically and

hydrolytically stable in aqueous and organic solutions between pH 2-8. If R is a bulky group, the bond will have even greater stability (Kirland *et al*, 1989).

$$YSiR_2X + M\text{-}OH \longrightarrow M\text{-}O\text{-}SiR_2Y + HX$$

Polymeric silane coupling agents have 3 hydrolisable groups and so can cross link with each other as well as forming an attachment to the oxide surface.

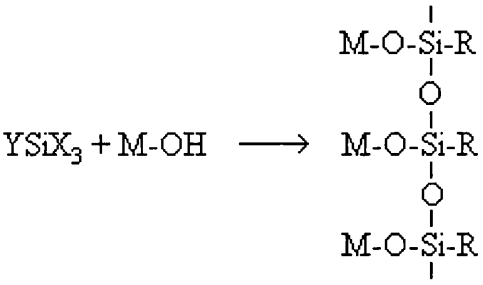

In these silane coupling agents Si-O-Si-C linkages are created. Water is required for efficient cross linking. The silane films that are produced vary in thickness from a monolayer to a few hundred monolayers.

Research has been carried out to elucidate the exact mechanism for the attachment of silane coupling agents to oxide surfaces (Bascom, 1968, Lee, 1968). The reaction seems to proceed via a 2 step hydrolysis and then condensation mechanism in aqueous solution. Hydrolysis first gives silanols which react with the oxide surface or condense to form a network of siloxanes. The hydrolysis is fast, making many silanes coupling agents moisture sensitive. The condensation polymerisation takes longer (several hours).

In non aqueous solution the mechanism is thought to work by the removal of water from the oxide surface. Oxide surfaces in contact with normal atmospheric conditions will carry enough moisture on their surfaces to hydrolyze methoxysilanes or chlorosilanes (Plueddeman, 1982). Hydrogen bonds can form between the hydroxyl groups of the oxide with the oxygen atoms of the silanes. The formation of covalent bonds between the surface oxygens and the silane was suggested in early research (Pluddemann, 1974, Ranney, 1974, Kaas, 1971) and much evidence now supports their existence (Pesek & Matyska, 1997).

2.5.3 Silanes Used in Conservation of Archaeological Iron

Silane coupling agents have been tested in industry as corrosion inhibiting treatments, used for painted and clean metal surfaces. They are intended as a replacement for the currently used, but toxic, chromate and phosphate treatments (Van Ooij & Child, 1998). Their use as inhibitors is still very much in the development stage. Some work has previously been carried out on using silane coupling agents to produce a hydrophobic surface on archaeological iron corrosion products (Al Ahmed, 1992). Three silane coupling agents were tested, vinyltriethoxysilane, $CH_2CH.Si(OC_2H_5)_3$, (VTS), γ-methacryloxypropyltrimethoxysilane, (MTS) and methyltriacetoxysilane, (MAS), using 10% solutions of each silane in toluene

In accelerated corrosion tests the performance of these silanes varied from almost no stabilisation in comparison to a control sample, in the case of MTS, to a moderate improvement in the stability of the objects treated with VTS and MAS. The Si-O-Fe bonds formed were found not to withstand attack by water as tests showed the silanes were desorbed in aqueous solution. Silanes were also reported to give objects a glossy and artificial looking surface (Al Ahmed, 1992).

2.5.4 Octadecyltrimethoysilane (ODTMS)

In this work it was decided to test another silane, octadecyltrimethoxysilane (ODTMS), $CH_3(CH_2)_{17}Si(OCH_3)_3$. ODTMS was chosen for its suitability as a hydrophobing agent. Due to its lack of reactive organic group, ODTMS is not used as a coupling agent (Harder *et al*, 1997), but is suitable for the proposed purpose. It has been used to create coatings that prevent free exchange of water in and out of smectite clays (Wasserman *et al*, 1997, 1998).

A methoxysilane was chosen as the equivalent trichlorosilane is very reactive and moisture sensitive and spontaneously polymerises in aqueous solution (Taylor, 1996). The methoxysilane is still reactive enough to work in non-aqueous solution. ODTMS will react with an oxide surface as previously described. The hydrolysis is strongly pH dependent.

The hydrolysis rate of remaining groups increases once one methoxy group has been hydrolysed (Linden *et al*, 1996).

Experimental work on deposited monolayers of ODTMS suggests the molecules form highly ordered films with the aliphatic hydrocarbon chains aligned in a near vertical arrangement, pointing upwards from the surface that the molecules are deposited on (Taylor *et al*, 1996). If this arrangement were mirrored on an iron oxide surface, an effective hydrophobic barrier may be created. Concentrations of between 0.01M and 0.1M have been used to create these close packed films (Banga et al, 1995, Britt & Hlady, 1999).

Figure 2.2 The linear, surface polymer formed by ODTMS (Sjöblom et al, 1995)

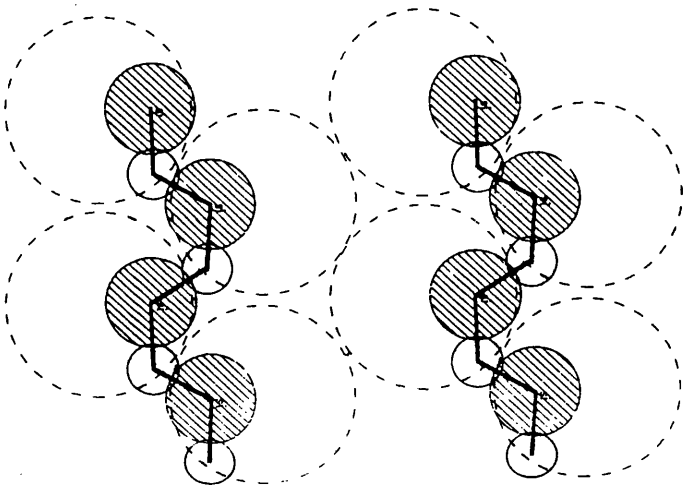

Hydrocarbon chains: dashed circles, Si: circles with hatching, O: circles with solid outline

Recent work on ODTMS polymerised films formed at the air-water interface (known as Langmuir -Blodgett films) has been carried out to investigate the exact configuration of these polymers. Sjoblan *et al* (1995), assume bond lengths of 1.90Å for Si-C, and 1.70Å for Si-O bonds. They conclude that steric hindrance due to the hydrocarbon chain would force the polymer into a linear configuration rather than a cross linked polymer. Figure 2.2 illustrates this effect. These linear polymer chains adopt random coil configurations. The hydrocarbon chains are divided equally on both sides of the polymer chain, however the hydrocarbon chains themselves are randomly coiled, although at low temperatures the trans configuration (with the 2 parts of the carbon chain on opposite sides) is favoured (Vidan and Leblanc, 1998). Research carried out on Octadecyltriethoxy Silane molecules

bonded to a silica surface, indicated that below 40°C, 80% of the C-C bonds of the hydrocarbon chain were trans, and the remaining 20% were disordered and were constantly exchanging between the trans and gauche configurations (Cheng *et al*, 1996).

In this work the ODTMS used was supplied by Sigma -Aldrich chemicals, 90% purity, and used without further purification. Being moisture sensitive it was stored in a nitrogen or Argon atmosphere dry box. Physical data for ODTMS is shown in table 2.1 The toxicity of silanes are generally thought to be low (Lenga, 1988), however the usual laboratory precautions should be taken in handling this material. Silanes may cause irritation on contact with skin and may be a respiratory irritant.

Table 2.1 Physical data for ODTMS

FORMULA	$CH_3(CH_2)_{17}Si(OCH_3)_3$
APPEARANCE	Colourless liquid
FORMULA WEIGHT	374.69
MELTING POINT	16-17°C
FLASH POINT	140°C
REFRACTIVE INDEX	4390
DENSITY	$0.883gcm^{-3}$
SOLUBILITY	toluene, benzene

2.6 FLUORINATED SILANE COUPLING AGENTS

2.6.1 The Hydrophobic Properties of Fluorocarbons

Saturated fluorocarbons are even more hydrophobic than hydrocarbons and also show oleophobic properties (oil repelancy). For this reason they are widely used in polymers for producing non stick and water proof surfaces. These properties can be explained by considering the nature of fluorine, and in particular the fluorine carbon bond. Fluorine is the most electronegative element which accounts for the C-F bond being very strong. The strength of each C-F bond increases the more fluorine that is bonded to one carbon. A bond energy of 484kJmol^{-1} is given for a C-F bond in CF_4, whilst the C-H bond in CH_4 is quoted as 416kJmol^{-1} (Yoshino & Teranaka, 1997). The bond length also shortens. It is possible to pack all the fluorine's necessary to produce a saturated fluorocarbon with no overcrowding. This would not be possible with chlorine for example. The increased size of the fluorine atoms in comparison to hydrogen, means that the carbon backbone is well shielded from chemical attack. The covalent radius of fluorine is 0.72Å, whilst that of hydrogen is only 0.37Å (Shriver, Atkins & Langford, 1990, 68). This shielding effect accounts for the highly inert behaviour exhibited by fluorocarbons with respect to chemical attack. This inherent stability also accounts for the low boiling points in comparison to equivalent hydrocarbons, and the very low inter-molecular forces. In liquid phase fluorocarbons are usually immiscible with polar species (such as water) and also most hydrocarbon based organic molecules (Tatlow, 1979). The hydrophobicity of fluorocarbons with more than six carbons, is due to these very weak intermolecular forces causing a very low surface free energy (Fielding, 1979).

XRD studies were carried out on the perfluoro n-alkane, n-$C_{16}F_{34}$ to ascertain the molecular geometry of fluorocarbons. It was found to have a zig-zag carbon chain (trans conformation), but twisted to relieve the repulsion's between fluorine's on alternate carbon atoms. A full rotation of 360° was achieved with a 26 carbon chain (Tatlow, 1979).

2.6.2 Fluorinated Silane Coupling Agents

Recently there has been a great interest in synthesising fluorocarbon silane coupling agents to use as surface active agents. They are desirable for the properties described above, that is, the hydrophobic and olephobic properties that they can confer on a surface. A variety of differing fluorocarbon silane coupling agents are mentioned in the literature. They all tend to be bonded to the silane group via the $-CH_2CH_2-$ hydrocarbon linkage. This is related to an alkene group being used in the synthesis of such silane coupling agents (Yoshino *et al*, 1992, 1994a, 1995, 1996, Sawada *et al*, 1991). Fluorocarbons such as the straight chain perfluoroalkyl groups, $CF_3(CF_2)_nCH_2CH_2-$, and the branched $(CF_3)_2CF(CF_2)_nCH_2CH_2-$ have all been used in silane coupling agents (Yoshino *et al*, 1993a, 1994a, 1996, 1997). Other groups used are perfluoroalkyl phenyl groups such as $C_8F_{17}(C_6H_4)C_2H_4Si(OCH_3)_3-$, which have the advantage of being more soluble in hydrocarbons (Yoshino *et al*, 1995), and coupling agents with two fluorocarbon chains such as $C_3F_7(CH_2CHSi(OCH_3)_3)C_3F_7$ (Sawada *et al*, 1991). Silane coupling agents with either three methoxy groups, two methoxy groups and one methyl group, or three isocyanate (NCO) groups bonded to the silicon have been synthesised (Yoshino *et al*, 1993a,b, 1994a,b, 1996).

Fluorocarbon silane coupling agents have been applied to oxide surfaces such as silica and the hydrophobic and oleophobic properties of the films formed have been tested. It has been showed that the longer the fluorocarbon chain, the more hydrophobic the surface produced (Yoshino *et al*, 1996, 1997). It was shown that a minimum concentration of 0.015M polyfluoroalkylsilane was neccessary to maximise the hydrophobicity of an oxide surface (Yoshino *et al*, 1993).

2.6.3 1H,1H,2H,2H-Henicosafluorododecyltrimethoxysilane (HFTMS)

In this work, 1H,1H,2H,2H-Henicosafluorododecyltrimethoxysilane, (HFTMS), $C_{10}F_{21}C_2H_4Si(OCH_3)_3$, was chosen to test as a surface modifying hydrophobing treatment for archaeological iron. This silane was synthesised by Yoshino *et al* (1993) and tested on glass plate for its hydrophobic and oleophobic properties. A surface more hydrophobic than polytetrafluoroethylene (PTFE) was produced with this surface treatment, which also performed better than the equivalent dimethoxymethylsilane. This may be due to closer

packing of the trimethoxysilane due to the formation of siloxane networks, in a similar manner to hydrocarbon silanes (Arkles, 1977). This arrangement is illustrated in figure 2.3. AFM studies of a glass surface modified with this silane were carried out and showed that a 59Å, double layer or a 89Å triple layer of the silane had formed at the glass surface (Yoshino, 1994b). Figure 2.4 illustrates the conformation of these bilayers (Yoshino *et al*, 1997). The modified surface showed good stability and resistance to oxidation in testing with hot concentrated nitric acid.

Figure 2.3 Model of silane modified silica surface

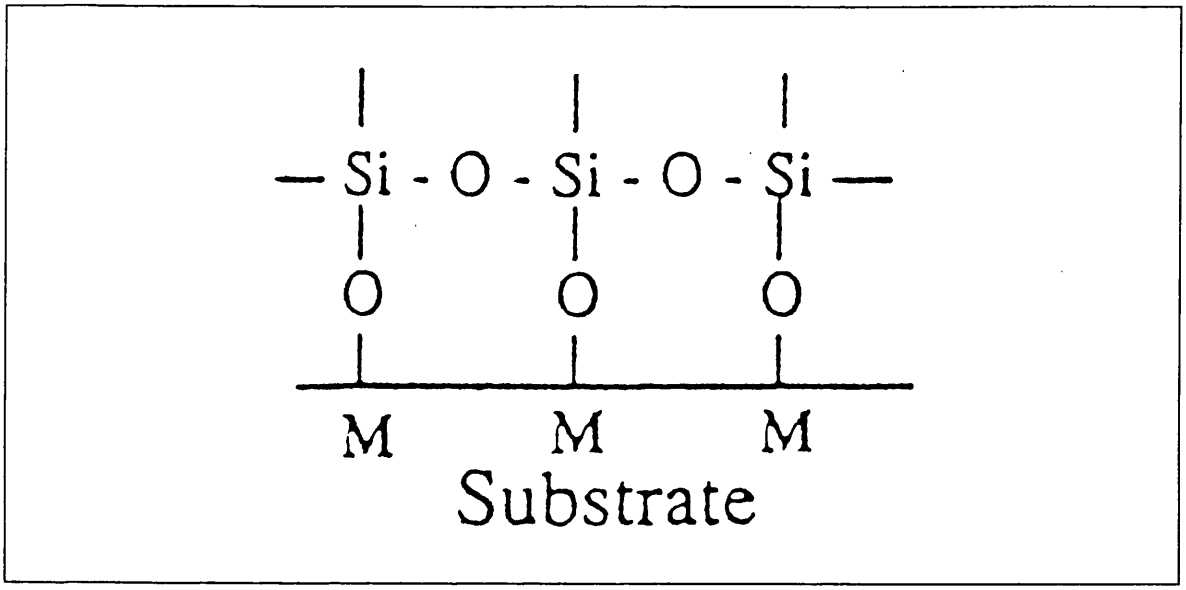

Figure 2.4 Proposed model of glass modified with $CF_3(CF_2)_nCH_2CH_2Si(OCH_3)_3$ (Yoshino et al, 1997)

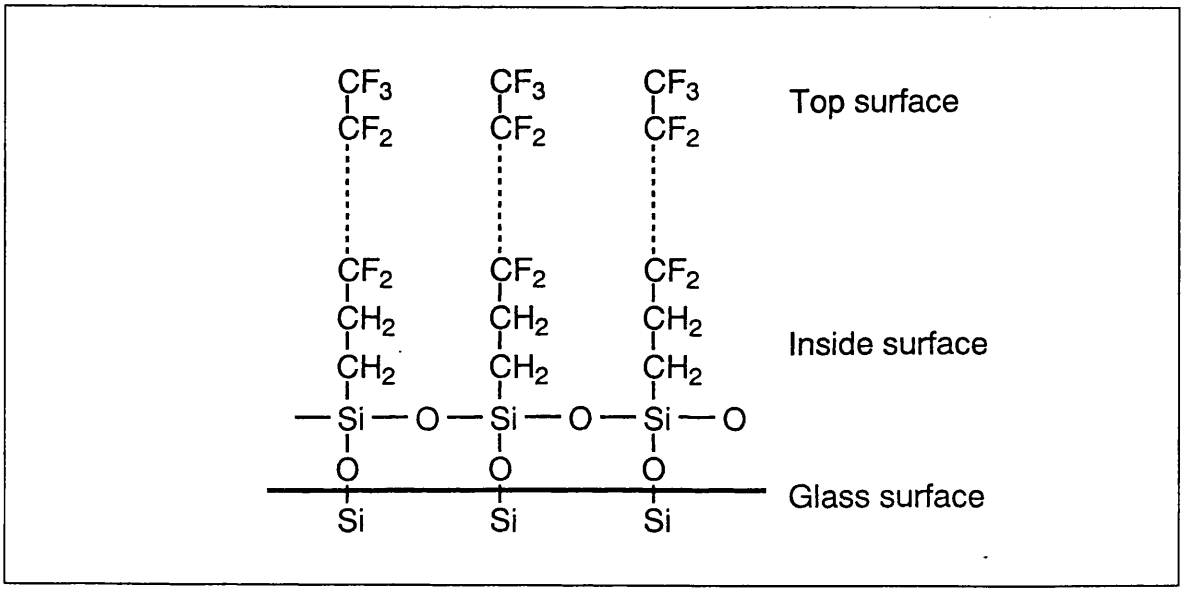

This silane coupling agent has been tested as a surface modification treatment for dentures (made of polymers with silica filler), to provide a contamination free surface (Yoshino *et al*, 1993b). A 0.03M solution in the fluorinated solvent F-113 was used. Surface modified dentures were tested over a four month period of normal use. The modified samples showed a significant improvement after four weeks. Studies were also performed on surface modification of metals, giving a highly water repellent surface (Yoshino *et al*, 1997). Physical data for HFTMS is shown in table 2.2.

Table 2.2 Physical data for HFTMS

FORMULA	$C_{10}F_{21}C_2H_4Si(OCH_3)_3$
APPEARANCE	Colourless Liquid
FORMULA WEIGHT	668
BOILING POINT	93-94°C/53 Pa
SOLUBILITY	F-113

The HFTMS used in this work was provided by Dr Norio Yoshino, Tokyo University. 5ml ampoules contained 0.015M and 0.03M solutions of HFTMS in F-113, fluorinated solvent (1,1,2 trichlorotrifluoroethane, $CF_2ClCFCl_2$). No toxicity or safety data was available for the polyfluoroalkylsilane, however it is likely to have the low toxicity of most other silanes. Similar precautions to those suggested for ODTMS should be taken.

2.7 TITANATE COUPLING AGENTS

2.7.1 Introduction

Titanium, as with silicon can form organofunctional compounds, known as titanate coupling agents. They are used in a similar way to silane coupling agents. They are molecular bridges between inorganic oxides and organic polymers. Titanate coupling agents were developed in the 1980s and were at one time found superior to silane and other coupling agents in some composite systems (Monte, 1983). They are used widely as coupling agents in fibre reinforced composites (Monte, 1978, 1985). Like silane coupling agents they react with surface hydroxyl groups on inorganic oxides and form an organic monolayer on the surface. The organic group may have various properties enabling it to react with an organic polymer interface. Titanate coupling agent treated surfaces will become hydrophobic (Monte & Sugerman, 1981) and often able to withstand high temperatures and humidity as well as improving the impact strength and mechanical properties of the systems they are used in (Monte, 1988a, 1988b). Titanate coupling agents have also been used to coat aluminium nitride powder, to improve the stability of dispersions used in polyolefin based ceramic injection moulding formulations (Liao *et al*, 1995).

2.7.2 Chemical Structure of Titanate Coupling Agents

The general formula of titanate coupling agents can be given as $(RO)_m$-Ti-$(O\text{-}X\text{-}R\text{-}Y)_n$ where RO- is a hydrolysable alkoxy group such as CH_3O- OR $(CH_3)_2CO$-, X is an organic functional group which will have an effect on the chemistry of the compound and the way it reacts with the other substrates. This could be a carbonyl, sulphonyl, phenolic, phosphate, pyrophosphate or phosphine group. R will be an alkyl group, most often a long carbon chain. Y may be an organic functional group that can react with the organic surface the molecule is to be coupled to. This can be a methacrylate or an amine. The numbers that m and n represent can be 1, 2, or 3, depending on the number of organic chains required on each coupling agent molecule.

Titanate coupling agents react in a similar way to the silane coupling agents previously described. They react with hydroxyl groups on inorganic oxide surfaces resulting in a reaction such as:

$$(RO)\text{-}Ti\text{-}(O\text{-}X\text{-}R\text{-}Y)_3 + M\text{-}OH \rightarrow M\text{-}O\text{-}Ti\text{-}(O\text{-}X\text{-}R\text{-}Y)_3 + ROH$$

The new chemical and physical properties of the surface will be determined by the nature of the -X-R-Y groups, now present at the surface. The tetravalent titanium can act as an electron donor or acceptor and can therefore catalyse reactions, such as the rearrangement and redistribution of the molecular structure of a polymer phase (Monte and Sugerman, 1988a). The X group may also participate in bonding with the inorganic oxide surface.

2.7.3 The Use of Titanate Coupling Agents for Corrosion Inhibition and Conservation of Archaeological Iron

Titanium coupling agents have been tested and used as corrosion inhibiting treatments (Monte & Sugerman, 1985), both on clean metals, and as a primer for metals that are to be painted. Several titanates, were tested as inhibitors for carbon steels and aluminium (Monte & Sugerman, 1988). The monolayer of coupling agent formed an effective passive film and was shown to inhibit corrosion. The coupling agents tested were the monoalkoxy titanates, titanium IV 2-propanolato, trisisoctadecanoato-0 titanium IV 2-propanolato, trisdioctylpyrophosphato-0 titanium IV 2-propanolato, tris[2,-((2-amono-ethyl) amino)-ethanolato-0], and the neoalkoxy titanates, titanium VI neoalkenolato tris(dioctyl)phosphato-0, titanium VI neoalkenolato tris(dioctyl)pyrophosphateo-0, and titanium VI neoalkenolato tris(2-ethylenediamino)ethylato (Monte and Sugerman, 1988).

Titanates have been tested for use as a surface modifying treatment for the conservation of archaeological iron. Kaneko suggested the use of the titanate isopropyltriisostearoyl titanate (TTS). He tested its performance on FeOOH powder and found it to be effective for the hydrophobing of iron oxyhydroxide surfaces (Kaneko, 1989). Al Ahmed (1992), tested both silane and titanate coupling agents on high and low chloride content corroded iron artefacts. The titanates were found to offer superior protection to the silanes, whose use has already been discussed in section 2.5. Two titanates were tested, isopropyltri(dioctyl)pyrophosphatotitanate (KR38S) and isopropyltriisostearoyltitanate

(KRTTS). 0.05M solutions in toluene were used to treat iron objects. Both were found to provide some protection from corrosion. With marine iron objects containing high concentrations of chloride ions the treatments were found to be less effective. In these cases, additional fluoride washing treatments were found to be a more important factor in the stabilisation of the iron. It seems that for marine iron some sort of desalination was still required. The treatment however seemed a very useful one to assist in further stabilisation of iron objects. The titanates were found to have little effect on colour and no effect on metallurgical structure due to the low temperatures used in the treatment. Other materials such as leather, bone, textile, and wood seemed unaffected by the treatment which was cheap and easy to perform.

2.7.4 Titanium IV, 2-propanolato, tris isooctadecanoato-0 (Isopropyl triisostearoyltitanate) - (TTS)

In this work is was decided to continue testing the previously used titanate, isopropyltriisostearoyltitanate, known as Ken React TTS (KRTTS). This was found to be the most successful surface modification treatment tested for archaeological iron (Al Ahmed, 1992, Kassianidou, 1994) and was therefore used to compare the other treatments tested in this work.

Table 2.3 Physical data for TTS

FORMULA	$CH_3.CH.CH_3OTi(OCO.C_{17}H_{35})_3$
APPEARANCE	transparent reddish brown liquid
VISCOSITY	50-200cps @ 25°C
SPECIFIC GRAVITY	0.95 ± 0.02 @ 16°C
FLASH POINT	93.3 °C
BOILING POINT	300°F
SOLUBILITY	isopropyl alcohol, xylene, toluene at less than 5%, and mineral oil

KRTTS, $CH_3.CH.CH_3OTi(OCO.C_{17}H_{35})_3$, was designed originally for use as a dispersant for zinc oxide in naphthenic oil and mineral fillers in polyolefins. It use has now expanded

to many other applications, such as an adhesion promoter in epoxy/copper/fibreglass printed circuitboards, a dispersant in carbon black for photocopier toner, and metal primers and corrosion inhibitors. Most recently this coupling agent has been used to strengthen the interface between carbon fibres and the matrix phenolic resin material in carbon fibre reinforced carbon composites, used for ultra-high temperature applications, such as space craft and hydrogen combustion gas-turbine blades (Iwashita *et al*, 1995).

The TTS used in this study was obtained from Kenrich Petrochemicals Inc (KRTTS) and was 95% pure. It was used with no further modification. The physical data on KRTTS is shown in table 2.3

Safety data provided by Kenrich Petrochemicals states that KRTTS presents little or no immediate significant hazard if spilled and no unusual hazard if involved in a fire. Upon thermal decomposition it may emit toxic fumes. The substance has the potential of being a respiratory tract irritant and prolonged or repeated skin contact may cause skin irritation. Contact with eyes may cause irritation and swallowing may be harmful. The long term health effects are not known.

2.8 LONG CHAIN ALIPHATIC AMINES

2.8.1 Introduction

The inhibiting effect of amines on iron and steel has been known for many years. Both aromatic and aliphatic amines show inhibiting properties. They belong to the organic or adsorption class, and are mixed inhibitors, inhibiting both the anodic and cathodic reactions. The mechanism by which they inhibit involves the chemisorption of the amine nitrogen onto the metal surface (Jones, 1992). Amines are used to inhibit in the pickling and acid cleaning of mild steel in hydrochloric acid. Examples of amines commonly used as inhibitors include Octylamine, $C_8H_{17}NH_2$, (Muralidhoran *et al*, 1994), Cetyltrimethyl ammonium bromide, $[CH_3(CH_2)_{15}](CH_3)_3N^+Br^-$, (Malik, 1995) and pyridines (Andropov, 1974).

2.8.2 The Structure and Inhibitive Mechanism of Amines

Amines have the formula NR_3. They can be subdivided into primary, $R\text{-}NH_2$, secondary, $R_2\text{-}NH$ or tertiary R_3N amines. Amines can be aliphatic or aromatic, where the nitrogen forms part of the aromatic ring. The properties of amines are often associated with the lone pair of electrons on the nitrogen, that can form co-ordinate bonds to other atoms.

Studies of the comparative inhibition of primary, secondary and tertiary amines have been carried out (Andropov *et al*, 1972, 1974). A connection between the electron donor properties of the nitrogen and the inhibiting capability of the amine was found and this therefore suggests the direct participation of the nitrogen in the formation of a bond between the inhibitor and the metal. The above also means that inhibiting properties are a direct function of the basicity of an amine. With amines of equal pK_a the protective effect of the amines diminishes in the order

$$R_3\text{-}N > R_2\text{-}NH > R\text{-}NH_2$$

This is due to the ability of tertiary amines to mechanically 'shield' the metal surface. With amines of high pk_a however differences are evened out as the electron donor properties play a much larger part in the inhibition mechanism.

Pyridines and diamines have also been studied (Andropov, 1974). It was found that the introduction of electron donor substituents on the pyridine molecule results in an increased inhibition, so 2-methylpyridine is a better inhibitor than pyridine itself. Diamines are better inhibitors than pyridines as the two amine groups can adsorb simultaneously on the metal surface giving a stronger amine-metal interaction (Andropov, 1974).

Aromatic amines such as aniline have also been studied with respect to corrosion inhibition (Banerjee & Malhotra, 1992). It has been found that they act by adsorption of several types of species. If the metal surface is positively charged, chloride ions will be adsorbed and then the inhibitors nitrogen will adsorb, giving a layer of perpendicular anilinium ions. If the metal is negatively charged the nitrogen of the protonated aniline will adsorb directly onto the surface. At zero charge the aromatic ring will be physisorbed to the metal surface through its' π orbitals (Banerjee & Malhotra, 1992).

2.8.3 Amines in Conservation

The use of amines to treat archaeological iron has often been suggested. Walker (1982) noted that organic inhibitors such as straight or chain amines may be advantageous as they are organic molecules, and may be more easily removed, making the treatments reversible. He also states that amines with C_{16} or C_{18} chains have been found to give about 80% inhibition at a concentration of 100 to 200 ppm for steel in sea water.

James Argo carried out work on using the amine ethylenediame as a corrosion inhibitor for the washing of archaeological iron in aqueous solution. He suggests that the amine chemisorbs onto iron corrosion product and inhibits corrosion by forming a hydrophobic surface (Argo, 1985). This inhibition allowed the washing away of chloride ions from an average of 9600ppm to 150ppm. A treatment for iron was devised consisting of immersing the iron in a bath of 5% ethylenediamine in water at 70°C for 7-10 days, and then repeating this procedure with successive solutions for 50-60 days in all. The objects are finally removed and washed in water and acetone. This method was found to be successful, with only 4% of objects treated becoming unstable (Selwyn & Logan, 1993).

Amines are widely used as corrosion inhibitors in industry, however many aromatic amines are highly toxic (Lunn & Sansone, 1994) and their use would not be favoured by conservators. Aliphatic amines are not toxic and there is much scope for further research into their use as inhibitors in washing solutions and as protective surface treatments

2.8.4 Long Chain Aliphatic Amines

Long chain aliphatic amines are often used as corrosion inhibitors. These are amines where the R groups is a long hydrocarbon chain from C_3 upwards. The comparative abilities as the chain length increases from $C_3H_7NH_2$ to $C_{11}H_{23}NH_2$ has been studied (Braun *et al*, 1993). In this study inhibition was found to increase with increasing amine chain length up to about 10 carbons. Little further improvement in inhibiting capability was found between 11 and 14 carbons. The longer the chain the more hydrophobic the amine therefore allowing less water to penetrate to the metal surface. The amine is thought to be attached to the metal surface through the nitrogen or via hydrogen bonding (Braun *et al*, 1993).

High molecular weight aliphatic amines (C_{16}-C_{18} amines) have been used as corrosion inhibitors, but they are insoluble in aqueous solution and so must be dissolved into solvents such as kerosene and added to aqueous solutions with small amounts of non-ionic surfactants (Fujii & Aramaki, 1960). Such amines are commonly used as inhibitors in steam boilers at concentrations of 1-3ppm (Jones, 1992).

Experimentation with additional side chains to the hydrocarbon was undertaken by Fujii & Aramaki (1960). Long chain amines were reacted with long chain carboxylic acids to make complex compounds. Differently branched hydrocarbon chains on the amines were compared. The anti-corrosivity was found to increase as the side chain moved further from the nitrogen adsorption site. Branches attached near the nitrogen would hinder the ability of the inhibitor to adsorb on the metal surface compactly. The branches attracted solvent molecules and therefore increased the inhibitive effect.

Some studies into the adsorptive properties of iron oxides modified with long chain amines such as octadecylamine have been made (Dernovaya *et al*, 1993). When γ-Fe_2O_3 was

treated with octadecylamine a considerable decrease in the number of adsorption sites available on the oxide surface was found. This was with respect to the adsorption of hydrocarbons such as hexane, octane and benzene, and polar molecules such as nitromethane and ethanol. The surface properties of other minerals such as $Mg_3Si_4O_{16}(OH)_2$ (Talc) have also been modified with octadecylamine (Li *et al*, 1993). The treatment increases the hydrophobicity of the minerals' surface. The adsorbed amines were found to be attached with their nitrogen atom to the surface and the hydrocarbon tails orientated distally. Up to a monolayer coverage was reported. Dodecylamine chloride was used to treat china clay, kaolin (a mixture of 70% kaolinite ($Al_2(OH)_4Si_2O_5$), 12% quartz (SiO_2), and 18% mica ($KAl_2(OH)_2(AlSi_3O_{10})$). The treatment made the surface more hydrophobic, at coverage of less than a monolayer. As little as 0.125 dodecylamine chloride monolayer drastically changed the wetting conditions for water, the surface becoming unwettable (Jańczuk *et al*, 1990). Studies of docecylamine adsorbed onto galena (PbS) and fluorite (CaF_2) have also been carried out. Impedance measurements were used to differentiate between this physisorption and other molecules that chemisorbed onto the mineral's surfaces (Bessière *et al*, 1995).

Long chain aliphatic amines were selected to test as a surface hydrophobing and corrosion inhibiting treatment in this work. Their effectiveness was compared to the titanate treatment already investigated (Al Ahmed, 1992). It was considered that the smaller size of the nitrogen group may allow a closer packing of the surface hydrocarbon chain layer than in the case of TTS and therefore provide a more hydrophobic barrier. Micale *et al* experimented with large silane type coupling agents and the smaller molecule methanol. On γ-Fe_2O_3 and γ-FeOOH surfaces, the cross sectional area of a surface hydroxyl group was taken to be $10Å^2$, whereas each trimethylsilicon group on the surface (the result of adsorption of hexamethyldisilazane) take up $30\text{-}40Å^2$. Therefore by this calculation only a third of the surface hydroxyl groups could be blocked by the silane (Micale and Pendleton, 1988). Methanol being much smaller can give a greater surface coverage. An activation temperature of 400°C was used and a surface hydroxyl concentration on α-Fe_2O_3, of less than 1 hydroxyl group per $100Å^2$ was found after the treatment as compared to 7.8 hydroxyl groups per $100Å^2$ before the treatment. The silane treatment could reduce the hydroxyl concentration to 4.9 (with heating to activate) hydroxyl groups per $100Å^2$

(Micale *et al*, 1985). The principle is therefore illustrated - a molecule with a smaller cross section may be better able to hydrophobe a surface. To this end it was proposed to test long chain aliphatic amines. The adsorption of these onto the iron oxide surface may provide a more compact hydrophobic layer with long hydrocarbon chains close packed.

Such close packed films of long chain amines have been reported as crystalline Langmuir-Blodgett (LB) films. These are monolayer films that are spread out on an aqueous surface in an organic phase such as chloroform, and then transferred to a solid surface using a constant perimeter trough. n-Alkyl amines with chains of 18 or fewer carbons have formed monolayers. Multilayers of amines such as n-docosylamine have also been formed using the LB techniques (Gaines, 1982, Ganguly *et al*, 1993).

Figure 2.5 Crystal structure of $(C_{10}H_{21})_2MnCl_4$ viewed as a bilayer

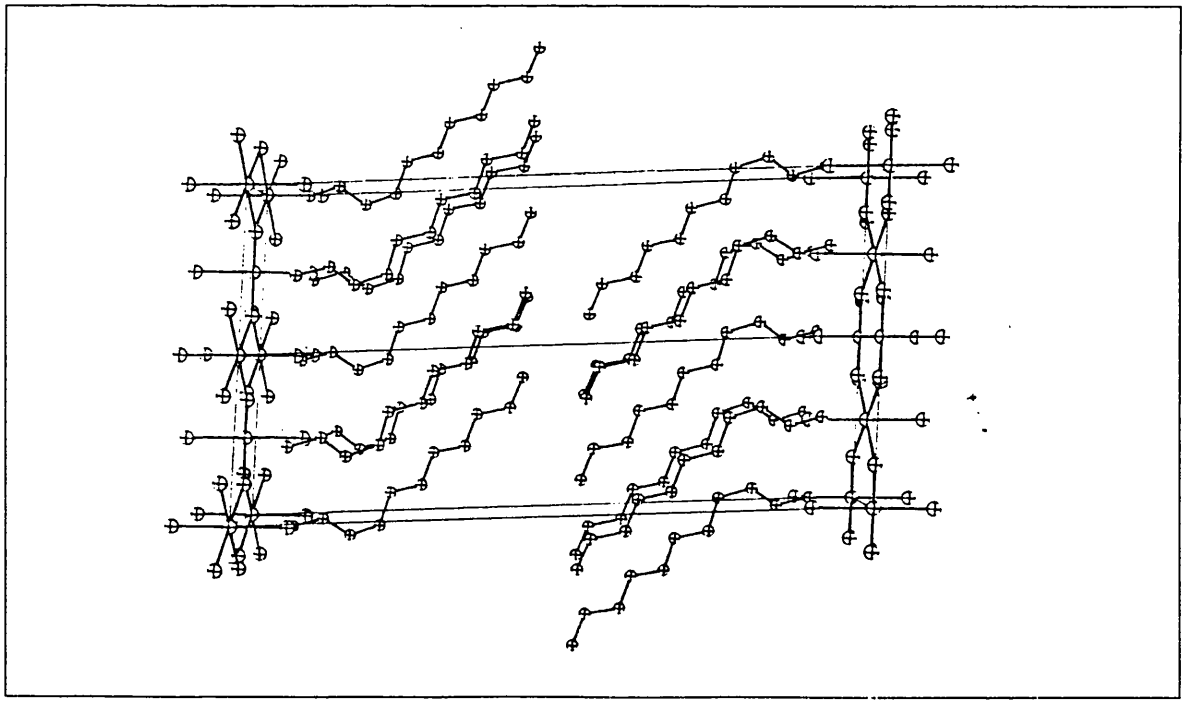

Solid compounds have also been reported that contain arrays of long chain amines with the hydrocarbon chains close packed. These are often quasi-two dimensional systems with bilayer structures. A series with the formula $(RNH_3)_2MX_4$ has been synthesised where R is a long chain hydrocarbon. The compounds have been synthesised with several divalent transition metals such as Mn^{2+}, Fe^{2+}, Cu^{2+}, Co^{2+}, Hg^{2+}, Zn^{2+} and Cd^{2+} (Needham *et al*, 1984, Willet *et al*, 1973). The metal halide portion is octahedrally coordinated giving two

dimensional perovskite type sheets of corner sharing octahedra. The ammonium group is hydrogen bonded to a chloride ion, holding in place the hydrocarbon tails which stack together. A diagram illustrating such a compound is shown in figure 2.5. The hydrocarbon chains are arranged in the trans configuration except for a gauche bond at the C_1-C_2 or C_2-C_3 bonds where the chain is attached to the nitrogen. This causes the chains to be inclined at an angle of 40° from the normal to the lattice (Needham *et al*, 1984). The lattice of tantalum sulphide TaS_2 has also been synthesised with intercalated octadecylamine layers lined up within the crystal structure. Figure 2.6 illustrates this arrangement (Day, 1983, 310).

Figure 2.6 TaS_2 layer intercalated with Octadecylamine

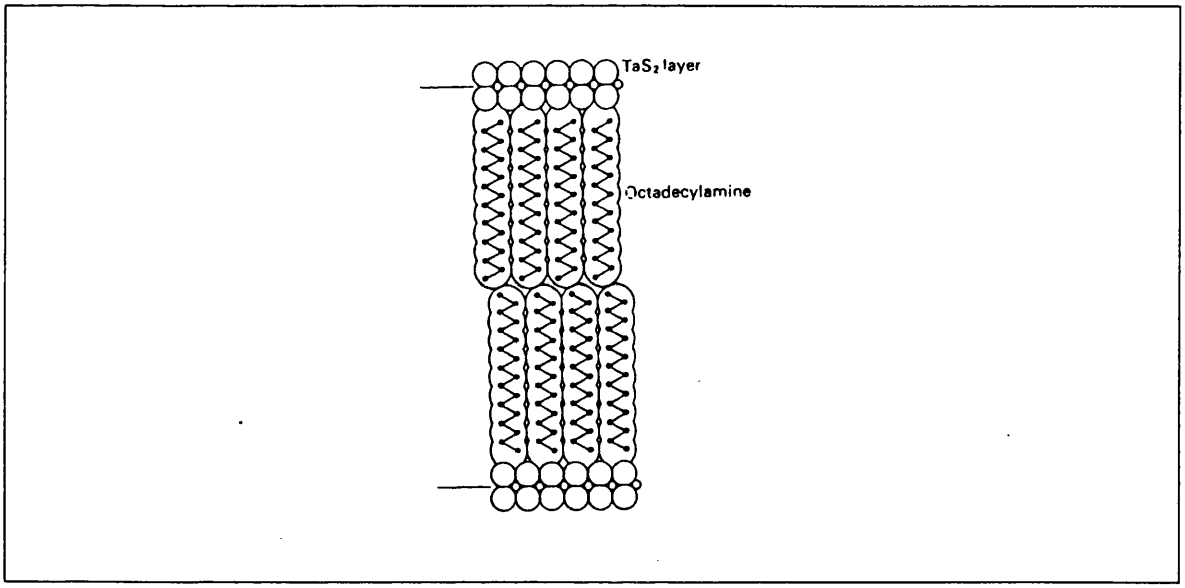

Long chain aliphatic amines combine the inhibitive properties of amines, with the hydrophobic properties of hydrocarbon chains. They may therefore provide a suitable and effective treatment for archaeological iron objects.

2.8.5 Decylamine (DCA) and Octadecylamine (ODA)

The amines tested in this work are from the same homologous series of amines. Decylamine, $C_{10}H_{21}NH_2$, and Octadecylamine, $C_{18}H_{37}NH_2$ were both initially tested. As the hydrocarbon chain length increases the amines change their state from liquid to waxy solids that are insoluble in aqueous solution. The amines used were purchased from

Aldrich and used with no further modifications. Physical data is given in table 2.4. The purity of the Octadecylamine used was 98%.

Both Octadecylamine and Decylamine have moderate to low toxicity. They are caustic in nature and therefore are skin and eye irritants. They are harmful if swallowed, inhaled or absorbed through the skin and can cause burns and respiratory problems. They should be handled with care, using protective gloves and clothing (Lenga, 1988).

Table 2.4 Physical properties of decylamine and octadecylamine

NAME	*DECYLAMINE*	*OCTADECYLAMINE*
SYMBOL	DCA	ODA
FORMULA	$C_{10}H_{21}NH_2$,	$C_{18}H_{37}NH_2$
FORMULA WEIGHT	157.30	269.52
MELTING PT/BOILING PT	12-14°C/216-218°C	55-57°C
DENSITY	0.787g/ml	0.777g/ml
FLASH POINT	85°C	110°C
COLOUR/APPEARANCE	Colourless liquid	White waxy solid
SOLUBILITY	water, alcohol, benzene, ethanol, acetone	toluene, benzene, ethanol

CHAPTER THREE

Coupons for Corrosion Testing

3.1 INTRODUCTION

Corrosion inhibitors and other treatments are often tested on archaeological material to assess their success in stabilising objects and there suitability as conservation treatments (Al Ahmed, 1993, Kassianidou, 1994). The action of corrosion inhibitors as described in chapter two, are particular to a metal and set of conditions in which the inhibitor is to be used. Although many assessments of the performance of inhibitors can be found in the literature, it is essential to test an inhibitor in the conditions it is to be used, to gain any comparative information on the performance of different inhibitors. Tests on archaeological material suffer from the variability of the material used in the tests. The variability in archaeological materials means that large numbers of objects must be tested to produce meaningful results. It is not always possible to obtain such a quantity of archaeological material, especially as the testing procedures may be destructive.

After some initial accelerated corrosion tests on archaeological iron, it was decided to attempt the production of iron test coupons for corrosion testing. The use of coupons of uniform size and shape for corrosion testing is widespread in industry (Carter, 1982). Their use allows a standard testing procedure from which the performance of many different treatments can be assessed. However, in industry corrosion tests are carried out on polished and clean metal surfaces, which differ greatly to the surfaces of archaeological objects.

Previously coupons for testing corrosion inhibitors for archaeological copper artefacts have been prepared with copper corrosion products on their surface that model the type of corrosion products found on corroded copper artefacts (Faltermeier, 1995). It was decided

to synthesis similar pre-corroded coupons from iron to be used in accelerated corrosion testing of the various surface treatments described in the previous chapter. The corrosion products found on archaeological iron have been described in section 1.4 They are numerous and vary in accordance with the burial conditions of the archaeological object. The most damaging phase to the future stability of an object has been found to be the β-FeOOH phase and it was therefore decided to produce coupons containing this oxide in the corrosion product layer formed on the coupon surface. The production of a pre-corroded coupon would provide a standardised material on which corrosion testing could be carried out.

3.2 POWDER X-RAY DIFFRACTION (XRD)

This technique was used to characterise the corrosion products formed on coupons. Different compounds existing within the corrosion products can be identified by comparing results with the literature. The technique works on the principle that X-rays are diffracted when passed through a crystal as their wavelengths are comparable to the separation of crystal lattice planes. If crystal lattice planes are regarded as a reflective surfaces, each one separated from the next plane by the distance d, constructive interference will occur only at specific angles of the incoming X-ray beam. An equation relating these properties, known as the Bragg Equation is given as follows:

$$\lambda = 2d \sin \theta$$

This means that a specific crystal lattice will have a characteristic X-ray diffraction pattern. XRD can be carried out on powders as well as single crystals. A monochromatic X-ray beam is used. The powder will contain crystals lying in all directions and so the diffracted beam will lie in a cone around the incident beam.

In this work, diffraction patterns were obtained using a Siemens D5000 X-ray diffractometer, with Cu $K_{\alpha 1}$ radiation. Interpretation of data was carried out using the Siemens Diffrac auxiliary programme, version 3.2. Samples were ground to a fine powder and then smeared evenly onto a small piece of transparent tape. This was then covered with another piece of tape. The sealed sample was then loaded into the diffractometer sample holder. Readings were taken over a period of 2 hours. Diffraction patterns were compared to a library of data supplied with the diffractometer.

The diffraction patterns of α-FeOOH and β-FeOOH powders are shown in figures 3.1 and 3.2. The methods of preparation of these powders are given in chapter Five. The diffraction pattern of a sample of the corrosion products produced on pre-corroded coupons is shown in figure 3.3. β-FeOOH can be seen to be present in this corrosion product, although the diffraction patterns of this and the other samples are of low intensity. This may be related to the strong absorption of Cu K_{α} radiation by iron rich phases. The absorption causes a loss of X-ray intensity and a high background due to fluorescence radiation (Schwertmann & Cornell, 1991).

Figure 3.1 Powder diffraction pattern of α-FeOOH

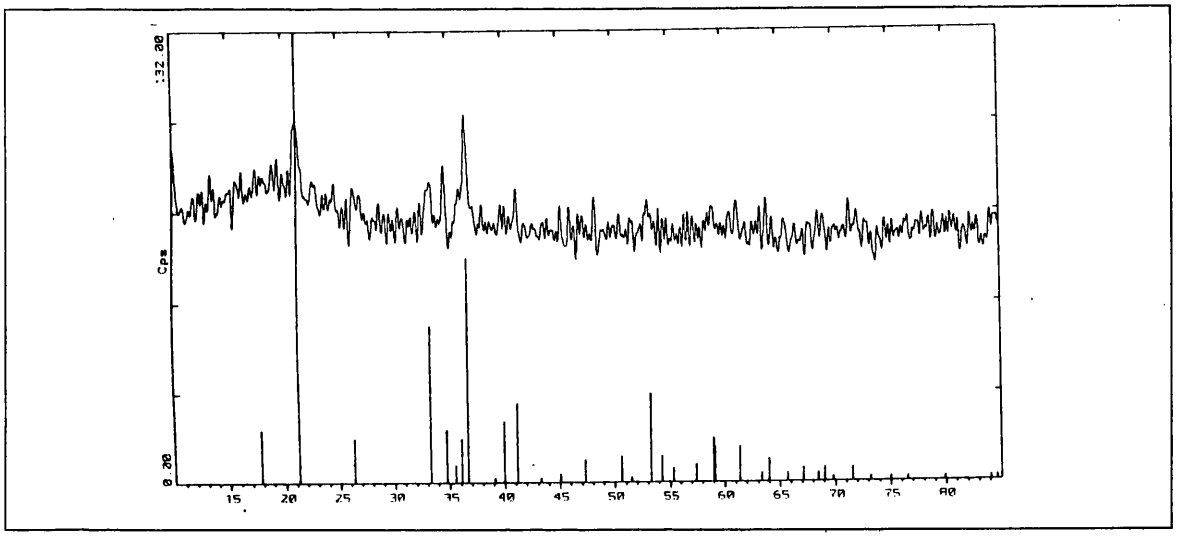

Figure 3.2 Powder diffraction pattern of β-FeOOH

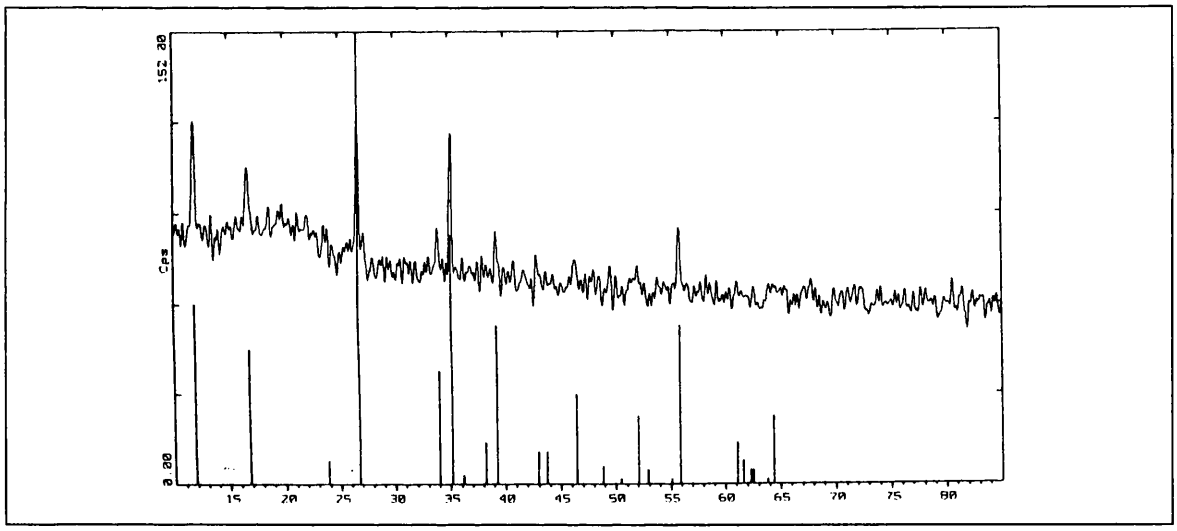

Figure 3.3 Powder diffraction pattern from pre-corroded (Method B) coupon.

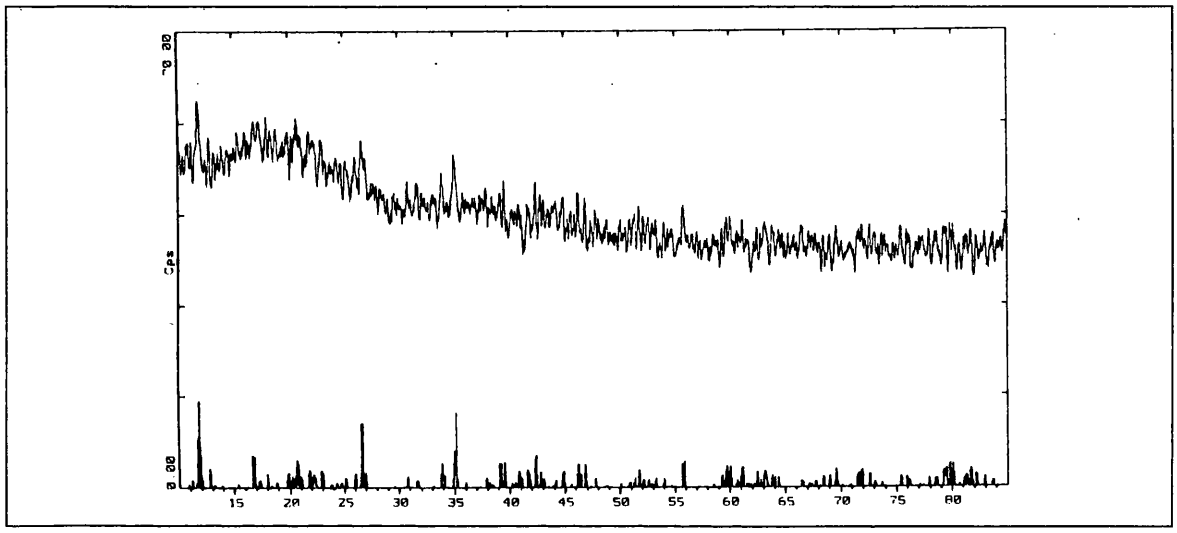

3.3 PRODUCTION OF CORRODED COUPONS

3.3.1 Method A

Coupons were initially made by following the method used by Hjelm-Hansen *et al* (1993) The iron used was purchased from Advent research materials Ltd, in the form of 10cm by 10cm iron sheets of temper hard, 99.5% Purity. These sheets were cut into 2cm by 5cm coupons. To produce the artificial corrosion layer the following procedure, known as method A, was followed:

Method A:

1. degrease the iron coupons in acetone
2. Stand coupons above 1M HCl in a closed desiccator for 1 week partly immersed in a water bath at 40°C.
3. Coupons then removed from desiccator and stored over silica gel before use

This produced an adherent layer of corrosion product and was used in initial accelerated corrosion experiments. However these coupons were very variable in appearance, consisting of corrosion products of varying colour. A dark brown corrosion product was formed on most of the coupons, however spots of black and orange/yellow corrosion products occurred on some coupons. The extent of corrosion also varied depending on the position of the coupon within the round desiccator. This effect was minimised by moving the coupons each day. XRD data was difficult to interpret as much of the corrosion product was amorphous. The most easily identifiable phase was γ-FeOOH. Traces of the oxides γ-Fe_2O_3, Fe_3O_4, and β-FeOOH were also detected

To prepare more evenly corroded coupons, it was decided to use a rectangular tank, rather than the desiccator previously used. A glass tank, 40cm by 25cm by 30cm, was modified as shown in figure 3.4. Glass rods were glued 10cm from the top of the tank to form a support on which the coupons could be placed. 1M HCl could then be poured underneath and a lid placed on top of the tank. The whole tank was then left at 40°C. The coupons were turned over everyday so that the small area in contact with the glass rods was exposed. After 1 week the coupons produced by this method were inspected and found to

be covered by a dark brown uniform corrosion layer. XRD data showed this to be an amorphous corrosion product

Figure 3.4 Glass tank used to corrode coupons

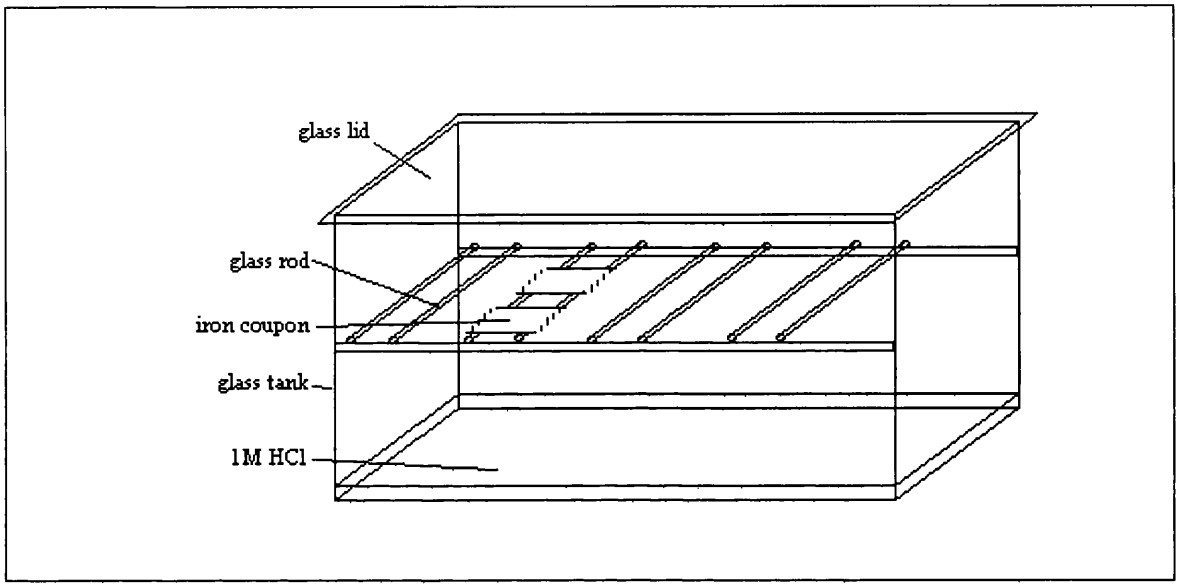

3.3.2 Method B

It was intended to produce uniform artificial coupons that could be used to model the behaviour of archaeological iron, and in particular, the damaging corrosion layer that causes archaeological iron to be unstable. This requires the presence of β-FeOOH. It was therefore necessary to produce coupons with a corrosion layer containing β-FeOOH. Akaganeite, β-FeOOH can be prepared by the hydrolysis of iron (III) solutions containing chloride or fluoride ions (Bernal *et al*, 1959, Nomura *et al*, 1988). Solutions of ferric chloride and Hydrochloric acid when heated within the range 60 to 100°C for up to 2 weeks precipitate β-FeOOH crystals (Matijevic & Scheiner, 1978). The literature also notes its formation by the hydrolysis of FeOCl (Keller *et al*, 1936), precipitation from $FeCl_3$ and K_2CO_3 (Hofer *et al*, 1946) and the damp oxidation of $FeCl_2.4H_2O$ crystals (Mackay, 1960).

It has also been shown that Akaganeite forms from the dry aerial oxidation of β-$Fe_2(OH)_3Cl$ which will precipitate from slightly acidic solutions of ferrous chloride at room temperature (Misawa *et al*, 1971, 1974). Further work has recently been carried out on the

link between β-$Fe_2(OH)_3Cl$ and β-FeOOH and the mechanism of oxidation of β-$Fe_2(OH)_3Cl$ in solution that may lead to the formation of β-FeOOH (Refait & Genin, 1997).

Figure 3.5 Oxidation of β-$Fe_2(OH)_3Cl$

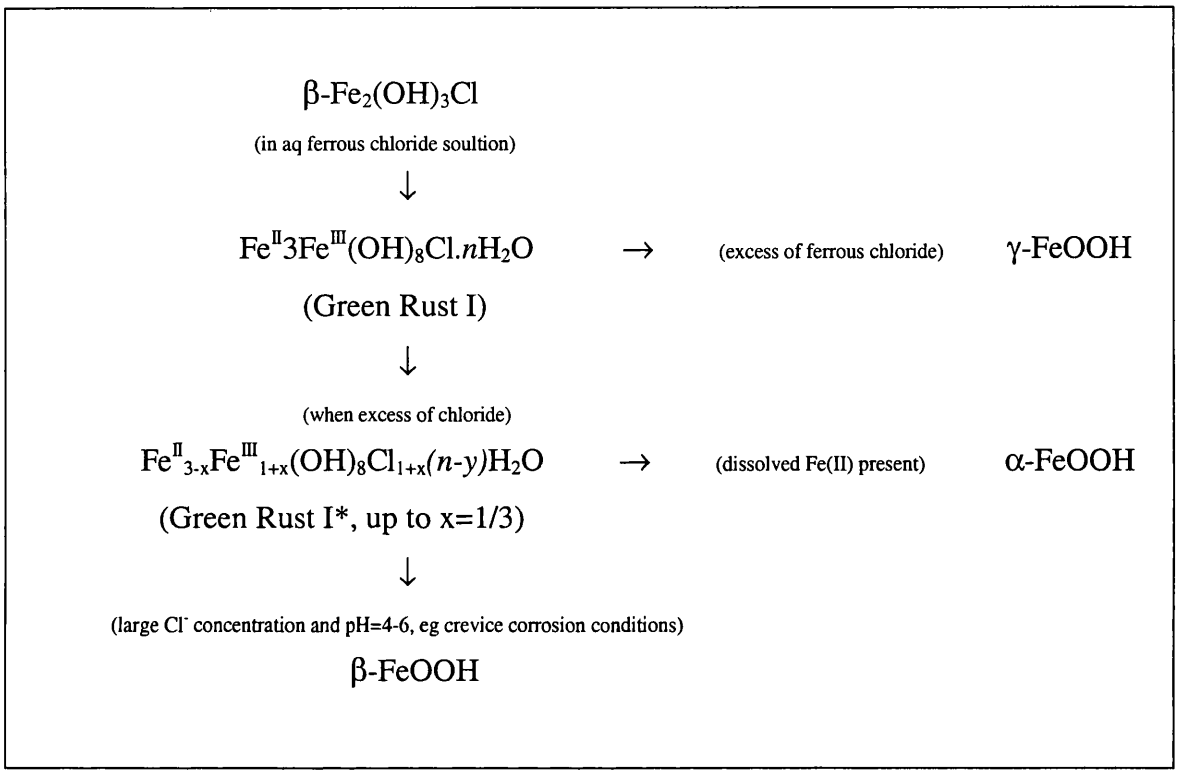

β-$Fe_2(OH)_3Cl$ was discovered by Keller (1948). It has a rhombohedral $Co_2(OH)_3Cl$ structure with a cubic close packed array of anions. Its existence as a mineral has also been confirmed (Springer, 1989). Misawa *et al* have found that β-$Fe_2(OH)_3Cl$ will give rise to Green Rust I complexes in aqueous ferrous chloride solutions (Misawa *et al*, 1969, 1970). Refait and Genin have carried out XRD and Mössbauer spectroscopy on the intermediate species and the final products in the precipitates formed from ferrous chloride and sodium hydroxide solutions. The final product formed will be one or more of the iron oxyhydroxide phases, α, β, and γ-FeOOH. There is a competitive process occurring in the formation of the oxyhydroxides, with differing ferrous to chloride ion ratios favouring the production of different phases oxyhydroxides (Refait & Genin, 1997). A reaction scheme is given in figure 3.5 to show the oxidation of β-$Fe_2(OH)_3Cl$ from the results of Refait and Genin.

This indicates that Akageneite forms with high chloride concentrations, of at least 2 or 3 moles per litre and a pH of between 4 and 6. In practice these are the conditions that occur in localised areas at the interface of metals and corrosion products or in crevices (Refait & Genin, 1997), and therefore the above reaction scheme may account for the production of β-FeOOH in corrosion products, and the observation that β-FeOOH is formed when steel is exposed to a fairly dry atmosphere after having been attacked by air containing HCl or Cl_2 vapour (Handa *et al*, 1985).

Figure 3.6 Reactions Occurring when Iron Corrodes in Sodium Chloride Solution

Initial Reaction:

$$Fe \rightarrow Fe(OH)^+ \rightarrow Fe(OH)_2^+ \rightarrow Fe(OH)_4^- \rightarrow \gamma\text{-FeOOH}$$

When supply of OH- is suppressed:

$$Fe(OH)_2^+ + (2\text{-}x)OH^- + xCl^- \rightarrow [Fe(OH)_{4-x}Cl_x]^- \rightarrow \beta\text{-FeOOH}(Cl_x) + 2H_2O$$

Experimental work has also been carried out to produce β-FeOOH on iron immersed in sodium chloride solutions - as occurs in marine corrosion. Nomura *et al* (1987) found that to produce β-FeOOH on iron coupons within 6 days, a 3% sodium chloride solution in a sealed bath at 45°C was needed. It was found that a low oxygen concentration favoured the production of β-FeOOH as opposed to γ-FeOOH which was formed with higher oxygen concentrations. It seems there is a competition between the inclusion of hydroxide or chloride groups in the Fe(III) complexes formed on corrosion of iron. It is only when the concentration of hydroxide ions is limited by a decreased oxygen concentration, that the β phase is formed. The reaction scheme for the species formed is illustrated as in figure 3.6.

It has been noted that β-FeOOH usually forms on steel present in sea-water for large periods of time, which would fit with the above scheme which would predict the initial formation of γ-FeOOH when hydroxide ions are available. The inner corrosion layers however would eventually be deficient in hydroxide ions due to the restriction of oxygen

supply by the γ-FeOOH layer. Ferric hydroxide species in solution would therefore react with chloride ions present to form β-FeOOH.

Bearing the above literature in mind, a series of tests using different methods were carried out to try and produce coupons with a consistent, even corrosion layer containing β-FeOOH in a short time scale. Each resulting coupon was visually examined and some of the corrosion products were scrapped off for XRD analysis to discover what phases of iron oxide and oxyhydroxide were present. The methods used and resulting appearance and XRD results are given in table 3.1 The coupons used were of the same size and material of those described in method A

The results of the corrosion product test therefore gave rise to an improved methodology for producing uniformly corroded coupons with β-FeOOH present in the corrosion products. The XRD data seems to suggest that coupons corroded in an HCl atmosphere will produce a layer of amorphous, or γ-FeOOH. However when 1M HCl solution is added to the pores of this corrosion product, a proportion of the existing corrosion product re-dissolves, forming a mixed Fe(II), Fe(III), solution containing a high concentration of Cl^- ions. It is likely that β-$Fe_2(OH)_3Cl$ will precipitate out of this solution, and when left to dry in air, β-FeOOH will form, as detected by the XRD results for the corrosion product tests. It is possible that Green Rust I intermediate species form as intermediate stages in this oxidation process (Refait & Genin, 1997). A greenish colouration can be observed in the coupons during the oxidation process, before they finally become brown/orange coloured.

The method used to produce these corroded coupon will be referred to as method B and each stage in the procedure is described below:

Method B

1. Degrease the iron coupons in acetone.
2. Place coupons on glass rods in corrosion tank over 1M HCl solution, place glass lid on tank.
3. Leave coupons at 40°C for 7 days, turning the coupons over every day.
4. Dip coupons in 1M HCl solution, blotting the excess from each side of the coupon.

5. Place coupon horizontally on weighing boat and leave to dry in air, turning the coupon after several hours.
6. Store coupons in a desiccator over silica gel before use.

Figure 3.7 Corrosion Products Test Methods

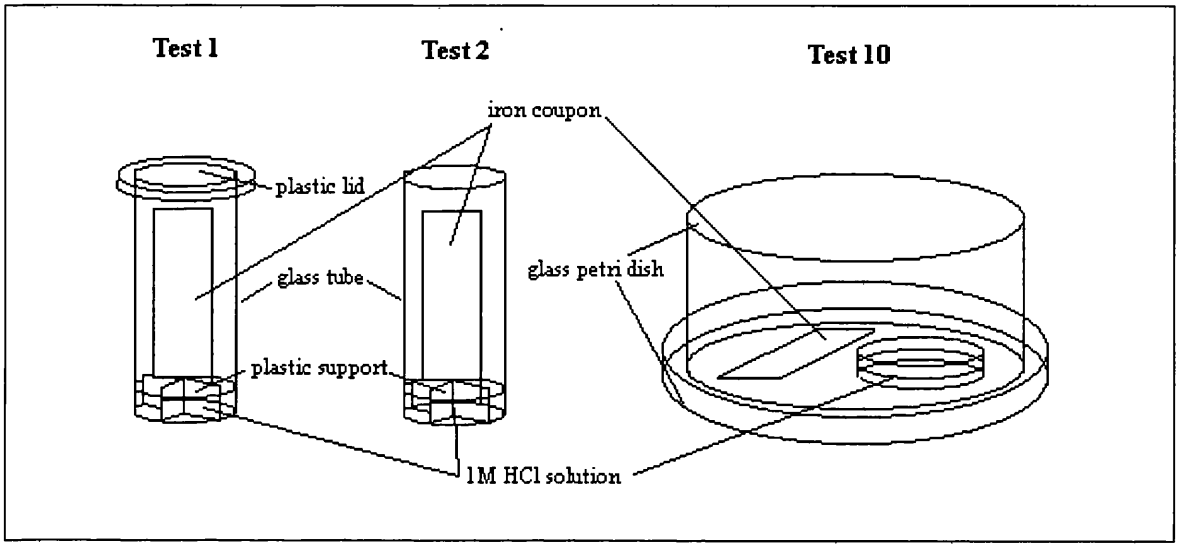

Table 3.1 Corrosion Product Tests

Corrosion Product Test	*Experimental Method*	*XRD and visual inspection results*
TEST 1 (see figure 3.7)	1) Clean coupon placed in sealed glass tube with 1M HCl 2) Left overnight in closed desiccator at 40°C	No consistent corrosion product formed. Corrosion product darker at the bottom end.
TEST 2 (see figure 3.7)	1) Clean coupon placed in open glass tube with 1M HCl 2) Left overnight in closed desiccator at 40°C	Corrosion product inconsistent, some black patches occurred. More corrosion product formed at end of coupon nearest the HCl solution
TEST 3	1) Clean coupon placed in open glass tube with IM HCl 2) Placed in desiccator containing more IM HCl 3) Left for 2 days in closed desiccator at 40°C	Water droplet fell onto coupon causing inconsistent corrosion product layer
TEST 4 (see figure 3.4)	1) Clean coupon placed horizontally above 1M HCl 2) Left in closed tank for 2 days at 40°C	Consistent even corrosion layer produced
TEST 5	1) Coupon corroded as in test 4 2) Corroded coupon placed in 1M NaCl solution for 24h 3) Coupon then left to dry in air	NaCl, Fe_3O_4 present
TEST 6	1) Coupon corroded as in test 4 2) Corroded coupon placed in 1M NaCl solution for 24h 3) Coupon rinsed in distilled water 4) Coupon left to dry in air	Fe_3O_4 present

Corrosion Product Test	*Experimental Method*	*XRD and visual inspection results*
TEST 7	1) Coupon corroded as in test 4 2) Coupon placed into 1M HCl	Corrosion product dissolves from the surface of the coupon
TEST 8	1) Clean coupon placed into 1M HCl	Corrosion product does not form on the surface
TEST 9	1) Coupon corroded as in test 4 2) Coupon placed in 1M NaCl solution for 1 week 3) Coupon rinsed in distilled water 4) Coupon left to dry in air	γ-Fe_2O_3 present
TEST 10 (see figure 3.7)	1) Coupon placed under glass dish with 1M HCl for 2 days 2) Left in air for 2 days	β-FeOOH formed on side of coupon exposed to air. $FeCl_2.4H_2O$ also present
TEST 11	1) Coupon corroded as in test 4 2) Coupon left in air, upright in glass sample bottle	A very small amount of β-FeOOH detected
TEST 12	1) coupon corroded over 1M HCl in tank at room temperature for 4 days	Small amount of α-FeOOH, γ-FeOOH

Corrosion Product Test	*Experimental Method*	*XRD and visual inspection results*
TEST 13	1) Coupon corroded as in test 4 2) Coupon left in air for 2 days 3) Coupon rinsed in distilled water for several hours 4) Coupon dried in air for 1 day	Corrosion Product turns black on placing in water. Fe_2O_3 detected
TEST 14	1) Coupon corroded as in test 4 2) Several drops of 1M HCl solution placed on corroded coupon surfaces 3) Coupon replaced in desiccator at 40°C for 2 days	β-FeOOH present but also darker corrosion products. Corroded surface very uneven with areas of yellow 'sweat'
TEST 15	1) Coupon corroded as in test 4 2) Drops of 0.1M HCl placed on the corroded coupon surface 3) Coupon left to dry in air	No phase identified. Corrosion product amorphous
TEST 16	1) Coupon corroded as in test 4 2) Drops of 1M HCl placed on the corroded coupon surfaces 3) Coupons left to dry in air	β-FeOOH and γ-FeOOH present

Corrosion Product Test	*Experimental Method*	*XRD and visual inspection results*
TEST 17	1) Coupon corroded as in test 4 2) 1M HCl dropped onto the corroded coupon 3) Coupon replaced in corrosion tank but at room temperature	γ-FeOOH and very small amount of β-FeOOH, however corrosion product uneven, blistered with some black areas and yellow/brown spots.
TEST 18	1) Coupon corroded as in test 4 2) Drops of 1M HCl placed onto the corroded coupon 3) Coupon left upright in glass bottle to dry over 2 days	β-FeOOH and γ-FeOOH detected. But more of the light coloured corrosion product is found at the bottom of the coupon where the solution has dripped downwards
TEST 19	1) Coupon corroded as in test 4 2) Drops of 1M HCl placed onto the corroded coupon 3) Coupon placed flat in weighing boat and left to dry overnight	β-FeOOH, γ-Fe_2O_3 present. Corrosion product darker on the underside of the horizontally placed coupon
TEST 20	1) Coupon corroded as in test 4 2) Corroded coupon dipped in 1M HCl solution and then blotted on both sides to remove excess solution. 3) Coupon placed in weighing boat and left to dry overnight, turning over the coupon after several hours	β-FeOOH present. A consistent, even, light and dark brown mottled corrosion layer is produced

3.4 SCANNING ELECTRON MICROSCOPE (SEM)

A Scanning Electron Microscope, SEM, was used to obtain images of the corrosion products formed on coupon surfaces. A very fine 'probe' of electrons at energies of 30-40keV is focused on the surface of the specimen and scanned across it in parallel lines. The impact of the electron beam causes the emission of secondary electrons and the re-emission of the electrons from the original beam, known as backscattered electrons. The intensity of the electron emission is related to the topology of the surface (especially with backscattered electrons) and the elemental composition of the surface (with secondary electrons), and thus images of these two characteristics are gained.

Elemental analysis was also carried out using X-rays emitted from the surface of the corrosion product samples. The method of x-ray analysis used is known as EDAX (Energy Dispersive Analysis of X-rays). A semiconductor detector classifies the radiation according to its energy by converting the incident radiation into pulses of current whose size are proportional to the energy of the x-radiation. The energy of an x-ray is specific to the element from which is was emitted, and therefore an analysis of these x-rays can give quantitative data on the elemental composition of a sample.

In this study a Hitatchi s-570 SEM was used, with a LINK SYSTEMS A.N. 1000 X-Ray Microanalysis system. EDAX was carried out with a Lithium drifted Silicon detector. This can give quantitative analysis of elements down to and including beryllium, at an accuracy of 0.1%(wt). A ZAF/PB quantitative software package was used for the electron beam analysis.

3.4.1 SEM Images

SEM images were acquired of the surface of a coupon corroded via Method B. A micrograph is shown in figure 3.8. This is a backscattered electron image of the corroded coupon surface. The 'floret' shape growth of the corrosion products is shown. These florets are between 20-30um in size and are made up of dendritic crystal growth.

Figure 3.8 SEM Image of the surface of corroded coupons

3.4.2 Quantitative Analysis

Quantitative analysis was carried out on several different samples of corrosion products. An electron beam energy of 20.00kV was used and the time of analysis for each quantitative analysis was 100 seconds. Before each sample was analysed, the SEM was standardised using a Cobalt standard sample. The resulting data gives the weight percentages of each element analysed and also a normalised weight percentage. The quantities of iron and chloride present in the samples were analysed and these figures were converted into an atomic ratio of Fe:Cl.

Several different samples were analysed so a comparison could be made between the synthetically produced corrosion product, the α and β-iron oxyhydroxides, and corrosion

products found on actual archaeological objects. The synthesis of the α-FeOOH and β-FeOOH will be described in detail in chapter five. Archaeological iron from the same sources as analysed was used in the corrosion tests described in chapter four. The material came from two sources, the first batch, Roman nails from a hoard found at Inchtuthill, Scotland (Angus *et al*, 1962), were obtained from English Heritage and the second batch, unprovenanced medieval nails were obtained from the Museum of London (Ganairis, 1998). Analysis was also carried out on a sectioned iron coupon and corrosion products formed in moist air (not in an acidic, chloride rich environment). The samples used and the results obtained are listed in table 3.2. Samples 1-3 and 5-7 were powdered in a pestle and mortar and pressed into discs which were used for the quantitative analysis. Samples 4 was an iron coupon sectioned with a saw and mounted in epoxy resin before polishing the iron surface.

The quantitative analysis of iron and chloride ions in the oxyhydroxides α-FeOOH and β-FeOOH samples 1 and 2, give the results that would be expected from the literature. The α-FeOOH sample had only a negligible amount of chloride present, which is consistent with the formula α-FeOOH, containing no chloride within its structure. The remaining element analysed was iron. Oygen is undetectable by EDAX analysis, but can be inferred from the missing percentage weight. In nearly all the analyses some trace elements were also detected which can be attributed to impurities.

Three points on the β-FeOOH pellet were analysed, giving fairly homogeneous results. A chloride weight percentage of between 4.5 - 4.7 wt% (see table 3.2) matches closely the literature value of 4.6% (Childs *et al*, 1980). This corresponds to a formula $Cl(H_2O)Fe_8O_7(OH)_9$ and could be understood as a chloride ion occupancy of every second tunnel site. Childs *et al* (1980) state that due to the size of the chloride ion (3.6Å) only half of the tunnel sites can be occupied with chloride ions. However Post and Buchwald (1991), give a value of 1.35 chlorides per unit cell, consistent with two thirds of the tunnel sites occupied by chloride ions, with no water detected in tunnels at all. A displacement of the chloride in the tunnel site, away from other occupied sites would accommodate the extra chloride.

Table 3.2 SEM-EDAX Quantitative Analysis

Sample	*Description*	*Fe*		*Cl*		*Fe:Cl Molar Ratio*
		% (wt)Element	*% (wt) Normalised*	*% (wt) Element*	*% (wt) Normalised*	
1	α-FeOOH	50.5	99.9	0.0	0.0	-
2	β-FeOOH	45.9	86.7	4.5	13.3	5.8:1
		46.2	86.3	4.7	13.7	5.6:1
		45.2	86.2	4.6	13.8	5.6:1
3	Corroded Coupon	46.8	85.7	5.0	14.3	5.3:1
	(Method B)	49.1	86.7	4.8	13.3	5.8:1
4	Iron in centre of	99.4	99.8	0.1	0.1	-
	sectioned corroded coupon	99.9	99.9	0.1	0.1	-
5	Corrosion product from	48.3	99.7	0.1	0.2	400:1
	surface of freshly	41.17	97.2	0.7	2.8	31:1
	corroded coupon	61.7	99.8	0.1	0.2	535:1
6	Corrosion Product	52.4	99.7	0.1	0.3	343:1
	from English Heritage	52.6	99.9	0.0	0.0	-
	Nails	48.6	89.9	3.5	10.1	7.9:1
7	Corrosion Product	1.0	90.8	0.1	9.2	8.8:1
	from Museum of	9.5	98.7	0.1	1.3	65:1
	London nails	44.5	99.3	0.2	0.7	129:1

Akageneite has been synthesised with varying amounts of chloride present, for example, Johnston and Logan (1979) reported an initial chlorine content of 6.9 wt%, decreasing to 3.5 wt% after 8 days of washing with water. Therefore, too much significance should not be given to the above analyses as an indication that the chloride ions are necessarily located in tunnel sites, rather than replacing the structural hydroxide ions as suggested by Rezel and Genin (1990).

Sample 3, the corrosion product synthesised by Method B, gives similar results to the β-FeOOH analysis. The analysis gives us excellent evidence that a chloride containing corrosion product has been found. The XRD data proves that some of this, at least, is β-FeOOH, although the colloidal nature of the corrosion products does make the diffraction pattern diffuse. The similarity of the analysis data in samples 2 and 3 would suggest that a large proportion of the corrosion product formed on the corroded coupon is β-FeOOH.

Analysis of the iron used to make the corroded coupons, shows the composition and purity of the iron. Up to 0.1 wt% impurities were found to be contained in the iron, including traces of chlorine, phosphorus and manganese. A corrosion product formed on the iron coupon surface, formed in moist air, rather than being exposed to an HCl environment was also analysed, so as to compare its composition to the corrosion product formed by Method B. On this coupon only a small quantity of chloride was detected, although up to 0.7% was found to be present in one analysis.

Samples 6 and 7, the corrosion products from actual archaeological objects also show fairly low chloride concentrations compared to the corrosion products which were specifically synthesised to contain a high chloride ion concentration. One analysis did show a significantly high chloride percentage, indicating that the corrosion product are not homogeneous and perhaps some high chloride compounds are present. Sample 6 shows chloride ion concentrations comparable to sample 5, however sample 7, the medieval nails show a very variable iron composition and a large number of other element present such as magnesium, silicon, phosphorus, potassium, and calcium. This indicates that much of the corrosion product on the surface of the objects are not iron oxide or oxyhydroxides at all, but silicate inclusions from sand and grit. These other compounds have become included into the corrosion products during burial and the corrosion process, and are now firmly

cemented together by the iron corrosion products that have formed around them. Chloride ions are also present between 0.1-0.2 wt%, similar levels to sample 5.

Levels of less than 0.01 wt% chloride ions (100ppm) has been considered 'safe', i.e. not detrimental to the stability of the artefact (North and Pearson, 1978), so the archaeological iron objects analysed in this work, may require some treatment to remove the chloride ions and stabilise the objects. Marine cast iron can typically contain 13 wt% chloride ions (although this may not be evenly distributed within the sample, a higher chloride concentration occurring nearer to the corroding surface). The objects used in this study do not have this high level of chloride ions, however this composition has been reproduced in the corroded coupons synthesised for corrosion inhibitor testing.

CHAPTER FOUR

Corrosion Testing

4.1 ACCELERATED CORROSION TESTING

4.1.1 Standard Accelerated Corrosion Tests

Accelerated corrosion testing is used to evaluate the extent to which selected metals and alloys can resist corrosion in the environmental conditions applied. Real time corrosion testing would be the only totally reliable test to measure the actual corrosion resistance of an object in the environment it is to inhabit or in which is it to function. However, this would be a lengthy process. To obtain data within a more acceptable time scale, accelerated corrosion tests are specifically designed to reproduce the corrosion occurring naturally in years, within the space of a few weeks. The environmental conditions applied during the test do therefore have to be much harsher than those that would occur naturally. The objective of short term accelerated testing has been defined as "reproducing the natural corrosion and degradation processes inside the test chamber in a reduced time frame but without changing the corrosion/degradation mechanisms that occur in natural environments" (Skerry & Simpson, 1993). The selection of an appropriate set of conditions for a corrosion test is therefore a compromise between producing the correct mechanisms of corrosion and obtaining results in the shortest possible time (Baboian, 1995).

There are some problems in interpreting accelerated corrosion test results, with respect to comparing the degree of corrosion that would actually occur in a real time scale and in a natural environment (such as the museum environment), to the artificial accelerated test results. However, standardised accelerated corrosion testing, where an appropriate test is chosen, is the best available method for evaluating the performance of materials such as

inhibitors and coatings. Many standard tests are available for testing a variety of materials in a variety of environments (Carter, 1982). In simple humidity tests, objects are placed in high humidity environments, often at elevated temperature. Cyclic humidity tests, where the humidity is cycled between low and high values over a period of hours, are also used. Other more complex tests can also be carried out. A common accelerated corrosion test is the salt fog test, where objects are tested against exposure to a salt mist environment, such as sodium chloride solutions or synthetic brines (containing sodium and magnesium chlorides, magnesium sulphate, potassium bromide and chloride, sodium hydrogen carbonate and calcium chloride). Salt fog tests are performed on materials that are to be used in very harsh environments and are therefore less applicable to testing the performance of objects in museums. Careful interpretation is needed with the results of more complex accelerated corrosion tests, as the conditions are not just more severe, but are specific to the environmental reproduced and therefore could be misleading. Other more sophisticated tests may involve the control of variables such as air flow, gaseous composition and u.v. radiation (Baboian, 1995).

Standard corrosion tests have been devised for industrial purposes. Organisations such as governments, the military and private companies all have designated standard corrosion tests by which they can test and compare materials for use in a variety of environments. The American Society for Testing Materials (ASTM) has produced several special technical publications on laboratory corrosion testing and these offer guidance on standard conditions for many different corrosion tests such as, ASTM B117, the test method of salt spray testing or ASTM B287, the method of acetic acid salt spray testing (used to simulate exposure to an aircraft carrier environment).

A commonly used corrosion test for simulating outdoor atmospheric corrosion is ASTM G60, cyclic humidity test. This test involves cycling the humidity of the test environment from a minimum of 20% or less, to a maximum of 95% or more in 8 hour cycles, three times a day. When the highest humidity is reached the samples are dipped into an aqueous solution containing 1% sodium chloride, 1% calcium chloride and 0.1% sulphuric acid (by weight). Three 5 minute immersions are recommended with 1 minute for draining between each immersion. The test is carried out at 52±1°C for 20 days (ASTM, 1997).

4.1.2 Accelerated Corrosion Test Methodology

4.1.2.1 Accelerated Corrosion Test Method

The standard corrosion tests described in the previous section have all been devised to simulate specific environments in which to test the performance of materials. For example, the test ASTM G60 has been designed with the automotive industry in mind, that is, atmospheric exposure, where little protective rust may form. To devise a suitable accelerated corrosion test for this study, the museum environment in which objects are located must be considered. Obviously museum environments will vary depending on the location and sophistication of any air filtering or conditioning systems available. The recommended relative humidity is 40-60% (Ambrose & Paine, 1993). Pollutants found in many museum environments include particulates, sulphur dioxide, ozone and oxides of nitrogen. Much of this originates from the burning of fossil fuels and so pollution will be greater in urban and industrial areas. Concentrations of outdoor atmospheric pollutants can range up to 300$\mu g/m^3$ in London. It has been estimated that when no air filters are employed, indoor pollutant levels may be approximately half the outdoor values (Thomson, 1997).

The standard industrial tests previously described are not appropriate for modelling the museum environment due to the harsh and corrosive conditions applied, commonly designed to simulate outdoor environments. In an attempt to accelerate the rate of corrosion, but without changing the corrosion mechanism, it was decided use an increased temperature and humidity (in comparison to the museum environment) in accelerated corrosion tests. No additional pollutants were added to the testing environment, as it was judged that the corrosion products surrounding the objects or coupons would themselves lead to the formation of a more acidic localised environment.

In all the corrosion tests, batches of samples, untreated and treated with the inhibitors as described in section 4.2, were subjected to aggressive conditions with respect to temperature and humidity. Samples, contained in pre-weighed plastic weighing boats, were placed in the humidity cabinet at a fixed relative humidity of 90%, and a temperature of 40°C. The humidity cabinet was placed on indirect cool mode. Samples were kept under

these conditions for at least 21 days. Samples were removed for short periods of time during the test for observation and mass measurement.

4.1.2.2 Humidity Cabinet

Accelerated corrosion tests were carried out in a Fisons humidity cabinet with a Eurotherm 910D dual loop thermostatic controller. The internal space of the cabinet has dimensions of roughly 60cm deep, 80cm high, and 100cm long. The cabinet consists of a working chamber above an air treatment chamber. In the treatment chamber the humidity and temperature of the air is controlled. The air is then circulated through specifically designed ducts so that the flow remains unaffected by shelves inside the working chamber and all parts of the chamber are circulated with air of the same temperature and humidity. The air treatment chamber contains a heating element, a refrigerator coil, a chilled water heat exchanger coil and an atomiser which injects water to give the required humidity. Lower temperatures (below 30°C) and humidity can be obtained by running the refrigeration unit continually - known as direct refrigeration mode. For temperatures between 15 - 95°C the chilled water heat exchanger is used to control the refrigeration, known as indirect refrigeration mode. Humidity and temperature were set using the thermostatic control, however fluctuations in the humidity of ±10% and in temperatures of ±2°C did occur.

4.1.3 Evaluation of the Degree of Corrosion in Corrosion Tests

The rationale of any corrosion test is to determine and compare the extent of the corrosion that has occurred in each batch of samples. A wide choice of methods for assessing corrosion damage exist. Much corrosion testing is done as part of quality control assessment. A simple pass/fail criteria is therefore often applied which will depend on an assessment of whichever property is under scrutiny, for example, change in appearance, type of corrosion produced or mechanical properties. In many cases any kind of visual indication of corrosion will be classed as a failure.

In initial experiments visual inspections of samples were undertaken. If any new corrosion product could be seen on the surface of the sample it was classed 'unstable'. New corrosion products were visible against the existing darker corrosion layers. Often new

corrosion product has a shiny crystalline appearance and a lighter orange colour. Flaking of small or large fragments from the surface was also used as a sign of corrosion and instability.

When the degree of corrosion, rather than just its presence is to be assessed a good indicator is to examine the change in mass. Mass calculations in corrosion tests are often calculated on the basis of the mass of metal lost in the corrosion test. This involves the acid stripping of all corrosion products to leave behind only the uncorroded metal which can then be weighed and compared to the initial mass (ASTM G1, 1997). This method does not however allow for assessments to be made during the corrosion test. It was therefore decided to monitor the mass increase occurring on corrosion.

As corrosion occurs, the oxidation process leads to an increase in mass. The percentage increase in mass will indicate the amount of corrosion that has occurred and can be used to compare the extent of corrosion in different samples tested. Measuring the increase in mass will allow the detection of small amounts of corrosion that are not clearly visible, especially on already corroded metal objects or coupons used to simulate objects. A quantitative approach such as this will also allow the comparison of the extent of corrosion occurring in different batches which may not be apparent by visual inspection alone.

In all experiments mass calculations were made to compare the amount of corrosion occurring in each batch of samples. Initial masses were recorded, and then masses recorded at intervals during the corrosion test so as to calculate the mass increase of each sample. Results were made comparable by calculating a percentage mass increase for each sample (as the actual initial mass of each sample varied). The percentage mass increases were calculated as follows:

$$\%\,\textbf{Mass Increase} = \left[\left(\frac{\textbf{Mass} - \textbf{Initial Mass}}{\textbf{Initial Mass}}\right)\textbf{x100}\right]$$

To calculate a mean % mass increase value for each batch of samples used in an accelerated corrosion test a normal distribution is required. With any given batch of samples a random range of values will be obtained so that the average of several values gives a truer picture. A histogram can be constructed to confirm a normal distribution in % mass increase values. To confirm this to be the case in this work, a pilot corrosion test was

carried out (further details are given in section 4.3.3). 50 iron coupons (2cm x 5cm) corroded by Method B were subjected to the accelerated corrosion test described in section 4.1.2.1. The % mass increase values after 21 days have been plotted in the histogram shown in figure 4.1. Although the relatively small number of samples do not provide a complete picture, a normal distribution is indicated.

Figure 4.1 Histogram showing normal distribution of the % mass increase of coupons in pilot test 2

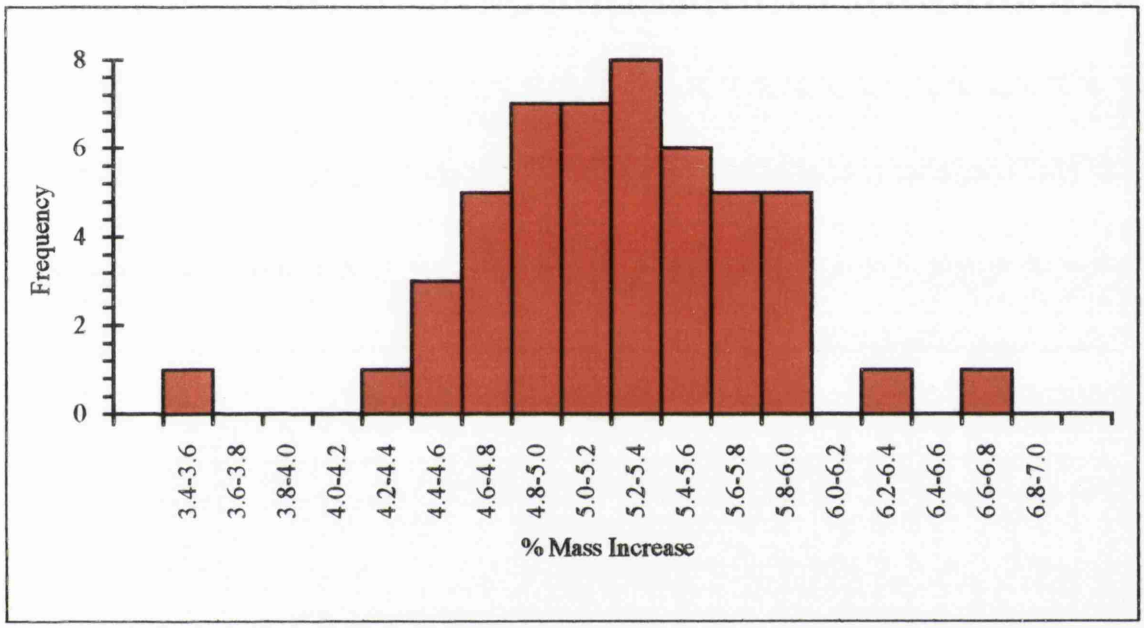

4.2 TREATMENT OF MATERIAL FOR CORROSION TESTING

4.2.1 Samples Used in Accelerated Corrosion Tests

To test the inhibitive treatments described in chapter two, accelerated corrosion tests were performed on batches of archaeological iron nails and synthetically corroded coupons, prepared as described in chapter Three. The same number of coupons or nails were used in each differently treated batch, in an experiment. The ASTM standard guide for conducting corrosion coupon tests states that five to ten replicated coupons should be used in each test (ASTM, 1997). A larger sample will give a more representative mean value. In the accelerated corrosion tests performed in this work batches of coupons and nails were made as large as possible within the constraints of availability and space.

4.2.1.1 Archaeological Iron

Archaeological material tested were batches of Roman nails from Inchtuthill, Scotland, given by English Heritage. Most of these nails contained a substantial iron core, well covered with several mm of iron oxyhydroxide, magnetite and other corrosion products. In a few cases, only a thin layer of corrosion products was visible. Nails varied in size from 2cm to 12cm long. A photograph of a selection of the nails used is shown in figure 4.2. EDAX analysis of the corrosion products of these nails is given in chapter three.

Figure 4.2 A selection of nails used in accelerated corrosion tests

Unlike the coupons used, all the nails varied in size (volume), shape and mass and therefore some attempt was made to select similar groups of nails for each batch. The total quantity of nails available were divided into small, medium and large nails based on a brief visual inspection. Each batch of nails taken to be treated with inhibitor, was made up of the same number of small, medium and large nails, randomly chosen from the three groups into which the nails had been divided. An attempt was also made to evaluate the condition of the nails and ensure each batch contained a similar number of highly corroded and less corroded nails.

4.2.1.2 Corroded Iron Coupons

The annual book of ASTM standards states that "the size and shape of test specimens are influenced by several factors and can't be rigidly defined" (ASTM, 1997). It is however also stated that coupons should be as large as can be conveniently handled. Several types of standard coupon sizes are suggested such as, circular coupons of 38mm diameter and 3mm thickness with an 11mm hole in the centre, or 25mm by 50mm by 3mm rectangular coupons. In this work two sizes of iron coupons were used. Initially 50mm by 20mm by 1mm coupons were selected. Due to the need for treatment by silanes to be carried out in a moisture free environment, later corrosion tests were carried out with smaller coupons that would fit inside the glassware used. These coupons were 25mm by 10mm by 1mm.

Coupons were produced to be homogeneous, that is, all the same size, amount and type of corrosion product within the limits possible. Therefore no further sampling was necessary when choosing batches to be treated.

4.2.2 Pre-Treatment of Samples

4.2.2.1 Archaeological Iron Nails

All nails were cleaned with an air abrasive unit using 5.3μm Al_2O_3 powder to remove any concretions and extraneous soil and sand adhering to the surface of the object. Some of the lighter orange surface corrosion product was also removed. The nails were then rinsed in acetone to degrease the surfaces before further treatment.

4.2.2.2 Corroded Coupons

All coupons were degreased in acetone before inhibitive treatments were applied. No other pre-treatment was carried out.

4.2.3 Treatment of Samples

4.2.3.1 Heating to 150°C Under vacuum

As some of the treatments involved heating samples, it was decided to investigate the effect of heating samples alone, so that any change in corrosion rate due to heating a sample could be differentiated from the effect of an inhibitive treatment. Some samples were therefore heated to 150°C under a vacuum of 800mbar for 12 hours.

4.2.3.2 Treatment with ODTMS

4.2.3.2.1 Treatment with a 0.015M solution of ODTMS

A treatment procedure was followed as advised by Dr Norio Yoshino (1997). Samples to be treated were immersed in a 0.015M solution of ODTMS in toluene. The solution was prepared in a dry box purged with nitrogen or argon as ODTMS is moisture sensitive. A schlenk line (a combined nitrogen and vacuum line) was used for the experiment so that it could be carried out in a moisture free environment. Figure 4.3 illustrates this apparatus. Samples were placed in a schlenk tube and this was then alternately filled with nitrogen and evacuated and eventually left filled with nitrogen. The 0.015M ODTMS solution was then transferred from another schlenk tube using a delivery tube until all the samples were totally immersed in the solution. The samples in solution were heated to a temperature of 50°C for 4 hours. The solution was then transferred back into another schlenk tube via a delivery tube, so that it could be re-used. The samples were rinsed in ethanol and then rinsed in distilled water for 1 minute. The samples were then dried and placed in an oven at 150°C for 30 minutes.

4.2.3.2.2 Treatment with a 0.03M solution of ODTMS

The same procedure as described above was also carried out with 0.03M solutions of ODTMS in toluene.

Figure 4.3 Illustration of a Schlenk Line (Coyne, 1997)

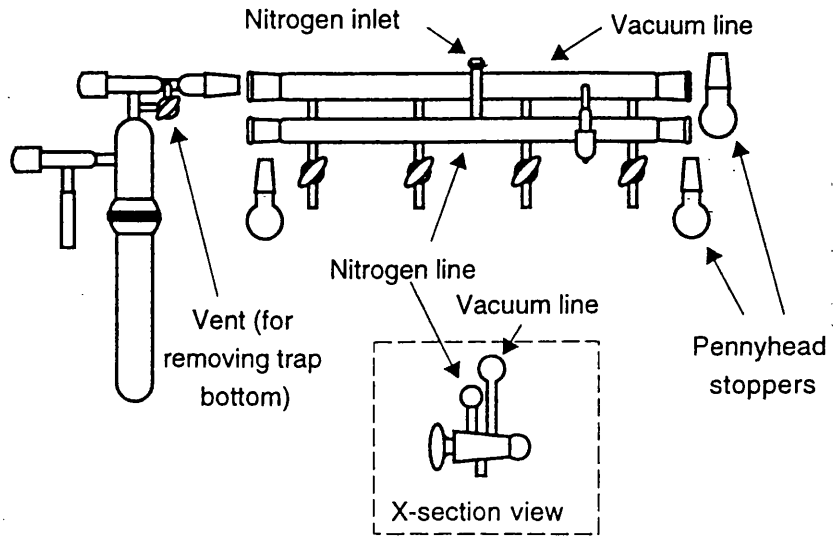

4.2.3.3 Treatment with HFTMS

4.2.3.3.1 Treatment with a 0.015M solution of HFTMS

Ampoules of 0.015M HFTMS in F-113 solution, supplied by Dr N. Yoshino, were opened inside a dry box, and the solution added to a shlenk tube. Samples were placed in a schlenk tube and this was then alternately filled with nitrogen and evacuated and eventually left filled with nitrogen. Initially a schlenk tube with a narrow neck was used so small 1cm x 2cm coupons had to be treated. A round bottomed flask with a side arm and tap was then used. This had a larger neck so that larger 2cm x 5cm samples and nails could be treated. The 0.015M HFTMS solution was transferred from another schlenk tube using a delivery tube into the tube containing the samples, until all the samples were totally immersed in the solution. The samples in solution were heated to a temperature of 50°C for 4 hours.

4.2.3.3.2 Treatment with a 0.03M solution of HFTMS

The same procedure as described above was also carried out with 0.03M solutions of HFTMS in F-113 which were supplied in ampoules.

4.2.3.3.3 Treatment with a 0.03M solution of HFTMS followed by a 0.03M solution of pyridine

The same procedure as described in section 4.2.3.3.2 was carried out. These samples were then immersed in a 0.03M solution of pyridine (C_5H_5N) in toluene and left for twelve hours at room temperature (roughly 25°C). Samples were rinsed twice in toluene and left to dry in air

4.2.3.3.4 Treatment with a 0.03M solution of pyridine followed by a 0.03M solution of HFTMS

Samples were initially immersed in a 0.03M solution of pyridine in toluene and left for twelve hours at room temperature (roughly 25°C). Samples were then rinsed in toluene and left to dry in air. These samples were then treated with 0.03M HFTMS as described in section 4.2.3.3.2.

4.2.3.3.5 Testing of Effect of Solvents Used

To examine if the solvents used to deliver the inhibiting treatments had any effect on the corrosion rates, samples were treated with the solvents and then subjected to accelerated corrosion tests.

Treatment with Toluene:

Samples were immersed in toluene for 12 hours and then left to dry in air.

Treatment with F-113:

Samples were immersed in F-113 for 4 hours and then left to dry in air.

4.2.3.4 Treatment with TTS

4.2.3.4.1 Treatment with 0.05M TTS Solution

Samples were immersed in 0.05M solution of TTS in toluene and a 800mbar vacuum applied at 35°C for 12 hours. Samples were then removed from the solution and heated at 45°C to cure the coating. Samples were rinsed twice with toluene and left to dry in air.

4.2.3.4.2 Treatment with 0.015M TTS Solution

Samples were treated as described in section 4.2.3.4.1 using a 0.015M solution of TTS in toluene.

4.2.3.5 Treatment with ODA

A 0.01M solution of ODA in toluene was prepared using sonication to facilitate the dissolution process. Samples were immersed in this solution under a vacuum of 800mbars at room temperature, 25°C, for 12 hours. Samples were then rinsed twice in toluene and left to dry in air.

4.2.3.6 Treatment with DCA

Samples were immersed in a 0.05M solution of DCA in toluene, under a 800mbar vacuum, at room temperature, 25°C, for 12 hours. Samples were then rinsed twice with toluene and left to dry in air.

4.2.4 Storage of Samples

All samples were stored over silica gel in sealed containers after treatment and before use in accelerated corrosion tests.

4.3 SAMPLE SIZE USED IN ACCELERATED CORROSION TESTS

4.3.1 Introduction

The number of samples used in each batch of samples treated and then tested in accelerated corrosion tests were chosen based on the constraints of availability and practicality. Each accelerated corrosion test was carried out using coupons initially corroded in the same batch. This was done to limit the variation in thickness of the corrosion layers on coupons. However, this did limit the total number of coupons that could be tested in each experiment. The size of the humidity chamber was also a limiting factor to the number of coupons that could be used in each test. The same number of coupons or nails were used in each batch so that all the mean % mass increase values that were calculated were comparable .

Although the number of samples in a batch varied in different experiments, an attempt was made to understand the relationship between the number of coupons used in each batch of samples tested, and the margin of error of the mean % mass increases calculated. In this way the differences between the means of differently treated batches could be assessed and a judgement made on whether or not the differences in corrosion rates of different batches were statistically significant.

This statistical analysis was carried out for accelerated corrosion tests using coupons corroded by method B only. No statistical analysis was carried out for corrosion tests involving archaeological material or coupons not corroded using method B. It was decided that due to the large variability of the samples within these batches no further information could be gained by such an analysis.

4.3.2 Statistical Analysis of Sample Size of Corroded Coupons

The corroded coupons were produced in order to test the effect of the various inhibitive treatments discussed in chapter two. Accelerated corrosion testing was carried out to ascertain the extent to which each treatment prevented further corrosion. Each coupon will perform in a unique way in each corrosion test. Small differences in the coupons will lead

to differing corrosion rates and therefore it was necessary to use a number of coupons for each test and then calculate a mean corrosion rate. The number of samples used for each experiment would effect the margin of error and standard deviation of the mean corrosion rates calculated. When trying to evaluate the performance of several treatments, not only the mean corrosion rate, but the standard deviation from this mean, is very significant in making comparisons.

The aim of the statistical analysis carried out was to define what difference in % mass increase will actually make the recorded values significantly different, rather than within a margin of error that makes differentiation of two batches of differently treated corroding coupons impossible. This value will depend on the sample size - the number of corroded coupons used in each batch. Comparing the mean corrosion rates of two differently treated batches of coupons, each batch can be seen as a sample taken from an original population of corroding coupons.

The relationship between sample size and standard deviation can be theorised as follows. Two batches of samples, each of size n, are taken and the percentage mass increase occurring during an accelerated corrosion test for each coupon is calculated and mean values for each batch, $\bar{x}_1$, $\bar{x}_2$, are calculated for each batch. The batches have different means, but the variances, σ^2 of the populations, and thus the batches are assumed to be the same. The variance squared rooted equals the standard deviation, σ.

Null hypothesis statistical tests are used in the calculation of the margin of error acceptable for the mean % mass increase values with any given size of samples in each batch, n. The null hypothesis postulated in this case is that the mean % mass increase values of two batches of corroding samples under test represent a significant differences in the actual postulated mean % mass increases of the two populations of samples. In other words, with what percentage probability is data, gained from the batches of samples an accurate indication of the data that would have been gained from the actual populations. It is necessary to establish the probability that will be acceptable for rejecting or accepting this null hypothesis. The probability chosen is known as the confidence level. Confidence levels of 90% or 95% are commonly chosen (Harnett & Murphy, 1975). The maximum

difference, D, that is permissible between the estimate of a population parameter and a true population parameter must also be considered. D represents the amount of 'error' allowable. This value is crucial in comparing batches as two mean % mass increases within this value, can not be considered significantly different

The true means of two populations of corroding samples are known as $\mu._1$ and μ_2 The true standard deviation of these population is σ. Assuming a normal distribution, with a known standard deviation, the following statistical results can be expressed (Harnett & Murphy, 1975):

$$\text{variance}(\bar{x}_1 - \bar{x}_2) = \text{variance}(\bar{x}_1) + \text{variance}(-\bar{x}_2)$$
$$\text{variance}(\bar{x}_1 - \bar{x}_2) = \text{variance}(\bar{x}_1) + (-1)^2\,\text{variance}(\bar{x}_2)$$
$$\text{variance}(\bar{x}_1 - \bar{x}_2) = \text{variance}(\bar{x}_1) + \text{variance}(\bar{x}_2)$$

Given the result:

$$\text{variance}(\bar{x}) = \sigma^2/n$$

where σ^2 is the variance of the parent population and n is the size of each sampling batch:

$$\text{variance}(\bar{x}_1 - \bar{x}_2) = \frac{\sigma^2}{n} + \frac{\sigma^2}{n} = \frac{2\sigma^2}{n}$$

and therefore the standard deviation, σ, of this variance:

$$\sigma(\bar{x}_1 - \bar{x}_2) = \sqrt{2s^2/n}$$

If the difference between means, $(\bar{x}_1 - \bar{x}_2)$, can be seen as a normally distributed random variable, it can be expressed in terms of the standard normal random variable, z:. An expression for the standardised normal test statistic z, can be given:

$$z = \frac{x - \mu}{\sigma}$$

where x is a random variable, μ is the mean of the random variables and σ is the standard deviation. Therefore, in this case:

$$z = \frac{(\bar{x}_1 - \bar{x}_2) - (\mu_1 - \mu_2)}{\sqrt{2\sigma^2/n}}$$

and therefore:

$$z = \frac{(\bar{x}_1 - \bar{x}_2) - (\mu_1 - \mu_2)}{\sigma\sqrt{2/n}}$$

The value of $(\bar{x}_1 - \bar{x}_2) - (\mu_1 - \mu_2)$, is the difference between the batch means and the population means, and is therefore the factor D, the amount of 'error' allowable. Therefore:

$$z = \frac{D}{\sigma\sqrt{2/n}}$$

Using normal probability tables, for a confidence level of 90% (meaning it is 90% certain that the differences in values are statistically significant), Student's t tests can be used (Harnett & Murphy, 1975). This requires z to be greater or equal to 1.645 for the null hypothesis to be accepted. Therefore:

$$1.645 \leq \frac{D}{\sigma\sqrt{2/n}}$$

Rearranging this equation for sample size, n:

$$n \geq \frac{5.412\sigma^2}{D^2}$$

If the standard deviation of a population is known, the relationship between sample size, n, and the margin of error, D can therefore be calculated.

4.3.3 Pilot Tests to Calculate the Standard Deviation of the % Mass Increase of Corroded Coupons in Accelerated Corrosion Tests

To find the value of the standard deviation of percentage mass increase, two Pilot tests were carried out, on the two differently sized coupons used in the accelerated corrosion tests, PT1 using the 1cm x 2cm coupons and PT2 using the 2cm x 5cm coupons. In each case a population size of 50 untreated but corroded coupons was used (corroded by Method B). This number was chosen to provide a large but manageable population size from which the standard deviation could be calculated. Accelerated corrosion tests were carried out as described in section 4.1.2. Each accelerated corrosion test was carried out for three weeks (21 days). Percentage mass increase data was used to calculate the mean and standard deviation % mass increase of the populations, using the following formulae:

$$\bar{x} = \frac{\sum x_i}{n}$$

where x_i is the % mass increase and $\bar{x}$ is the mean % mass increase.

The standard deviation is the square root of the variance, σ^2, where:

$$\sigma^2 = \frac{\sum(x_i - \bar{x})^2}{n}$$

It was assumed that the standard deviation calculated from these pilot tests of untreated but corroded coupons would be the same as the standard deviation of a population of inhibitor treated coupons. The assumption that inhibiting treatments would not affect the statistical spread of the corrosion test results was made so that the same standard deviation could be used in all cases. Although a population of 50 coupons is not large, it was felt that it was an acceptable value given the practical constraints of the experimental conditions. All comparisons of data were taken from the values of the % mass increase after 21 days. This therefore also assumes that in each experiment identical conditions were employed over the 21 day period.

4.3.4 Results of Pilot Tests

The masses of all 50 samples in the pilot tests were recorded at the start of the tests and after 21 days. % mass increase values for each of the samples were calculated and from this data the standard deviations were calculated. The results are summarised as follows.

4.3.4.1 Pilot Test 1

Pilot test 1 used 1cm x 2cm corroded coupons. A standard deviation of 0.95% mass increase was calculated. Therefore at a 90% confidence level:

$$n \geq \frac{4.88}{D^2}$$

4.3.4.2 Pilot Test 2

Pilot test 2 for 2 x 5cm coupons, calculated a standard deviation of 0.53% mass increase. Therefore at a 90% confidence level:

$$n \geq \frac{1.52}{D^2}$$

As may be expected, the margin of error on the smaller coupons is larger then that for the larger coupons due to the more exaggerated effects of the irregularities caused by sides and edges for smaller surface areas.

4.4 ACCELERATED CORROSION TESTS RESULTS

As previously discussed, the inhibitor treatments tested in this work are intended to form a hydrophobic, inactive surface on the previously hydrophilic corrosion products that are found on archaeological iron objects. By blocking the surface adsorption sites of water and other corrosive agents, it is expected that further corrosion can be prevented and objects stabilised. Accelerated corrosion tests were carried out to compare the effectiveness of the suggested treatments at preventing corrosion.

Accelerated corrosion tests were carried out as described in section 4.1.2. The intention was to assess the stability of batches of samples treated with different inhibitors, and compare their performances with respect to preventing corrosion in the aggressive environment of the humidity cabinet. In each experiment an untreated control batch was also tested so that all treatment could be compared to untreated samples, as well as to other inhibitive treatments.

A series of experiments were carried out, using archaeological iron nails, and coupons, initially produced using method A, and subsequently method B. Initial experiments were carried out on archaeological material. The shortage of suitable archaeological material and the need for a more standardised tests lead to following accelerated corrosion tests to be carried out on coupons. Each experiment was carried out in response to the results of the previous experiment, testing different inhibitors or combinations of treatments. Experimental conditions and results are described in the following sections.

4.4.1 Experiment 1: Comparison of Amines and Titanate Using Archaeological Iron Nails

The first accelerated corrosion test was carried out with batches of archaeological material, due to the availability of a quantity of Roman nails from Inchtuthill. 4 batches of 20 nails were taken and each batch treated with the inhibitors. The inhibitor treatments for each batch of nails is given in table 4.1a and described in detail in section 4.2. The corrosion test was carried out for 47 days. The results of this corrosion test are given in tables 4.1b and 4.1c, and displayed graphically in figures 4.4 and 4.5.

Stability data was obtained by giving a value of 0 for stable nails, whilst unstable nails were assigned the value 1. Nails were considered stable where no signs of further corrosion were visible, as described in section 4.1.3. The total number of unstable nails against time has been shown for all the batches as well as the mean % mass increase data calculated from the individual mass increases of each sample.

From, both the mean % mass increase and the stability data, it can be seen that all three treatments, TTS, ODA and DCA provide some protection from corrosion. All three treatments have lower % mass increases than the untreated control batch of nails, and in all cases more of the treated nails remained stable than the untreated batch. The results show the TTS treatment to be the superior one. The TTS treated batch gained roughly a third of the mass gained by the untreated batch, however both amines gained about half of this value. The two amines behaved in a very similar way, with almost identical mass increases. In the first 35 days of the experiment the DCA treated samples increases in mass slightly more than the ODA treated samples, but by the 47th day, the trend had reversed. The difference is however so small, that it is unlikely to be statistically significant, and the effectiveness of the two treatments should be seen as identical.

General observations of the four batches tested was in agreement with the mean % mass increase results. The TTS treated nails were in a similar condition to their state prior to the experiment, however the untreated nails showed a considerable amount of new corrosion, including spots of paler coloured corrosion products and flaking and cracking of existing corrosion product layers. The condition of both batches treated with amines was somewhere between the untreated and TTS treated batches.

When the mass increase data is compared to the stability data (see tables 4.1b and 4.1c and figures 4.4 and 4.5) it can be seen that the pattern is very similar. By the end of the accelerated corrosion test 19 of the 20 nails in the untreated batch were classed as unstable, however in the batch treated with TTS only 8 nails were unstable, 12 having remained uncorroded. The two amine treatments show slightly more exaggerated differences in stability judges by appearance when compared to the results from mass increase data. 7 of the ODA nails remained stable whilst only four of the DCA nails were classed as stable after the completed test. The percentage mass increase data show that the

difference in the rates of corrosion of the two amine treatments are in fact very small, and therefore the stability test does show a larger degree of error. This is not surprising as the stability test is a fairly blunt assessment, differentiating only between no signs of corrosion and any slight sign of corrosion. No mechanism existed for examining the degree of corrosion occurring in each individual sample. In addition, the method was very subjective, depending on the visual inspection of one individual alone. Often a fine line existed between what would pass as stable, and what would be considered unstable. The stability tests do not seem to add any extra information that can not be gauged from recording mass increase data and for this reasons stability tests were discontinued and further experiments were judged on % mass increase calculations only.

Table 4.1a - Treatments used in experiment 1

BATCH NUMBER	TREATMENT
Batch 1	No Treatment
Batch 2	0.01M ODA (section 4.2.3.5)
Batch 3	0.05M DCA (section 4.2.3.6)
Batch 4	0.05M TTS (section 4.2.3.4.1)

Table 4.1b Numbers of unstable nails in experiment 1

NO OF DAYS		0	8	16	24	31	41	47
BATCH 1	*None*	0	5	13	15	16	17	19
BATCH 2	*ODA*	0	5	7	8	10	13	13
BATCH 3	*DCA*	0	4	7	11	13	14	16
BATCH 4	*TTS*	0	4	4	5	5	6	8

Table 4.1c Mean % mass increases for nails in experiment 1 (n=20)

NO OF DAYS		0	8	16	24	31	41	47
BATCH 1	*None*	0	0.150%	0.160%	0.179%	0.198%	0.231%	0.279%
BATCH 2	*ODA*	0	0.096%	0.119%	0.119%	0.118%	0.128%	0.131%
BATCH 3	*DCA*	0	0.103%	0.121%	0.125%	0.120%	0.127%	0.126%
BATCH 4	*TTS*	0	0.078%	0.089%	0.086%	0.081%	0.086%	0.082%

Figure 4.4 Experiment 1:Number of unstable nails against number of days in humidity cabinet

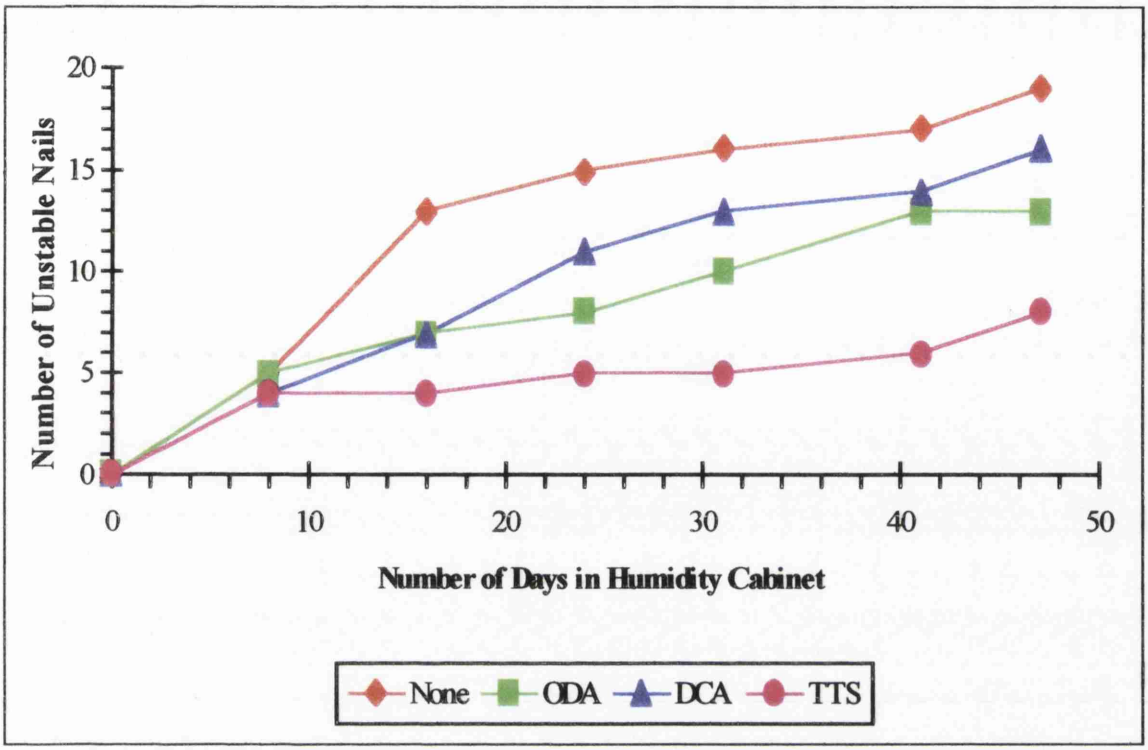

Figure 4.5 Experiment 1: Mean % mass increases against number of days in humidity cabinet

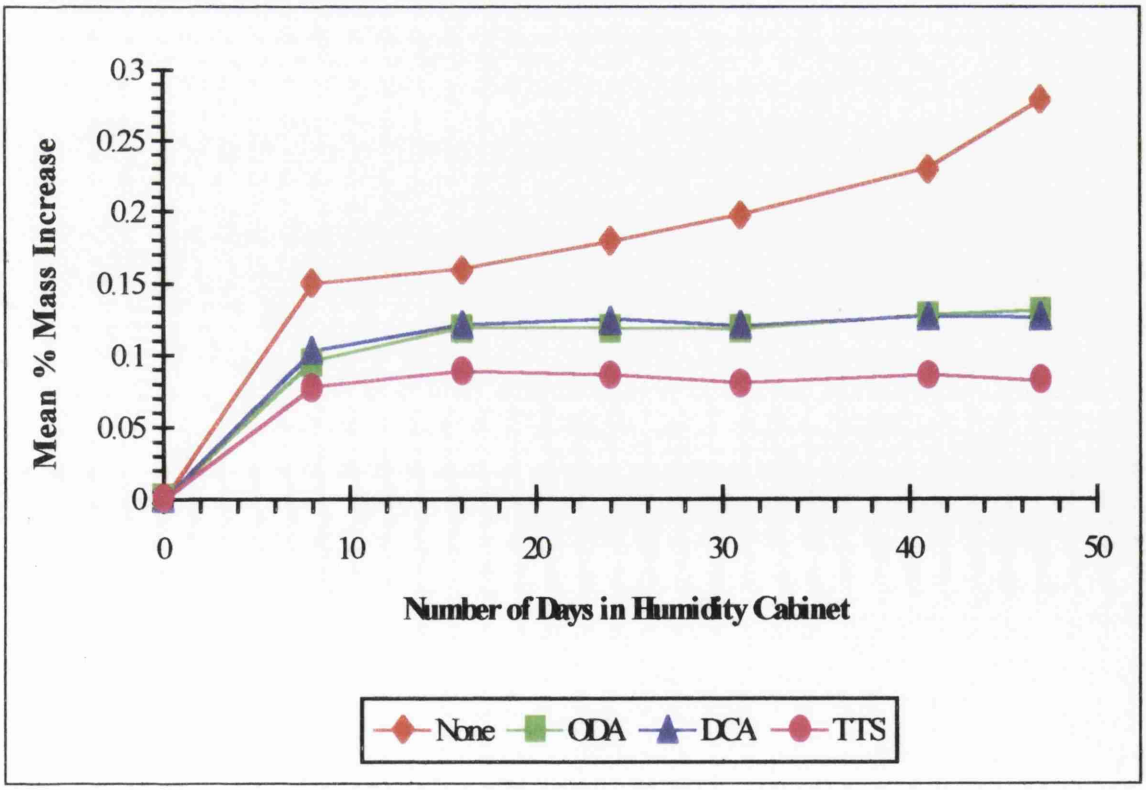

4.4.2 Experiment 2: Comparison of ODA and TTS Treatments Using Pre-corroded Coupons

Experiment 2 and all subsequent experiments were carried out using pre-corroded coupons produced as described in chapter three. The coupons used were produced by method A. Each batch contained 5 corroded iron coupons 2cm by 5cm in size. The treatment methods used are given in table 4.2a. Two batches of coupons with no inhibitor treatment were tested. One batch was the control group. The coupons in the other untreated batch had been heated to 150°C as described in section 4.2.3.1, so that the effect on the corrosion rate, if any, of heating the coupons could be assessed. The accelerated corrosion test was carried out for 41 days. The results of this test are given in table 4.2b and figure 4.6.

It is interesting to compare the extent of corrosion occurring on untreated coupons and untreated archaeological nails. From experiment 1, it can be seen that after 41 days the mass of a batch of untreated nails had increased by a mean value of 0.280%, whilst after 41 days the untreated coupons had increased in mass by a mean value of 8.36%. The thickness, density and composition of the corrosion product layer will explain these differences. Due to the much shorter time span in the production of the corrosion products on the coupons, they are much thinner and less dense than those found on the archaeological nails tested, and therefore, oxygen and water will more readily reach the metal within the corrosion layer. The archaeological nails may also contain a much higher proportion of magnetite, a less hydrophilic corrosion product. The coupons were synthesised by corrosion in HCl so that they would contain a high proportion of chlorinated iron oxyhydroxide corrosion products. In this way they are specifically modelling the high chloride concentration areas of archaeological iron, and areas where corrosion causes a low pH and a build up of chloride ions, as occurs in pitting or crevice corrosion (Rosenfeld *et al*, 1964). The coupons are therefore not identical to archaeological iron in the degree of corrosion occurring, but are models of the most corrosion-inducing factors, present in archaeological iron, and especially marine iron. They are therefore useful in examining the corrosion performance of the most unstable types of archaeological iron.

The results of this accelerated corrosion test again show that surface treatment by TTS or ODA improves corrosion resistance (see figure 4.6). In this experiment both TTS and ODA corroded by about 4% less than the untreated batches, whose mean % mass increases were over 8% after the 41 day test. In contrast to the first experiment however, very little difference could be detected in the performance of the titanate, TTS and the amine, ODA. This suggests that in more extreme conditions, of high humidity, temperature and high chloride concentration, even if only small quantities of water can penetrate the inhibitors hydrophobic layer, this is enough to initiate corrosion. The amount of corrosion in this case seems to be controlled by the catalytic effect of chloride ions present rather than the quantity of water that can penetrate the inhibitor layer. The chloride concentration is the rate determining factor, rather than the amount of water and so the differences that have been shown in experiment 1 are not seen in this experiment. In other words, if a significant quantity of chloride ions are present at the metal surface, the amount of water that can penetrate the hydrophobic inhibitor layer becomes less significant and differences in types of inhibitors are less pronounced.

It is also clear from this experiment, that the heating, to 150°C under vacuum has no effect on the corrosion rate of a batch of nails. The corrosion rate of the untreated batch and the heated batch was almost identical. This indicates that the improved corrosion resistance of samples treated with inhibitors can be attributed to the effect of the inhibitor rather than any effect that heating the sample during the treatment process may have. This also indicates that any increase in corrosion rates detected is not due to the heating of samples to 150°C.

Table 4.2a Treatments used in experiment 2

BATCH NUMBER	TREATMENT
Batch 1	No Treatment
Batch 2	Heated (section 4.2.3.1)
Batch 3	0.05M TTS (section 4.2.3.4)
Batch 4	0.01M ODA (section 4.2.3.5)

Table 4.2b Mean % mass increase results for experiment 2 (n=5)

NO. OF DAYS		0	3	8	14	21	28	35	41
BATCH 1	*None*	0%	1.89%	5.17%	6.59%	7.28%	7.68%	7.98%	8.36%
BATCH 2	*Heated*	0%	2.16%	5.33%	6.40%	6.88%	7.52%	7.89%	8.26%
BATCH 3	*TTS*	0%	1.43%	2.34%	2.76%	3.10%	3.34%	3.61%	3.84%
BATCH 4	*ODA*	0%	1.45%	2.50%	2.86%	3.19%	3.37%	3.63%	3.89%

Figure 4.6 ***Experiment 2: Mean % mass increases against number of days in humidity cabinet***

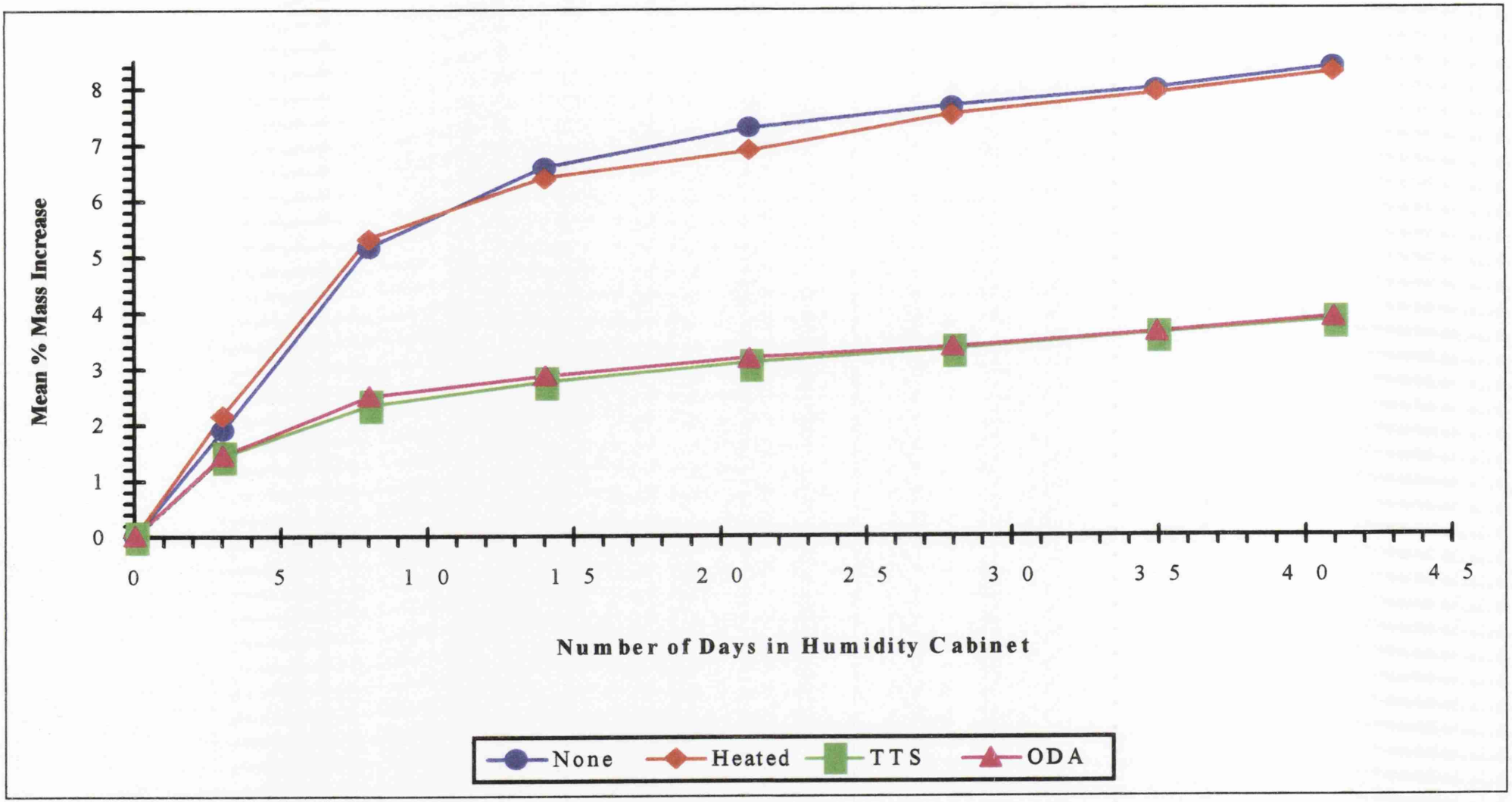

4.4.3 Experiment 3: Comparing, ODA, Silanes and TTS Using Corroded Coupons

A further accelerated corrosion test was carried out to test the silane inhibitors and assess their performance in comparison to ODA and TTS. Table 4.3a lists the treatments used. The coupons were corroded by method B. The coupons used were smaller than in the previous experiment. 1cm by 2cm coupons were used so that the silane treatments could be carried out in the available schlenk tube. To obtain mean % mass increase values of smaller error, larger batch sizes were used in this test. 15 coupons were used for each batch of differently treated samples. Table 4.3b and figure 4.7 show the results for the mean % mass increase for each batch. The accelerated corrosion test was carried out for 29 days, however the statistical analysis is based on the results after 21 days so as to correspond to the value of the standard deviation calculated from the pilot test carried out for 21 days.

Using the results of the pilot test I, the margin of error, D, for the mean % mass increase of a batch of 15 coupons after 21 days of the test, was found to be 0.57% at a 90% confidence level. Therefore values that differ by more than this amount can be considered statistically different. The results of this accelerated corrosion test show that the TTS and ODA treatments give some protection from corrosion whilst the ODTMS treatment can not be considered statistically different to the untreated sample and therefore can not be concluded to have given protection from corrosion to the coupons. In this experiment the ODA treatment has a slightly lower mean % mass increase, 3.54% after 21 days, compared to 3.85% and 3.82% for the two TTS treatments used. However, these values are within 0.57% and so the difference can not be considered as statistically significant and the performance of TTS and ODA can be considered equivalent.

In this experiment two TTS treatments were tested. Different concentration solutions of TTS were used in the treatments. The results for both batches are almost identical, showing that the concentration of this inhibitor treatment does not affect its efficiency. This confirms what would be expected. Above a critical concentration maximum surface coverage is achieved and therefore maximum inhibition is achieved. This relationship has been found for adsorption inhibitors, whose action on a metal surface has been described

using the Langmuir isotherm for monolayer adsorption (Sastri, 1998, 37). Further increase in the concentration of the initial treatment will not affect inhibitor efficiency. Both treatments were therefore carried out in an excess of titanate and it can be concluded that a 0.015M solution of TTS is adequate in providing maximum surface coverage. Any excess titanate is subsequently removed from the sample surface by rinsing in toluene.

The most unexpected result from experiment three is that the batch treated with HFTMS seems to have an accelerated rate of corrosion, in comparison to the untreated batch. After 29 days the untreated batch has a mean % mass increase of 5.06% whilst the HFTMS treated sample has a mean % mass increase of 7.90%, almost 3% greater than the untreated batch. Rather than inhibiting corrosion, the treatment has seemed to have increased the rate of corrosion.

To investigate this result further the standard deviations of the mean % mass increase values of each batch of coupons were calculated. These values are given in table 4.3c. The standard deviation (defined in section 4.3.2) is an indication of the spread of the values from which the mean is calculated. The standard deviation will obviously increase as the mean increases and therefore to compare the spread of each mean, the standard deviation as a percentage of the mean has also been calculated and given in table 4.3c.

It can be seen that the standard deviation and standard deviation expressed as a percentage of the mean value, for the batch treated with HFTMS, are much larger than those of all the other batches. The standard deviation as a percentage of the mean for the HFTMS batch ranges from 27.52% to 46.46%, whilst the other batches vary from 10.08% to 31.36%. A much wider range for the % mass increases of samples within the HFTMS batch, in comparison to the range in other batches is found. This suggests that rather than a uniform failure in the corrosion inhibition of the HFTMS treatment, only some of the coupons are failing, and causing an acceleration of corrosion, whilst other coupons within the batch are not corroding at an accelerated rate. Analysis of the raw mass increase data shows that after 2 days 11 of the coupons treated with HFTMS have individual % mass increases that are less than the mean % mass increase of the untreated batch, however after 29 days only 2 coupons are in this category. This shows that an increasing failure rate is occurring in the HFTMS treated coupons as the test proceeds.

Table 4.3a Treatments used in experiment 3

BATCH NUMBER	TREATMENT
Batch 1	Untreated
Batch 2	0.05M TTS (section 4.2.3.4.1)
Batch 3	0.015M TTS (section 4.2.3.4.2)
Batch 4	0.01M ODA (section 4.2.3.5)
Batch 5	0.015M HFTMS (section 4.2.3.3.1)
Batch 6	0.015M ODTMS (section 4.2.3.2.1)

Table 4.5b Mean % mass increase results for experiment 3 (n=15)

NO OF DAYS		0	2	4	7	14	21	29
BATCH 1	Untreated	0.00%	1.65%	2.33%	2.83%	3.77%	4.47%	5.06%
BATCH 2	0.05M TTS	0.00%	1.22%	1.84%	2.30%	3.17%	3.82%	4.37%
BATCH 3	0.015M TTS	0.00%	1.26%	1.87%	2.35%	3.20%	3.85%	4.42%
BATCH 4	0.01M ODA	0.00%	1.29%	1.85%	2.26%	2.96%	3.54%	4.06%
BATCH 5	0.015M HFTMS	0.00%	1.50%	2.63%	3.83%	5.66%	6.91%	7.90%
BATCH 6	0.015M ODTMS	0.00%	1.34%	1.91%	2.42%	3.25%	4.06%	4.39%

4.3c Standard deviations of mean % mass increases in experiment 3 (n=15)

NO OF DAYS		2			4			7			14		
		Mean	s.d	% s.d.	Mean	s.d	% s.d	Mean	s.d	% s.d	Mean	s.d	% s.d
BATCH 1	Untreated	1.65%	0.23%	13.94%	2.33%	0.35%	15.02%	2.82%	0.42%	14.89%	3.76%	0.58%	15.43%
BATCH 2	TTS	1.23%	0.17%	13.82%	1.83%	0.33%	18.03%	2.29%	0.42%	18.34%	3.17%	0.62%	19.56%
BATCH 3	TTS	1.26%	0.20%	15.87%	1.87%	0.35%	18.72%	2.35%	0.45%	19.15%	3.19%	0.63%	19.75%
BATCH 4	ODA	1.29%	0.13%	10.08%	1.84%	0.22%	11.96%	2.26%	0.28%	12.39%	2.95%	0.37%	12.54%
BATCH 5	HFTMS	1.49%	0.41%	27.52%	2.63%	0.92%	34.98%	3.83%	1.47%	38.38%	5.66%	2.38%	42.05%
BATCH 6	ODTMS	1.33%	0.27%	20.30%	1.91%	0.39%	20.42%	2.41%	0.48%	19.92%	3.25%	0.65%	20.00%

NO OF DAYS		21			29		
		Mean	s.d	% s.d	Mean	s.d	% s.d
BATCH 1	*Untreated*	4.47%	0.70%	15.66%	5.06%	0.79%	15.61%
BATCH 2	*TTS*	3.81%	0.77%	20.21%	4.36%	0.88%	20.18%
BATCH 3	*TTS*	3.85%	0.79%	20.52%	4.42%	0.91%	20.59%
BATCH 4	*ODA*	3.53%	0.50%	14.16%	4.05%	0.59%	14.57%
BATCH 5	*HFTMS*	6.91%	3.08%	44.57%	7.90%	3.67%	46.46%
BATCH 6	*ODTMS*	4.05%	1.27%	31.36%	4.38%	0.92%	21.00%

where s.d = standard deviation of the mean (as defined in section 4.3.2), % s.d = standard deviation expressed as % of the mean

Figure 4.7 ***Experiment 3: Mean % mass increases against number of days in humidity cabinet***

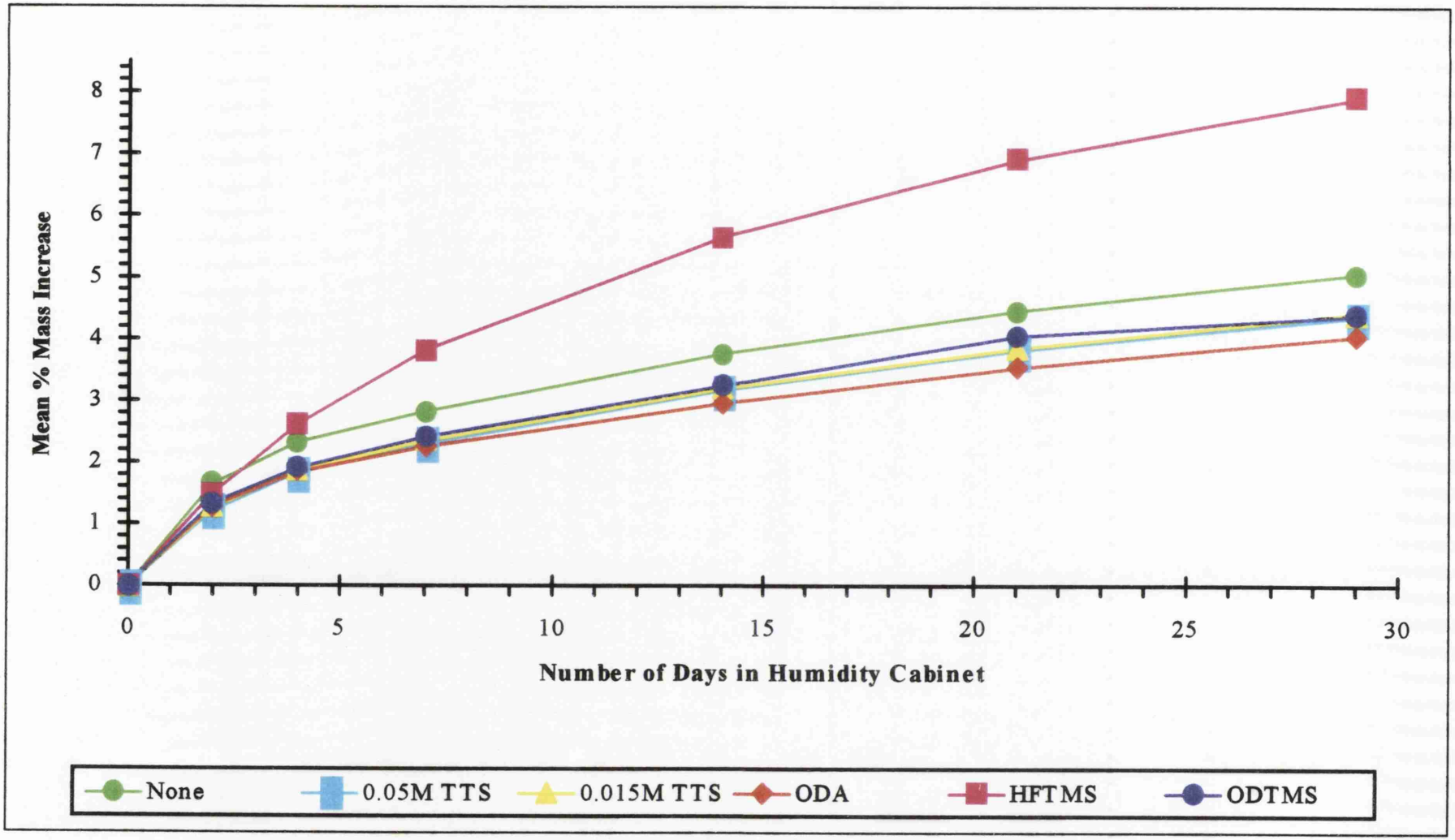

4.4.4 Experiment 4: Comparing HFTMS and Untreated Coupons

To confirm the unexpected acceleration of corrosion caused by the HFTMS treatment, another accelerated corrosion test was carried out. 2 batches of 9 coupons were tested. The coupons were 2cm by 5cm in size and corroded by method B. The treatment methods used are given in table 4.4a and the accelerated corrosion test results given in table 4.4b and figure 4.8. Using the results of pilot test II, the value of D (the acceptable margin of error at a 90% confidence level) was calculated to be 0.41%.

The results mirror those obtained in experiment 3. The mean % mass increase of the HFTMS coupons was more than 2% greater than that of the untreated coupons after 21 days. This shows that the HFTMS coupons corroded at a significantly greater rate than untreated coupons.

4.4.5 Experiment 5: Testing the Solvents Toluene and F-113

In an attempt to explain the causes of the accelerated corrosion for coupons treated with HFTMS, the effect of the solvent used to transport the inhibitor treatments to the sample surface was also tested. The HFTMS was dissolved in the solvent 1,1,2 trichlorotrifluoroethane ($CF_2ClCFCl_2$), F-1132, whilst in all other cases toluene was used as the solvent. Batches of 16 2cm by 5cm coupons, corroded by method B were treated with toluene and F-113 respectively as shown in table 4.5a. An accelerated corrosion test was carried out on these samples for 21 days. The results are shown in table 4.5b and figure 4.9.

The factor D, the allowable margin of error was calculated to be 0.31% after 21 days. The results therefore show no significant difference between the two batches treated with different solvents. In fact, although the rates of corrosion can not be considered statistically different, the batch treated with toluene has a percentage mass increase 0.3% greater than the F-113 batch after 21 days, therefore discounting any possibility that the F-113 solvent has a corrosive effect.

Table 4.4a Treatments used in experiment 4

BATCH	TREATMENT
Batch 1	Untreated
Batch 2	0.015M HFTMS (Section 4.2.3.3.1)

Table 4.4b Mean % mass increase results for experiment 4 (n=9)

NO OF DAYS		0	3	7	15	21
BATCH 1	*Untreated*	0.00%	2.35%	3.65%	4.97%	5.77%
BATCH 2	*HFTMS*	0.00%	2.62%	4.71%	6.96%	7.83%

Table 4.5a Treatments used in experiment 5

BATCH	SOLVENT
Batch 1	Toluene
Batch 2	F-113

Table 4.5B Mean % mass increase results for experiment 5 (n=16)

NO OF DAYS		0	1	4	7	21
BATCH 1	Toluene	0.00%	0.94%	1.84%	2.15%	3.81%
BATCH 2	F-113	0.00%	0.95%	1.78%	2.02%	3.61%

Figure 4.8 Experiment 4: Mean % mass increases against number of days in humidity cabinet

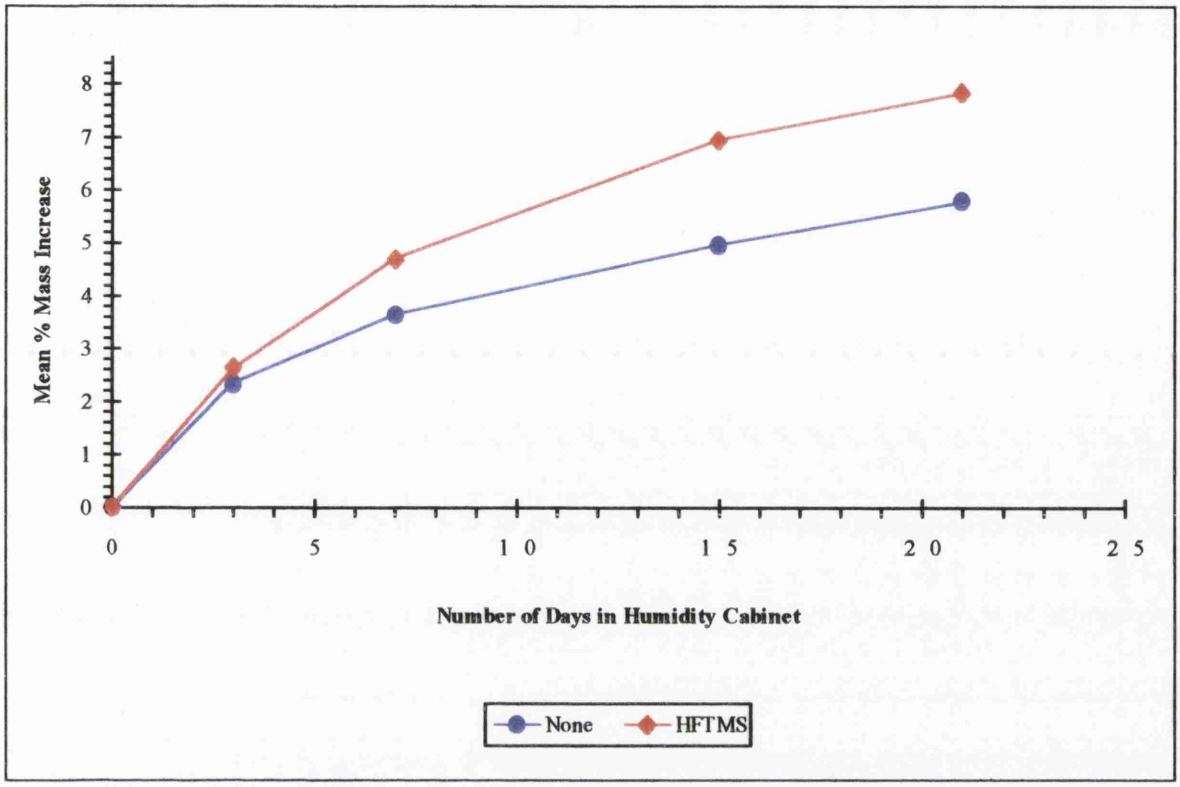

Figure 4.9 Experiment 5: Mean % mass increases against number of days in humidity cabinet

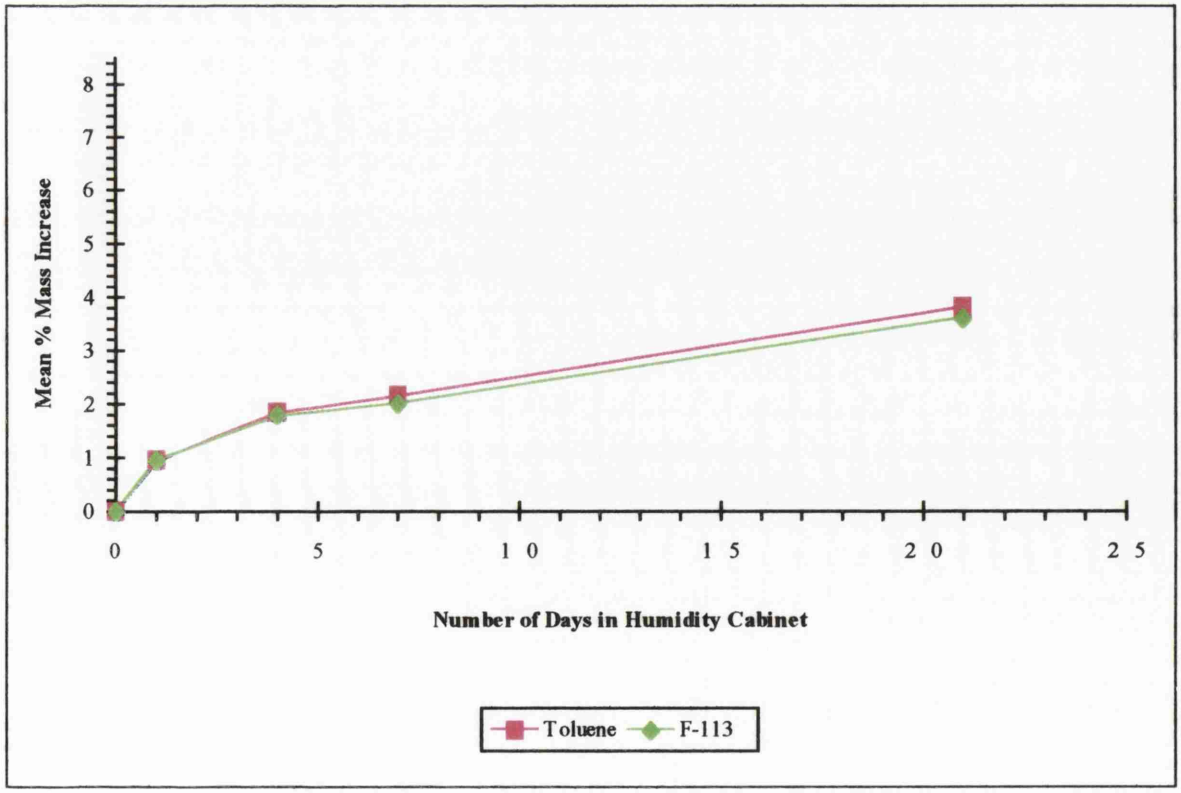

4.4.6 Experiment 6: Comparing ODTMS, HFTMS and HFTMS and Pyridine

It was hypothesised that when treated with HFTMS the hydrophobic layer formed by the treatment on the surface of the corrosion product layer prevented the formation of a condensed water layer. Its absence may lead to a greater diffusion of oxygen to the corroding surface, where a small amount of water contained within the corrosion products may already exist. The greater oxygen concentration may thus facilitate a faster rate of corrosion. Untreated samples have layers of condensed water on the surfaces of the corrosion products (Corvo *et al*, 1997, Clarke & Hall, 1991, Zettlemoyer *et al*, 1966), and this would limit oxygen diffusion and thus the rate of corrosion would be less (Williams, 1997). Although this hypothesis fails to explain the difference in the performance of other treatments, it was decided to carry out further investigations.

It was decided to test the hypothesis by treating HFTMS batches with a further inhibitor. It was hoped that the addition of a second inhibitor would prevent the mechanism by which corrosion was being accelerated. A second inhibitor adsorbed onto the metal or corrosion product surfaces would prevent the oxygen that diffuses through the HFTMS barrier from reaching the corroding surface, and thus reverse the effect that caused the acceleration of the corrosion rate of coupons treated with HFTMS. Coupons were treated with pyridine, C_5H_5N, a known organic corrosion inhibitor for iron (Jones, 1992, 507). Treatment with pyridine was carried out on 2 batches of coupons, one treated before the HFTMS treatment and one after the HFTMS treatment. This is described in sections 4.2.3.3.3 and 4.2.3.3.4.

Batches of 13 2cm by 5cm coupons, corroded by Method B, were treated as shown in table 4.6a. The accelerated corrosion test was carried out for 35 days. The results of the accelerated corrosion test are given in table 4.6b and figure 4.10. Using the standard deviation value from pilot test 2, the margin of error D, was calculated to be 0.34%. The results show that as in previous experiments the coupons treated with HFTMS alone have an accelerated rate of corrosion in comparison to the untreated batch. The mean % mass increase after 21 days being 6.50% as compared to 4.13% for the untreated batch. The batch treated with ODTMS has a slightly lower rate of corrosion than the untreated

control batch, however the difference in % mass increases after 21 days is within the factor D, and therefore the difference can not be seen as statistically significant.

Both batches treated with HFTMS and pyridine have almost identical mean % mass increases. This seems to indicate that the order in which the treatments are carried out has no effect on the corrosion inhibition. The rate of corrosion, as inferred from % mass increase data for both HFTMS and pyridine treated batches is substantially less than from the batch treated with HFTMS alone. However the corrosion rates are not lower than the untreated batch, if anything being slightly higher. The addition of the pyridine treatment does seem to have prevented the acceleration of the corrosion rate, but the batches still do not have a better survival rate than the untreated batch. The decrease in the corrosion rate observed may be explained from the inhibitive effect of the pyridine alone and we can not accept the original hypothesis that the addition of a second inhibitor will convert the HFTMS treatment from a treatment that accelerates corrosion to a treatment that inhibits corrosion.

Table 4.6a Treatments Used in experiment 6

BATCH NUMBER	TREATMENT
Batch 1	Untreated
Batch 2	0.03M ODTMS (section 4.2.3.2.2)
Batch 3	0.03M HFTMS (section 4.2.3.3.2)
Batch 4	HFTMS/Pyridine (section 4.2.3.3.3)
Batch 5	Pyridine/HFTMS(section 4.2.3.3.4)

Table 4.6b % Mass Increase Results for experiment 6

NO OF DAYS		0	2	7	14	21	35
BATCH 1	*Untreated*	0.00%	1.41%	2.66%	3.58%	4.13%	4.97%
BATCH 2	*ODTMS*	0.00%	1.52%	2.62%	3.40%	3.90%	4.46%
BATCH 3	*HFTMS*	0.00%	1.49%	3.89%	5.69%	6.50%	6.91%
BATCH 4	*HFTMS/Pyridine*	0.00%	1.29%	2.94%	4.10%	4.63%	4.90%
BATCH 5	*Pyridine/HFTMS*	0.00%	1.28%	2.60%	3.82%	4.47%	4.83%

Figure 4.10 Experiment 6: Mean % mass increases against number of days in humidity cabinet

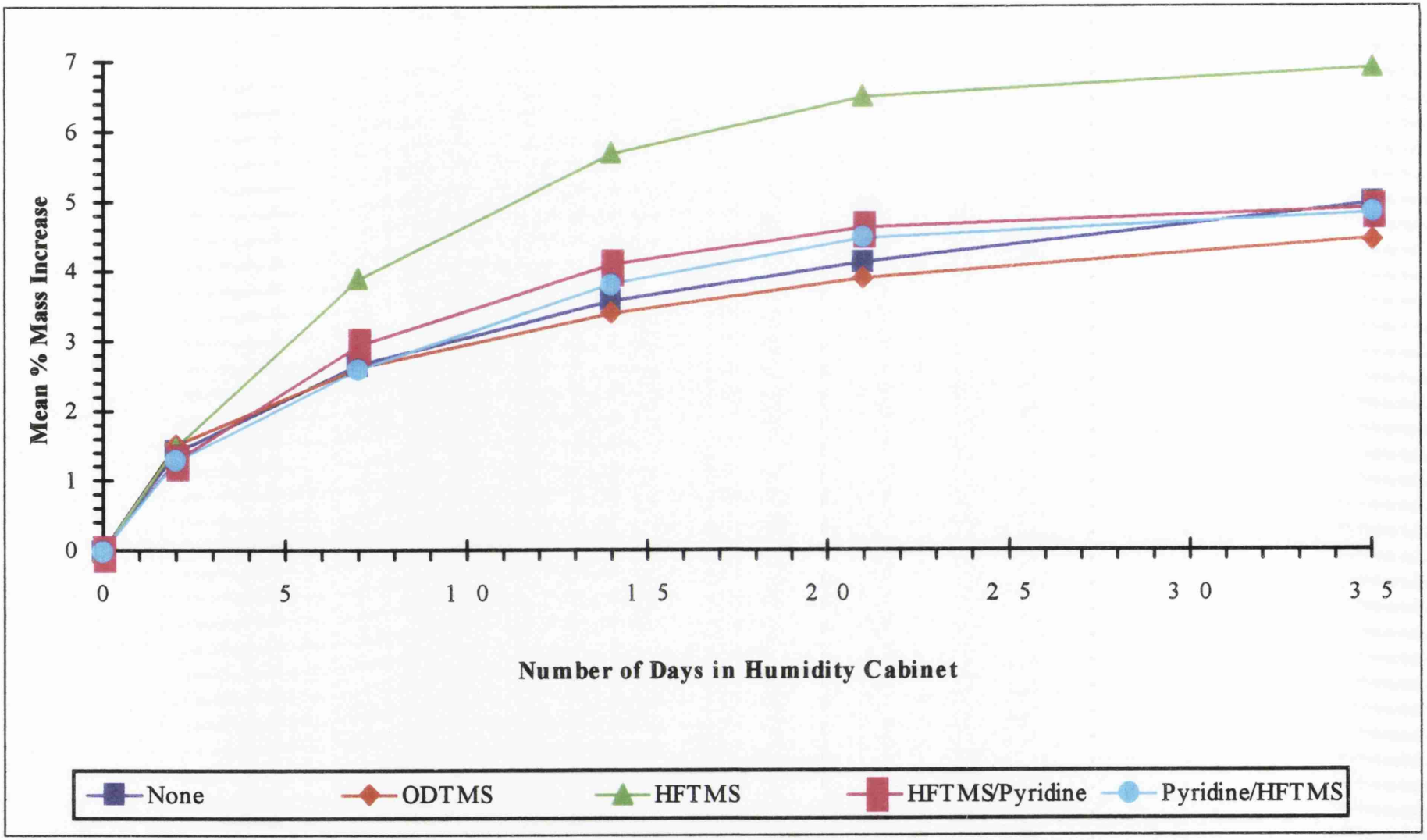

CHAPTER FIVE

Water Adsorption Isotherms, Floatation Tests and Electrochemical Monitoring

5.1 WATER ADSORPTION ISOTHERMS

5.1.1 Introduction

Atmospheric corrosion occurs due to a layer of water adsorbed onto a metal surface. The amount of water adsorbed will depend on the relative humidity of the atmosphere and on the chemical and physical properties of the metal surface (Corvo *et al*, 1997). When a layer of corrosion products exists between the metal-atmosphere interface, the adsorption properties of those salts will greatly effect the amount of water on the corroding surface and thus effect the rate of corrosion. The composition, structure and physical characteristics of corrosion products present will also affect the extent of water adsorption. Research has shown chloride or sulphate containing corrosion products will adsorb polymolecular water layers, whilst low chloride or sulphate concentration corrosion products will only absorb a monomolecular layer of water (Corvo *et al*, 1997). The porous nature of many corrosion products also increases the water retained in corrosion products due to capillary condensation.

The presence of a water film on a metal surface is linked to the ambient humidity of the atmosphere. The point at which water vapour condenses to form a film is known as the critical relative humidity. At this point corrosion can occur. It has already been argued that the presence of corrosion product salts can greatly decrease the critical relative humidity due to their hydroscopic nature (Evans & Taylor, 1972). Generally, the critical humidity is

close to the vapour pressure of a saturated solution of the salts that make up the corrosion products.

The approach taken in this work is to try and prevent the condensation of water films on the metal and the metal oxide surfaces. If the formation of a water layer can be prevented, then the likelihood of further atmospheric corrosion will be reduced. The inhibiting treatments used are all molecules that form a hydrophobic layer. A measure of the effectiveness of the inhibitors used would therefore be to assess the extent of water adsorption occurring on treated and untreated samples of the compounds that are contained in corrosion layers. The effectiveness of inhibitor treatments can then be examined and comparisons of the amount of water adsorbed can be made. This can be carried out by measuring small changes in the mass of iron oxyhydroxide samples as the humidity is changed. When water is adsorbed the mass will increase. The size of the increase is dependent on the amount of water that is adsorbed onto the iron oxyhydroxides samples. This is the theoretical basis for the measurement of water adsorption isotherms. Measurements have been made on iron oxyhydroxide powders to simulate the effect of water adsorption on the surface of corroded iron objects. Oxyhydroxides have been tested as these corrosion products are often found on the surfaces of archaeological iron objetcs. The mechanisms by which they absorb water and other gases have been described in chapter one. Although the corrosion products on archaeological objects have more compact surfaces than the powders tested, the use of α-FeOOH and β-FeOOH powders in this study allows for comparative quantitative measurements to be made.

5.1.2 Water Adsorption Isotherms

5.1.2.1 Structure of Adsorbed Water

The adsorption of water onto iron oxyhydroxides has already been described in section 1.5.4. The basic model of adsorption of water on most iron oxide and oxyhydroxides is that of chemisorption by a dissociative mechanism, whereby OH^- and H^+ are absorbed onto surface ferric ions, so forming 2 hydroxyl groups at the oxide surface. β-FeOOH also has tunnel sites in which water can be adsorbed (Kaneko *et al*, 1975). Further

physisorption then occurs with an immobile first layer, with successive layers undergoing a gradual transition through a mobile second layer to an ice-like structure in the next few layers (McCafferty *et al*, 1969).

The first physically adsorbed water is doubly hydrogen bonded to the underlying hydroxyl layer (Zettlemoyer *et al*, 1966, Kaneko *et al*, 1974, 1979). After initial physisorption by hydrogen bonding, some water molecules will give an electron to the oxide surface, and become chemisorbed. The chemisorbed water molecules donate an electron to the t_{2g} orbital of the Fe(III) site on the oxyhydroxide lattice:

$$H_2O(\text{chemisorbed}) \quad \Leftrightarrow \quad H_2O^+(\text{chemisorbed}) + e(t_{2g})$$

where $e(t_{2g})$ denotes the electron in the t_{2g} orbital (Kaneko & Inouye, 1979). Water molecules are connected to the FeOOH surface by both hydrogen bonding and weak charge transfer.

The subsequent mobile layers of water also have some structure and have been shown to hydrogen bond in the manner of ice for the first 2 to 3 water layers. The adsorbed water molecules are connected to each other by tetrahedral hydrogen bonding (Kaneko *et al*, 1979). Further water layers (up to seven layers have been detected) tend towards a liquid water structure as the ordering influence of the surface is overcome (MaCafferty *et al*, 1969). This however may be more appropriately viewed as an order-disorder transition of hydrogen atoms, rather than a solid-liquid phase transition (Kaneko *et al*, 1979).

5.1.2.2 Adsorption Isotherms

A free gas and an adsorbed gas are in dynamic equilibrium. The fractional coverage of a solid surface with a gas, θ, depends on the pressure of the overlying gas. The dependence of θ on the pressure at a set temperature is called an adsorption isotherm. Different types of gas adsorption have been modelled by different adsorption isotherms. The simplest model is the Langmuir isotherm, which is based on the assumption that all adsorption sites are equivalent and that the probability of adsorption at any particular site is independent of that occupancy of other surface sites. If the dynamic equilibrium is shown as:

$$A(g) + M(\text{surface}) \quad \Leftrightarrow \quad AM(\text{surface})$$

with a rate constant K_a for adsorption, and K_d for desorption, the rate of change of surface coverage due to adsorption will be proportional to the pressure (P) of A and the number of vacant sites, $N(1-\theta)$, where N is the total number of sites:

$$\frac{d\theta}{dt} = K_a PN(1-\theta)$$

The rate of change of θ due to desorption is proportional to the number of adsorbed species, $N\theta$, and therefore:

$$\frac{d\theta}{dt} = K_d N\theta$$

At equilibrium these two rates are equal and so we can obtain the Langmuir isotherm

$$\theta = \frac{KP}{1 = KP} \quad \text{where} \quad K = \frac{K_a}{K_d}$$

The Langmuir isotherm however is only a valid model for monolayer adsorption. It levels off to the same saturated value rather than rising indefinitely at higher pressures as would be expected for multilayer adsorption. Therefore for multilayer adsorption the B.E.T. (named after Brunauo, Emmett and Teller) adsorption isotherm is most widely used (Atkins, 1990). The B.E.T isotherm can be defined as follows:

$$\frac{V}{V_{mon}} = \frac{cz}{[1-z][1-(1-c)z]} \quad \text{where} \quad z = \frac{P}{P^*}$$

where P^* is the vapour pressure above a macroscopically thick layer of the pure liquid on the surface, V is the volume of adsorbed gas, V_{mon} is the volume of adsorbed gas corresponding to monolayer coverage and c is a constant. The B.E.T. isotherm can also be expressed in the form:

$$\frac{z}{(1-z)V} = \frac{1}{cV_{mon}} + \frac{(c-1)z}{cV_{mon}}$$

The constant c is related to the enthalpy of desorption from a monolayer and the enthalpy of vaporisation of the adsorbate. When the enthalpy of desorption is large in comparison to the enthalpy of vaporisation, the coefficient c is large ($c >> 1$) and the B.E.T isotherm simplifies to:

$$\frac{V}{V_{mon}} = \frac{1}{1-z}$$

The B.E.T. isotherm fits observed results moderately well, but it tends to underestimate the extent of adsorption at low pressure and overestimates adsorption at high pressures. This failure is due to the factors that the B.E.T model does not account for, such as, the

heterogeneous nature of most surfaces (so that adsorption on all sites does not have an equal probability) and the horizontal interactions (parallel to the surface) between adsorbed molecules, especially at high coverages (Gregg & Sing, 1967). Figure 5.1 illustrates isotherms that fit the Langmuir and B.E.T. models. The B.E.T. model divides isotherms into 5 basic types. Type I is the equivalent of Langmuir type adsorption. The type of isotherm produced will depend on the type of surface a material possesses and factors such as porosity, pore size and frequency.

Figure 5.1 The five types of adsorption isotherm in the B.E.T. classification (Gregg & Sing, 1967)

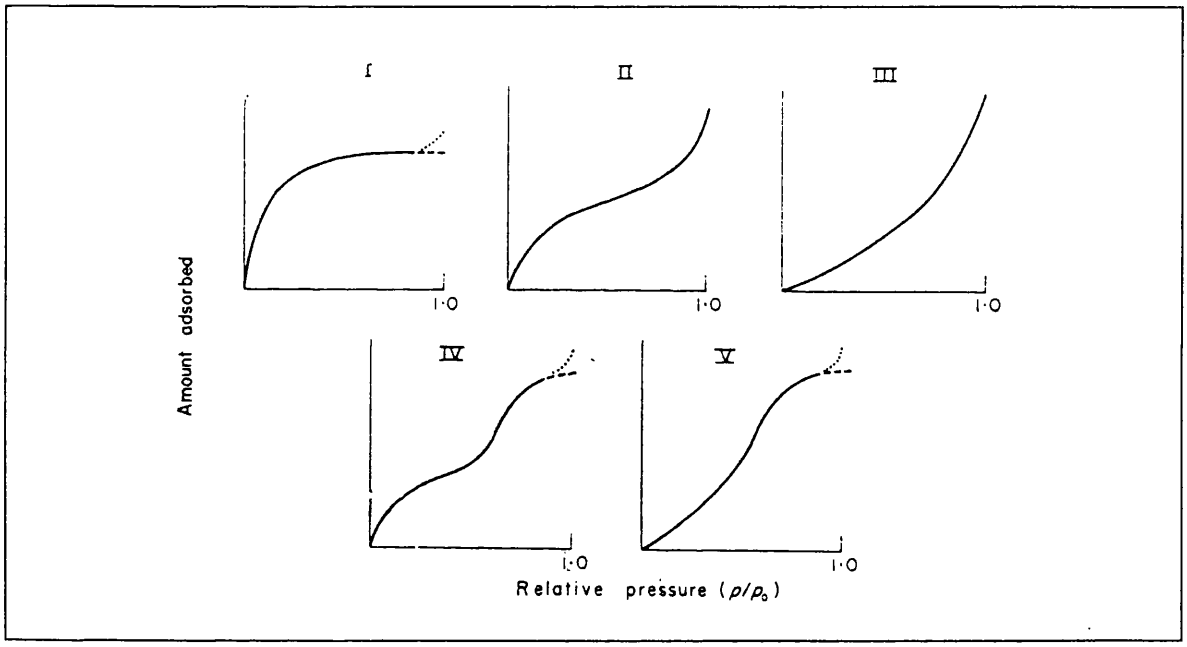

5.1.2.3 Water Adsorption Isotherms

A water adsorption isotherm is a measure of the amount of water that is adsorbed onto the surface of a solid with changing partial pressure of water vapour (humidity). The amount of water adsorbed per gram of solid will depend on the partial pressure and temperature. Adsorption can be measured in grams, milligrams, moles or centimetres squared.

In this work, water adsorption isotherms were obtained by measuring mass changes in a sample of iron oxyhydroxide powder as the relative humidity was varied from 0% to 80% or 100%. The α-FeOOH and β-FeOOH phases of iron oxyhydroxide were synthesised and used to mirror the effect of water vapour on corrosion products. α-FeOOH is a corrosion

product predominantly found near the surface corrosion layers. The role of β-FeOOH in post excavation corrosion has already been described in section 1.5.1

It is common to look at the adsorption of a gas such as Nitrogen and the record an adsorption isotherm by measuring mass or volume changes with change in pressure of the gas. However, for water adsorption the case differs slightly in that water vapour is carried in air. Rather than varying the absolute pressure of this gas mixture, the proportions of water vapour to air in the mixture is varied, effectively changing the partial pressure of the water vapour (at constant temperature), in other words, varying the humidity. The partial pressure of water vapour was measured in terms of relative humidity, RH, which is given as a percentage and is defined as follows:

$$RH\% = \frac{AbsoluteHumidity}{SaturationHumidity} x100$$

A relative humidity of 100% indicates totally saturated air, whilst 0% relative humidity indicates completely dry air. Varying relative humidity can therefore be formed by mixing differing proportions of dry air and water vapour saturated air, so that relative humidity, RH, can also be defined as:

$$RH(\%) = \frac{P_{wv}}{P_{WV} + P_D}$$

where P_{wv} = the pressure of water vapour saturated air and P_D = the pressure of dry air.

5.1.3 Synthesis of Iron Oxyhydroxides

5.1.3.1 Synthesis of α-FeOOH

α-FeOOH, goethite, was prepared following the method originally given in Atkinson *et al* (1967). 200ml of 2.5M potassium hydroxide was added dropwise to 825ml of 1.25M aqueous ferric nitrate solution, $Fe(NO_3)_3$. The solution was continuously stirred during the addition, and then left stirring at 60°C for 24 hours. The precipitate formed was then separated by centrifugation. It was washed several times with dilute potassium hydroxide and then with distilled water. The precipitate was finally dried in air at 42°C overnight and stored in a sealed sample tube until used.

5.1.3.2 Synthesis of β-FeOOH

The synthesis of β-FeOOH was carried out following the method originally given by Matijevic *et al* (1978) and also used by Paterson and Rahman (1983). A 3 litre aqueous solution of 0.09M ferric chloride, $FeCl_3$, and 0.01M hydrochloric acid was made. This solution was then heated to 95°C and stirred for 24 hours. The solution was then left to cool to room temperature and centrifuged, pouring off the liquid. The precipitate obtained was then redispersed several times until no soluble iron could be detected. Soluble iron was tested for using thiocynate indicator paper. The precipitate of β-FeOOH was dried in air overnight at 42°C and stored in a sealed sample tube until used.

5.1.4 Treatment of α-FeOOH and β-FeOOH Samples with Inhibitive Treatments

5.1.4.1 Treatment with a 0.015M solution of ODTMS

1g of both α-FeOOH and β-FeOOH were separately treated with 0.015M solution of ODTMS in toluene in a similar manner to that described in section 4.2.3.2.1. The concentration of 0.015M was chosen in all treatments, being large enough for maximum inhibitor coverage. 1g of powder was treated with $10cm^3$ of the inhibitor solution. Care was taken when evacuating the schlenk tube, so that the powder was not sucked upwards. Once treated powders were rinsed in ethanol which was then removed via a delivery tube covered with filter paper. The powders were then rinsed in distilled water, which was again removed via a delivery tube. The powders were then placed in an oven at 150°C for 30 minutes. After treatment powders were stored in sealed sample tubes.

5.1.4.2 Treatment with 0.015M HFTMS

1g of both α-FeOOH and β-FeOOH were separately treated with 0.015M HFTMS as described in section 4.2.3.3.1. The differences to this procedure are the same as those differences described in section 5.2.4.1. After treatment powders were stored in sealed sample tubes.

5.1.4.3 Treatment with 0.015M TTS

1g of both α-FeOOH and β-FeOOH were separately treated with 0.015M TTS in toluene solution as described in section 4.2.3.4.1. However no vacuum was applied in the reaction as the sample was in loose powder form and so it was decided that there was no need for a vacuum to help the solution penetrate. The powders were removed from the TTS solution by centrifugation. The powders were rinsed twice in toluene and centrifuged to recollect the powders, which were finally allowed to dry in air overnight and stored in sealed sample tubes.

5.1.4.4 Treatment with 0.01M ODA

1g of both α-FeOOH and β-FeOOH were separately treated with a 0.01M solution of ODA in toluene as described in section 4.2.3.5.1. However, no vacuum was applied. Samples were rinsed twice with toluene, centrifuging between washes to reclaim the precipitate. The powders were dried in air overnight, and stored in sealed samples tubes.

5.1.5 Experimental Method for Recording Water Adsorption Isotherms of Inhibitor Treated and Untreated Samples of α-FeOOH and β-FeOOH

Water adsorption isotherms were measured using the microbalance apparatus illustrated schematically in figure 5.2. A Cahn D-200 microbalance was used to measure the changing mass of powdered samples. The microbalance consists of a quartz boat to contain a sample suspended from a platinum wire, counterbalanced by another quartz boat on a platinum wire which was used to contain weights to counterbalance the sample. The balance consists of the weighing unit which detects the actual weight, and a control unit which contains most of the electronics and from where the output data is sent to a computer. The balance works by converting a force to an electrical current. The balance beam pivots about an axis of rotation when a force is applied. An electric current flowing in a torque motor located in a permanent magnetic field at the pivot point also produces a force about the axis. This will be equal to the force from the quartz boat when the beam is at the beam reference position. The reference position is detected by a sensing system. The current necessary to produce the required torque motor force is therefore a direct measure of the mass of the sample and sample boat. Calibration of this current allows measurement in

units of weight. The balance has a sensitivity to change as small as 0.1mg. The mass of the sample is electronically recorded and displayed using the Cahn D-200 software on a computer. The data could be copied as standard data file. The whole balance was contained in a vibration free box.

Figure 5.2 Schematic diagram of Cahn D-200 microbalance (Cahn D-200 Instrument Manual, 1992)

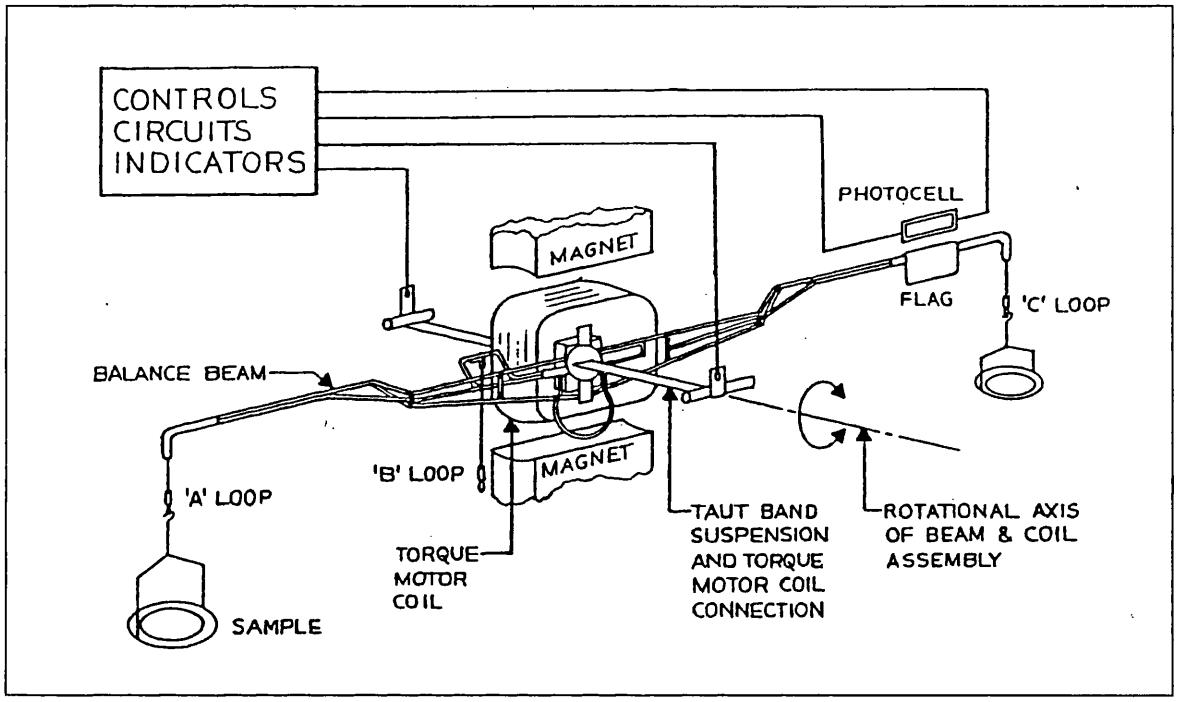

The balance was calibrated before each experiment using an 100mg weight. Roughly 10mg (±0.5mg) of powder, was placed in the quartz sample holder, after setting the balance to zero with the empty quartz sample holder. The sample holder was suspended on a platinum wire. This was placed inside a glass tube with an inlet for the water vapour supply. A plastic stopper was placed in the neck of the inlet arm to seal the glass tube. The vacuum pump attached to the apparatus was then used to evacuate the glass tube containing the sample. The powder was left under vacuum overnight to drive off any water adsorbed onto the powder surface.

Mass recording were then obtained at a range of relative humidity. A flow of water vapour was connected to the microbalance via the inlet arm on the glass tube which had previously been stoppered. A total gas flow of 500cm^3/min was used, and differing relative humidity

obtained by mixing the correct proportions of a totally dry air flow with a water saturated air flow, obtained by passing the air through a water bubbler. The air flow was controlled by gas flow controllers, which were controlled by a computer program. The computer program controlled the relative humidity and also the length of time at which gas flow of any particular relative humidity was to flow over the powdered sample. Experiments were carried out at room temperature, 20-25°C.

For an equilibrium value of water adsorption to be recorded, several hours were needed at each relative humidity. At higher humidity longer times were needed as more absorption was taking place. For 0% and 20% relative humidity, readings were taken after 6 hours. For 40% and 60%, readings were taken after 8 hours. For 80% relative humidity, the mass was recorded after 10 hours and for 90% and 100% relative humidity, the mass was recorded after 20 hours. From the data obtained and the original mass of the dry sample, the mass increases were determined, and therefore the mass of water adsorbed by 1g of α-FeOOH and β-FeOOH was calculated. This data was collected for untreated oxyhydroxide samples and samples treated with inhibitors. Water adsorption isotherms in the form of mass of water adsorbed by 1g of solid, against relative humidity were plotted for all samples.

5.1.6 Water Adsorption Isotherm Results

Figure 5.3a illustrates the resulting adsorption isotherms from α-FeOOH powder and α-FeOOH powders treated with the various inhibitors tested. It can be seen that the isotherm for α-FeOOH matches a B.E.T. type II adsorption isotherm. This is confirmed in the literature (Clarke & Hall, 1991, Gonzalez Calbet *et al*, 1981).

All treated α-FeOOH samples show a considerably reduced amount of adsorbed water present at all relative humidities, and certainly between 50% and 70%, the range that might be expected in ambient museum environments. The samples treated with TTS, ODTMS and HFTMS show especially low levels of water adsorption. The ODA treated α-FeOOH does not perform as well and adsorbs significantly more water. Its isotherm has a similar shape to that of the untreated α-FeOOH indicating that as in this case, B.E.T. type II

multilayer adsorption is occurring. The desorbtion of ODA molecules must therefore be occurring, leading to the adsorption of further water molecules.

The measurement made for samples treated with TTS, ODTMS, and HFTMS show a slightly different behaviour. The amount of water adsorbed, even at 90% humidity is significantly lower than that of the untreated or ODA treated powder. The HFTMS treated sample adsorbed the least amount of water followed by the TTS treated powder and then the ODTMS treated powder. The differences are very small and can not be considered significant, but must be seen as within the degree of experimenal error caused by small fluctuations in temperature during the experiment.

The shape of these three isotherms also differs from that of the B.E.T type II isotherm observed for α-FeOOH. They fit the B.E.T. type I or Langmuir model. This indicates that only monolayer adsorption is occurring. A linear plot can be derived from the Langmuir isotherm if it is expressed as follows:

$$KP\theta + \theta = KP$$

If $\theta = V/V_\infty$, where V is the volume of gas adsorbed and V_∞ is the volume corresponding to complete coverage of all available adsorption sites in a monolayer, this becomes:

$$\frac{P}{V} = \frac{P}{V_\infty} + \frac{1}{KV_\infty}$$

Therefore if P/V is plotted against P, a gradient of the reciprocal of the monolayer coverage will be obtained.

Substituting the relative humidity for the value P, and the mass of water absorbed onto 1g of α-FeOOH as V, a pseudo-Langmuir plot can be obtained for the absorbtion of water onto the TTS, ODTMS and HFTMS treated α-FeOOH powders. Relative humidity divided by Mass of water adsorbed has been plotted against relative humidity. This is shown in figure 5.4. From the gradients of these best fit linear plots, monolayer coverages of 4.55mg/g, 6.02mg/g and 7.66mg/g were calculated respectively for the HFTMS, TTS and ODTMS treated α-FeOOH samples.

Similar trends can be seen in the water adsorption isotherms for β-FeOOH powders treated and untreated. The isotherm for the untreated β-FeOOH is of the B.E.T. type IV, as confirmed in the literature (Brunaver *et al*, 1940, Gonzalez Calbet *et al*, 1981). Type IV isotherms resemble type II isotherms but occur with porous materials. This means that adsorption occurs not only on the surface of the material but also inside the pores. Type II and IV differ in their desorption behaviour, the later retaining adsorbed water due to capillary condensation which causes the formation of hysteresis loops (Gregg & Sing, 1967, 121).

As with the α-FeOOH, all β-FeOOH samples treated with inhibitors absorb less water than the untreated sample. In this case the ODA treated powder behaves in a similar hydrophobic manner as the other treatments until about 80% relative humidity. At this point it can be postulated that desorbtion of the ODA molecules causes the increase in the amount of water adsorbed.

The other three treatments behave in a similar manner with very little differences. These isotherms do however still have the B.E.T. type IV isotherms and do not fit the Langmuir model of monolayer adsorption. This indicates that even when treated with hydrophobic molecules, some multilayer adsorption, perhaps within pores, still occurs with β-FeOOH.

The study of the water adsorption isotherms of α-FeOOH and β-FeOOH has shown that the three treatments, TTS, ODTMS, and HFTMS do provide a hydrophobic coating to iron oxyhydroxide powders and greatly reduce the extent of water adsorption. The reduction of water adsorption is much less for ODA which acts as a less efficient hydrophobing agent. The performance of these surface treatments on oxyhydroxide powders gives an indication of how the treatments will change the hydrophilic nature of corrosion products and the surfaces of archaeological iron objects.

Figure 5.3a Water adsorption isotherms for α-FeOOH, showing the amount of water adsorbed onto 1g of α-FeOOH in mg against percentage relative humidity

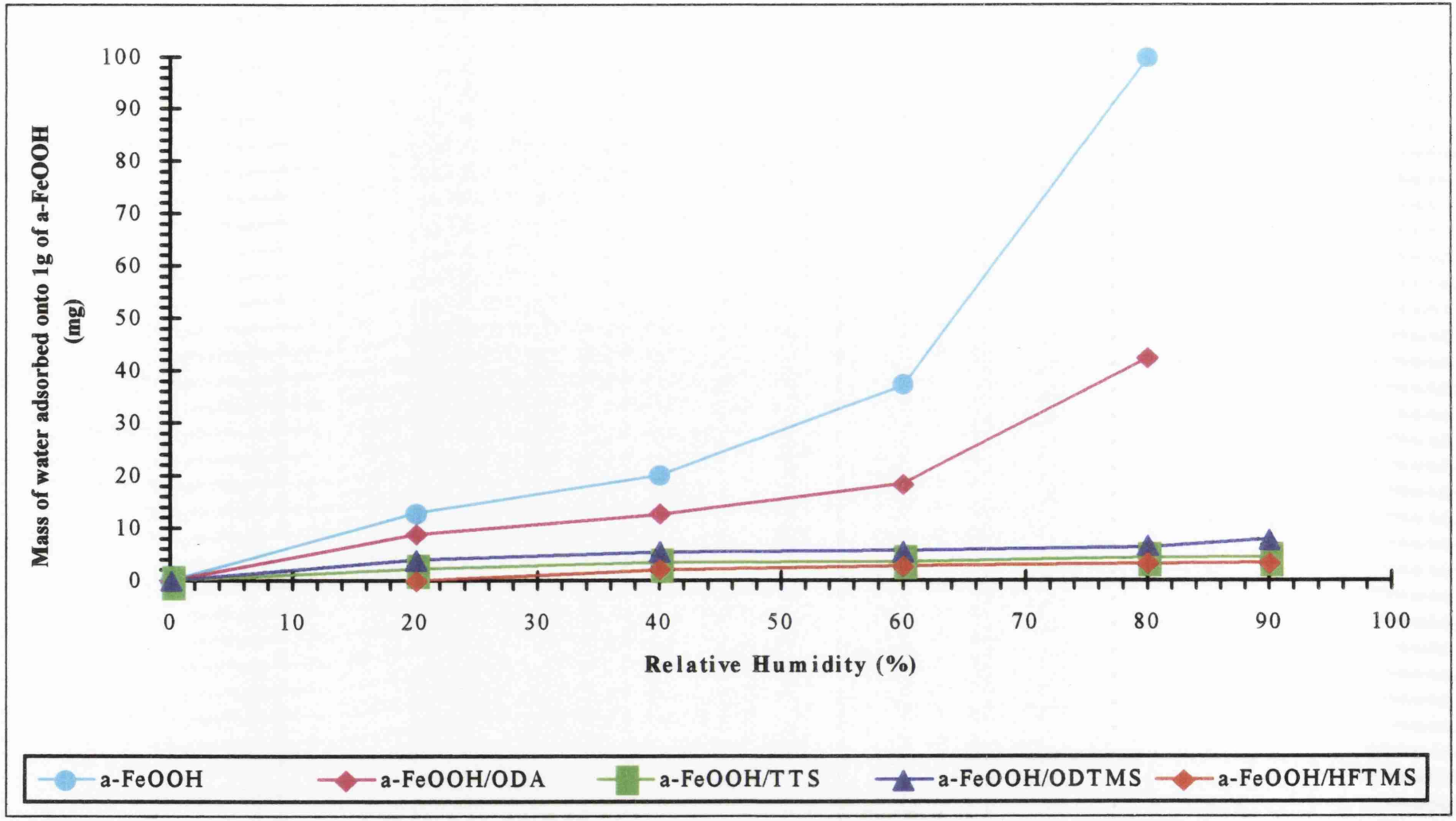

Figure 5.3b Water adsorption isotherms for β-FeOOH, showing the amount of water adsorbed onto 1g of β-FeOOH in mg against percentage relative humidity

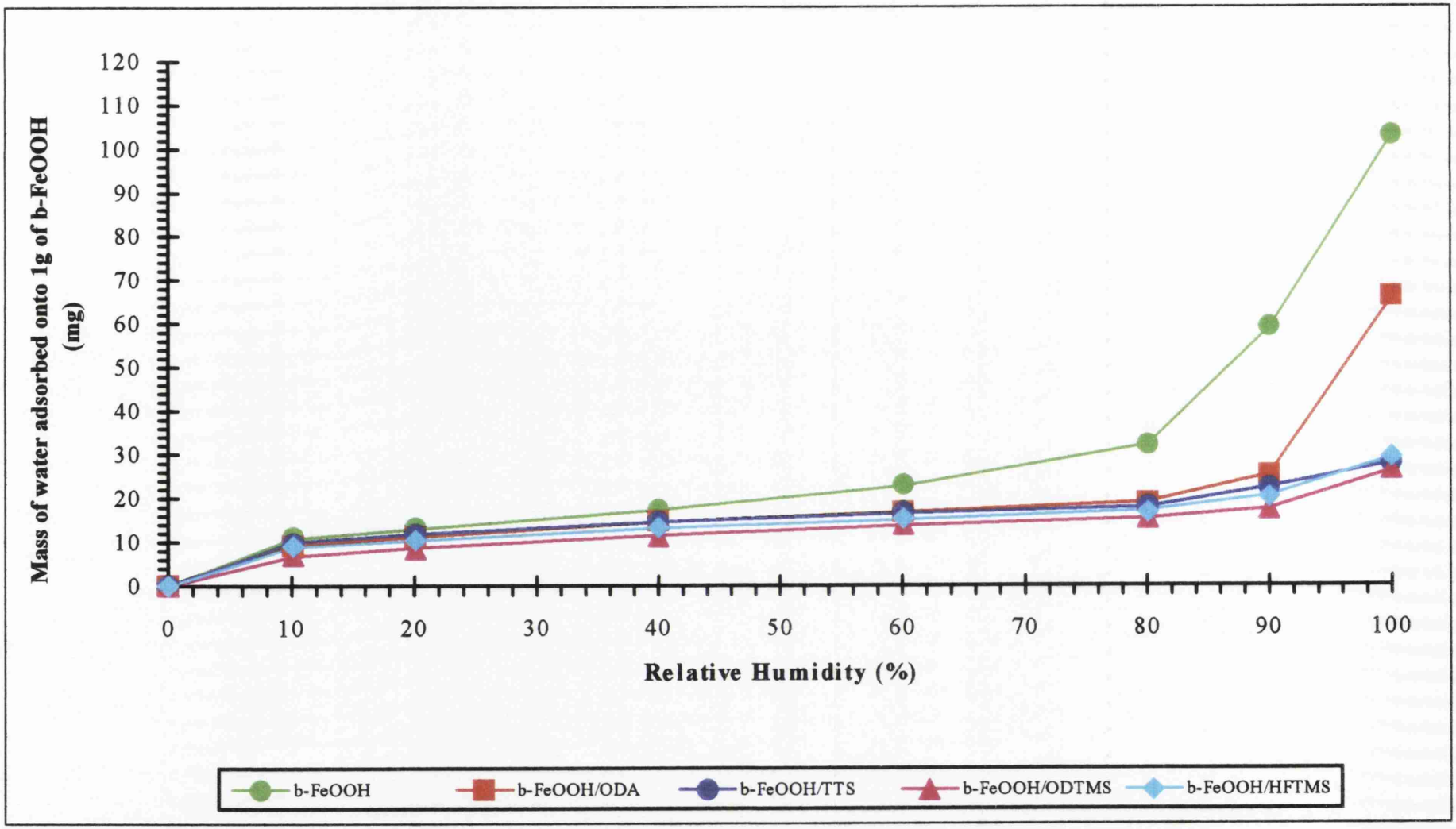

Figure 5.4 Pseudo-Langmuir plots for α-FeOOH treated with TTS, ODTMS and HFTMS

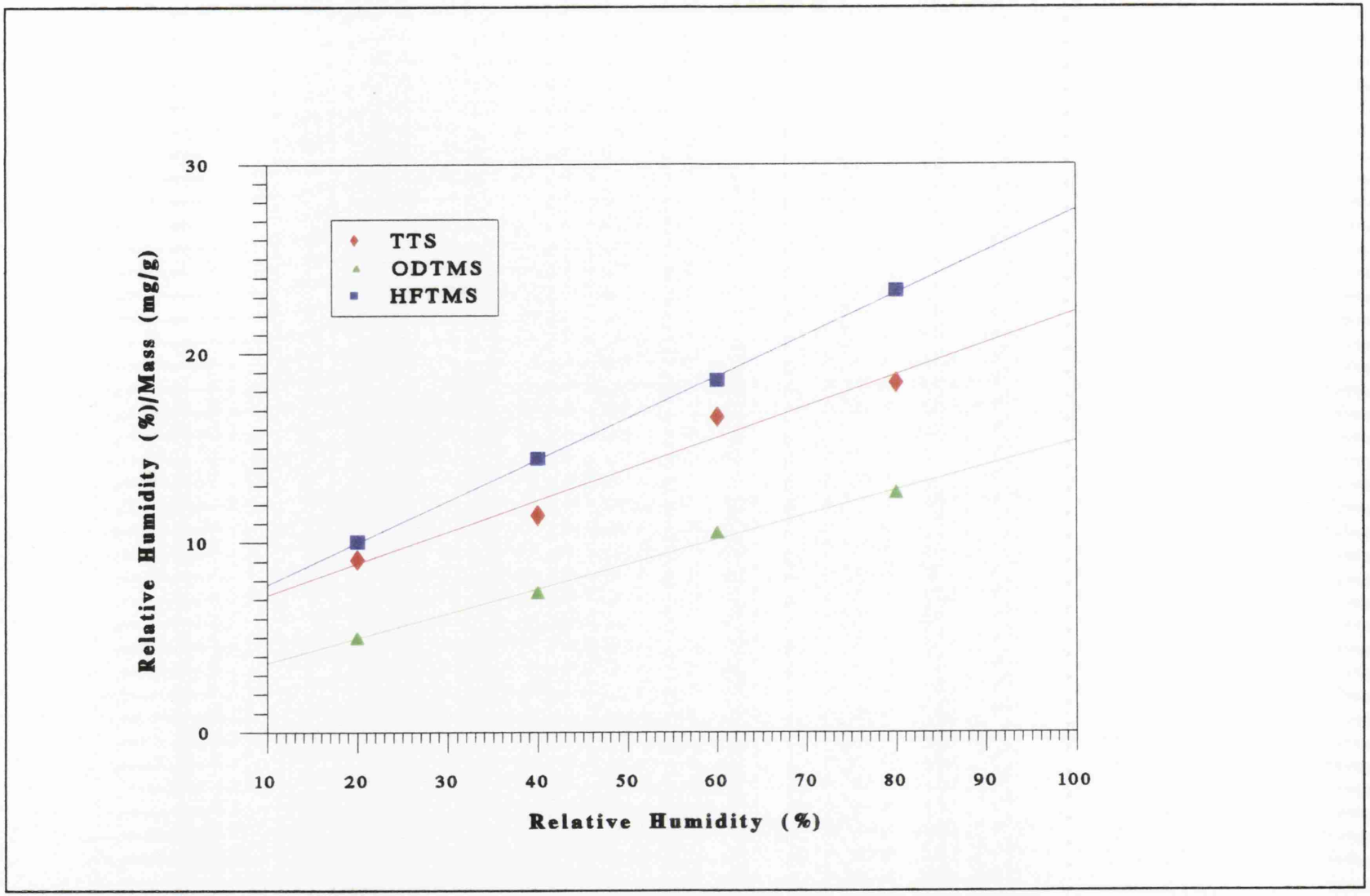

5.2 FLOATATION TEST TO EVALUATE STABILITY OF INHIBITORS

5.2.1 Introduction

Failure of inhibitive treatments may be attributed in part to the breakage of the bonds formed between the inhibitive molecules and the iron oxyhydroxide corrosion product surfaces. Interfaces are vunerable to chemical attack by corrosive agents making these bonds the weakest links. The bonds may be broken in the presence of water as there is a strong possibility that hydrolysis will occur. To some extent the interface is protected by the long hydrocarbon or fluorocarbon chains present on all the inhibitors tested. The hydrophobicity will prevent water penetration, however if water does penetrate, hydrolysis can occur, causing debonding of the inhibitor molecules and its removal from the oxyhydroxide surface. The surface will no longer be protected from further penetration of water which may reach the metal surface and cause corrosion. The rate of debonding will be governed by the nature and strength of the bond between the oxyhydroxide and the inhibitor, the hydrophobicity of the surface and other factors such as temperature and pH (Rosen, 1980).

5.2.2 Floatation Test

The extent of debonding occurring when inhibitor treated samples are exposed to direct attack by water can be measured qualitatively in a simple way (Al Ahmed, 1993). When the surface of an iron oxyhydroxide powder has inhibitor molecules bonded to its surface, the powder becomes hydrophobic. The powder will not be wetted when placed in water and will therefore float on the water surface. The powder will remain floating if it can withstand water attack and hydrolysis.

Once water molecules penetrate and replace inhibitor molecules at the surface of the iron oxyhydroxide, the surface starts to become less hydrophobic. When debonding occurs to the extent that the surface becomes hydrophilic, the sample will become wetted and sink. The observation of how long inhibitor treated samples of iron oxyhydroxide powders float on water can therefore be used as an indication of the rate of desorption of the inhibitor

molecules, and ultimately the stability of the inhibitor. This simple test will give an indication of the permanence of the inhibitor treatments and can be used to assess the long term benefit of these treatments for use as treatments for the conservation of archaeological iron.

5.2.3 Experimental Method

Samples of α-FeOOH and β-FeOOH were synthesised and treated with the inhibitors ODTMS, HFTMS, TTS and ODA as described in section 5.2. 0.5g of these powders were carefully sprinkled onto a sample tube containing 10ml of water. These sample tubes were examined at intervals over several months to observe whether the iron oxyhydroxide powders were floating on the surface of the water or had sunk to the bottom of the sample tubes.

5.2.4 Floatation Test Results

Untreated β-FeOOH and α-FeOOH powders sank instantaneously upon being wetted by water. β-FeOOH and α-FeOOH powders treated with ODA also sank within the first few minutes, although at a slower rate to the untreated powders. All other powders treated with TTS, HFTMS, and ODTMS floated. The samples were observed over a six month period and no further changes were observed.

This indicates little debonding occurs with iron oxyhydroxide powders treated with TTS, HFTMS and ODTMS. A permanent unhydrolysable bond seems to be formed between the oxide and inhibitor. However, in the case of ODA, immediate debonding occurs to the extent that the powders become hydrophilic and wettable within the first few minutes. This indicates that the bonding interactions formed between the iron oxyhydroxide surface and the amine ODA are easily hydrolysable.

5.3 ELECTROCHEMICAL MONITORING

5.3.1 Introduction

As stated in section 1.1.1, corrosion is an electrochemcial process. The rate of a corrosion process can be measured from the corrosion current density, i_{corr}. From mixed potential or Evans diagrams (see figure 1.6) it can be seen that corrosion current density is related to the electrochemical potential of a corroding metal. For a corroding system such as iron in hydrochloric acid, it is observed that as the corrosion current density increases (i.e. as the rate of corrosion increases), the corrosion potential will become more negative. Therefore a measure of the rate of corrosion of a particular metal, E_{corr}, can be obtained from simply observing the potential of a corroding metal with respect to a reference electrode.

The corrosion potential of variously treated pre-corroded samples of iron in distilled water were recorded over time. The actual rate of corrosion of these samples could then be compared, and therefore the inhibitive properties of the various treatments assessed. The measurement of corrosion potentials is well established in the monitoring of archaeological iron from shipwrecks still in marine environments (North, 1982, Carpenter & MacLeod, 1993). Electrochemcial methods have also been used to assess the behaviour of archeological iron in various stabilising solutions (Hjelm-Hansen *et al*, 1993). It must be considered that the aqueous corrosion environment used to perform the electochemical measurements is not identical to the atmospheric environment in which the treatments are intended to inhibit corrosion of archaeological iron. These experiments are however useful in adding further information on the comparative performance of the tested treatments.

5.3.2 Corrosion Potential Under Open Circuit Conditions

The surface potential of a corroding metal, M, with respect to a reference electrode, is the mixed or corrosion potential, E_{corr}. Changes in the corrosion potential under open circuit conditions, with time, can be informative. These results can be easily interpreted, as a shift in potential to more negative value indicates an increase in the activity of a metal and thus indicates an increase in the rate of corrosion. This method gives a simple indication of how

corrosion rates change with time and can be useful when assessing inhibitive coatings and coating failures leading to further outbreaks of corrosion after an initial period of passivity.

E_{corr} must be measured under open circuit or zero current conditions. This means the net current density will be zero (i.e. no net flow of current). The electrochemical cell will consist of the corroding metal (the working electrode) and a reference electrode in an electrolyte solution. The voltage of this cell is recorded whilst zero current is maintained. The corrosion potential recorded in this way can be called the open circuit potential. Its measurement over time has been used to assess the corrosion inhibiting properties of coatings such as polyaniline (Ahmed & MacDiarmid, 1995).

5.3.3 Treatment of Samples

Corrosion potential data was obtained for an untreated pre-corroded coupon (using method B, see section 3.3.2), and for pre-corroded coupons treated with ODA, TTS, ODTMS, and HFTMS. The treatments were carried out as described below. The HFTMS solution supplied for this experiment was in ampuoles of 0.03M HFTMS in F-113. Therefore ODTMS and TTS treatments were carried out at a concentration of 0.03M. Due to its sparing solubility the ODA treatments was carried out at a concentration of 0.01M. All coupons were degreased in acetone before inhibitive treatments were applied.

5.3.3.1 Treatment with a 0.03M solution of ODTMS

Samples to be treated were immersed in a 0.03M solution of ODTMS in toluene. The solution was prepared in a dry box purged with nitrogen or argon as ODTMS is moisture sensitive. A Schlenk line (a combined nitrogen and vacuum line) was used for the experiment so that it could be carried out in a moisture free environment. Samples were placed in a round bottomed flask with side arm and this was then alternately filled with nitrogen and evacuated and eventually left filled with nitrogen. The 0.03M ODTMS solution was then transferred from another Schlenk tube using a delivery tube until all the samples were totally immersed in the solution. The samples in solution were heated to a temperature of 50°C for 4 hours. The solution was then transferred back into another Schlenk tube via a delivery tube. The samples were rinsed in ethanol and then rinsed in

distilled water for 1 minute. The samples were then dried and placed in an oven at 150°C for 30 minutes to complete the cross linkaging reaction.

5.3.3.2 Treatment with a 0.03M solution of HFTMS

Ampoules of HFTMS solution were opened inside a dry box, and the solution added to a shlenk tube. Samples were placed in a round bottomed flask with side arm and this was then alternately filled with nitrogen and evacuated and eventually left filled with nitrogen. The 0.03M HFTMS solution was transferred from another schlenk tube using a delivery tube into the tube containing the samples, until all the samples were totally immersed in the solution. The samples in solution were heated to a temperature of 47°C for 4 hours. The solution was then transferred back into another schlenk tube via a delivery tube. The samples were rinsed in ethanol and then rinsed in distilled water for 1 minute. The samples were then dried and placed in an oven at 150°C for 30 minutes to complete the cross linkaging reaction

5.3.3.3 Treatment with 0.03M TTS Solution

Samples were immersed in 0.03M solution of TTS in toluene and a 800mbar vacuum applied at 35°C for 12 hours. Samples were then removed from the TTS solution and heated at 45°C for 12 hours to cure the coating. Samples were then rinsed twice with toluene and left to dry in air.

5.3.3.4 Treatment with 0.01M ODA

A 0.01M solution of ODA in toluene was prepared. Samples were immersed in this solution under a vacuum of 800mbars at room temperature, 20-25°C, for 12 hours. Samples were then rinsed twice in toluene and left to dry in air.

5.3.4 Measurement of Corrosion Potentials

5.3.4.1 Preparation of Samples

Samples for the measurement of corrosion potential were the corroded iron coupons previously used in accelerated corrosion tests. Coupons corroded by method B (see

section 3.3.2) were used. The coupons were first treated with the inhibitor treatments as described in section 5.3.3. The coupons were then carefully handled to try and reduce flaking and removal of corrosion products or inhibitor coatings. Corrosion product layers were removed from one end of the coupon using abrasive sand paper until the shiny iron metal could be seen. A crocodile clip was then soldered to this end using, a 60% tin:40% lead solder. This assured that good electrical contact between the coupon and the clip was achieved. A multimeter was used to test that electrical contact had been made. A water resistant varnish was then painted onto the coupons so that all but a 2cm by 2cm (±0.5mm) area of the coupon was covered. This would ensure that a working electrode of the same area (±2mm^3) would be used in each experiment. The varnish was left to dry for several hours.

5.3.4.2 Experimental Method

Corrosion potential measurements were made using a two electrode cell. A corroded iron coupon was used as the working electrode and a standard calomel electrode was used as the reference electrode (SCE) This is a mercury, mercury (I) chloride, potassium chloride electrode, the half cell reaction being:

$$Hg_2Cl_2 + 2e^- \Leftrightarrow 2Hg + 2Cl^-$$

The potential of the reference electrode is controlled by the activity of the chloride anion. When saturated KCl solution is used, the standard calomel electrode has a potential of +0.242V vs the standard hydrogen electrode (Crow, 1994, 110).

Both the working and reference electrodes were connected to a cell, containing distilled water. The electrolyte itself would form from the salts contained within the corrosion product layers. The cell was connected to a Picolog analogue-to-digital converter, which was connected to a computer running the Picolog data logger program. The experimental set up is illustrated schematically in figure 5.5. The Picolog data logger consists of an analogue to digital converter which has channels that are used to measure a voltage, which is a representation of a real world parameter such as pressure, temperature or in this experiment, voltage. The reference and working electrodes were connected to different channels on the analogue-to-digital converter. The Picolog program then takes readings from these channels and combines them to output the cell voltage. The program collects readings at regular intervals. In this experiment, data was recorded every 15 minutes.

Experiments were continued for 8500 minutes (between 5 to 6 days) for each sample. Picolog data could be stored as standard data files.

Figure 5.5 Experimental set up for measurement of corrosion potential

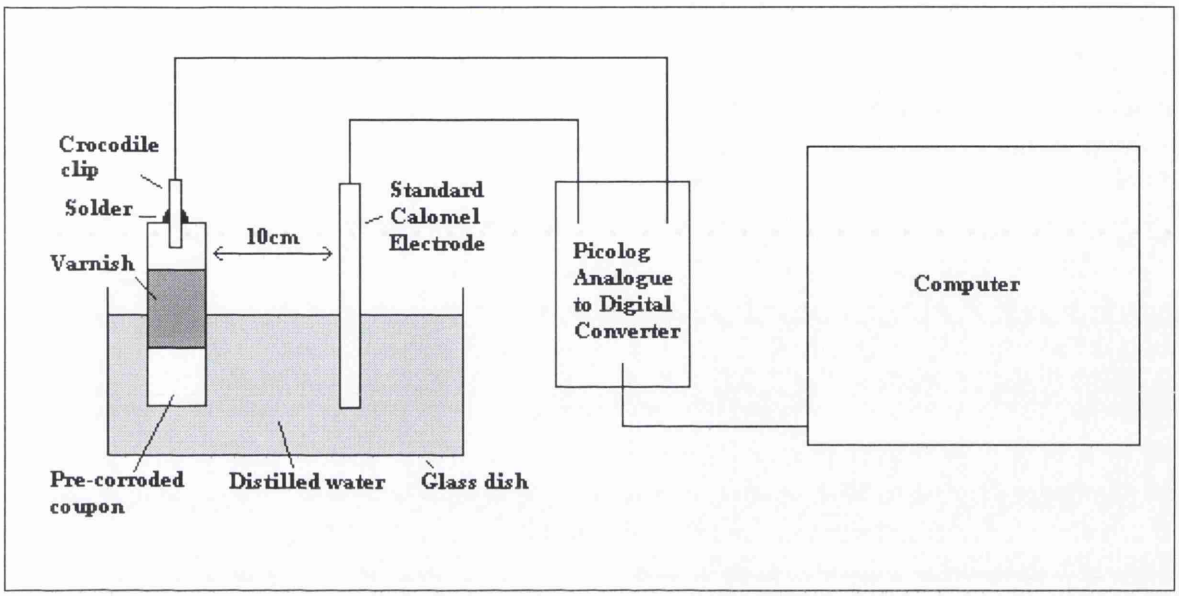

5.3.5 Corrosion Potential Results

The corrosion potentials measured are not half cell electrode potentials but mixed potentials, meaning they fall between the half cell electrode potentials of the anodic and cathodic reactions occurring in the corrosion process. A polarisation process occurs when a metal is exposed to the electrolyte solution and it's potential is drawn away (polarised) from its equilibrium potential. An overpotential starts to develop. The speed at which an overpotential develops and the magnitude of the corrosion potential are both indications of the rate of corrosion occurring in the tested samples. The corrosion potentials of various different metals, in different environments can not be used to indicate comparative rates of corrosion, as the rate of corrosion is dependant on kinetics not thermodynamics. However it is valid to use corrosion potentials to compare the corrosion rates of the same metal in similar environmental conditions. In this case the corrosion potential is indicative of the rate of corrosion. A logarithmic relationship exists. This relationship has been confirmed in research into the corrosion rates of archaeological iron analysed *in situ* at shipwreck sites in Australia (MacLeod, 1995). The relationship between d, annual depth of corrosion in mm per year, and E_{corr}, the corrosion potential was expressed as:

$$\log d = aE_{corr} + b$$

where a and b are constants, related to the particular conditions at each shipwreck site. This logarithmic relationship implies that a small change in corrosion potential will have a much larger change in corrosion rate.

Examples of the electrochemical results recorded in this work are shown in figure 5.6. For each inhibitor data was collected from several treated coupons. Data was recorded for coupons treated with the inhibitors HFTMS, ODTMS, ODA and TTS. The potential of an untreated sample was also recorded for comparison. An error of ±0.025V was found for the value of the corrosion potential for each particular inhibitor treatment. The rate of change of corrosion potential was also characteristic for each inhibitor treatment. The corrosion potential value and rate of change in corrosion potential of each coupon tested has been used to assess the corrosion inhibiting properties of the treatments. The results show that up to 6000 minutes, about 4 days, the untreated sample has the lowest corrosion potential, and is thus corroding at the fastest rate. After this time the corrosion potential of the ODA treated sample falls below that of the untreated sample. All the other treatments have lower corrosion rates than the untreated sample for the length of the experiment.

As well as looking at the absolute values of the corrosion potentials, it is also interesting to compare the gradient of each data series, that is the rate of change of corrosion potential. In the initial few days the greatest drops in corrosion potentials occur. The time taken for this drop to occur is an indication of the time taken for the metal to become more active and relates to the efficiency of each surface treatment in preventing corrosion.

The ODA treated sample initially has the highest corrosion potential. In fact it corrodes at a slower rate than the other samples in the first 2500 minutes (just under 2 days). The corrosion potential then falls more rapidly than the other treatments so that it eventually has the lowest corrosion potential. The initial good performance of the ODA treatment may be related to the amine acting as a corrosion inhibitor in addition to the hydrophobic actions of the hydrocarbon chain. The corrosion inhibiting properties of amines are related to several factors. Their basic nature allows them to neutralise the acidic solutions that start to form at corroding surfaces (Jones, 1992, 502). Amines are also electron donors and can act as adsorption inhibitors (Braun *et al*, 1993, Dernovaya *et al*, 1993).

However, the results of the floatation experiment seem to show that ODA is not permanently bonded to the corrosion product surface, and this may explain the subsequent fall in corrosion potential observed. Once a large proportion of ODA is no longer bonded to the iron oxyhydroxide surface after the first 2000 minutes, the corrosion potential falls more rapidly than is the case for any of the other samples.

Although the accelerated corrosion tests showed ODTMS had very little impact on the corrosion rate, and HFTMS actually increased the corrosion rate, the corrosion potentials measured for samples treated with both inhibitors seem to show the biggest decrease in corrosion rates when compared to the untreated sample. These treatments show the highest corrosion potential values. After 8535 minutes (about 6 days) the untreated sample is at a potential of -0.645V, whilst the ODTMS treated sample is at -0.624V and the HFTMS treated sample at -0.592V. It is however interesting to note that the potentials of these sample drop more rapidly within the first 500 hours than either of the other treatments.

The TTS treated sample shows a consistently higher corrosion potential than the untreated sample. After 1000 minutes it does fall below the potentials of the HFTMS and ODTMS treated samples. The initial fall in corrosion potential is more gradual than that of the former treatments, which perhaps indicates that this treatment (as seems to be the case) would be a better inhibitive treatment in atmospheric conditions (rather than in solution).

Figure 5.6 Corrosion potential vs time for pre-corroded coupons treated with inhibitors

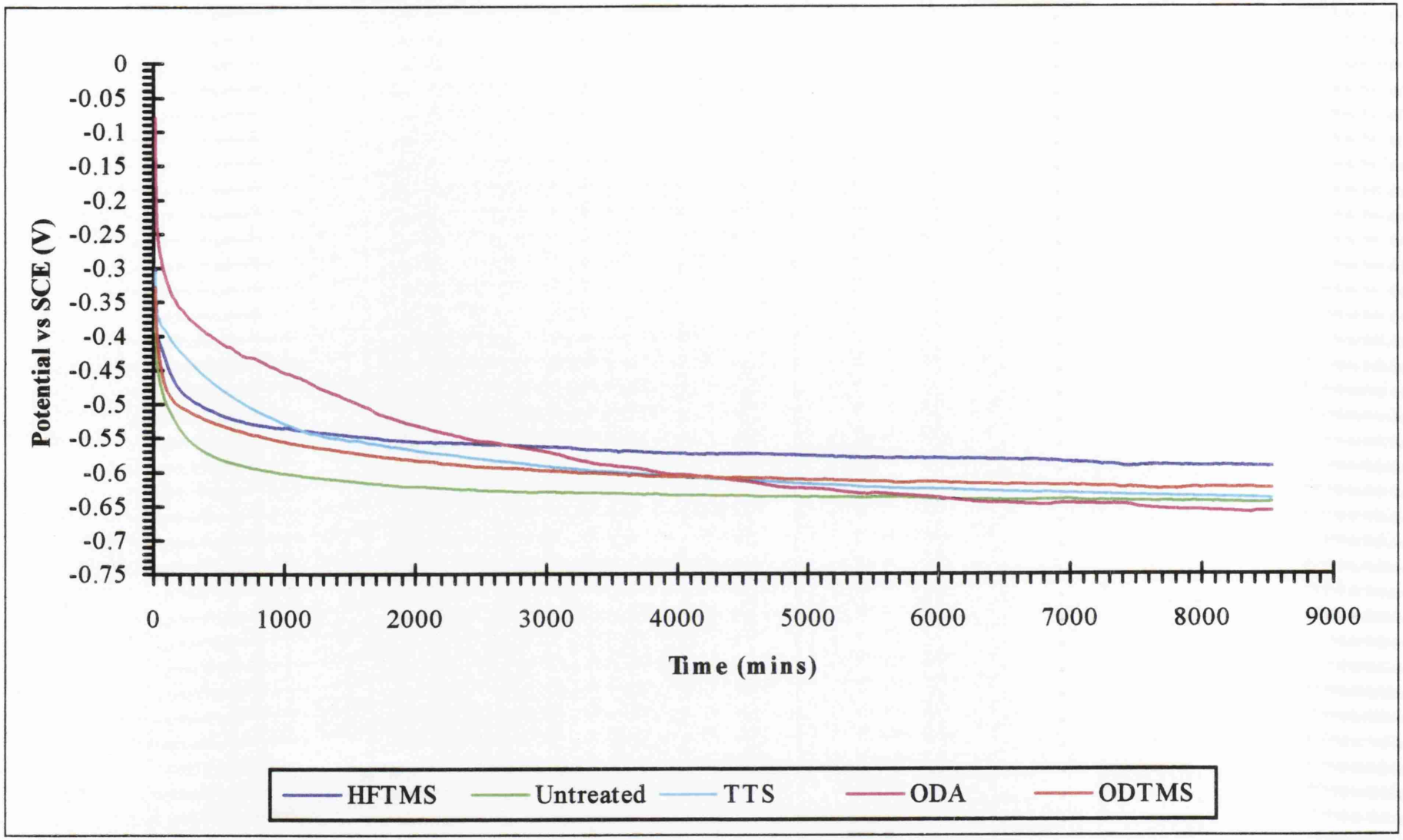

CHAPTER SIX

FTIR and XPS Surface Analysis

6.1 SURFACE ANALYSIS

In recent years many analytical techniques have been developed specifically for examining the surfaces and interfaces of materials (rather than their bulk composition or structure). The majority of analytical techniques will penetrate a materials surface and analyse the bulk, but for the study of corrosion inhibitors, techniques are necessary that can analyse the first few molecular layers. Methods of surface analysis allow the investigation of the bonding and composition of surface layers and are therefore of increasing importance in the study of corrosion and corrosion inhibitors.

What is meant by 'surface' is often defined in terms of the particular problem under examination. For example, when considering the reaction of gas molecules with a metal, the surface would be defined as the adsorbed gas molecules and the first molecular layer of metal atoms, however when examining segregation within a metal alloy, the surface layer may be considered to extend to the depth at which the composition is indistinguishable from that of the bulk. A more general definition of the surface layer is simply the interface between two media. The extent of this interface or surface is the region where the properties of the material deviate from those of the bulk media (Brune *et al*, 1997, 3).

Surface analysis techniques are now almost as numerous as the techniques available for bulk analysis. Surface selective and sensitive versions of most widely used analytical techniques have been devised by varying certain aspects of the experimental procedures. Amongst the most commonly used surface analysis techniques are x-ray photoelectron spectroscopy (XPS), secondary ion mass spectroscopy (SIMS), Auger spectroscopy and surface sensitive forms of FTIR and Raman spectroscopies. All these techniques can provide differing information on surfaces, such as identification of chemical compounds

and bonds or quantitative elemental analysis. The appropriate analytical technique must therefore be chosen which can probe the particular problem in question. Often only by using several techniques can the nature and of a surface be fully illuminated.

In this work two surface analysis techniques have been used to investigate the interactions between the inhibitor treatments TTS, ODA, HFTMS and ODTMS, and the corrosion product substrates. A surface sensitive form of FTIR, known as DRIFT has been used to gain information on the bonding interactions that exist between the inhibitor treatments and iron oxyhydroxides. x-ray photoelectron spectroscopy (XPS) was also used. This technique provides quantitative information on surface compositions.

6.2 VIBRATIONAL SPECTROSCOPY

6.2.1 Fourier Transform Infra Red Spectroscopy (FTIR)

Infrared spectroscopy is a powerful analytical technique for the characterisation of the molecular structure of inorganic and organic compounds. It is based on the absorption of infrared radiation by a sample, causing transitions from one vibrational state to a higher vibrational state. An infrared spectrum is therefore a set of absorption bands whose intensities and frequencies provides information on the structure and bonding in a molecule.

In the past infrared spectroscopy was carried out with instruments that would record the energy transmitted through a sample as a function of wavelength. However, modern infrared spectroscopy is carried out using Fourier transform infrared spectrometers. Fourier transformation is a computational mathematical method used for splitting a curve into a sum of sine and cosine functions. FTIR instruments employ a Michelson Interferometer instead of a monochromator. In the interferometer, the radiation first hits a beam-splitting mirror after passing through the sample. The two halves of the beam are then reflected back from mirrors. These beams then recombine. If monochromatic radiation is used, constructive or destructive interference occurs depending on the difference in the path lengths of the split beams. If one of the reflecting mirrors is moved backwards, the interference will periodically change from constructive to destructive and a sine wave will be detected. With polychromic radiation, the combination of many sine wave signals produces a complex interferogram however using the fourier transform technique the intensities of individual frequencies of radiation can be calculated.

An FTIR spectrometer produces a plot of intensity of infrared radiation against frequency. The scan time for the moving mirror dictates the speed at which the spectrum can be recorded. Spectra can be acquired in time spans of a few milliseconds, however slower scans allow the accumulation of more intense signals and increase the signal-to-noise ratio. It is these factors that make FTIR a vastly superior technique in comparison to conventional infrared spectroscopy. When a monochromator is used, as in conventional infrared, most of the radiation from the source does not pass through the sample, but is

lost by the monochromating process. This leads to poor sensitivity. FTIR has a much higher radiation throughput and coupled with the increase in signal-to-noise due to the summation and averaging of many scans, a very high sensitivity is obtained. Conventional infrared spectrometers also suffer from wavelength inaccuracies associated with the backlash in mechanical movements such as rotating mirrors and gratings. These are reduced in FTIR spectroscopy so that a resolution of up to $0.1cm^{-1}$ is obtainable (Kemp, 1987, 80). Due to its speed, FTIR can be used as an analytical technique for in-situ studies such as its use in gas chromatography or electrochemistry.

The value of FTIR is further increased by the ability to manipulate spectra using computer subtraction. In this way background absorbtion of water and carbon dioxide in the atmosphere can be removed. If a spectra of the background is first recorded, this may be subtracted from any sample spectrum to give a spectrum of absorbtion attributable to the sample only.

6.2.2 Surface Analysis and Infrared Spectroscopy

Initial attempts to use infrared spectroscopy to study surfaces were not successful. Little information about the structure and composition of surfaces could be inferred from infrared spectra. The infrared bands of chemisorbed species and other surface structures are weak and broad in comparison to the signal obtained from the bulk. The concentration of deposited surface layers can be low, in the order of monolayers and thus a concentration below the detection limit of conventional infrared. A sensitivity and selectivity beyond the ability of conventional dispersive spectrometers was required. Added problems included the complexity of spectra containing a bulk material with a different surface species as adsorption bands of chemisorbed species may overlap bands from the bulk material.

It has only been with the advent of FTIR in the late 1960s, with its superior sensitivity and selectivity, that surface analysis has become possible. The advantages previously described allow for the detection of absorbence bands attributed to surface species. The use of computers also allows for better structure elucidation by means of digital subtraction of the bulk spectra, leading to magnification and enhancement of the weak surface signal.

FTIR has allowed infrared spectroscopy to complete with other surface techniques. Its mode of use for surface analysis differs from that used for bulk analysis. Specialised infrared techniques that are suitable for surface analysis include reflective-absorption spectroscopy and diffuse reflectance spectroscopy. Those methods unlike some high vacuum techniques are non destructive and able to give structurally specific information.

Surface analysis using FTIR can normally be carried out on standard commercial instruments with which special attachments can be added. Absorption signals of the order 10^{-4} to 10^{-2}A are typically detected in surface analysis (Brune *et al*, 1997, 370). Simple transmission FTIR has been used for surface analysis as has photoacoustic spectroscopic techniques, however, the most successfully used methods are those using reflection techniques, such as internal reflection (IRS, ATS), external reflection (ERS, IRRAS) and diffuse reflectance (DRIFT). Radiation reflected, rather than transmitted through a sample will have a higher component of its signal originating from surface adsorption.

Infrared spectroscopy is useful for the characterisation of functional groups on the surfaces of powdered solids and their interactions with adsorbate molecules. Species adsorbed onto metals (such as CO_2 or CO), can also be studies with FTIR. The technique is widely used in research into catalysis, and many other fields of material science that relate to surface properties (Brune *et al*, 1997). FTIR is a useful tool in the study of corrosion inhibitors and their interactions with metal surfaces (Okabayashi *et al*, 1997, Braun *et al*, 1993). Numerous studies have been carried out. Information gained by FTIR can help elucidate the mechanisms of inhibition and thus assist with the selection of more efficient inhibitors.

6.2.3 DRIFT Spectroscopy

When infrared radiation is directed towards a sample, the majority will be adsorbed and transmitted through the sample. However, a small proportion will be backscattered. Infrared radiation can be absorbed, reflected or penetrate a sample before being backscattered. Diffuse reflectance spectroscopy is based on the penetration of infrared radiation that occurs before scattering. This radiation had been adsorbed by the first few

surface layers and then re-emitted and backscattered. This gives an absorbence spectra of predominantly the surface layers.

The accessory used in this technique is shown in figure 6.1. The infrared beam is focused onto the solid sample and the diffusely scattered radiation is collected and returned to the detector. Samples are usually analysed as powders and can be mixed with potassium bromide or potassium chloride or analysed without dilution. The powder loosely placed in the sample cup is levelled off to give a flat surface.

Figure 6.1 Schematic representation of a DRIFT accessory (Brune et al, 1997)

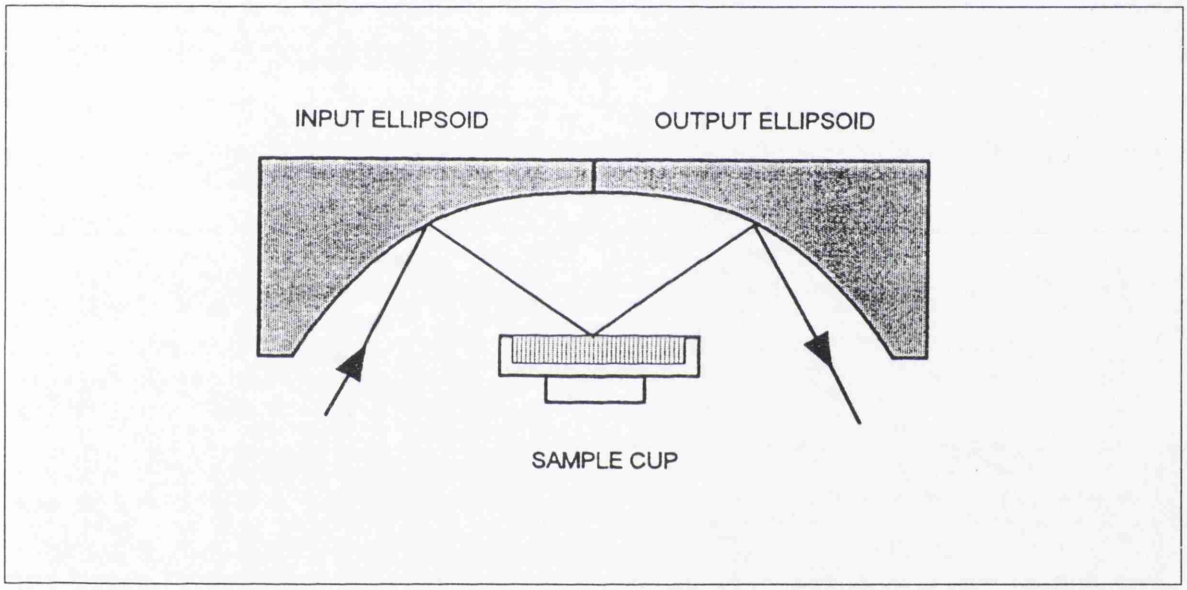

DRIFT is mainly used in the characterisation of surface layers on powders. In comparison to transmission spectroscopy of powder surfaces there is a greater sensitivity when the DRIFT technique is used and sharper peaks can be obtained. However DRIFT is sensitive to particle size and compression and so quantitative analysis and structural assignment can be difficult (Hrebicik *et al*, 1997).

6.2.4 Samples Analysed by DRIFT Spectroscopy

α-FeOOH and β-FeOOH powders were synthesised and treated with the inhibitors ODTMS, HFTMS, ODA and TTS as described in chapter 5. DRIFT spectra of these samples and untreated β-FeOOH and α-FeOOH were collected.

6.2.5 DRIFT Spectra Collection

DRIFT spectra were collected using a Perkin Elmer 2000 spectrometer supported by control and data processing software. A diffuse reflectance accessory was used (see figure 6.1). The sample container was filled to the brim with powdered sample and levelled off. Spectra were recorded from $400cm^{-1}$ to $1000cm^{-1}$. All spectra were taken at a resolution of $4cm^{-1}$ in transmitance mode. 250 scans were recorded for averaging to obtain an improved signal-to-noise ratio.

Spectra of the untreated and treated iron oxyhydroxide samples were recorded. The absorbence contribution of the iron oxyhydroxide was digitally subtracted so that a spectra consisting of the absorbence of the inhibitor and inhibitor-oxyhydroxide interaction can be studied.

6.2.6 FTIR Spectra of Inhibitor Molecules

FTIR spectra of the inhibitor molecules, ODTMS, HFTMS, ODA and TTS were recorded. These liquids or solutions were dropped onto potassium bromide discs (potassium bromide pressed into transparent discs) and the spectra immediately recorded in transmittance mode. These spectra were compared to the DRIFT spectra of the inhibitors absorbed onto the iron oxyhydroxide surfaces.

6.2.7 FTIR Results

A complete assignment of all peaks recorded in each FTIR spectrum was not attempted. Only those peaks of interest in the interpretation of the nature of the interactions between the inhibitors and iron oxyhydroxides were considered. These interactions could be best studied by subtracting the contribution of the iron oxyhydroxides to the recorded DRIFT spectra. This left only the vibrations of the inhibitor molecules and any new bonds formed between the inhibitor and bulk oxyhydroxide. Comparing the subtracted spectra to the spectra of the inhibitor molecules alone indicated the presence of vibrations associated with bonds formed between the inhibitor and oxyhydroxide. Assignment of infrared peaks was based on a survey of literature values for similar molecules and bonding interactions

(Al Ahmed, 1992, Kurth & Bein, 1993, 1995, Brousseau *et al*, 1998, Ishida & Koenig, 1978a, 1978b, Culler *et al*, 1986, Demjen *et al*, 1997, Leyden *et al*, 1985, 1988, Harwood & Moody, 1989, Braun *et al*, 1993, Okabayashi *et al*, 1997, Socrates, 1994, Bellamy, 1975, Miller & Ishida, 1986). Figure 6.2a-d illustrates the spectra of the four inhibitor molecules in the region 400-2000cm^{-1}. Figure 6.3a-b illustrates the spectra of α-FeOOH and β-FeOOH. The DRIFT spectra of the treated samples are shown in appendix A, alongside the FTIR spectra of the inhibitor treatment alone, and the spectra of the inhibitor and inhibitor-oxyhydroxide interactions that has been formed by subtracting the iron oxyhydroxide spectra. Relevant sections of these subtracted spectra are illustrated in this chapter in figures 6.4-6.7.

Table 6.1 gives the assigned peaks for the FTIR spectra of ODTMS and the subtracted spectra of ODTMS on α-FeOOH and β-FeOOH. The spectra are illustrated in figures 6.4a-b. Many of the peaks are very weak, and so there identification in all cases was not possible. A peak detected at 1137cm^{-1} in the spectra of ODTMS subtracted from α-FeOOH treated with ODTMS was assigned from literature values as the asymmetric stretching vibration of Si-O-Si. Two bands at 781cm^{-1} and 636cm^{-1}, from the ODTMS spectra subtracted from β-FeOOH treated with ODTMS were assigned as symmetric stretches of Si-O-Si. The presence of these vibrations indicates that the silane is present on the oxyhydroxide surfaces in its polymerised siloxane form.

Further evidence for polymerisation of the silane can be inferred from the absence of Si-O-CH_3 vibrations, which are clearly present in the spectrum of ODTMS (see figure 6.2a) at 1190cm^{-1} and 1091cm^{-1}, the former being the OCH_3 rocking vibration and the later the asymmetric stretch. The absence of these bands in both subtracted spectra suggests that the silane has reacted with the iron oxyhydroxide and other silane molecules. Evidence for bonds between the silane and the iron oxyhydroxide surfaces could also be found from the presence of asymmetric and symmetric stretching vibrations of the Fe-O-Si bond at 1200cm^{-1} and 1178cm^{-1} respectively. These were detected in the subtracted spectrum of ODTMS on β-FeOOH.

A weak band at 915cm^{-1} was detected in the subtracted spectrum of ODTMS on α-FeOOH. This was assigned as the stretching vibration of the Si-OH group. Its presence indicates that the polymerisation of the silane is not complete and some of the silane had been hydrolysed to give Si-OH groups.

The spectra for α-FeOOH and β-FeOOH treated with HFTMS after the subtraction of the oxyhydroxide part of the specta are shown in figures 6.5a-b. Table 6.2 list the assigned peaks of interest. Several vibrations were assigned to Si-O-Si symmetric and asymmetric stretches on both α and β-FeOOH powders treated with HFTMS. These peaks were not detected in the HFTMS spectrum and therefore indicates that polymerisation has occurred between silane molecules on the iron oxyhydroxide surface.

Fe-O-Si bands are located between 1100-1250cm^{-1}. These vibrations could not be detected due to the very strong adsorption of the C-F stretching vibration in this region. On all spectra of HFTMS (see figure 6.2b, 6.5a-b) at least three strong adsorptions were present between 1151-1253cm^{-1} which can be assigned to the complex series of vibrations that occur with poly-fluorinated carbon chains. Si-OH symmetric stretch vibrations were weakly detected for both subtracted spectra in the region 895-935cm^{-1}. The presence of these bands indicates that polymerisation may not be complete and some unpolymerised silane is present on the iron oxyhydroxide surfaces. The final difference that can be observed is the absence, in the spectra of the iron oxyhydroxides treated with HFTMS, of the strong peak in the HFTMS spectra at 1094cm^{-1} This peak was assigned as the Si-OCH_3 asymmetric stretch. Its absence in the subtracted spectra indicates that some reaction has occurred on the α and β-FeOOH surfaces.

The spectra recorded for TTS treated α and β-FeOOH after subtracation of the relevant oxyhydroxide spectra are shown in figure 6.6a-b. The assignment of significant peaks is given in table 6.3. The presence of the long C_{18} chains can be detected in all three spectra of TTS (see figures 6.2c and 6.6a-b), by the strong -CH_2- symmetric and asymmetric stretching vibrations at 2927cm^{-1} and 2854cm^{-1} respectively. The C-C stretch (1179cm^{-1}) and C-O stretch (1147cm^{-1}) of the O-C$(CH_3)_2$H group can be seen in the spectrum of TTS (figure 6.2c), however these peaks are not found in either of the subtracted spectra. This

indicates that TTS has reacted, with the alkoxy group being the leaving group in this reaction. This also suggests the formation of a bond between the titanium and the iron oxyhydroxide surface.

Further interactions between TTS and the surface of the iron oxyhydroxides can be inferred from changes in the position and intensity of the strong carbonyl stretch C=O at 1736cm^{-1} in TTS. In both the subtracted spectra (figures 6.6a-b), this band is much less intense and has shifted to several peaks at lower frequencies, between 1680-1720cm^{-1}. This change suggests that there are now several carbonyl vibrations, meaning that the carbonyls are not all bonded in the same way. The lowering of the vibration frequency suggests that some of the carbonyl groups are participating in hydrogen bonding to hydroxyl groups on the iron oxyhydroxide surface. This provides resonance stability and thus lowers the frequency of the carbonyl vibration.

Spectra recorded for ODA treated α and β-FeOOH after subtraction of the respective oxyhydroxides are illustrated in figure 6.7a-b. The assigned peaks are listed in table 6.4. As with the other cases, the long hydrocarbon chain of ODA is evident in all three spectra of ODA species (see figure 6.2d and 6.7a-b) from the two -CH_2- bend modes at 2927cm^{-1} and 2854cm^{-1}.

In the ODA spectrum (figure 6.2d) there are many peaks present at frequencies that are indicative of a primary amine. N-H symmetric and asymmetric stretches were assigned to the peaks at 3341cm^{-1} and 3268cm^{-1} respectively, N-H deformation to 1605cm^{-1} and a C-N stretch at 1089cm^{-1}. Some of these primary amine peaks can also be detected in the subtracted spectra (figures 6.7a-b). They can more clearly be seen on the spectra of ODA subtracted from β-FeOOH treated with ODA. The N-H deformation can be seen at 1609cm^{-1} and a C-N stretch at 1094cm^{-1}, however no N-H stretches were detected at the frequencies assigned to a primary amine.

Additional peaks are also present in the subtracted spectra that are not present in the ODA spectra. The presence of charged species is indicated by the presence of peaks at 1542cm^{-1} and 1510cm^{-1} in the subtracted β-FeOOH/ODA spectrum. These were assigned as the

symmetric and asymmetric deformations of $-NH_3^+$ groups. Peaks more characteristic of secondary amines were also detected, indicating that some reaction had occurred with the iron oxyhydroxide surface which had changed the nature of the amine. A band at 3512cm^{-1} in the β-FeOOH/ODA spectrum was assigned as a secondary amine N-H stretch, and a secondary amine C-N stretch was assigned as the peak at 1151cm^{-1}. A secondary amine in plane deformation was also detected in both subtracted spectra at 444-448cm^{-1}. The existence of secondary amine peaks gives a strong indication that bonds may have been formed between the iron oxyhydroxide surface and ODA, with the loss of a hydrogen atom. The presence of $-NH_3^+$ groups also indicates that the amine may be attached to the FeOOH surface via hydrogen bonds between the surface hydroxyls and ODA nitrogens.

Surface Fe-O-H hydroxyl groups stretches on both iron oxyhydroxides are assigned to the broad vibration in the 3100-3700cm^{-1} region (Urban, 1993, 189). If these hydroxyl groups are now bonded to inhibitor molecules on treated surfaces, a decrease in the intensity of this region might be expected in the spectra of the inhibitor treated samples. The spectra of the treated molecules (before the subtraction of the iron oxyhydroxide contributions) are shown in appendix A. It can be seen that all spectra show a broad peak within this region, however it is not easy to differentiate between surface hydroxyl groups and other hydroxyl groups such as Si-O-H or water adsorbed onto the surface. It is therefore not possible to make any conclusion on the relative number of surface hydroxyls groups present in the treated and untreated iron oxyhydroxide surfaces.

Table 6.1 Assignment of ODTMS peaks

ASSIGNMENT	MODE	ODTMS	α-FEOOH/ODTMS	β-FEOOH/ODTMS	REFERENCE
Fe-O-Si	Asymmetric Stretch	-	-	1200cm^{-1}(vw)	Al Ahmed, 1992
$Si(OCH_3)_3$	OCH_3 rock	1190cm^{-1}(s)	-	-	Kurth & Bein, 1995
$Si(OCH_3)_3$	Asymmetric Stretch	1091cm^{-1}(s)	-	-	Brousseau *et al*, 1998
Fe-O-Si	Asymmetric Stretch	-	-	1178cm^{-1}(vw)	Kurth & Bein, 1995 Ishida & Koenig, 1978a
Si-O-Si	Asymmetric Stretch	-	1137cm^{-1}(w)	-	Kurth & Bein, 1993 Culler *et al*, 1986 Demjen *et al*, 1997
Si-OH	Si-O Asymmetric stretch	-	915cm^{-1}(w)	-	Ishida & Koenig, 1978a,b Leyden *et al*, 1985
Si-O-Si	Symmetric stretch	-	-	781cm^{-1}(w)	Ishida & Koenig, 1978a
Si-O-Si	Symmetric stretch	-	-	636cm^{-1}(w)	Brousseau *et al*, 1998
$Si(OCH_3)_3$	Asymmetric deformation	453cm^{-1}(w)	-	-	Socrates, 1994

Table 6.2 Assignment of HFTMS peaks

ASSIGNMENT	MODE	HFTMS	α-FEOOH/HFTMS	β-FEOOH/HFTMS	REFERENCE
CF_3-CF_2-	C-F stretch	1250cm^{-1}(s)	1250cm^{-1}(vs)	1253cm^{-1}(vs)	Bellamy, 1975, Socrates, 1994
CF_3-CF_2-	C-F stretch	1211cm^{-1}(vs)	1225cm^{-1}(vs)	1218cm^{-1}(vs)	Socrates, 1994
CF_3-CF_2-	C-F stretch	1151cm^{-1}(vs)	1158cm^{-1}(s)	1154cm^{-1}(s)	Socrates, 1994
$Si(OCH_3)_3$	Asymmetric stretch	1094cm^{-1}(vs)	-	-	Brousseau *et al*, 1998
Si-O-Si	Asymmetric stretch	-	1100cm^{-1}(w)	1108cm^{-1}(m)	Ishida & Koenig, 1978a
Si-O-Si	Asymmetric stretch	-	1070cm^{-1}(w)	1077cm^{-1}(m)	Miller & Ishida, 1986 Kurth & Bein, 1993, 1995
Si-OH	Symmetric stretch	-	918cm^{-1}(w)	895-935cm^{-1}(w)	Ishida & Koenig, 1978a Leyden *et al*, 1988 Culler *et al*, 1985
Si-O-Si	Symmetric stretch	-	-	781-794cm^{-1}(w)	Ishida & Koenig, 1978a
Si-O-Si	Symmetric stretch	-	590cm^{-1}(s)	588cm^{-1}(s)	Ishida & Koenig, 1978a

Table 6.3 Assignment of TTS peaks

ASSIGNMENT	MODE	TTS	α-FEOOH/TTS	β-FEOOH/TTS	REFERENCE
$-CH_2-$	Asymmetric stretch	$2927cm^{-1}$(s)	$2927cm^{-1}$(s)	$2927cm^{-1}$(s)	Harwood & Moody, 1989
$-CH_2-$	Symmetric stretch	$2854cm^{-1}$(s)	$2854cm^{-1}$(s)	$2854cm^{-1}$(s)	Harwood & Moody, 1989
O-RC=O	C=O stretch	$1736cm^{-1}$(s)	$1680\text{-}1720cm^{-1}$(w)	$1680\text{-}1720cm^{-1}$(w)	Harwood & Moody, 1989
$=C(CH_3)_2$	C-C stretch	$1179cm^{-1}$(s)	-	-	Socrates, 1994
$O\text{-}C(CH_3)_2H$	C-O stretch	$1147cm^{-1}$(s)	-	-	Harwood & Moody, 1989
Fe-O-Ti					

Table 6.4 Assignment of ODA peaks

ASSIGNMENT	MODE	ODTMS	α-FEOOH/ODTMS	β-FEOOH/ODTMS	REFERENCE
2y amine, R_2NH	N-H stretch	-	-	$3512cm^{-1}$(m)	Socrates, 1994
1y amine, RNH_2	N-H sym stretch	$3341cm^{-1}$(s)	-	-	Braun *et al*, 1993
1y amine, RNH_2	N-H asym stretch	$3268cm^{-1}$(m)	-	-	Braun *et al*, 1993
$-CH_2-$	bend	$2927cm^{-1}$(vs)	$2927cm^{-1}$(m)	$2927cm^{-1}$(s)	Okabayashi *et al*, 1997
$-CH_2-$	bend	$2854cm^{-1}$(vs)	$2854cm^{-1}$(m)	$2854cm^{-1}$(s)	Okabayashi *et al*, 1997
1y amine, $-NH_2$	N-H deformation	$1605cm^{-1}$(m)	-	$1609cm^{-1}$(m)	Okabayashi *et al*, 1997
$-NH_3^+$	N-H Sym deform	-	-	$1542cm^{-1}$(m)	Okabayashi *et al*, 1997
$-NH_3^+$	N-H Asym deform	-	-	$1510cm^{-1}$(m)	Okabayashi *et al*, 1997
2y amine, R_2NH	C-N stretch	-	-	$1151cm^{-1}$(m)	Socrates, 1994
1y amine, RNH_2	C-N stretch	$1089cm^{-1}$(w)	-	$1094cm^{-1}$(m)	Socrates, 1994
R_2NH	R-NH-R deformation	-	$444cm^{-1}$(w)	$448cm^{-1}$(s)	Socrates, 1994

Figure 6.2a FTIR spectrum of ODTMS in transmittance mode

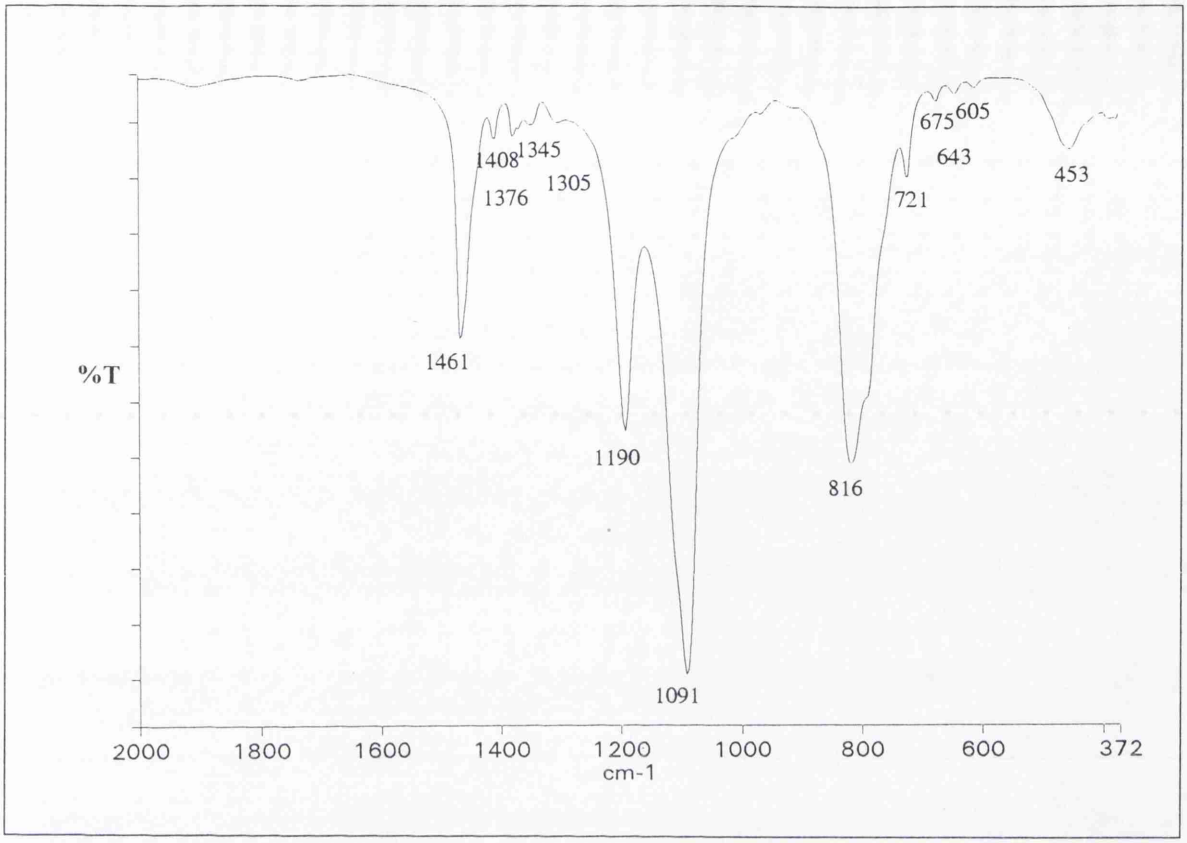

Figure 6.2b FTIR spectrum of HFTMS in transmittance mode

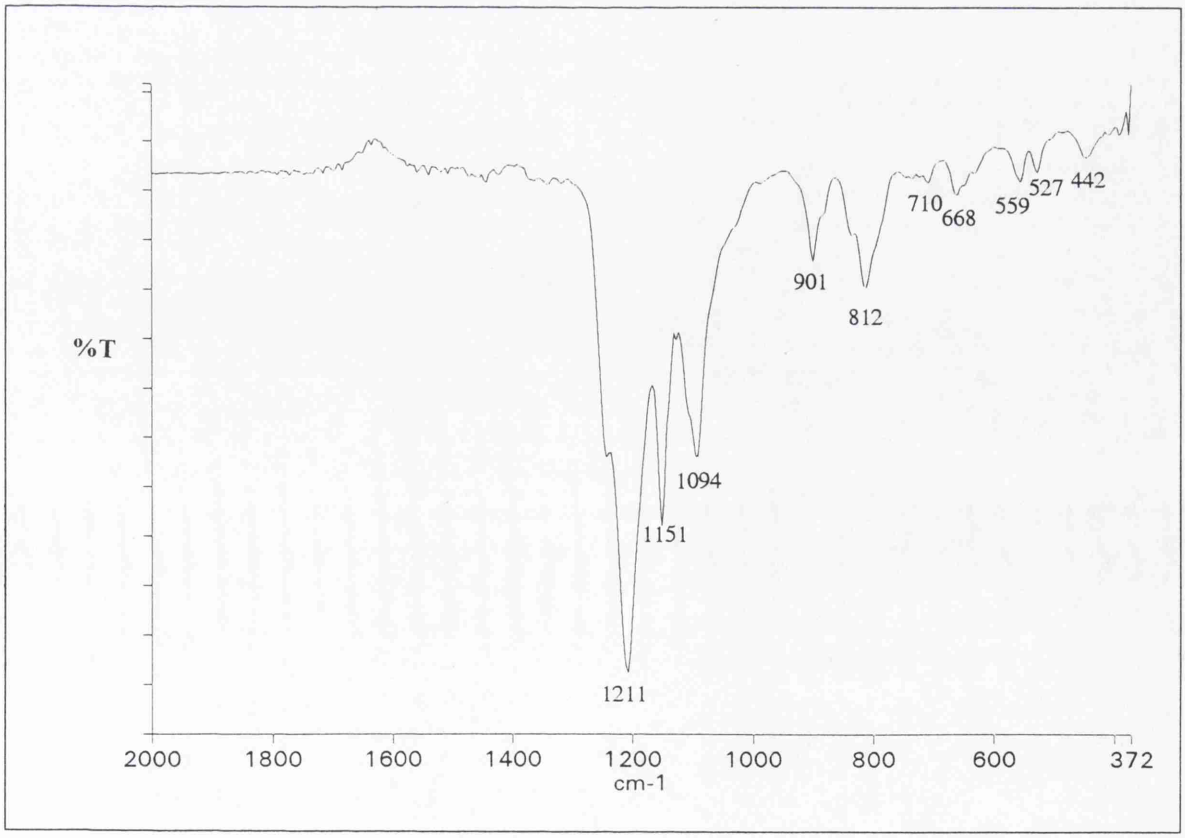

Figure 6.2c FTIR spectrum of TTS in transmittance mode

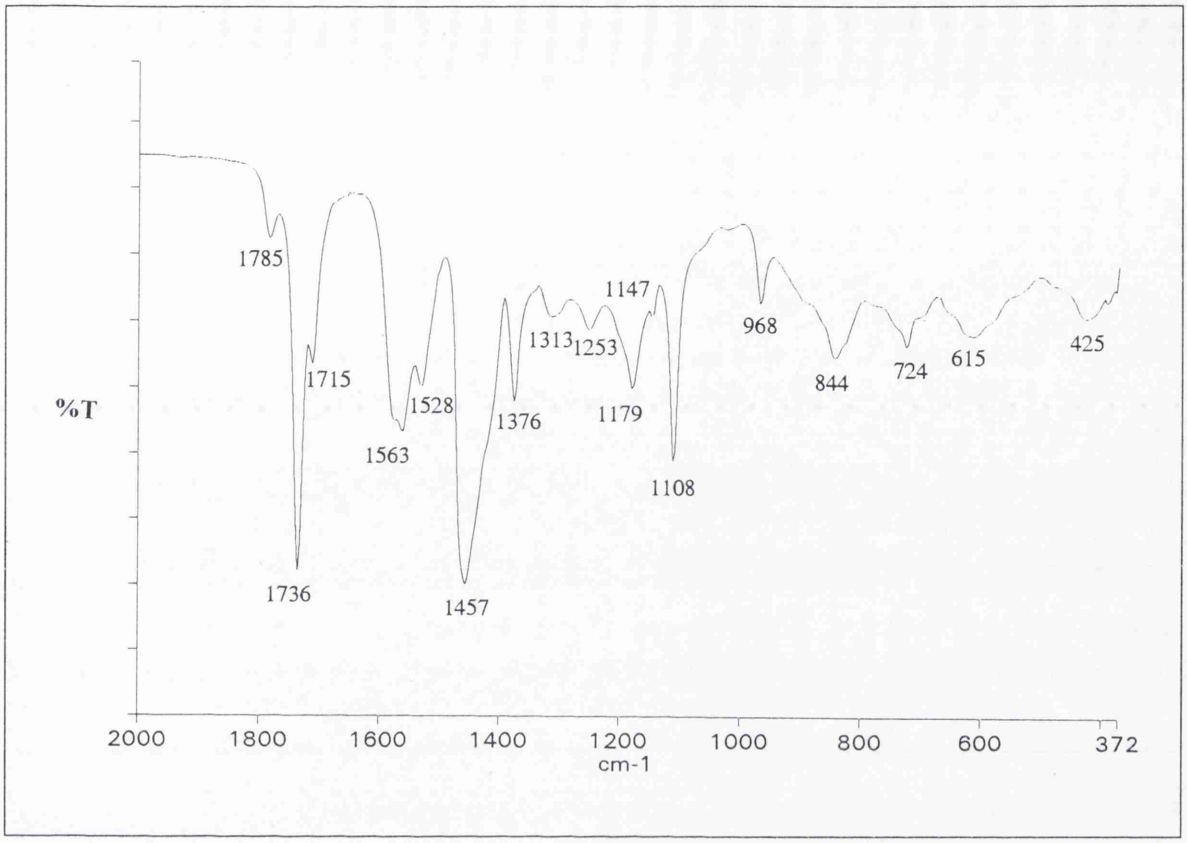

Figure 6.2d FTIR spectrum of ODA in transmittance mode

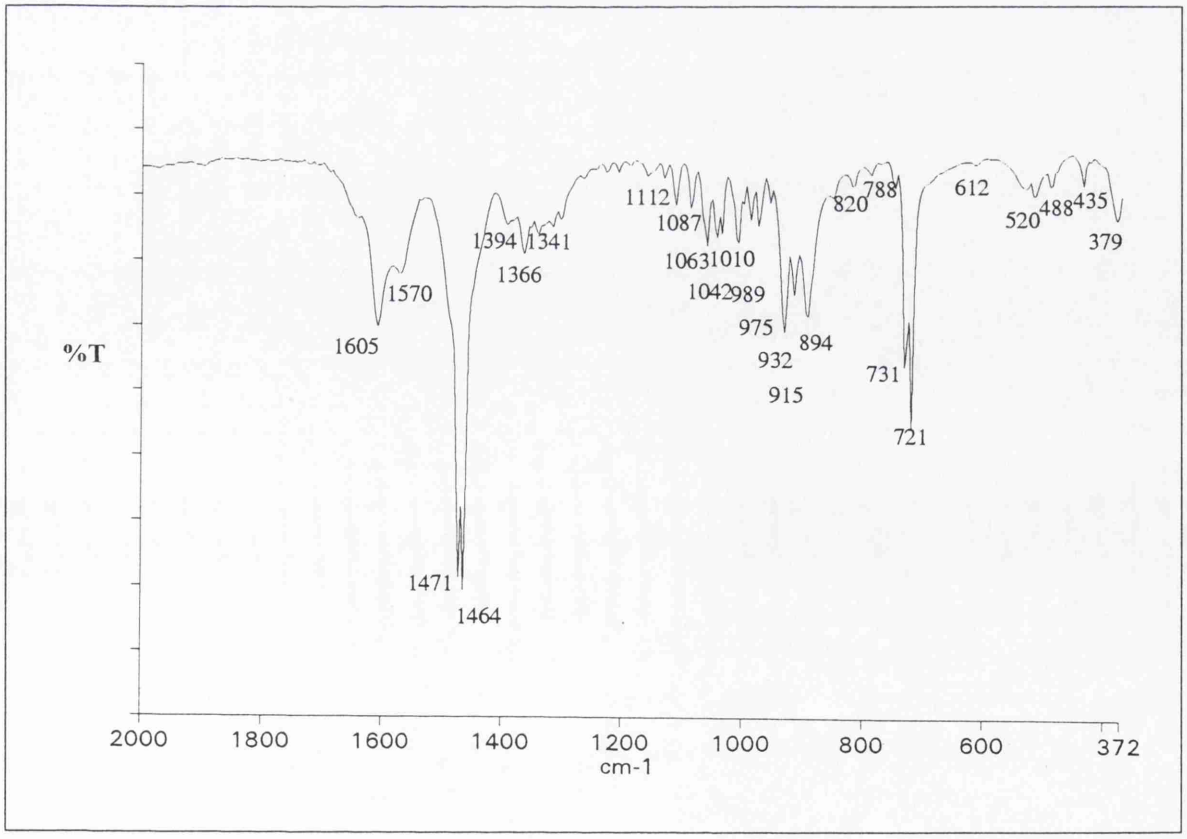

Figure 6.3a FTIR spectrum of α-FeOOH in transmittance mode

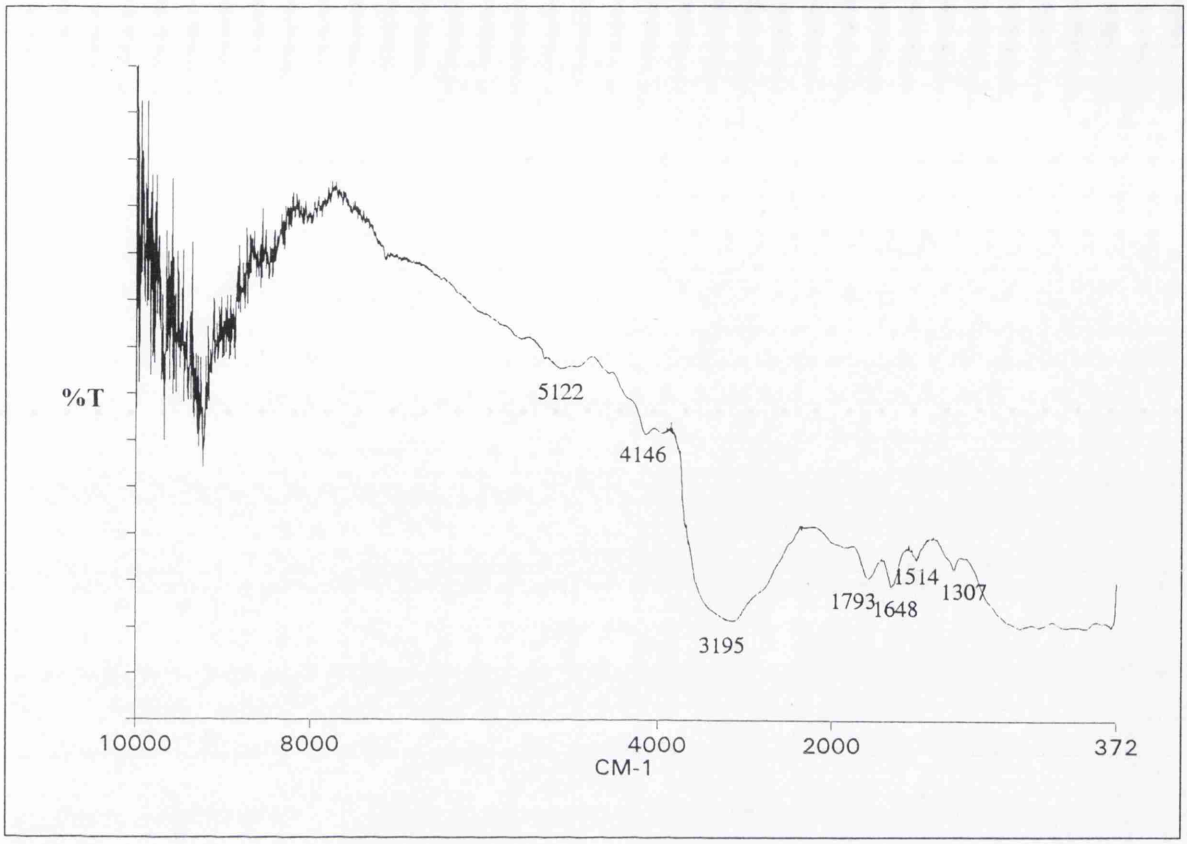

Figure 6.3b FTIR spectrum of β-FeOOH in transmittance mode

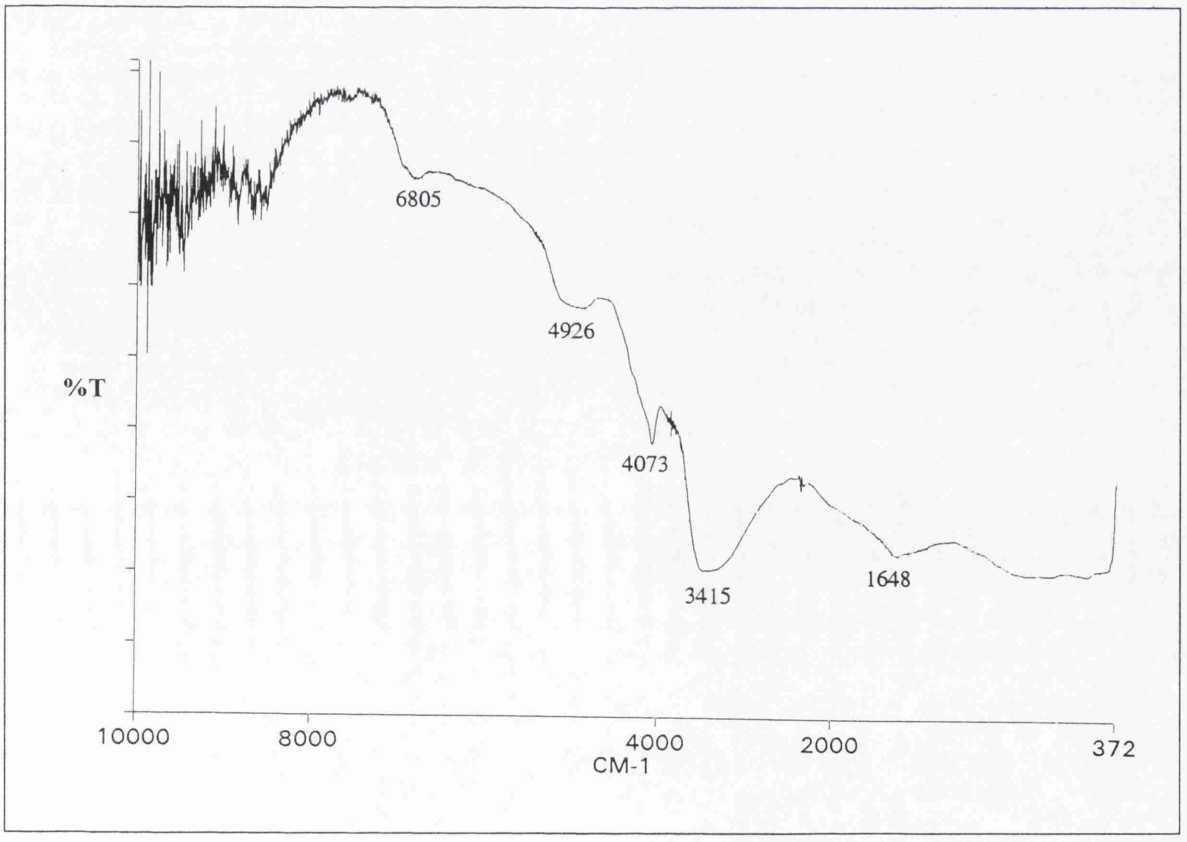

Figure 6.4a DRIFT spectrum of ODTMS on α-FeOOH surface, after subtraction of α-FeOOH

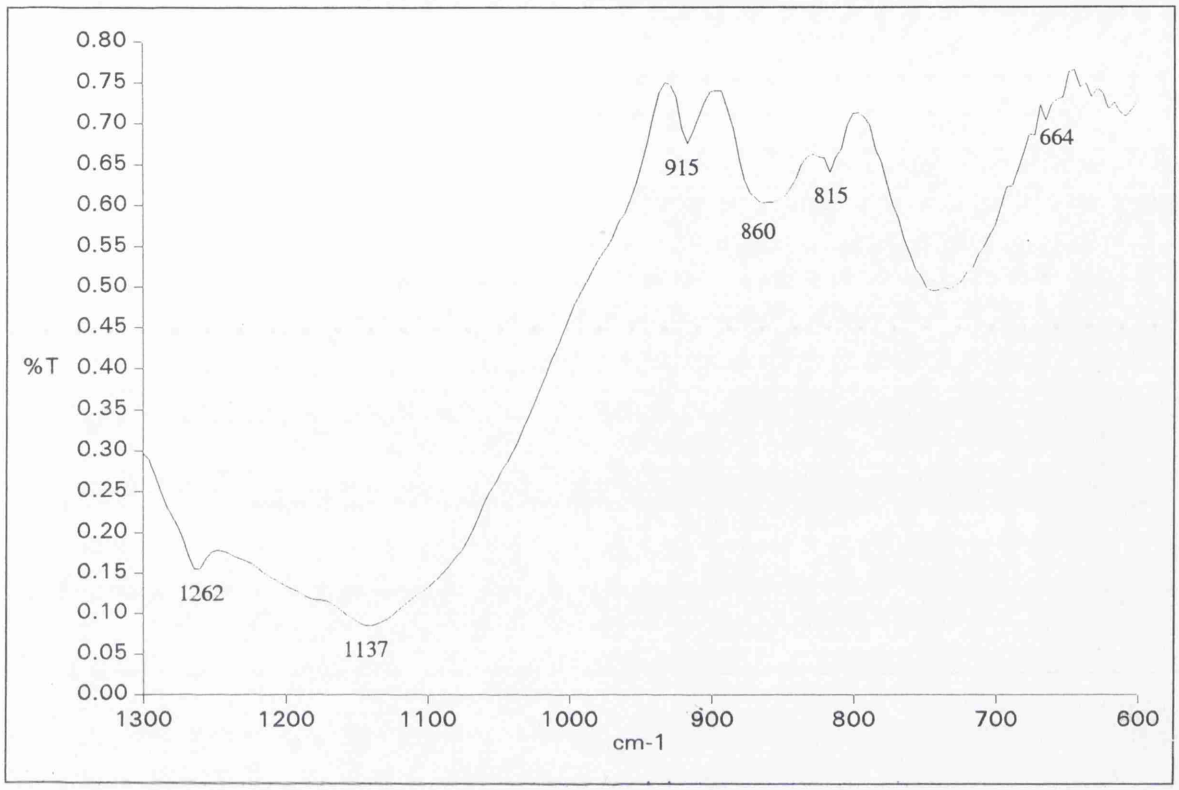

Figure 6.4b DRIFT spectrum of ODTMS on β-FeOOH surface, after subtraction of β-FeOOH

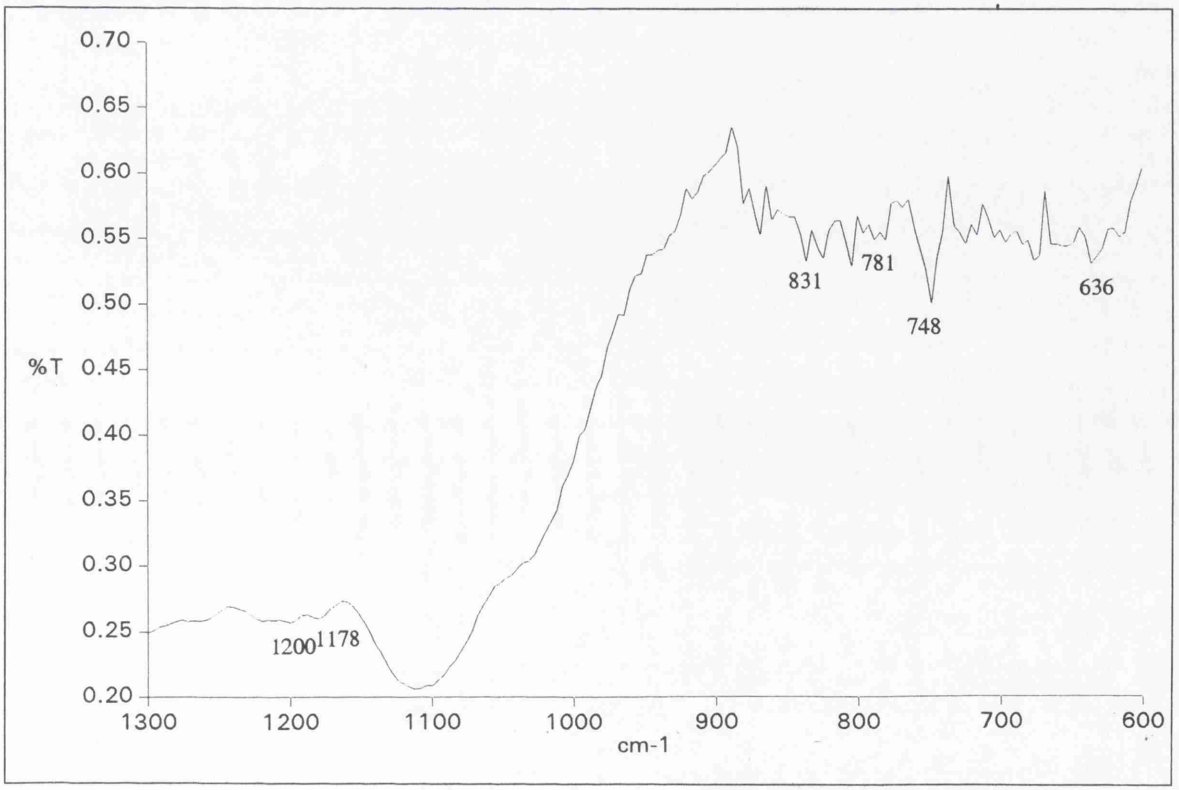

Figure 6.5a DRIFT spectrum of HFTMS on α-FeOOH surface, after subtraction of α-FeOOH

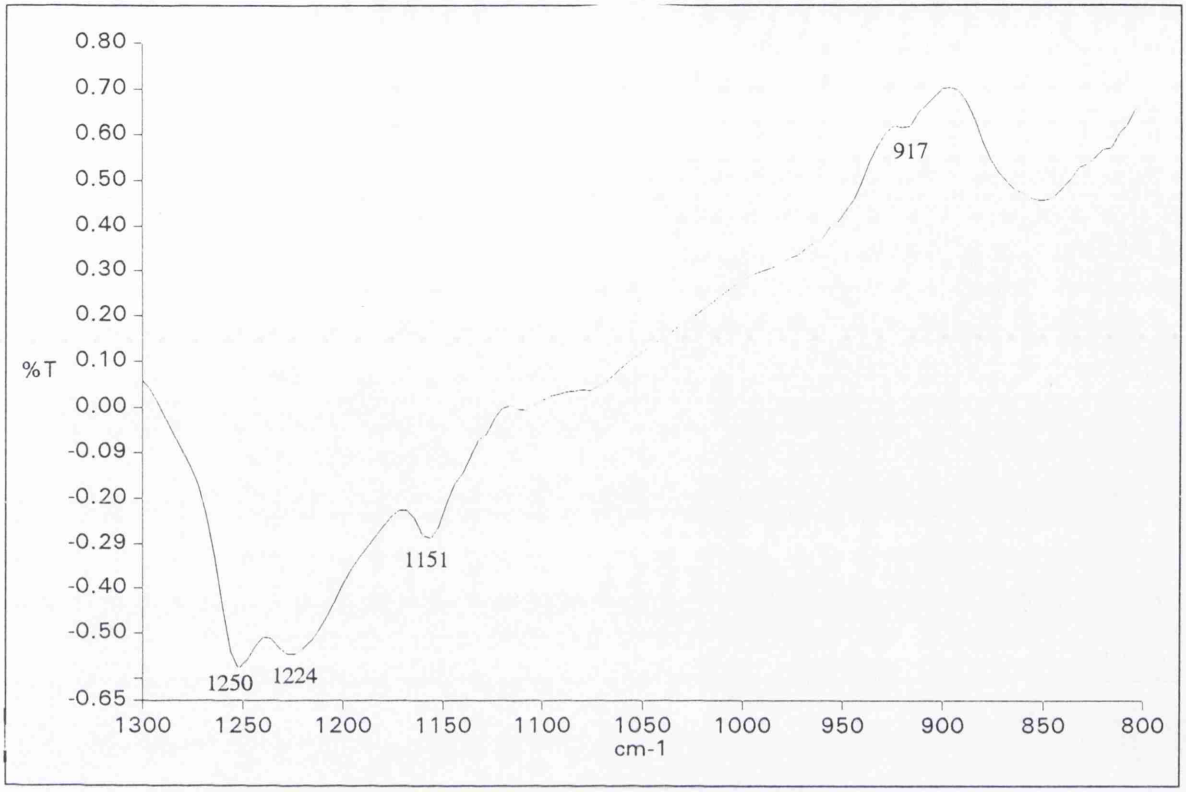

Figure 6.5b DRIFT spectrum of HFTMS on β-FeOOH surface, after subtraction of β-FeOOH

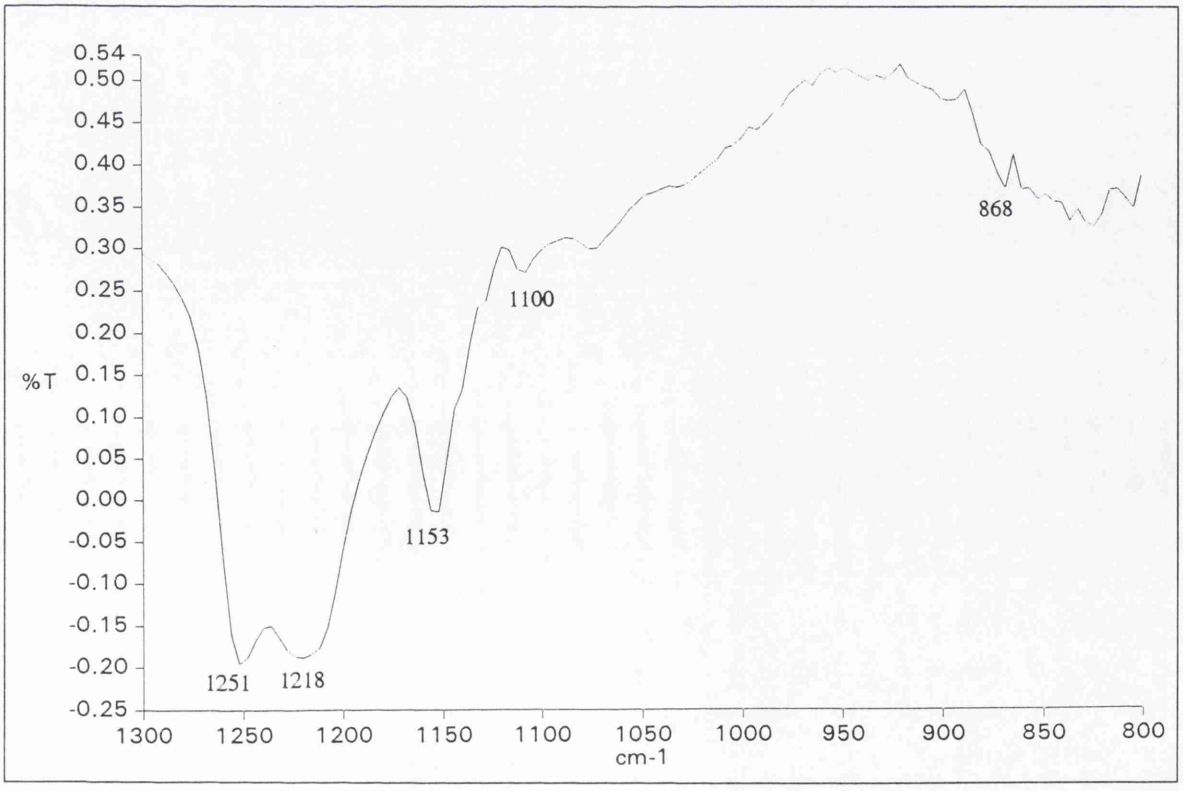

Figure 6.6a DRIFT spectrum of TTS on α-FeOOH surface, after subtraction of α-FeOOH

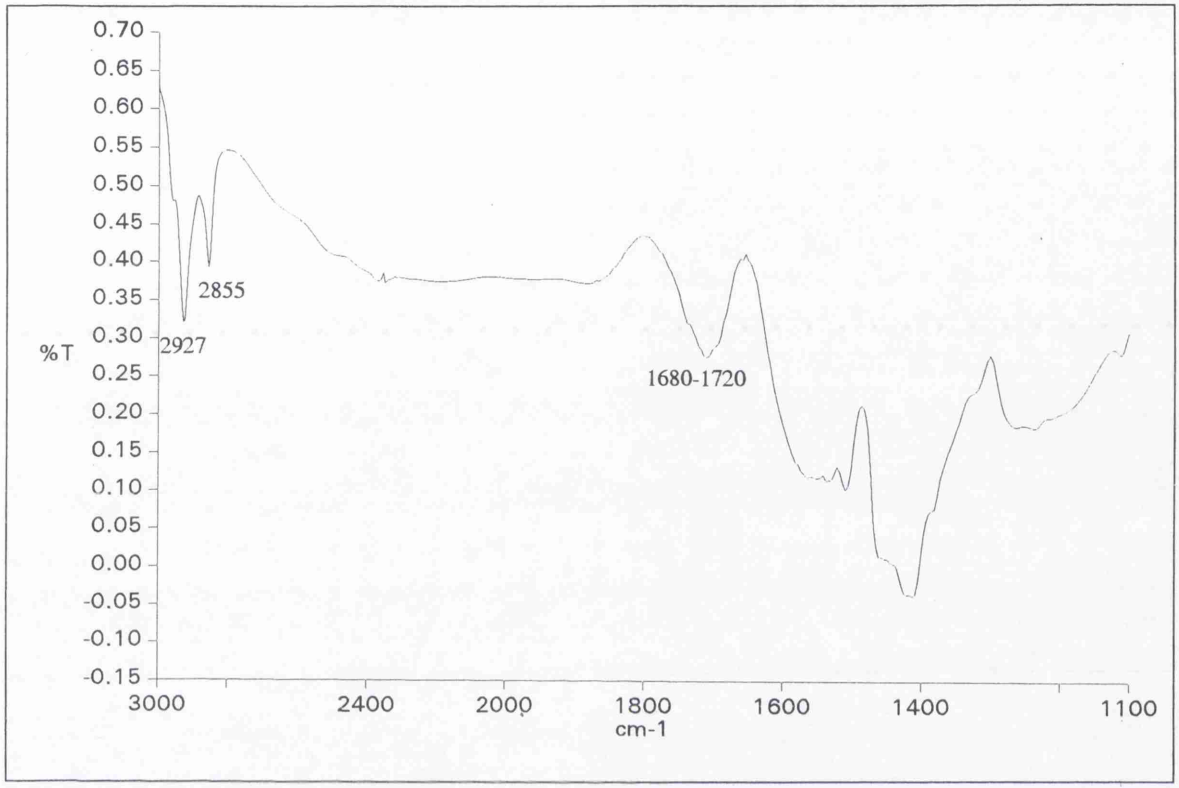

Figure 6.6b DRIFT spectrum of TTS on β-FeOOH surface, after subtraction of β-FeOOH

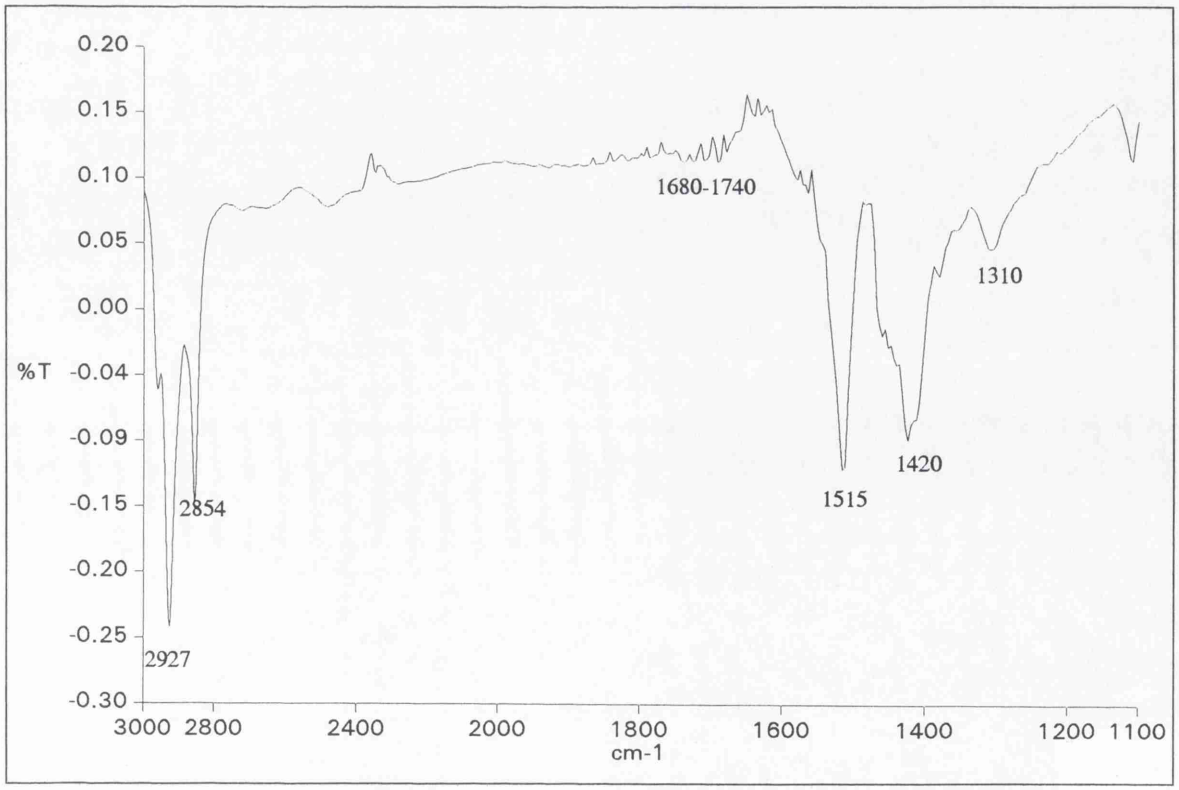

Figure 6.7a DRIFT spectrum of ODA on α-FeOOH surface, after subtraction of α-FeOOH

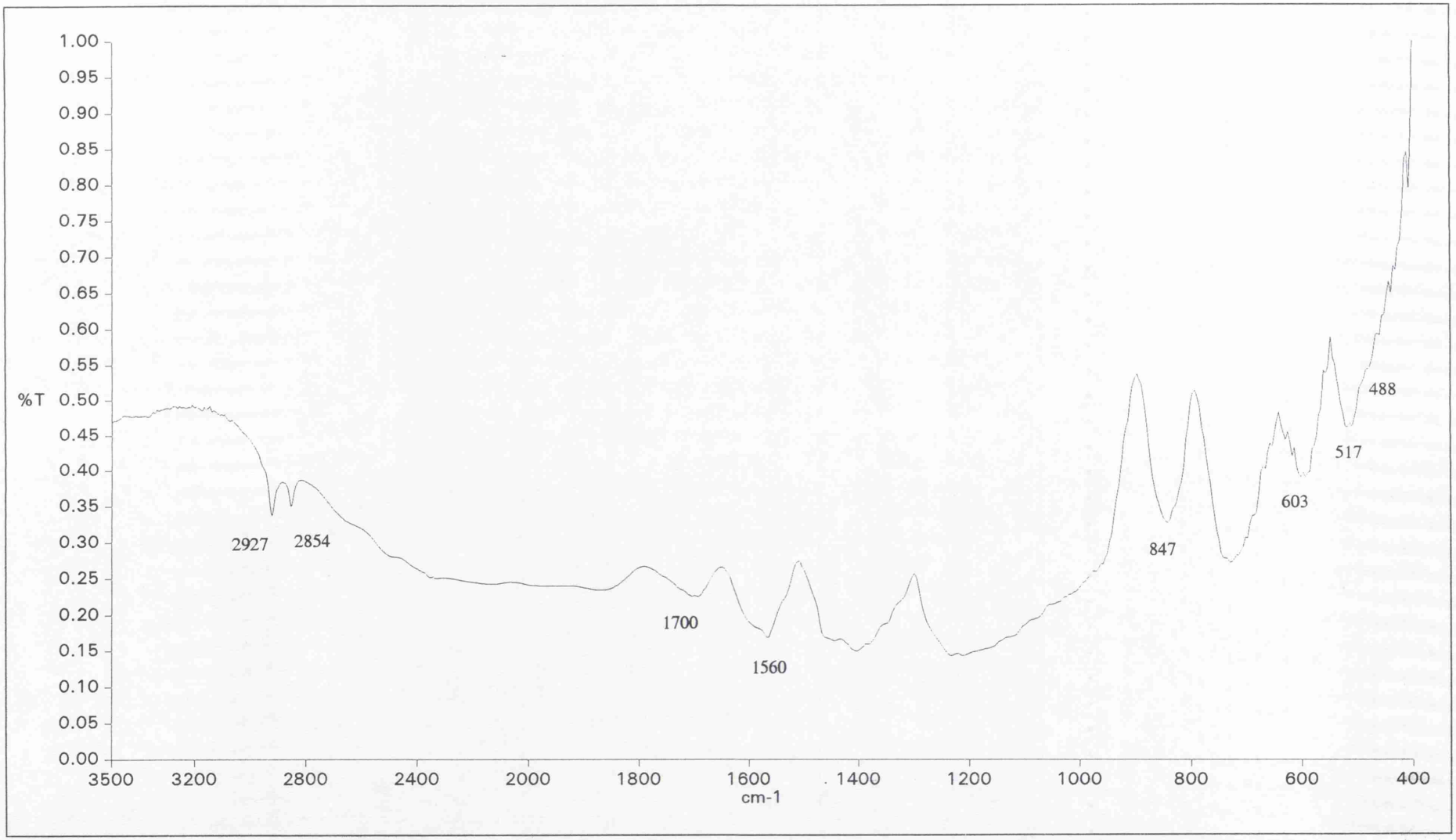

Figure 6.7b DRIFT spectrum of ODA on β-FeOOH surface, after subtraction of β-FeOOH

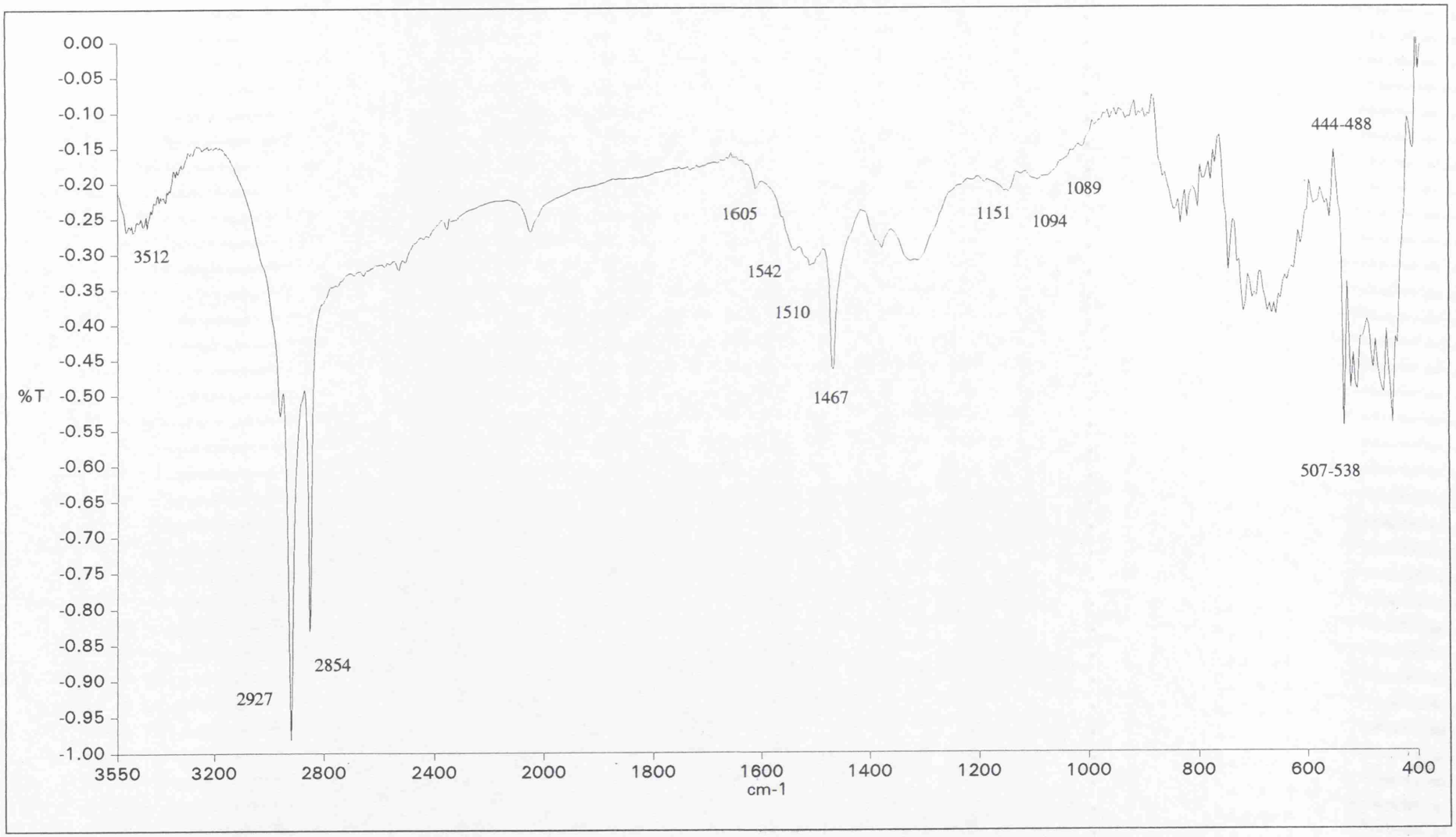

6.2.8 Raman Spectroscopy

6.2.8.1 Raman Spectroscopy

Raman spectroscopy is another form of vibrational spectroscopy. On irradiation by a laser, scattered light can be detected at the frequency known as the Rayleigh Line, and at additional frequencies symmetrically arrayed either side of the Rayleigh Line (Stokes and anti-Stokes lines). The differences between the Rayleigh Line frequencies and the other weaker Raman lines correspond to the vibrational frequencies present in the molecules of the sample.

Due to the different selection rules for the vibrations that appear in infrared or Raman spectra, vibrations can be classed as infrared active or Raman active (or both) and vibrations that are weakly observed or not present in infrared spectra may become strongly absorbing in Raman spectra (such as C=C and C=-C). The two techniques are therefore complimentary. The information that can be gained by Raman spectroscopy make it a good alternative or additional technique to FTIR.

6.2.8.2 Samples Analysed and Raman Spectra Acquisition

α-FeOOH and β-FeOOH powders were synthesised and treated with the inhibitors ODTMS, HFTMS, ODA and TTS as described in chapter 5. Spectra of these samples were collected by Amanda Hardy of UCL Chemistry Department. Spectra were recorded on a Renishaw Raman System 1000. A He-Ne air cooled laser was used to provide an excitation line at 632.8nm (red). Spectra were recorded over the range 120-1800cm^{-1} using data collected over 5 accumulations of 10 second duration.

It was however found that no peaks attributable to inhibitor molecules could be detected. In all cases only a weak signal attributed to the iron oxyhydroxide sample was detected. The technique was not sufficiently surface sensitive to record the vibrations of the molecules adsorbed onto the surface. Iron oxides are also weak Raman scatterers and so the signal produced was of low intensity with a poor signal to noise ratio.

6.3 X-RAY PHOTOELECTRON SPECTROSCOPY

6.3.1 X-Ray Photoelectron Spectroscopy

The photoelectric effect was first discovered by Einstein (for which he received the 1921 Nobel prize for physics). When x-rays are used to excite an atom, the emission of electrons (named photoelectrons) from core energy levels may occur. Figure 6.8 illustrates this schematically. The binding energy, E_B, of an electron in a particular electronic energy level can be calculated by measuring the kinetic energy of the photoelectron emitted from this level, E_{kin}, where:

$$E_B = h\nu - E_{kin} - \phi$$

$h\nu$ being the energy of the characteristic x-ray, h being Planks constant and ν being the frequency. ϕ is the work function of the spectrometer and sample, which is a constant. As these core energy levels are characteristic of particular atoms, there detection gives a method of elemental analysis.

Figure 6.8 Schematic illustration of photoelectron emission

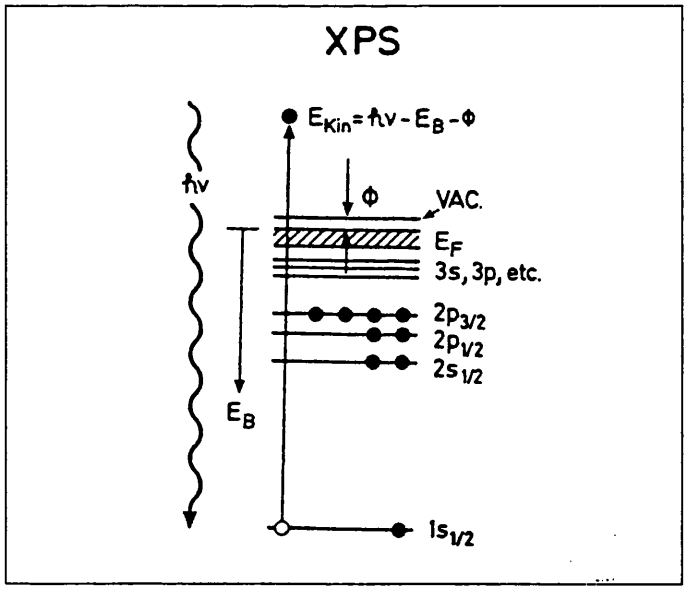

The binding energy of an electron in a core energy level of an atom is also dependant on the chemical state of an atom. For example the binding energy for a metal and its corresponding oxide may differ, the oxide being shifted by 2-3eV to a higher binding energy. This difference is known as the chemical shift. This shift makes determination of individual chemical states possible in addition to elemental analysis. The effect arises from

the differences in charge distribution of an atom when in different chemical states. Removal of a valence electron creating a positive ion will increase the binding energies of the remaining electrons whilst negative ionisation will have the opposite effect.

The first photroelectron spectroscopy experiments were carried out by Robinson and Rowlinson in 1914, but the technique was not successfully developed until the early 1950's by Prof Kai Siegbahn (Brune *et al*, 1997, 291). The technique is also known as ESCA (Electron Spectroscopy for Elemental Analysis) due to its ability to distinguish chemical states as well as elemental analysis. The main components of an x-ray photoelectron spectrometer are the x-ray source, sample stage, lens analyser and detector. These are all enclosed in an ultra high vacuum chamber (10^{-10} Torr). Photoelectrons produced are focused by an electrostatic lens system, onto the analyser. Energy discrimination of the photoelectrons is obtained by sweeping the potentials in the lens system. The x-rays are normally from an aluminium or magnesium monochromatized source.

XPS peaks appear on a background which must be removed to calculate peak intensities. The background continuously increases with electron energies, but there is also a stepwise increase, originating from inelastic scattering of electrons in the solid. These electrons appear at higher binding energies than the main peak. Quantitative analysis using XPS is relatively straightforward. An empirical method is normally used, referring to previously published data and standards. Accuracy of ±10% are to be expected for quantitative data (Christie, 1989, 157). Sensitivity of detection is in the range of 2-0.5%, although improvements have been made in newer instruments giving detection limits of 0.1-1% (Brune et al, 1997, 308).

6.3.2 Surface Analysis and XPS

XPS is a surface sensitive technique. With electron energies in the range 500-1500eV. Their mean free path, λ (the average distance the ejected electron can travel before inelastic collisions occur) is between 4 and 8 monolayers, in the range of 5nm (Brune *et al*, 1997). This means that only electrons originating from the surface layers will be emitted from the sample and reach the analyser.

The use of surface analytical techniques such as XPS to elucidate the nature of inhibitor layers on metal surfaces is becoming widespread in corrosion research (Swift *et al*, 1993) It is useful in many other fields such as metallurgy, catalysis, electronics and environmental control (Brune *et al*, 1997). The analysis of adsorbed or deposited layers is very difficult due to the low concentration of the layer. A high selectivity and sensitivity is needed, which is not found in some other commonly used techniques. On top of this, XPS can probe the elemental composition and chemical structure of a surface. XPS now has a detection limit in the range 0.1-1atomic %. Some modern instruments also have imaging facilities that have resolutions of 10μm (Brune *et al*, 1997).

6.3.3 Sample Preparation

XPS analysis was carried out on corroded iron samples. An iron rod, 5mm in diameter, from Johnson-Matthey (Specpure grade, total metal impurities: 15ppm or less), was cut into cylinders of height 5mm, so that the samples would be of convenient size for placing into the XPS analysis chamber. These samples were then corroded using method B, as described in chapter three, section 3.3.2. The corroded samples were then treated with the inhibitors ODTMS, HFTMS, ODA, and TTS as described in chapter five, section 5.3.3. A sample treated with DCA was also investigated, th treatment carried out as described in chapter four, section 4.2.3.6. Samples were stored in a desiccator over silica gel before use. Spectra of treated and untreated samples were recorded. Samples were placed on conductive tape before placing on the sample stage.

6.3.4 Spectra Collection

Spectra were collected on a VG ESCALAB 220i-XL from Fisons Instruments, in the laboratory of Professor D. Williams, UCL Chemistry Department. It was operated with Al-K_α monochromatised x-rays at 120W, with a spot size of 300μm and a vacuum of less than 1 x 10^{-9} Torr inside the analysis chamber. The analyser was operated in CAE (Constant Analyser Energy) mode with a pass energy (the kinetic energy of the electrons passing the analyser) of 20 - 80 eV. Spectra were acquired in large area XL lens mode, with step size of 200-800meV.

Only preliminary XPS studies on a limited series of samples was possible due to the unavailability of the XPS instrument. Further studies planned were not able to be carried out due to instrument failure and down time. Studies planned included the analysis of samples before and after exposure to a high humidty environment, to examine any differences that this exposure may cause.

6.3.5 XPS Results

Quantitative elemental surface compositions were calculated using the XPS software. Literature values of binding energies for particular transitions of each element were used to identify peaks. The 1s transitions of oxygen, carbon, fluorine and nitrogen, the 2p transition of chlorine and silicon and the $2p_{3/2}$ peak for iron and titanium were used for the quantitative analysis. After the subtraction of the background, using the Shirley method, the area of each peak was computed. Using literature sensitivity factors (Wagner *et al*, 1981), quantitative data was obtained. The binding energies and quantitative information for each sample analysed is given in table 6.5. Peak position do vary in each analysis which may be due to sample charging. Charging is exacerbated with rough and uneven surface. Figure 6.9 gives an example of the XPS spectra recorded.

Looking at the quantitative results it can be seen that in all cases a considerable change in the surface compositions has been achieved. The data for the ODA, TTS and ODTMS treated samples all show a considerable increase in the amount of carbon present on the iron corrosion product surfaces. The untreated sample also has 12.8% (atomic) carbon present on its surface, due to adsorbed organic molecules that are present on most surfaces. The increase in the amount of carbon is obviously due to the long C_{18} hydrocarbon chains of the inhibitor molecules. In the HFTMS treated sample fluorine, as well as a smaller amount of carbon was detected, originating from the polyfluoroalkyl chain on each inhibitor molecule. Additionally there is a decrease in the amount of oxygen present on the surfaces of those samples treated with inhibitors compared to the untreated samples. This would be expected as the presence of the inhibitor molecules will mean that less oxygen from the oxyhydroxide corrosion products will be detected in the treated samples. Chlorine, from the corrosion products is detected in all samples, although the atomic % varies from 1.1%-3.4%.

Table 6.5 XPS quantitative data for inhibitor treated and untreated corroded iron samples.

SAMPLE	PEAK	BINDING ENERGY (EV)	PEAK AREA	ATOMIC %
Untreated	Fe $2p_{3/2}$	712.40	0.00972	24.4
	O 1s	531.80	0.02462	61.7
	C 1s	285.40	0.00512	12.8
	Cl 2p	199.20	0.00044	1.1
ODTMS treated	Fe $2p_{3/2}$	710.50	0.00299	11.7
	O 1s	528.20	0.01092	42.6
	C 1s	283.40	0.01020	39.8
	Cl 2p	197.81	0.00079	3.1
	Si 2p	92.75	0.00073	2.8
HFTMS treated	Fe $2p_{3/2}$	713.00	0.00137	5.7
	F 1s	685.25	0.01132	47.0
	O 1s	533.60	0.00602	25.0
	C 1s	288.40	0.00397	16.5
	Cl 2p	203.00	0.00035	1.4
	Si 2p	106.20	0.00105	4.3
TTS treated	Fe $2p_{3/2}$	712.70	0.00388	9.2
	O 1s	532.00	0.02323	54.9
	Ti $2p_{3/2}$	461.50	0.00016	0.4
	C 1s	286.40	0.01426	33.7
	Cl 2p	203.50	0.00082	1.9
ODA treated	Fe $2p_{3/2}$	707.80	0.00223	6.4
	O 1s	525.15	0.00724	20.9
	C 1s	283.00	0.02282	65.7
	Cl 2p	195.85	0.00126	3.6
	N 1s	399.40	0.00116	3.4

Figure 6.9 Example of XPS spectrum recorded

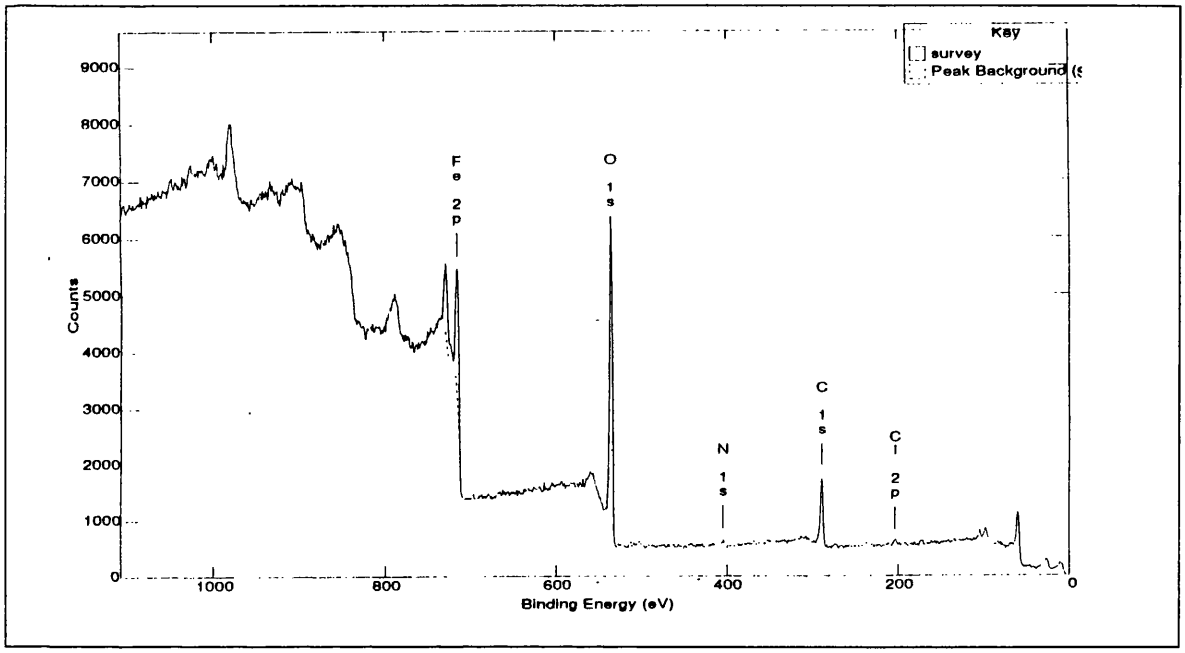

The presence of other elements found in the inhibitor molecules, on the surface of the treated samples gives added evidence for their presence on the corrosion product surface. Silicon was detected on the surfaces of both silane treated samples and nitrogen was detected on the ODA treated samples. Only a very small trace of titanium was detected on the TTS treated sample. The peak detected was barely above the background photoelectron level, however this is not surprising as unlike silicon or nitrogen in the other inhibitor molecules, the amount of titanium present in TTS is small. The ratio of carbon to titanium in TTS is 54:1, as compared to a ratio of carbon to silicon in ODTMS of 18:1.

The atomic percentage of iron analysed for each sample is given in table 6.5. These percentages are also expressed fractionally as the ratio of the percentage of iron for each inhibitor treated sample over the percentage of iron on the surface of the untreated corroded iron sample. These values are given in table 6.6. The interpretation of this data is more complex than might be thought. Iron analysed on inhibitor treated samples may be seen as an indication of areas of the surface not covered with inhibitor molecules (Al Ahmed, 1992). However XPS has a depth of analysis of about 5nm (Brune *et al*, 1997), but monolayers of molecules with long hydrocarbon chains such as ODTMS, octadecyldimethylmethoysilane (C_{18} chains) and cetyltrimethylammonium bromide (C_{16} chain) have been shown to have depth of between 2-3nm depending on the chain length

and chain orientation with respect to the surface (Horr *et al*, 1995, Sjoblom *et al*, 1995). Therefore the XPS spectra will consist of photoelectron energies from the inhibitor layer and the iron oxyhydroxide underneath. The percentage of iron analysed is therefore related to the depth of the inhibitor layer as well as its consistency. In fact, both these factors relate to the efficiency of the inhibitor. A thicker, more dense film is likely to provide better inhibition to corrosion.

Table 6.6 Ratios of iron percentages

	UNTREATED	ODTMS	HFTMS	TTS	ODA
Atomic % of Fe	24.4%	11.7%	5.7%	9.2%	6.4%
$\frac{\textit{\% Fe Inhibited}}{\textit{\% Fe Untreated}}$	-	0.48	0.23	0.38	0.26

The percentage of iron analysed on each surface is shown in table 6.6. It can be seen that there is a significant decrease in the percentage of iron analysed on all treated corroded surfaces, from 24.4% for the untreated corroded surface to between 11.7-5.7% for the inhibitor treated samples. The ratio of the percentage of iron on each inhibited sample divided by the percentage on the untreated surface is used to compare the different treatments. This value can be seen as being related to the efficiency of a treatment in terms of depth and percentage surface coverage. The lowest ratio, 0.23 is found for the HFTMS treated sample, the highest, 0.48 for the ODTMS treated sample. This indicates that the ODTMS treatment does not give as good a surface coverage, which would explain in part why it was not found to be a good inhibiting treatment. The HFTMS treatment was found to accelerate corrosion in the accelerated corrosion tests, however, from this technique it would appear to give good a good surface covering.

The ratio for the ODA treated sample, 0.26 is lower than that of the TTS treated sample, at 0.38. This indicates that ODA does form an inhibitor layer with a surface coverage better, if not equal to that provided by TTS when in a dry environment. However, the floatation tests have shown that the bonds between the iron oxyhydroxide and ODA nitrogen are easily hydrolysed, removing the inhibiting layer from the corroded surface in the presence of water.

A sample treated with DCA was also investigated, and in particular the peak obtained for nitrogen was examined. The peak showed the presence of $-NH_3^+$ species as well as NH_2 species. This spectra is shown in figure 6.10. The nitrogen peak of a corroded iron sample treated with DCA is shown with the nitrogen peak from an untreated corroded iron surface. The nitrogen found to be present on this surface is due to physisorbed organic molecules that often exist on surfaces. The nitrogen peak recorded from the DCA treated sample contrasts to the former peak by the presence of NH_3^+ species. This confirms the FTIR data in which evidence of protonated amine species were also found.

Figure 6.10 XPS spectra showing nitrogen peak for ODA treated sample

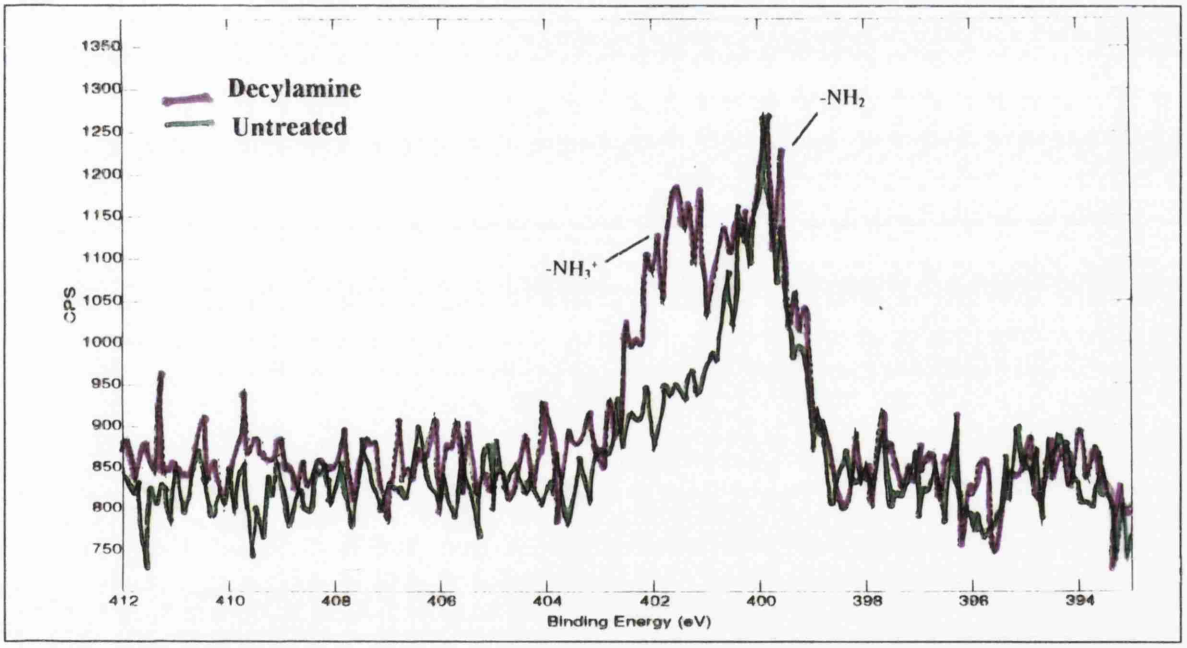

Further XPS studies, so that the surfaces of samples could be characterised again, after exposure to high humidity, were planned. In this way, the extent of the breakdown of the inhibitor layer could have been investigated. It was also intended to carry out XPS imaging experiments, using the imaging facility available on the VG ESCALAB 220i-XL instrument. Imaging the elemental composition of the surface of treated samples may indicate the distribution of the various inhibitor treatments on the sample's surface, and thus show the presence of any gaps or flaws in the treatments. Further work however was not possible due to the breakdown of the x-ray photoelectron spectrometer.

CHAPTER SEVEN

Assessing Polyaniline as a Corrosion Inhibiting Coating for Archaeological Iron

7.1 INTRODUCTION

Research into conducting polymers such as polyaniline has only recently gained momentum. The first conferences and meetings in this field occurred in 1989 (Przyluski, 1991). These new materials are often called organic metals or intrinsically conducting polymers (ICP) as the polymers themselves are conducting. Filled polymers, in which materials such as carbon or silver are compounded with a base polymer are also described as conducting polymers, but differ from these new ICPs in that the polymer itself is not conducting. An interesting new application for conducting polymers is there use as corrosion inhibitors (Deberry, 1985, Wessling, 1994). They have been found to be efficient inhibitors for iron and it was therefore decided to assess the performance of the conducting polymer polyaniline as a corrosion inhibiting treatment for archaeological iron. No previous studies have been carried out on the performance of this polymer on pre-corroded material.

Materials can be classified as insulators, semiconductors and conductors, depending upon their ability to conduct electricity. Intrinsically conducting polymers can behave as semiconductors, or even insulators, but in specific chemical states they become conductors. Intrinsically conducting polymers with conductivities as high as 10^5 Scm^{-1} have been synthesised (Kathirgamanathan, 1991). This is nearly equal to the conductivity of copper. Intrinsically conducting polymers can be used in a variety of applications such as antistatic materials, gas sensors, ion sensors, biosensors, optoelectronic devices, conducting adhesives, electroprinting and fibre optics. More recently certain intrinsically conducting polymers have been found to successfully inhibit corrosion and have been used as corrosion inhibitors.

7.2 WHAT ARE CONDUCTING POLYMERS

Intrinsically conducting polymers, like metals, have delocalised electrons that can move between atoms and allow a flow of charge. Conducting polymers differ from other conductors, such as carbon black, as besides their metallic character they are also redox active materials. In their different redox states these polymers may have differing conductivities and differing properties such as colour. They can be divided into two main categories, ionically conducting and electronically conducting polymers (Kathirgamanathan, 1991). The conduction mechanism in both groups is facilitated by conjugated double bond systems (alternate single and double bonds in carbon chains), however these are formed by different processes.

7.2.1 Electronically Conducting Polymers

Electronically conducting polymers include polyacetylene, polypyrrole, polythiophens and polyphthalocyanines. All these polymers have high molecular weight conjugated carbon chains. In their insulating states these consist of alternate single and double bonds of different lengths. These can be seen as quasi one dimensional crystalline materials and therefore band theory, used to describe solids, can be used to model these polymers. Figure 7.1 illustrates that the polymer would have a band gap (found to be 1.4eV in the case of polyacetylene) as in the case of semi-conductors. For conductivity, electrons need to be present in the upper conduction band.

Unlike semi-conductors the band structures of one dimensional solids can be changed. By adding extra electrons to the one dimensional lattice a different band structure is formed. The band gap collapses and electrons can enter band gap electron sites. The one dimensional structure also changes from double and single bonds to a homogeneous bond length. The polymer thus becomes conducting. This transition from the non-metallic to the metallic state is known as the Peierls transformation (Przyluski, 1991).

The addition of electrons to polymers such as polyacetylene, is known as doping. This creates a polaron, an electron and a corresponding positive carbon site. Figure 7.2 illustrates a polaron. These sites serve as hopping sites for charge carriers. A variety of

different and more complex combinations of polaron sites can exist (Przyluski, 1991, 18). Doping is achieved by the addition of doping agents such as sodium, or by photo-excitation of electrons.

Figure 7.1 Metallic and insulator states of conducting polymers

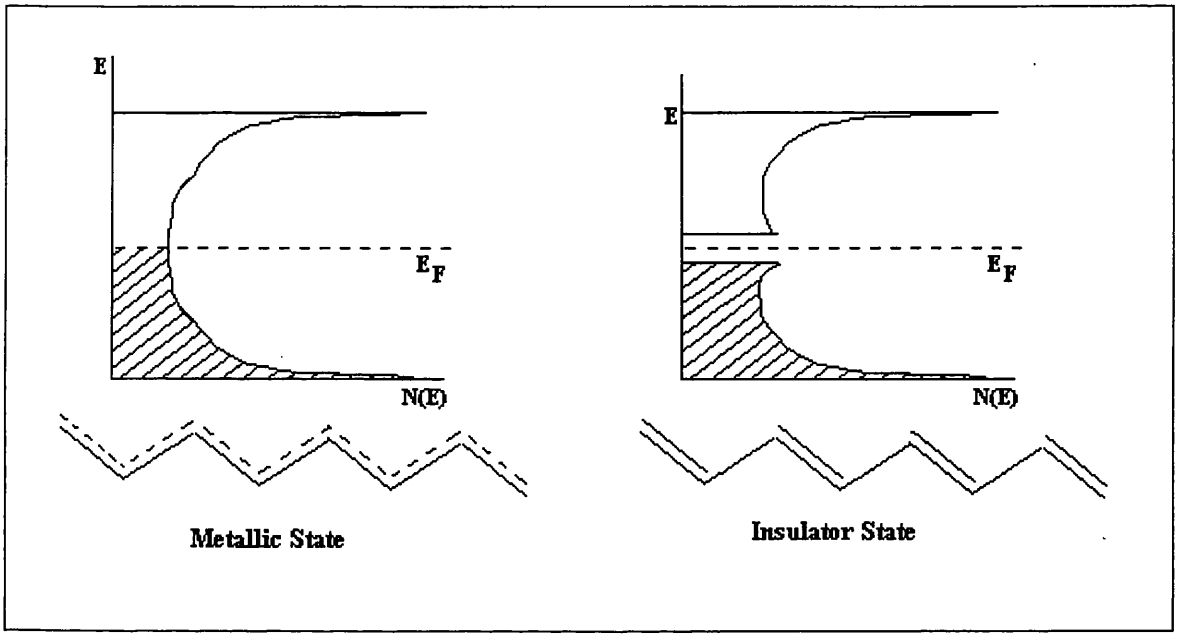

Figure 7.2 A polaron and its band structure (Przyluski, 1991)

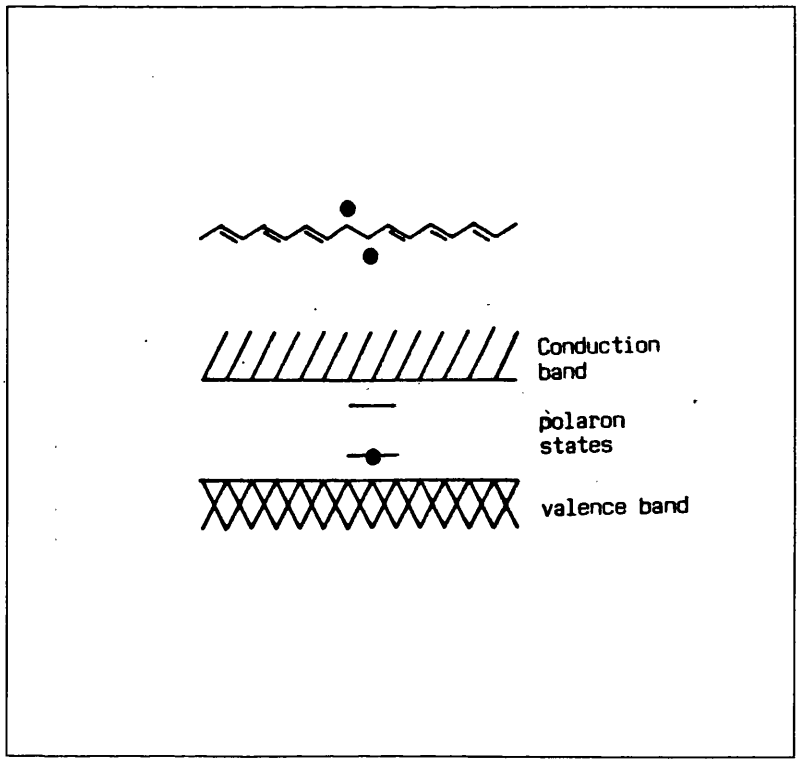

Electronically conducting polymers can also be described as heterogeneous, consisting of regions of high conductivity, 'metallic islands', separated by barriers of lower conductivity. If these barriers have high enough conductivity themselves, the polymer will be metallic in nature (Roth, 1986).

7.2.2 Ionically Conducting Polymers

Ionically conducting polymers are polymer salt complexes. These systems consist of a polymer and a metal salt or protonic acid in which polymer chains play the role of ligands. Examples of such polymer ligands are amines, imines, carboxyls, ketones, phosphonic acid groups and thiols. The conduction mechanism is complex and not completely understood. One theory suggested is the dynamic percolation theory (Rather *et al*, 1986) which explains conduction by the hopping of an ion from one site to another site of ionic occupancy.

Polymers suitable for the preparation of intrinsically conducting polymers often have a hetero-atom containing an electron pair with a donor power strong enough to co-ordinate a metal cation. As with electronically conducting polymers, ionically conducting polymers must be doped to become conductive. Doping is facilitated by the addition of a proton. Protonation leads to the rearrangement of the polymers electronic structure and the formation of polarons. This causes the breakdown of the polymers' band gap, leading to conductivity.

7.3 CORROSION INHIBITION WITH CONDUCTING POLYMERS

7.3.1 Introduction

A new approach to corrosion prevention based on the use of conducting polymer coatings has recently been proposed (Wessling, 1994, Lu *et al*, 1995, Troch-Nagel *et al*, 1992, Wrobleski *et al*, 1994). A form of anodic protection may be obtained by coating an active-passive metal, such as iron, with a redox species capable of maintaining the passive film on the metal. Some conducting polymers have the redox properties that allow this to occur. It has been found that conducting polymer coatings lead to a significant shift of the corrosion potential in the direction of noble metals and to the formation of a passive metal oxide layer on the surface of the metal (Yen Wei *et al*, 1995). Although work on these conductive coatings is still in its infancy, a coating has already been tested as a corrosion inhibitive primer for use by NASA on the surface of space shuttle launch pads, which previously needed to be repainted after every launch to stop rust developing (Phillips, 1994).

Conductive polymers suggested as corrosion inhibitors include, polythiophene-3-methanol (Polyakallio *et al*, 1995), poly 3-Methylthiophene (Ren & Barkey, 1992), polyaniline (Wessling, 1994, Wei-Kang Lu *et al*, 1995, Deberry, 1985, Yen-Wei *et al*, 1995, Wrobleski *et al*, 1994), polypyrole (Troch-Nagel *et al*, 1992), poly 2-vinylpyridine (Sekine *et al*, 1992), polythiophene (Borsch & Beck, 1993), poly ethoxy-aniline (Sathiyanarayanan *et al*, 1992), and poly o-methoxy-aniline (Sathiyanarayanan *et al*, 1994).

7.3.2 Corrosion Inhibition by Conductive Polymers

The mechanism of corrosion inhibition by conducting polymers can be explained as a form of anodic protection. A commonly practised form of corrosion prevention is to use a sacrificial anode such as a piece of zinc bolted to a steel ship. The zinc will corrode preferentially. This protection can be artificially produced by using a power supply to pump electrons into the metal to suppress metal dissolution. This is known as cathodic protection. For active-passive metals (iron, nickel, chromium and titanium) protection can also be afforded to a metal by using a power supply to remove electrons from the metal.

This will change the potential of the metal to a potential within the passive region and thus passivate the metal preventing corrosion. This process is known as anodic protection.

Electroactive and conductive polymers are thought to inhibit corrosion using a similar mechanism to anodic protection. Electrons from the metal can be taken up by the polymer and thus the metal becomes passivated. This process causes the oxidation of the metal, producing the passive iron oxide layer consisting of Fe_2O_3 and Fe_3O_4 (Lu *et al*, 1995). An accompanying reduction of the polymer film occurs. The polymer film may then be returned to its original chemical state by aerial oxidation, so being continuously regenerated, producing a long term stable protective film (Deberry, 1985).

The mechanism for corrosion inhibition has also been compared to that of other inhibitors having unsaturated bonds. These inhibitors are adsorbed onto metal surfaces due to the availability of π electrons and they replace surface water molecules and thus inhibit corrosion. Conducting polymers also have a delocalised structure and could therefore be classed as adsorption inhibitors, adsorbing via the delocalised π electrons (Sathiyanarayanan, 1992).

Conductive polymer coatings have been pursued as corrosion inhibitors as they seem to circumvent the problem of crevice corrosion occurring with insulating coatings (Deberry & Viehbeck, 1984). In corrosive environments, conductive polymer inhibitors have been reported not only to passivate a metal but to repassivate areas where the coating becomes damaged, for example, by a scratch. This repassivation can prevent localised corrosion and pitting.

7.4 POLYANILINE

7.4.1 Polyaniline as a Corrosion Inhibitor

Polyaniline is the intrinsically conducting polymer most studied for its possible industrial applications. This includes its use as a corrosion inhibitor. It was therefore decided that polyaniline was the most appropriate intrinsically conducting polymer to be tested as a conservation treatment for archaeological iron. It is at present being introduced to the commercial market by Ormecon Chemie, a subsidiary of Zipperling Kessler and Co, based in Ahrensburg, near Hanover in Germany. It is the first conducting polymer material to be commercially available (Zipperling-Kessler, 1996) for corrosion protection and for the manufacture of printed circuit boards.

Considerable research into using polyaniline as a corrosion inhibitor has been carried out. An initial study was carried out in 1985 and reported that stainless steel electrodes electrochemically deposited from perchloric acid solution, with thin films of polyaniline, remained passive for long periods of time in acid solutions in which they would normally be active and corrode at high rates. The stainless steel resisted pitting for the 30 day trial and corrosion did not occur even after the electroactive polyaniline coating had been scratched, in contrast to other passivated samples (Deberry, 1985).

In more recent years there has been an increase in the literature published on this subject. In a study by Wrobleski *et al* (1994), polyaniline was spray coated onto mild steel samples that were then doped with p-toluenesulphonic acid or zinc nitrate and an epoxy top coat added to the samples. Corrosion testing was carried out by immersing the samples in aerated 3.5% NaCl solutions or 0.1M HCl solutions and monitoring their appearances over an 8 to 12 week period. Some samples were scratched. The samples coated with the polyaniline primer showed much better corrosion resistance in both solutions and showed no signs of corrosion on the edges or in the scratched areas. Further tests over a seven month period gave further indications that doped polyaniline (emeraldine salt) was an effective corrosion inhibitor (Wrobleski *et al*, 1994).

Wessling (1994) coated stainless steel and copper with several layers of a dispersion of polyaniline. Corrosion currents and potentials were obtained for these samples and it was found that a significant and reproducible shift in the corrosion potential of up to 800mV for iron was achieved, together with a decrease in corrosion current. SEM and EDAX analysis showed the presence of a passivated iron oxide layer underneath the polyaniline coating (Wessling, 1994). ESCA and Auger studies by Lu *et al* (1995) indicated this oxide to be γ-Fe_2O_3 and Fe_3O_4 layers. It was also concluded that corrosion protection was achieved by the galvanic coupling of the polyaniline layer to the metal substrate. The corrosion protection afforded by polyaniline extended to exposed areas of metal (i.e. areas not covered by the polyaniline coating) that are also galvanically coupled to the polyaniline coated steel, thus explaining the protection afforded to even scratched areas of the metal (Lu *et al*, 1995).

A series of electrochemical measurements were also made on steel covered with polyaniline and polyaniline doped with hydrochloric acid. Contrary to what might be expected the basic form of polyaniline was found to offer better corrosion protection than the salt form. Both forms of polyaniline offered corrosion protection that was not gained from nonconjugated polymer coatings such as polystyrene and epoxys (Wei *et al*, 1995).

Substituted polyanilines have also been tested as corrosion inhibitors such as poly o-ethoxyaniline and poly o-methoxyaniline (Sathiyanarayanan *et al*, 1992, 1994). Substitution occurs on the ortho position of the aniline. The substituent renders the polymer soluble in ethanol. Electrochemical and mass loss corrosion tests found that these polymers, undoped or doped with hydrochloric or sulphamic acid, inhibited the corrosion of steels. The undoped polymers were found to be more efficient inhibitors

7.4.2 The Structure of Polyaniline

Polyaniline is formed from the polymerisation of aniline, $C_6H_5NH_2$. It was first prepared by an electrochemical oxidation in H_2SO_4 solution over 100 years ago (Lethby, 1862). The green polyaniline hydrosulphate salt formed was named emeraldine. Polyaniline (PANI) can exist in various oxidation states characterised by the ratio of imine to amine nitrogens

and corresponding quinoid to benzoid carbon rings. The conductive form is the emeraldine salt. It has the intermediate oxidation state, with equal numbers of imine (–N=) and amine (–NH–) nitrogens. The structure of PANI depends on its oxidation state, which in turn depends on pH. MacDairmid *et al* (1985) suggested the reaction scheme illustrated in figure 7.3 for the different forms of polyaniline.

Figure 7.3 The different oxidation states of polyaniline

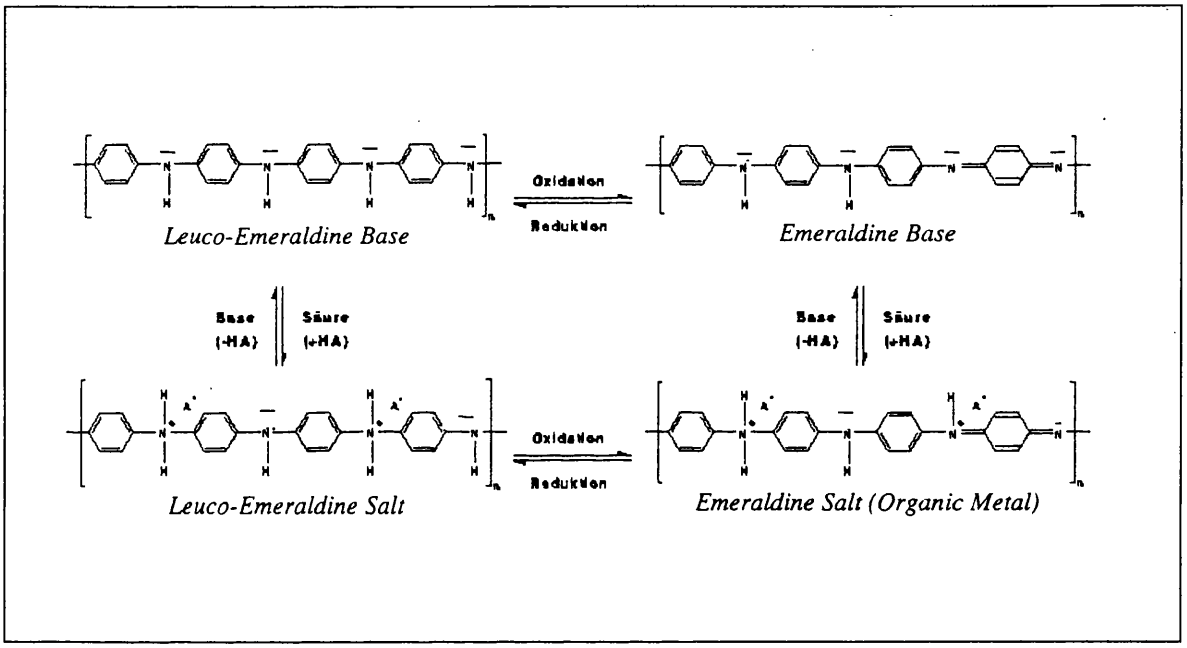

Polyaniline is electrochromic - in other words it changes its colour with oxidation and redox state. The metallic emeraldine salt phase forms transparent green films and the emeraldine base, transparent blue. Leuco-emeraldine is a white powder (Yen Wei *et al*, 1994). Both these oxidation states are stable up to temperatures of 200°C (Zipperling Kessler, 1996). Polyaniline can actually exist in a third oxidation state, pernigraniline base. This reduced phase is pale violet but is readily reoxidised. The pernigraniline salt is unstable and no characterisation has been carried out. Polyaniline films in the conducting metallic state have a resistance of 10^3-$10^5\Omega$ and a conductivity of up to $5Scm^{-1}$ (Zipperling Kessler, 1996). As a 'metal' it is nobler than iron or copper, ranging close to silver in the electrochemical series. The polymer is usually insoluble in any solvent.

7.4.3 The Conductivity of Polyaniline

Polyaniline falls into the intermediate category of mixed inherently conducting polymers. Electron transfer occurs via electronic and ionic mechanisms. The conducting emeraldine salt is formed from the protonation of emeraldine base. Protonation increases the conductivity by a factor of 10^{10} despite an unchanged electron concentration (Stafstrom *et al*, 1987). Protons can be introduced by the addition of a protonic acid such as hydrochloric acid. This proton doping leads to a phase segregation of unprotonated and fully protonated domains, thus creating a conductive polaronic metal. This process is shown diagramatically in figure 7.4. In the first stage protonation leads to the formation of a bipolaron, the unstable bipolaron structure then forms two polarons and these then separate to yield a polaron lattice (Stafstrom *et al*, 1987).

Figure 7.4 Doping of PANI to form conducting polymer: (a) before protonation and (b) -(d) after 50% protonation: (b) Formation of bipolarons and (c) of polarons; (d) the polarons separate, which results in a polaron lattice (Stafstrom et al, 1987)

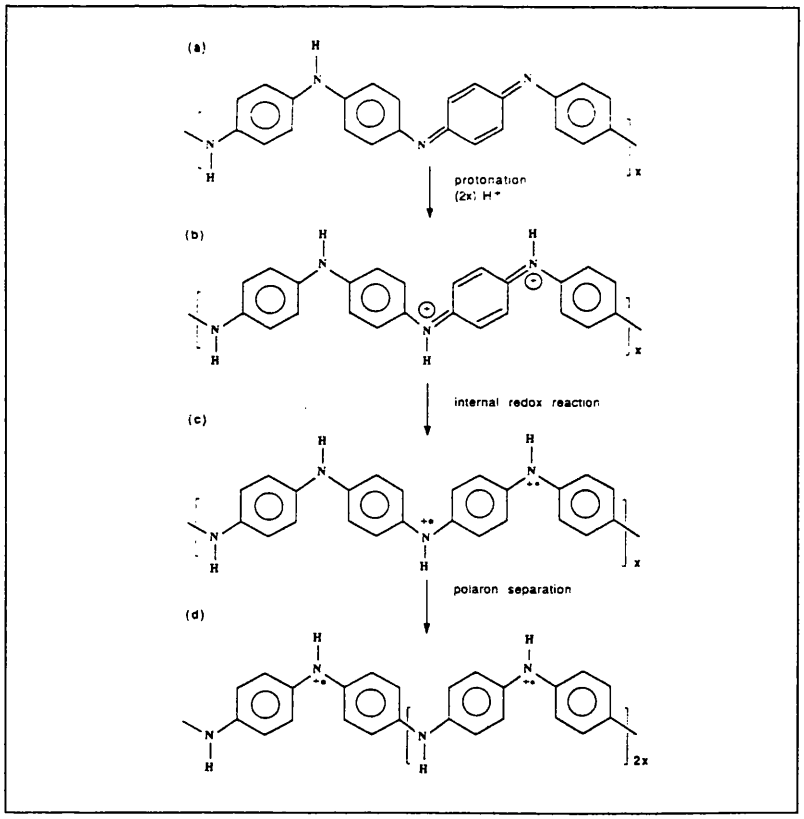

Proton exchange reactions play a central role in the conduction mechanism of polyaniline (Focke *et al*, 1987). The unprotonated imine nitrogens would be expected to act as a

barrier to conduction. However proton exchange reactions mean that these defects are not fixed in time and space but fluctuate in position. Intramolecular charge transfer involves the translation of a quinoid structure along the polymer backbone (see figure 7.5).

Figure 7.5 Migration of oxidation states along the polymer backbone by proton exchange and valence resonance (Focke et al, 1987)

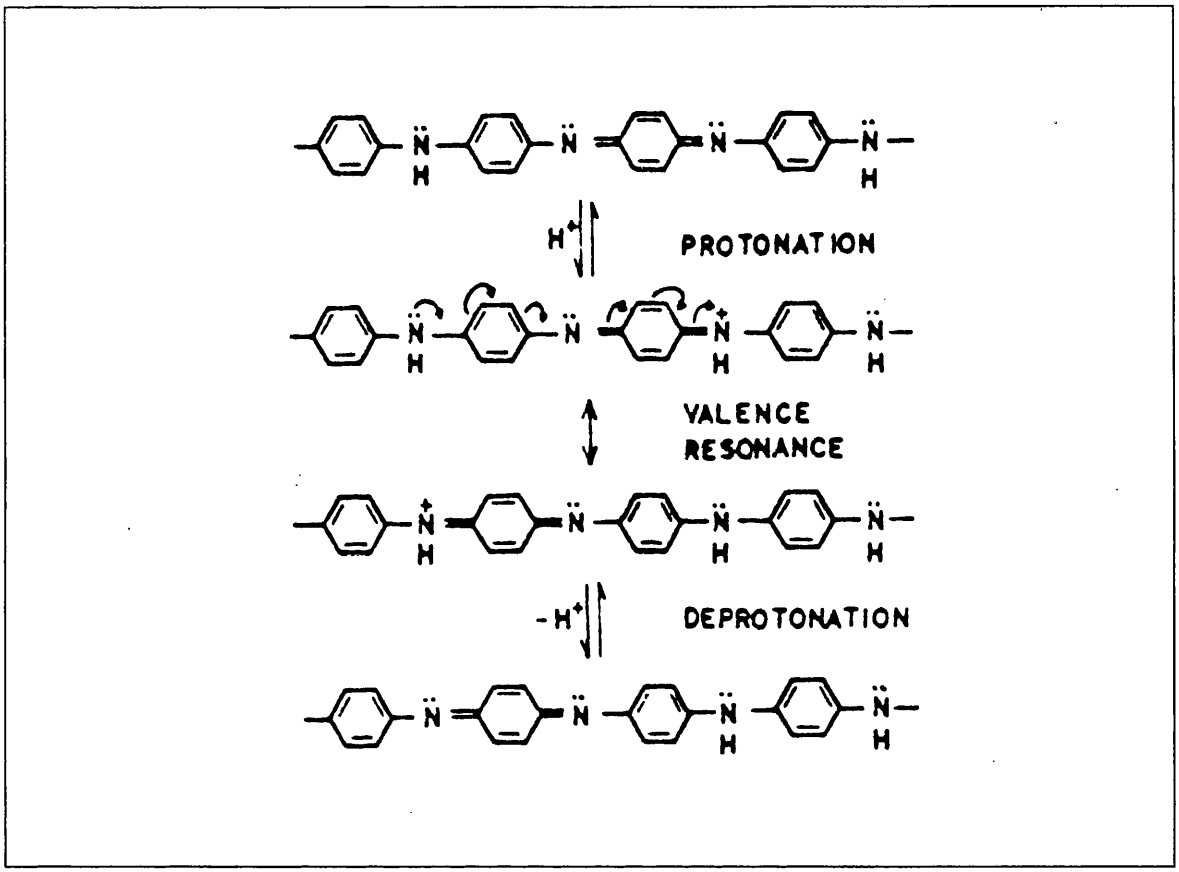

Translation over a distance of two rings is possible by valence resonance. Further translation can then be facilitated by deprotonation/protonation cycles as illustrated in figure 7.5. Interchain transport can also occur as illustrated in figure 7.6. This implies a coupling of electronic and ionic transport. PANI is found to increase its conductivity in the presence of water (Focke *et al*, 1987). This adds weight to the ion transport theory of the conductivity of polyaniline as water will aid proton transfer between chains of polyaniline via H_3O^+ ions.

Figure 7.6 Intermolecular charge transfer facilitated by proton-exchange reactions (Focke et al, 1987)

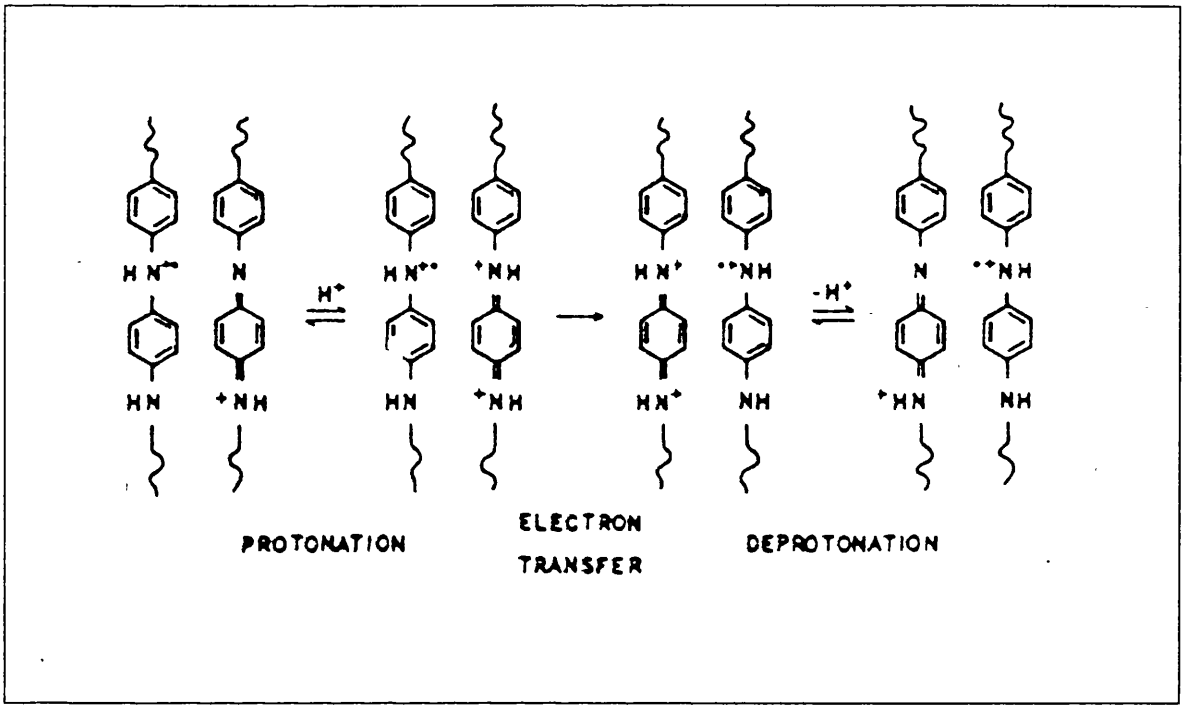

7.4.4 Mechanism of Corrosion Inhibition

The mechanism by which polyaniline inhibits corrosion is still much under discussion in the literature. Emeraldine salt, produced by doping polyaniline with a protonic acid such as hydrochloric or toluene-sulphonic acid, is the 'metallic' conducting phase. It is suggested, it inhibits corrosion by a form of anodic protection. It can be seen as a nobler metal that is galvanically coupled to the metal being protected, changing its potential and causing passivation.

There are some problems with the description of the corrosion inhibition of polyaniline, as the semiconducting, undoped form of polyaniline, the emeraldine base, has also been shown to inhibit corrosion. In this state polyaniline is not conducting and thus can not act as described above. Some studies have shown that emeraldine base inhibits corrosion to a greater extent than the conducting phase (Sathiyanarayanan *et al*, 1992. 1994). This suggest a different mechanism is at work, unrelated to the conducting nature of the emeraldine salt. A suggested mechanism for the inhibition of the undoped polymer is the presence of more imine groups. These positively charged nitrogen groups will act as sites

for adsorption onto a metal surface. The polymer is therefore working as an adsorption inhibitor, with a large size and therefore efficient corrosion inhibition.

7.4.5 Solubility of Polyanilne

The application of inherently conducting polymers for commercial purposes has been somewhat restricted by the fact that they are unprocessable. This means they can not be formed into films by dissolution and subsequent casting from a solvent or melt casting. For use as conducting films and coatings, some method must be available to dissolve or melt the polymer. Polyaniline films can be electrochemically deposited, however this is not a practical method if large areas or delicate objects are to be coated.

Polyaniline is insoluble in most common organic solvents due to its ridged 'backbone' structure (Sathiyarayanan *et al*, 1992). Melt processing is also not possible as the polymer decomposes at temperatures below a softening or melting point (Heeger *et al*, 1992). Emeraldine base is soluble to some degree in aqueous acetic acid, aqueous formic acid, dimethyl sulphoxide (DMSO), dimethylformamide (DMF) and N-methylpyrrolidone (NMP). Solubility will depend on the molecular weight of the polymer, the heavier polymers being less soluble. The solvent will extract the lower molecular weight polymers, the amount extracted depending on the solvent, for example THF dissolves 20% of the polymer by weight, whereas DMSO dissolves 80% of the polymer (MacDairmid *et al*, 1987). The conducting form of polyaniline, emeraldine salt, is totally insoluble in organic solvents. Polyaniline films (emeraldine base), can be cast from solution. To produce films of emeraldine salt, these emeraldine base films can then be doped by immersion in a protonic acid solution, such as 1M hydrochloric acid (Angelopoulos *et al*, 1988) or p-toluenesulphonic acid (Yen Wei *et al*, 1985).

Several methods have been devised to obtain soluble conducting forms of polyaniline. One method has been to use substituted aniline to create a soluble substituted polyaniline. Both o-methoxy polyaniline and o-ethoxy polyaniline are soluble. This has been accounted for by the increase in the torsional angle between adjacent carbon rings due to the steric strain exerted by the bulky groups substituted at the ortho position of the carbon rings. This

change in angle between rings, renders the polymer chain more flexible and thus more soluble without altering the electronic structure of the polymer (Sathiyarayanan *et al*, 1994). Co-polymers of aniline and substituted anilines were also produced in the effort to produce a soluble inherently conducting polymer. Various co-polymers of aniline, o-toluidine, o-ethylaniline, o-anisidine and o-aminophenol were synthesised. These were found to be soluble in water but less conductive than polyaniline (Kathirgamanathan *et al*, 1991)

A processable dispersion of doped polyaniline has been produced by Wessling *et al* (1996). The exact procedure used has not been revealed in the literature as it is part of a commercial venture. A new polymerisation method coupled with a new dispersion technique is said to lead to a soluble conducting polymer.

7.4.6 Counter Ion Induced Solubility of PANI-CSA

Processable, soluble conducting polyaniline has recently been produced by using a functionalized protonic acid to dope polyaniline base. This is reported to give a salt that is soluble in common organic solvents such as xylene, chloroform, m-cresol, formic acid and DMSO (Cao *et al*, 1992). A functionalized protonic acid can be denoted as $H^+(M^-–R)$. The counter anionic species ($M^-–R$), contains a functional group, R, which is compatible with nonpolar or weakly polar organic solvents. Examples of R groups used are dodecylbenzene in dodecylbenzenesulphonic acid, (DBSA), in which the long alkyl chain leads to solubility in solvents such as toluene, xylene, decalin, and chloroform, and camphorsulphonic acid (CSA) which leads to solubility in chloroform, m-cresol, and formic acid (Cao *et al*, 1992). In both these cases the M^- group is a sulphonate ion SO_3^-. The formulae of these functionalized protonic acids and solvents used are given in figure 7.7. The functionalized protonic acids act as surfactants, enabling the dissolution of conducting polyaniline, and the mixing with a variety of other polymers. They enable polyaniline to be cast from solution in the conducting phase and thus allow the production of conducting polymer films and coatings.

Figure 7.7 Formulae and structure of functionalised protonic acids used to dope polyaniline and the solvents in which they are soluble

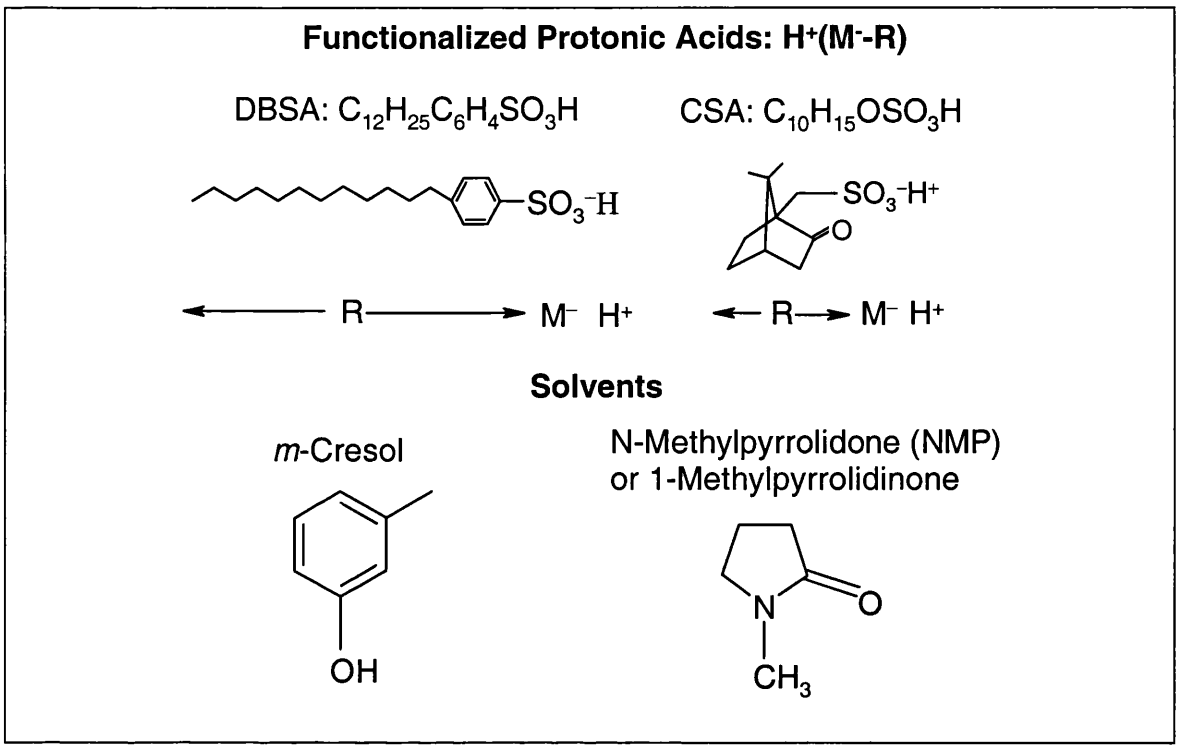

Polyaniline synthesised with camphor sulphonic acid (CSA) as the proton dopant falls into the category of counter ion induced soluble conducting polyaniline. The polymer is soluble in m-cresol, chloroform, formic acid and N-methylpyrrolidone (NMP). It is claimed that this form of doped polyaniline forms a pale green, almost colourless transparent film (Cao *et al*, 1992).

7.5 SYNTHESIS OF POLYANILINE

7.5.1 Chemical Synthesis of PANI-HCl - Emeraldine Salt

Following the method given by MacDiarmid *et al* (1987), polyaniline hyddrochloride was chemically synthesised for testing as a coating for archaeological iron. Polyaniline was synthesised from aniline and ammonium perxoydisulphate, $(NH_4)_2S_2O_8$. This gives a polymer of at least 160 repeat units (Cao *et al*, 1993). Aniline and ammonium peroxydisulphate were purchased from Aldrich chemicals. The aniline was purified by distillation under reduced pressure before use. Other chemicals were used as purchased.

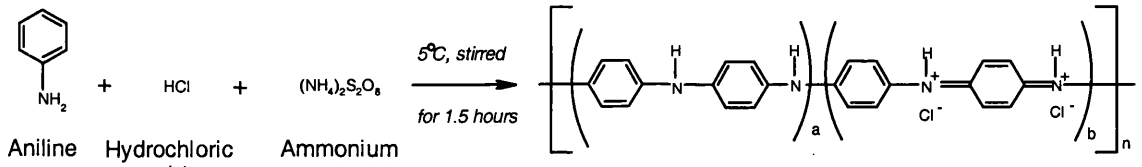

Aniline | Hydrochloric acid | Ammonium peroxydisulphate

Polyaniline hydrochloride (PANI-HCl)

11.5g of ammonium peroxysulphate was dissolved in 200ml of 1M HCl. This solution was cooled to 1°C. 20ml of Aniline was dissolved in 300ml of 1M HCl and this was also cooled to 1°C. Over a period of 1 minute the ammonium peroxysulphate was added to the aniline solution which was placed in an ice bath. The reaction was constantly stirred over a period of 1.5 hours and kept at a temperature below 5°C. After this period a blue-green precipitate was formed. The precipitate was collected by suction filtration and washed with 500ml of HCl in 60ml portions, until the initially pale violet filtrate became clear. Washing was performed carefully so that the liquid level remained above the top of the precipitate, thus preventing cracking of the precipitate cake which would result in inefficient washing. The precipitate was left to dry under suction for 10 minutes. This form of emeraldine salt is incompletely protonated, containing roughly 40% protonation (rather than the full 50% protonation that gives the highest conductivity phase of polyaniline) and so further reaction is needed.

The moist precipitate cake was therefore added to a 500ml solution of 1M HCl and stirred for 15 hours. The precipitate was then filtered and washed as previously described. The precipitate was again dried under suction for 10 minutes and then transferred to a vacuum desiccator and dried under dynamic vacuum for 4 hours. The semi dry precipitate was then

ground in a pestle and mortar and the dried for 48 hours under dynamic vacuum, at room temperature. The powder was then reground and stored over silica gel.

The powder was characterised by FTIR spectroscopy and the spectra recorded was found to be in agreement with literature spectra (Angelopoulos *et al*, 1988, Ping *et al*, 1996). The UV/Vis spectra of PANI-HCl was also obtained and found to be in agreement with the spectrum reported in the literature (Epstein *et al*, 1987, Monkman & Adams, 1991).

7.5.2 Chemical Synthesis of Polyaniline (PANI), Emeraldine Base

Polyaniline base was synthesised from polyaniline hydrochloride as described by MacDairmid *et al* (1987). Polyaniline hydorchloride was synthesised as described in section 7.5.1. The moist precipitate cake was obtained after 10 minutes of suction, and this was suspended in 500ml of 0.1M ammonium hydroxide solution, NH_4OH with constant stirring. After 10 minutes 1.0M NH_4OH was added dropwise until the solution had a ph of about 8. Stirring of the suspension was continued for about 15 hours. The precipitate was then filtered under suction, and washed with 500ml of 0.1M NH4OH in 60ml portions in the same manner described in section 7.5.1. The powder was then dried under suction for 10 minutes and then transferred to a desiccator and dried under dynamic vacuum for 4 hours. The powder was then ground and re-dried for 48 hours under vacuum. The powder was then stored over silica gel until used.

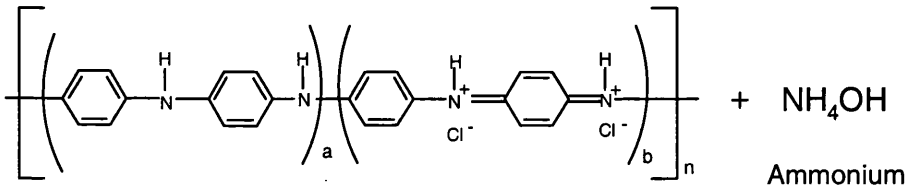

Polyaniline hydrochloride (PANI-HCl)

+ NH_4OH

Ammonium hydroxide

stirred

for 12 hours

NH_4Cl + H_2O +

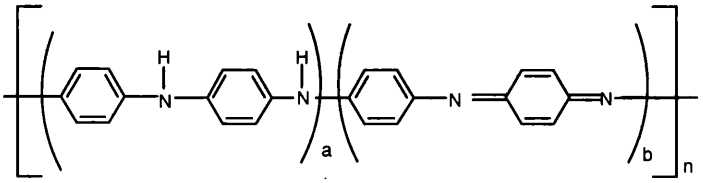

Ammonium chloride

Water

Polyaniline (PANI)

The powder was characterised by FTIR spectroscopy and the spectra recorded was found to be in agreement with published spectra (Angelopoulos *et al*, 1988, Ping *et al*, 1996).

The UV/Vis spectra of PANI was also obtained and found to be in agreement with the spectrum reported in the literature (Epstein *et al*, 1987, Monkman & Adams, 1991).

7.5.3 Synthesis of Polyaniline-Camphor Sulphonic Acid, PANI-CSA

An ion induced soluble form of polyaniline, PANI-CSA was synthesised based on the procedure given in the US Patent 5,232,631, for processable forms of electrically conductive polyaniline (Cao *et al*, 1993). All chemicals used in this synthesis were purchased from Aldrich chemicals. Aniline was purified by distillation under reduced pressure, however, all other chemicals were used in their as purchased states.

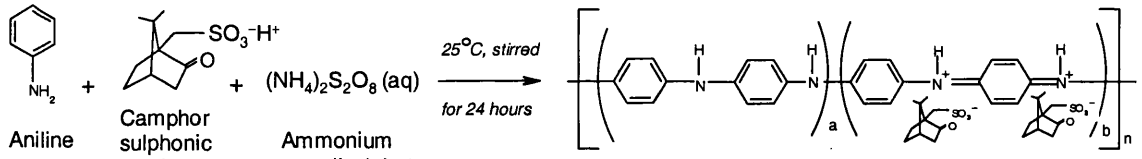

Aniline | Camphor sulphonic acid | Ammonium peroxydisulphate | Polyaniline CSA (PANI-CSA)

4.65g (0.05M) of freshly distilled aniline was added to 250ml of chloroform. 17.42g (0.075M) of Camphor Sulphonic acid was then added. The reaction was stirred and maintain at 25°C in a water bath. 4.68g of $(NH_4)_2S_2O_8$ in 20ml of distilled water was then added over a 30 minute period. The reaction was covered and left stirring at 25°C for 24 hours, after which period a green mixture is formed. This was then poured into 750ml of acetone which precipitates out the PANI-CSA complex. The complex was recovered by suction filtration, and washed with three 150ml portions of acetone, three 150ml portions of distilled water and three 150ml portions of acetone. The precipitated polymer was then left to dry under suction for 10 minutes and then placed in a desiccator under dynamic vacuum for 48 hours at room temperature. The green polymer was then ground into a powder and stored over silica gel until used. A yield of 3.38g of PANI-CSA was obtained. The polymer produced was characterised by FTIR and UV/Vis spectroscopy and compared to the spectra obtained for PANI and PANI-HCl.

7.5.4 Calculating Doping Ratio and Yield of PANI-CSA

To check that a doped form of polyaniline had been produced using the method described in section 7.5.3 and to calculate the amount of CSA dopant present, the amount of

emeraldine base recovered after reaction with ammonium hydroxide was compared to the amount of initial aniline monomer present in the polymer. Approximately 0.5g (0.52g) of PANI-CSA was weighed and added to 50ml of 0.1M NH_4OH solution. The reaction was stirred with a pre-weighed stirrer bean for 2 hours at room temperature. A preweighed sintered glass funnel was used to collect the PANI by suction filtration of the resulting solution. The precipitate was washed with distilled water until the filtrate had a pH of between 7 and 8. The PANI was then washed with methanol until a colourless filtrate was obtained. The PANI was dried under vacuum for 48 hours. The precipitate, funnel and stirrer bean were then re-weighed and the mass of PANI recovered, calculated to be 0.19g. The mass of CSA in the original polymer was then calculated to be 0.34g. The ratio of aniline units within PANI to CSA was then calculated to be 0.71, which approximates to 2 CSA molecules to every 3 aniline molecules, approximately two thirds doping.

The percentage yield of PANI-CSA synthesised was calculated. The amount of aniline present in the mass of PANI-CSA produced was calculated using the doping ratio 0.71. From 3.38g of PANI-CSA, 1.21g is PANI. An initial mass of 4.56g of Aniline was used in the synthesis and therefore a percentage yield of 26.54% was calculated.

7.5.5 PANI-CSA in *m*-Cresol

A 0.25% solution of PANI-CSA in *m*-cresol was supplied for evaluation as a corrosion inhibitor from the laboratory of Prof. P. Kathirgamanathan of South Bank University, London. This solution was dark blue/green in colour.

7.6 CHARACTERISATION OF SYNTHESISED POLYMERS

7.6.1 FTIR Spectroscopy

7.6.1.1 Experimental Method

Fourier transform infrared spectroscopy was used to characterise synthesised products. The technique has been outlined in Chapter Six. As with previous experiments, a Perkin Elmer 2000 model FTIR spectrometer was used in transmission mode. Spectra taken were compared with spectra of similar materials in the literature.

Very small amounts of samples for analysis (enough to just cover the end of a small spatula) were ground with about ten times the quantity of spectroscopic grade KBr. The KBr was dried before use by leaving in an oven at 200°C overnight. The powders were ground together in an agate pestle and mortar until and even consistency was produced. The powder was then carefully poured into a 13mm pellet press and a pressure of 10 tons applied for several minutes. The pressure was then released and the pellet that had formed was removed from the press. This pellet was then placed in a sample holder and this in the spectrometer for analysis. The spectrometer was flushed with nitrogen before analyses were carried out and a background scan was recorded. This background was then automatically subtracted from the final spectra

7.6.1.2 FTIR Results

The FTIR spectra obtained for PANI, PANI-HCl and PANI-CSA are shown in figures 7.8 The spectra are comparable to those given for doped and undoped emeraldine in the literature (Ping, 1996). Characteristic peaks in all the spectra can be used to differentiate between the doped and undoped polymer structures.

Many peaks in the spectra of the polymer salts, PANI-HCl and PANI-CSA are red shifted (shifted to a lower wavenumber) in comparison to the equivalent peaks in PANI. This can be seen in the peaks assigned to the C-H in and out of plane stretches of the aromatic rings, which are found between 700-1000cm^{-1} (Ping *et al*, 1996). The strongest peak in this region is found at 828cm^{-1} in the spectrum of PANI, but 819cm^{-1} and 815cm^{-1} in the spectra of PANI-CSA and PANI-HCl. The band at 1303cm^{-1} in the PANI spectrum has

Figure 7.8 FTIR spectra of PANI, PANI-HCl and PANI-CSA

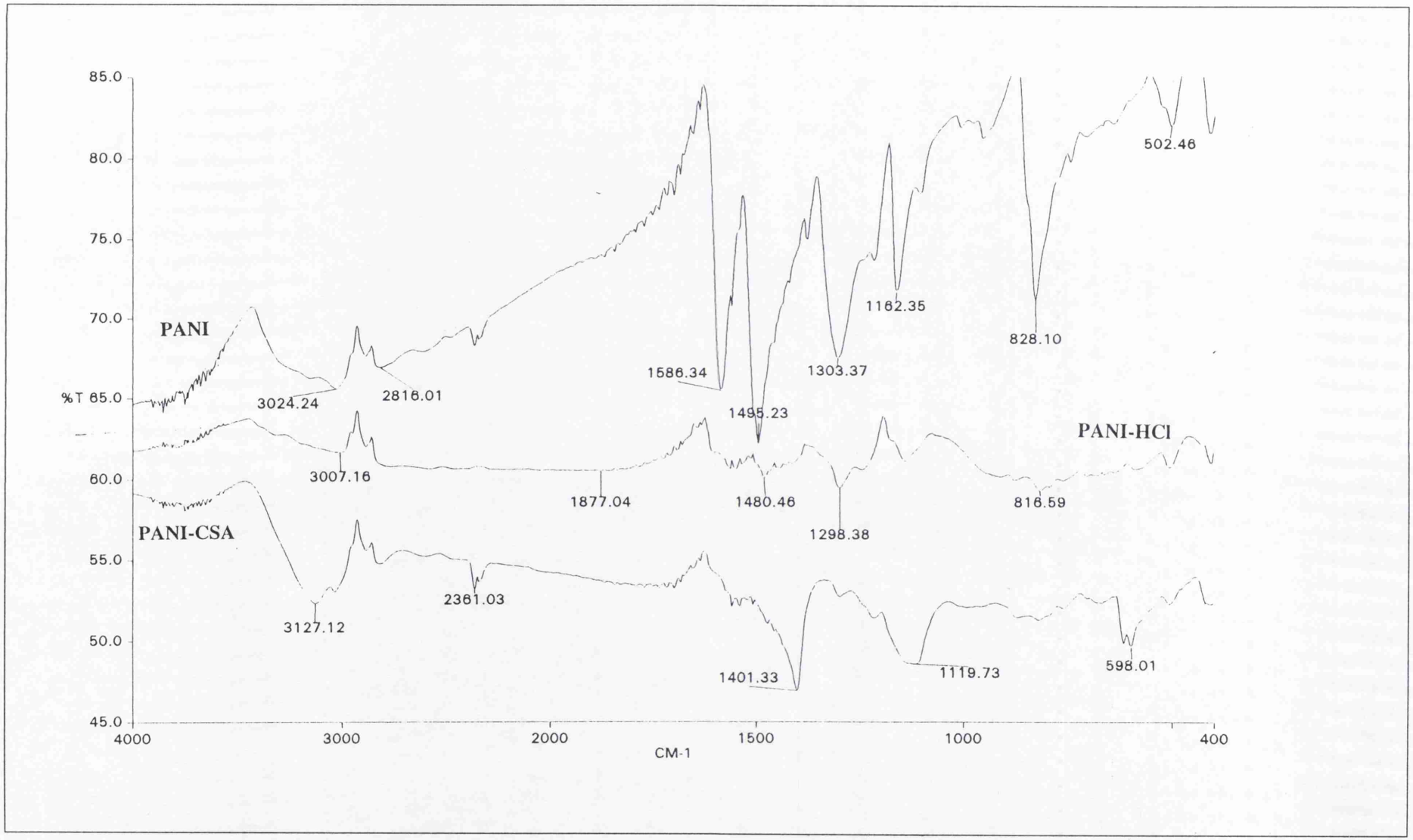

moved to 1297cm^{-1} in PANI-CSA and 1299cm^{-1} in PANI-HCl. This band has been assigned as the C-N stretch (Sariciftci *et al*, 1989). This red shift has been attributed to the different configuration of the polymer chain in the undoped semi-conducting and doped conducting forms. The protonation that occurs on doping induces π electron delocalisation and the formation of the polaron lattice, which leads to the different polymer conformation (Ping, 1996).

A difference between the doped and undoped polymers can also be seen in the peak that occurs at 1586cm^{-1} in the spectrum of PANI. This peak is related to the quinoid groups present in semi-quinoid PANI (Wang *et al*, 1991). This peak is not present in the spectra of PANI-HCl and PANI-CSA due to the benzenoid nature of the polaron lattice.

7.6.2 UV/Vis Spectroscopy

7.6.2.1 Experimental Method

A UV/Vis spectrophotometer measures absorbance in the ultra violet and visible regions (200-750nm). Absorbance in these regions is due to electronic transitions in the energy levels of a molecule. A monochromatic beam is split into two, with one beam passing through the sample and the other passing through a reference solvent.

UV/Vis Spectroscopy was carried out on a Perkin-Elmer Lambda 5 UV/Vis spectrophotometer. A slit width of 2nm was used with a scan speed of 120nm/min. Samples of PANI and PANI-CSA were prepared by dissolving 0.02g of the powders in 50ml of NMP. The insoluble PANI-HCl was analysed as a colloidal suspension in NMP which was formed by subjecting a mixture of PANI-HCl in NMP to sonication. Solutions were placed in quartz cells of depth 1cm. A quartz cell filled with only the NMP solvent was used as the reference/background sample.

7.6.2.2 UV/Vis Results

The UV/Vis spectra of PANI, PANI-HCl and PANI-CSA are shown in figure 7.9. These were compared to published spectra (Zipperling Kessler, 1996, Epstein *et al*, 1987, Monkman & Adams, 1991, Wang *et al*, 1991). The spectra of PANI has two sharp peaks

Figure 7.9 UV/Vis spectra of PANI, PANI-HCl and PANI-CSA

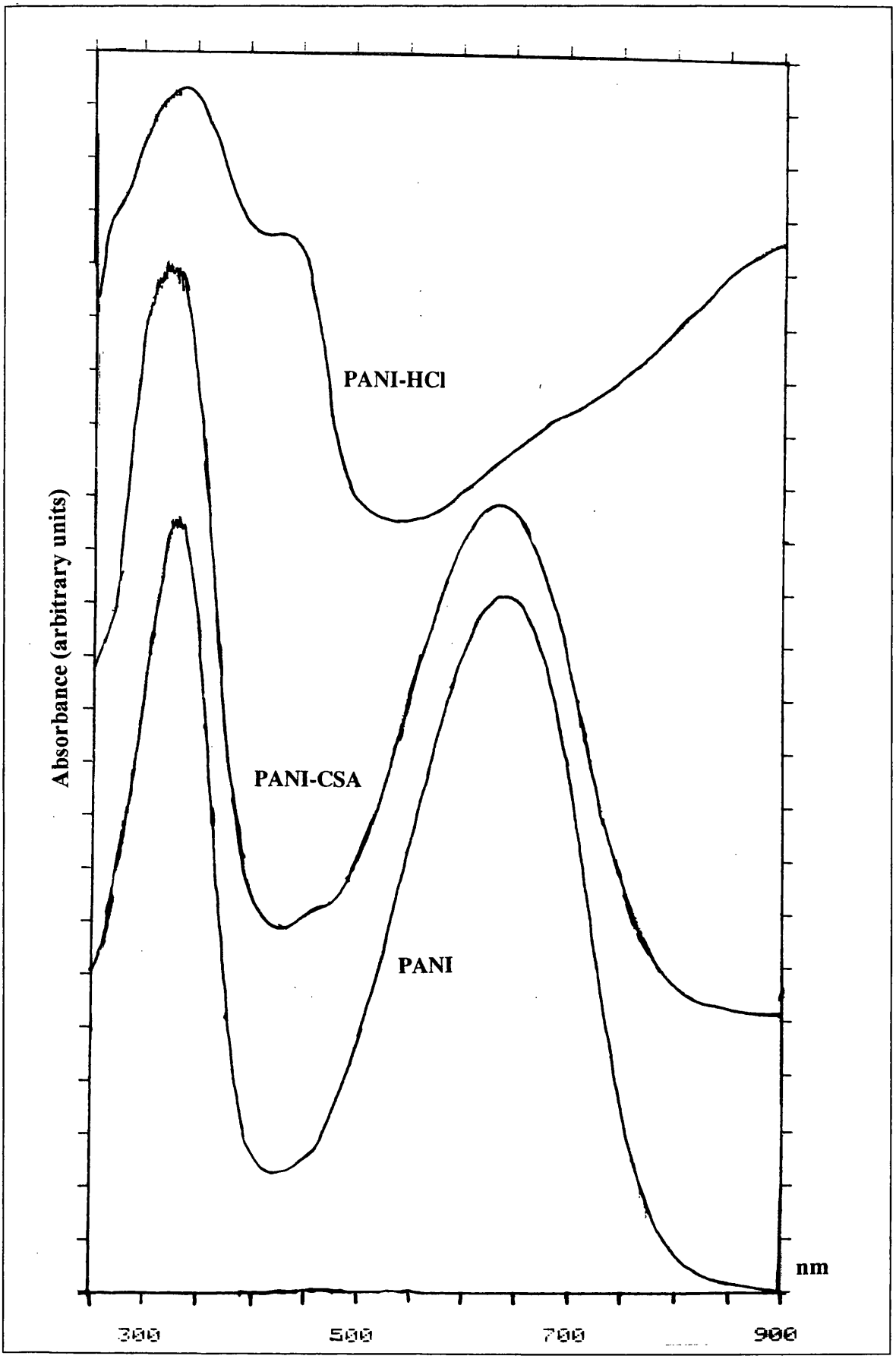

at 320nm and 610nm. These have been assigned to the $\pi \rightarrow \pi^*$ electronic transitions of the benzenoid and quinoid rings respectively (Wang *et al*, 1991). Absorption then falls off below 850nm. The spectra for the PANI-HCl suspension shows a broad adsorption band centred at 360nm. This has been assigned as absorption due to the $\pi \rightarrow \pi^*$ electronic transitions of the benzenoid species. No quinoid absorption is seen, indicating a change to the totally delocalised polaron structure (Monkman & Adams, 1991). The metal-like structure of PANI-HCl can also be seen in the increased absorption that occurs in the near infra red, starting at 500nm.

The spectra of PANI-CSA in NMP solution is similar to that of PANI, indicating that in solution PANI-CSA becomes deprotonated and non-conducting. This will be discussed further in section 7.6.3.

7.6.3 Solubility of Synthesised PANI-CSA

The actual solubility of the synthesised PANI-CSA was tested, alongside the solubility of the synthesised PANI and PANI-HCl. This was done by simply trying to dissolve a very small quantity of the solid in a sample tube filled with solvent. Solubility was easily visible as polyanilines form deeply coloured blue or green solutions when dissolved. The results are shown in table 7.1 Solubility of PANI-CSA was further tested. The effect of sonication on solubility was investigated by placing the same tube in a sonic bath for 10 minutes. The solutions were then filtered to remove any undissolved particulate material. The results are shown in table 7.2.

The PANI-CSA synthesised was only soluble in NMP, and slightly soluble in m-cresol and formic acid. The solution formed in NMP was blue, similar in appearance to PANI solutions and films, rather than the green colouration found in doped polyaniline films. This indicates than on solvation in the basic solvent NMP, deprotonation occurs, and thus the polymer is rendered soluble. Further evidence for this can be seen in the UV/Vis spectrum shown in figure 7.9. The spectrum is identical to that reported for PANI in the literature (Epstein *et al*, 1987, Monkman & Adams, 1991).and recorded in this work. This deprotonation has been reported previously, but it is stated that when the polymer is

subsequently brought out of solution, reprotonation occurs to form films or coatings of the conducting polyaniline salt(Cao *et al*, 1992).

Further studies in the solubility of PANI-CSA in NMP gave at first puzzling results. As further solid was added to the solvent a colour change developed from blue, to paler blue to very pale green to dark green. This anomaly seems to stem from a second colloidal phase of dispersed PANI-CSA which has a deep green colour. As this phase develops the overall appearance of the polymer is paler than the less concentrated solution due to the combined effect of the blue soluble PANI-CSA phase and the green colloidal phase.

Table 7.1 Solubility of PANI, PANI-HCl and PANI-CSA

SOLVENT	NMP	CHLOROFORM	TOLUENE	M-CRESOL	FORMIC ACID	1M HCL	TRIPROPYLAMINE
PANI	very soluble, deep blue solution	slightly soluble, pale green/blue solution	no	no	no	no	no
PANI-HCl	no	no	no	no	no	no	no
PANI-CSA	very soluble, deep blue solution	slightly soluble	no	no	slightly soluble, pale blue solution	no	no

Table 7.2 Solubility of PANI-CSA with sonication

SOLVENT	M-CRESOL	CHLOROFORM	FORMIC ACID	TOLUENE	TRIPROPYLENE	NMP
Before Sonication	not soluble	not soluble	no soluble	no soluble	not soluble	blue solution
After Sonication	dark green	dark green	dark green	dark green	very pale blue	blue solution
After Filtration	pale green/blue	colourless	pale green/blue	colourless	colourless	blue solution
Soluble?	slightly	no	slightly	no	no	yes

7.7 ELECTROCHEMICAL TESTING OF POLYANILINE COATINGS

7.7.1 Introduction

An electrochemical assessment of the corrosion inhibition produced by PANI and PANI-CSA coatings, formed on iron, was made using linear voltammetry . Using this method the corrosion potential and polarisation resistance of coated and uncoated iron could be calculated and therefore the inhibitive properties of the PANI and PANI-CSA films investigated.

7.7.2 Linear Voltammetry

The corrosion rate of a metal can be calculated using polarisation curves acquired during linear voltammetry. Figure 7.10 illustrates the electric circuit used for recording potentiodynamic polarisation curves using a potentiostat. A three electrode cell is used for electrochemical measurements of dynamic systems, that is, systems in which current flows. The cell current is measured between the working electrode (the metal sample) and counter electrode (platinum). The introduction of a reference electrode allows for the accurate measurement of the potential between the working electrode and the reference electrode. Potentiostats apply a predetermined potential to the working electrode so that measurement of the cell current can be made. The voltage is varied linearly with time and the resultant current is recorded. The external circuit necessary to collect this data requires a current measuring device, a potential measuring device, a source of potential (potentiostat) and an X-Y chart recorder. Computer driven instruments are now commonly used to produce potentiodynamic polarisation curves.

The polarisation curves recorded, when plotted as potential against log current, can be interpreted in terms of mixed potential theory. These plots are known as Tafel plots. At a positive applied potential a current is produced by the anodic half cell reaction (metal oxidation) and therefore this curve is known as the anodic polarisation curve. At negative applied potentials the current is produced by the cathodic half cell reaction and this is therefore known as the cathodic polarisation curve. These curves are non-linear at low currents. At higher currents they become linear on a semi-lorarithimic plot and this is

known as the Tafel region. The cathodic and anodic polarisation curves meet at the corrosion potential, E_{corr}, and this value can be simply read from a Tafel plot.

Figure 7.10 Basic circuit for a potentiostat and electrochemical cell, A.E; auxillary electrode, R.E; reference electrode, W.E; working electrode (Sheir et al, 1994)

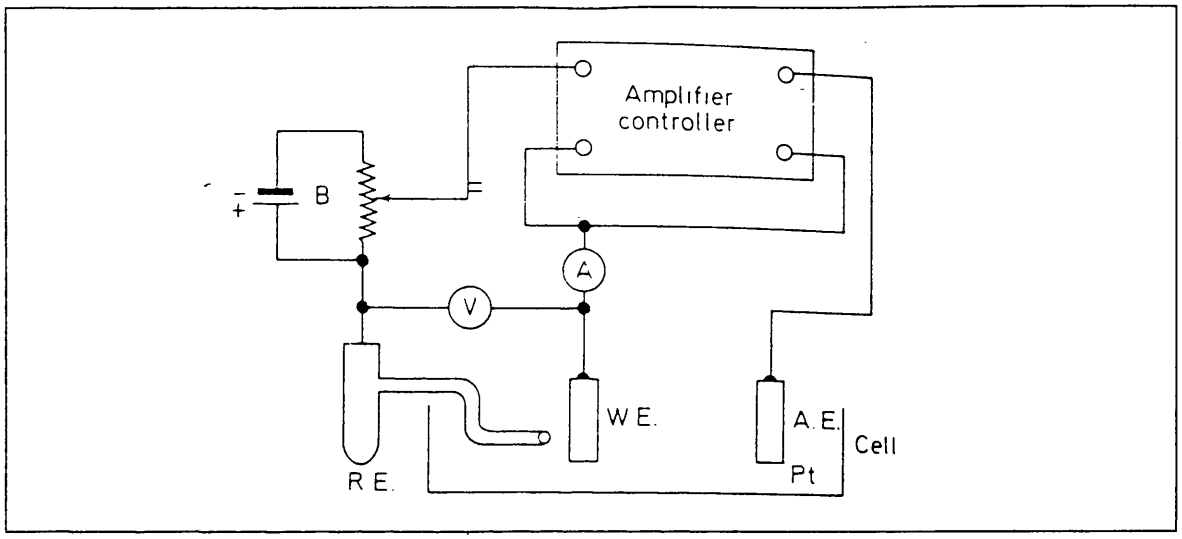

Corrosion rates can also be assessed by the value of polarisation resistance, R_p, using the same data recorded in linear voltammetry experiments. The applied current gives a linear plot with respect to the overpotential within 10mV more active or more noble than the corrosion potential (Fontana, 1987, 504). The slope of this linear polarisation curve is related to the kinetic parameters of the system by the equation:

$$\frac{\Delta E}{\Delta i_{app}} = \frac{\beta_a \beta_c}{2.3(i_{corr})(\beta_a + \beta_c)}$$

where β_a and β_c are the Tafel slopes of the anodic and cathodic reactions respectively. The slope of the linear polarisation plot is therefore the term $\Delta E/\Delta i_{app}$ and can be given in ohms. It can therefore be thought of as a resistance, the polarisation resistance, Rp. The slope of a linear polarisation curve is controlled mainly by i_{corr}, being insensitive to changes in the β values in this potential range. Therefore the above equation can be approximated (assuming the β values are on average 0.12V each) to:

$$\frac{\Delta E}{\Delta i_{app}} = \frac{0.026}{i_{corr}}$$

The polarisation resistance is therefore inversely proportional to the corrosion current, and can be used as a measure of corrosion rate.

7.7.3 Linear Voltammetry Measurements

Electrochemical experiments were carried out on iron samples coated with polyaniline in the laboratory of Prof. D. Williams, UCL Chemistry Department. The iron used was 5mm diameter Johnson-Matthey rods (Specpure grade, total metal impurities: 15ppm or less). Sections roughly 3mm long were cut and attatched to copper buttons with silver paint. These were then mounted in epoxy resin, in teflon cups. The teflon cup could be screwed into a copper electrode. The iron was polished with successively finer emery paper and finally with an Alumina powder suspension. Samples were then coated with PANI and PANI-CSA solutions (1g of polymer in 250ml of NMP) by pipetting one drop of the polymer solution on the iron electrode surface and leaving this to dry under dynamic vacuum for 48 hours. All samples were stored over silica gel before use.

Figure 7.11 Cell used in electrochemistry experiment.

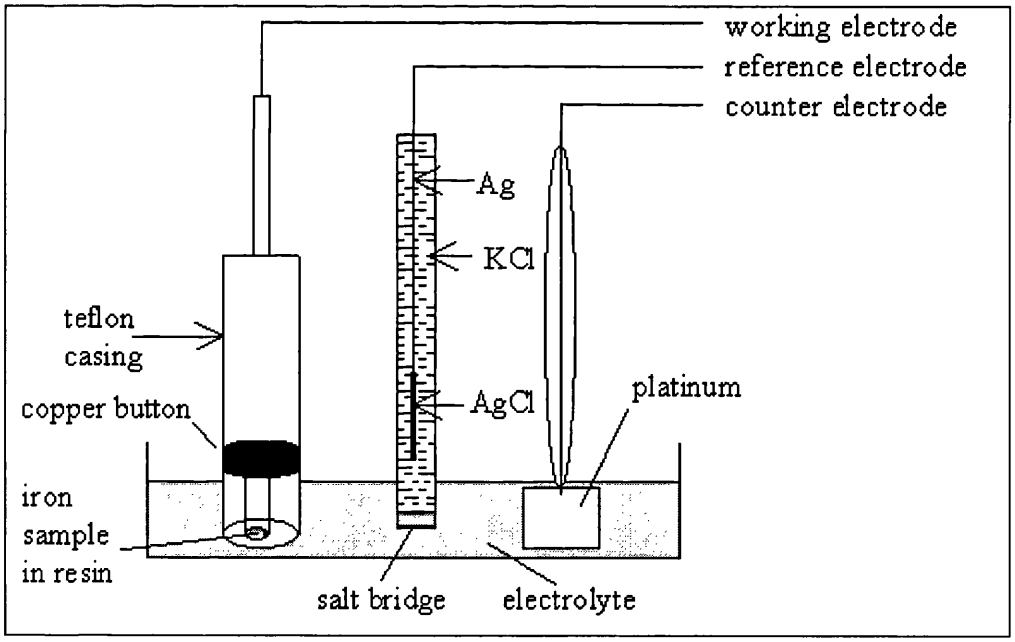

A cell containing the three electrode arrangement was used in linear voltammetry experiments. The iron sample was the working electrode with a Platinum counter electrode and a silver-silver chloride (Ag/AgCl/KCl) reference electrode. A 0.05M potassium hydrogen phthalate (C_6H_4COOK) and 0.1M potassium chloride solution was used as electrolyte. A diagram showing this arrangement is given in figure 7.11. Experiments were controlled by a computerised system - Eco Chemie Autolab. The current was recorded from -1.5V to 1.0V in 0.00244V steps at a rate of 0.002V/s.

7.7.4 Linear Voltammetry Results

The resulting potential against log current graphs (Tafel Plots) are shown in figure 7.12. Using the Autolab general purpose electrochemical system software (GPES, version 3.2), the corrosion potentials and polarisation resistances of iron and iron coated with PANI and PANI-CSA were calculated. These values are given in table 7.3.

Table 7.3 ***Corrosion potentials and polarisation resistance of electrodes***

Electrode	IRON	IRON/PANI	IRON/PANI-CSA
E_{corr}/V	-0.79	-0.61	-0.60
R_p/Ω	0.94×10^5	0.95×10^5	1.62×10^5

These values show that both electrodes treated with PANI and PANI-CSA have an inhibiting effect on the corrosion rate of iron. The corrosion potentials of both coated electrodes are more noble. The polarisation resistances of the coated electrodes are higher, indicating a lower corrosion current and therefore less corrosion. These results are a confirmation of the literature on the corrosion inhibiting properties of PANI, doped and undoped (Wessling, 1994, Wei *et al*, 1995, Lu *et al*, 1995, Wessling & Posdorfer, 1999). The doped PANI-CSA polymer coating was found to be slightly more inhibiting than the basic undoped form, which can be seen in the higher values of the corrosion potential, and almost double value for the polarisation resistance. This would confirm that the conducting form of the polymer has the best inhibiting properties (although some researchers have found the basic form of PANI to be a better inhibitor (Wei *et al*, 1995)).

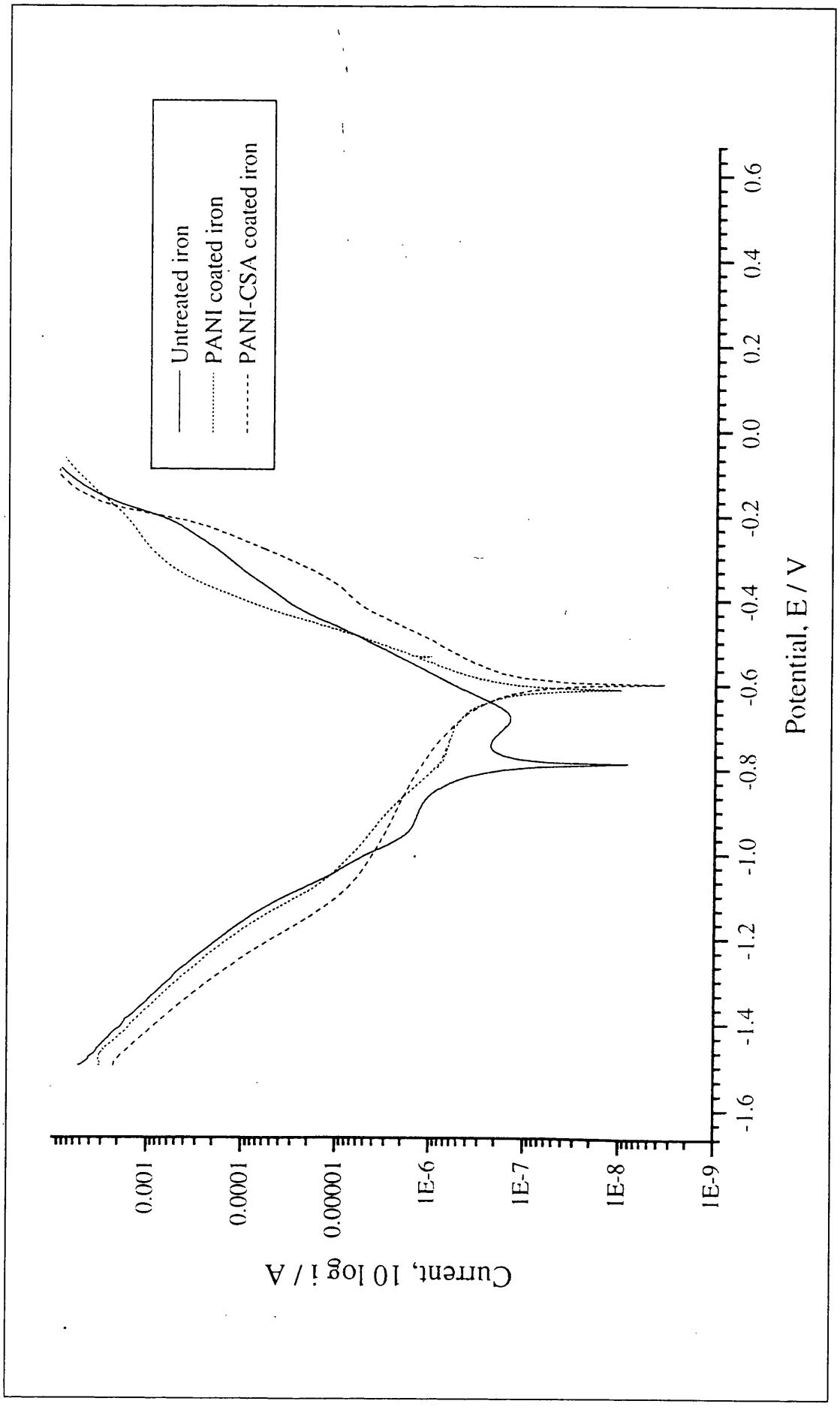

Figure 7.12 Log current vs potential for iron electrodes treated with PANI, PANI-CSA and untreated

7.8 ACCELERATED CORROSION TESTING

7.8.1 Introduction

Several forms of polyaniline were tested for there ability to inhibit the corrosion of archaeological iron. Accelerated corrosion tests were performed on pre-corroded coupons, and archaeological iron nails in the same way as described in chapter four. The performance of polyaniline coatings were compared to the TTS and ODA treatments as well as untreated samples. Testing of polyaniline coatings was carried out along with the corrosion test, experiment 2, described in chapter Four. In a second experiment archaeological nails treated with polyaniline were tested. Polyaniline coatings were formed by dipping samples into polyaniline solutions. Tests were carried out on corroded samples coated once and coated ten times. As in previous tests, the results of the accelerated corrosion tests were assessed by percentage mass increase measurements.

7.8.2 Treatment of Material for Corrosion Testing

7.8.2.1 Samples Used in Accelerated Corrosion Tests

An Accelerated Corrosion test was carried out on batches of 2cm by 5cm iron coupons, synthetically corroded by the method described as method A in chapter three (section 3.3.1). No further selection criteria were used in choosing coupons for the test. An accelerated corrosion test was also carried out on a batch of unprovenanced medieval nails provided by the Museum of London. Batches containing 10 nails each were selected in the same way as described in section 4.2.1.1

7.8.2.2 Pre-treatment of Samples

Coupons and nails were pre-treated in the same manner as described in section 4.2.2. The nails were cleaned with an air abrasive unit and both nails and coupons were degreased in acetone before treatment.

7.8.2.3 Treatment of Samples

7.8.2.3.1 Heating to 150°C Under Vacuum

This was carried out as described in section 4.2.3.1.

7.8.2.3.2 Treatment with 0.05M TTS Solution

This was carried out as described in section 4.2.3.4.1

7.8.2.3.3. Treatment with 0.01M ODA

This was carried out as described in section 4.2.3.5

7.8.2.3.4 Treatment with PANI in NMP

A solution of polyaniline was made up from 1g of PANI added to 250ml of NMP. This was sonicated for an hour to facilitate solution of the PANI. A dark blue solution was produced. Samples were heated to 150°C for 30 minutes. Samples were then dipped in the solution and the coatings left to dry. Samples were re-heated for 15 minutes to help drive off the solvent and dry the coating. Samples were prepared coated once, and coated 10 times. Samples were left to dry for 48 hours in a vacuum dessicator

7.8.2.3.5 Treatment with PANI-CSA in NMP

A solution of PANI-CSA was made up from 1g of PANI-CSA added to 250ml of NMP. This was sonicated for an hour to facilitate solution of the PANI-CSA. A blue solution was produced. Samples were heated to 150°C for 30 minutes. Samples were then dipped in the solution and the coatings left to dry. Samples were reheated for 15 minutes to help drive off the solvent and dry the coating. Samples were prepared coated once, and coated 10 times. Samples were left to dry for 48 hours in a vacuum dessicator

7.8.2.3.6 Treatment with PANI-CSA in NMP with vacuum drying

A solution of PANI-CSA was made up from 1g of PANI-CSA added to 250ml of NMP. This was sonicated for an hour to facilitate solution of the PANI. A blue solution was produced. Samples at room temperature were dipped into this solution and then dried under dynamic vacuum for 48 hours.

7.8.2.3.7 Treatment with PANI-CSA in NMP, applied under Vacuum

A solution of PANI-CSA was made up from 1g of PANI-CSA added to 250ml of NMP. This was sonicated for an hour to facilitate solution of the PANI. A blue solution was produced. Samples at room temperature were immersed into this solution and left under

vacuum for 12 hours. Samples were then removed from the solution, and left to dry for 48 hours in a vacuum dessicator, under dynamic vacuum.

7.8.2.3.8 Treatment with PANI-CSA in m-Cresol

Samples were heated to 150°C for 30 minutes. Samples were then dipped in the 0.25% solution of PANI-CSA in m-cresol and the coatings left to dry. Samples were reheated for 15 minutes to help drive off the solvent and dry the coating. Samples were prepared coated once, and coated 10 times. Samples were left to dry for 48 hours in a vacuum dessicator.

7.8.2.3.9 Storage of Samples

All samples were stored over silica gel in sealed container after treatment and before use in accelerated corrosion tests.

7.9 ACCELERATION CORROSION TEST RESULTS

7.9.1 Experiment 8: Comparing ODA, TTS and Polyaniline treatments

Experiment 8 was carried out using coupons produced by method A. Each batch contained 5 corroded iron coupons 2cm by 5cm in size. The treatments used are given in table 7.4. The Polymer treatments were applied as described in sections 7.8.2.3.4, 7.8.2.3.5 and 7.8.2.3.8. Coating were applied once (x1) or ten times (x10).

An accelerated corrosion test was carried out as described in chapter four. Results are shown in table 7.5 and figure 7.13. These results show that both the TTS and ODA treatments are far better at inhibiting corrosion than any of the polyaniline coatings. After the 41 days of the accelerated corrosion test the untreated control batch has increased in mass by 8.36%, whereas the TTS and ODA batches have increased in mass by only 3.84% and 3.89% respectively (as has been discussed in chapter four). This compares to mass increases of between 8.76% and 6.20% for the polyaniline coatings. It has also been confirmed that the heating of samples to 150°C has no effect on the rate of corrosion, as the heated but untreated batch, corroded at an almost identical rate to the untreated batch.

Although the polyaniline treatments do not prevent corrosion to the extent of the TTS or ODA treatments, most of the coating do perform better than the untreated batch in the corrosion test. The exception is the batch treated with PANI-CSA solvated in m-cresol, which after 14 days shows an mass increase greater than the untreated batch. The acidity of the m-cresol solvent applied to this batch, may account for this increase in the rate of corrosion.

Little difference can be seen in the performance of the undoped PANI and doped PANI-CSA polymers, however, it can be noted that batches coated with ten layers of each type of polyaniline perform better than the equivalent coating, treated with just one layer. This may indicate that the corrosion protection being afforded by these coatings is due to a barrier effect, rather than any electrochemical reaction. The thicker barrier, therefore reduces the occurrence of any gaps or flaws in the coating, and increases the corrosion inhibition.

Table 7.4 Treatments used in experiment 8

BATCH NUMBER	TREATMENT
Batch 1	No Treatment
Batch 2	Heated (section 7.8.2.3.1)
Batch 3	0.05M TTS (section 7.8.2.3.2)
Batch 4	0.01M ODA (section 7.8.2.3.3)
Batch 5	PANI x 1 (section 7.8.2.3.4)
Batch 6	PANI x 10 (section 7.8.2.3.4)
Batch 7	PANI-CSA (NMP) x 1 (section 7.8.2.3.5)
Batch 8	PANI-CSA (NMP) x 10 (section 7.8.2.3.5)
Batch 9	PANI-CSA (m-cresol) x 1 (section 7.8.2.3.8)
Batch 10	PANI-CSA (m-cresol) x 10 (section 7.8.2.3.8)

Table 7.5 Mean % mass increase results for experiment 8 (n=5)

NO. OF DAYS		0	3	8	14	21	28	35	41
BATCH 1	*None*	0%	1.89%	5.17%	6.59%	7.28%	7.68%	7.98%	8.36%
BATCH 2	*Heated*	0%	2.16%	5.33%	6.40%	6.88%	7.52%	7.89%	8.26%
BATCH 3	*TTS*	0%	1.43%	2.34%	2.76%	3.10%	3.34%	3.61%	3.84%
BATCH 4	*ODA*	0%	1.45%	2.50%	2.86%	3.19%	3.37%	3.63%	3.89%
BATCH 5	*PANI x 1*	0%	1.91%	4.09%	4.96%	5.57%	5.84%	6.36%	6.67%
BATCH 6	*PANI x 10*	0%	1.81%	3.98%	4.72%	5.30%	5.49%	5.90%	6.20%
BATCH 7	*PANI-CSA (NMP) x 1*	0%	1.44%	4.33%	5.61%	6.51%	6.85%	7.27%	7.62%
BATCH 8	*PANI-CSA (NMP) x 10*	0%	2.02%	4.09%	4.83%	5.44%	5.64%	6.06%	6.33%
BATCH 9	*PANI-CSA (m-cresol) x 1*	0%	2.88%	5.27%	6.60%	7.49%	7.85%	8.24%	8.76%
BATCH 10	*PANI-CSA (m-cresol) x 10*	0%	1.81%	4.15%	5.30%	6.06%	6.34%	6.76%	7.26%

Figure 7.13 Experiment 8: Comparing ODA, TTS with polyaniline treatments

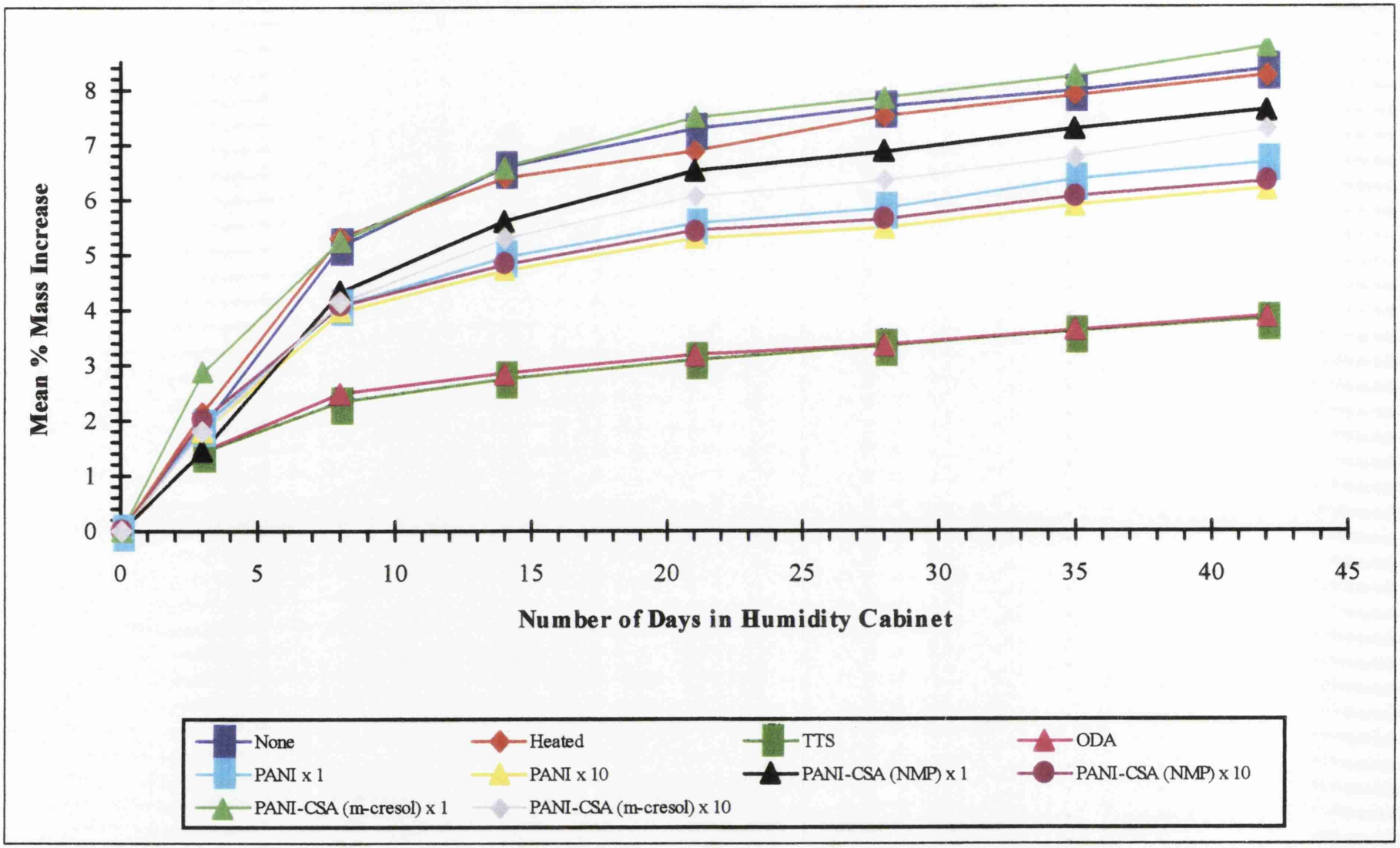

7.9.2 Experiment 9: Comparing TTS and PANI-CSA Treatments on Archaeological Iron

Experiment 9 was carried out using batches of nails from those given by the Museum of London. Each batch contained 10 nails, pre-treated as described above. The treatments used are given in table 7.6. The Polymer treatments were applied as described in sections 7.7.2.3.6 and 7.7.2.3.7 Coating were applied once.

An accelerated corrosion test was carried out as previously described in chapter four. The results are shown in table 7.7 and figure 7.14. This accelerated corrosion test using batches of archaeological iron nails, confirms the results obtained in experiment 8. After the 28 days of the test, the batch treated with TTS increased in mass by only 0.49%, as compared to 2.83% for the untreated batch. The batches treated with PANI-CSA show very similar corrosion rates to the untreated batch, indicating that these coatings do not provide inhibition to corrosion. Batch 3 was treated with the PANI-CSA in NMP solution under vacuum, to try and improve the penetration of the polymer coating within the corrosion layer. This batch has a slightly improved corrosion rate, increasing in mass by 2.73% after 28 days, however this improvement is very slight and unlikely to be statistically significant.

Polyaniline has been shown, in this work, and in the literature (Wessling *et al*, 1999), to inhibit corrosion when applied as a coating on clean iron. However experiments 8 and 9 have shown that this is not the case for corroded iron samples. Doped and undoped polyaniline have provided little or no protection when applied as a coating on corroded iron.

Table 7.6 Treatments used in experiment 9

BATCH NUMBER	TREATMENT
Batch 1	No Treatment
Batch 2	0.05M TTS (section 7.8.2.3.2)
Batch 3	PANI-CSA (vac) x1 (section 7.8.2.3.7)
Batch 4	PANI-CSA x1 (section 7.8.2.3.6)

Table 7.7 Mean % mass increase results for experiment 9 (n=10)

NUMBER OF DAYS		0	2	7	14	21	28
BATCH 1	*No Treatment*	0%	0.60%	1.23%	1.89%	2.44%	2.83%
BATCH 2	*TTS*	0%	0.12%	0.17%	0.26%	0.38%	0.49%
BATCH 3	*PANI-CSA (vac) x 1*	0%	0.47%	1.27%	1.89%	2.37%	2.73%
BATCH 4	*PANI-CSA x 1*	0%	0.49%	1.26%	1.95%	2.46%	2.84%

Figure 7.14 Experiment 9: Comparing TTS and PANI-CSA treatments on archaeological iron

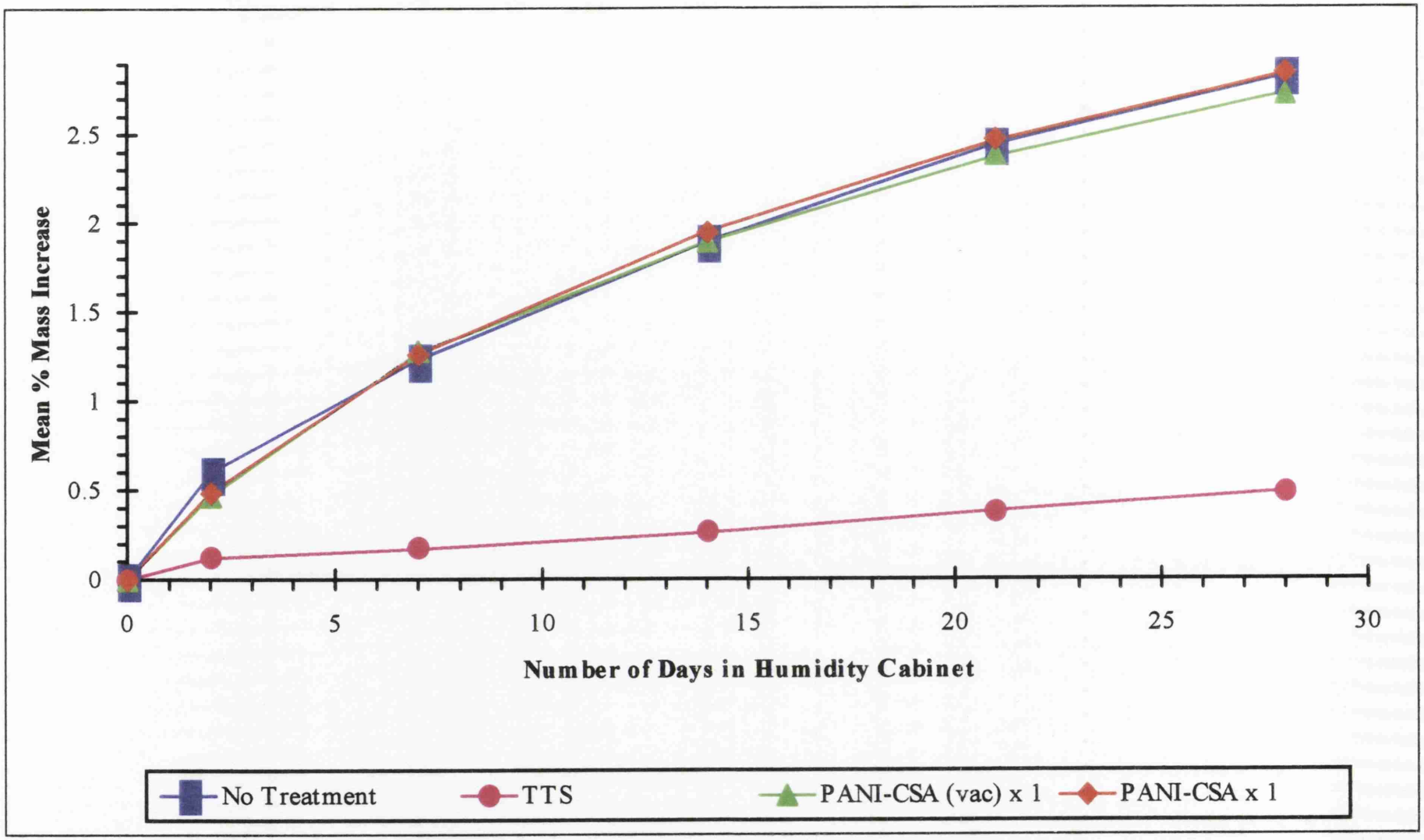

CHAPTER EIGHT

Discussion and Conclusions

8.1 Mechanisms of Interactions between Inhibitors and Corrosion Products

8.1.1 Mechanism of Interaction Between ODTMS and Corrosion Products

The information provided by the FTIR spectra, given in chapter six, indicates reactions have occurred between the iron oxyhydroxide surfaces and the ODTMS molecule. The absence of $Si(OCH)_3$ and the presence of Fe-O-Si and Si-O-Si vibrations in ODTMS treated samples, indicates that two types of reactions have occurred. A condensation reaction has occurred between ODTMS and hydroxyl groups on the surface of FeOOH, and the polymerisation of ODTMS molecules has also occurred. The mechanism and order of these reactions can be suggested, bearing in mind the method and conditions used in the application of the inhibitor.

For a reaction to occur the ODTMS molecule must undergo hydrolysis, replacing the methoxy groups with silanol groups. A mechanism has been suggested whereby silane coupling agents in anhydrous conditions may chemisorb onto mineral surfaces via hydrogen bonds (Piers & Rochester, 1995). For condensation reactions to occur between ODTMS molecules or between ODTMS and a substrate, hydrolysis must first occur (Plueddemann, 1982). Hydrolysis occurs stepwise, each methoxy group being replaced with an OH group to form first alkoxysilanols and then silane triols (Chovelon *et al*, 1995).

$$R\text{-}Si(OCH_3)_3 \leftrightarrow R\text{-}Si(OCH_3)_2OH \leftrightarrow R\text{-}Si(OCH_3)(OH)_2 \leftrightarrow R\text{-}Si(OH)_3$$

ODTMS was applied from a toluene solution. Although not an aqueous phase, the iron oxyhydroxide surface carries enough moisture to hydrolyse methoysilanes applied from anhydrous solvents (Plueddemann, 1982). Hydrolysis therefore occurs, producing at least $R\text{-}Si(OCH_3)_2(OH)$ molecules. In the presence of hydrolysable surface hydroxy groups, these molecules react via a condensation reaction to form covalent bonds between the silane and the iron oxyhydroxide. The exact mechanism of this reaction is still under investigation (Kurth & Bein, 1995, Chovelon *et al*, 1995). A mechanism involving initial hydrogen bonding has been postulated (Chovelon *et al*, 1995). This mechanism is illustrated in figure 8.1. It involves an initial chemisorption of the ODTMS molecule via a hydrogen bond. On the application of heat, a condensation reaction occurs leading to covalent Fe-O-Si bonds.

Figure 8.1 Mechanism for Formation of Fe-O-Si bonds

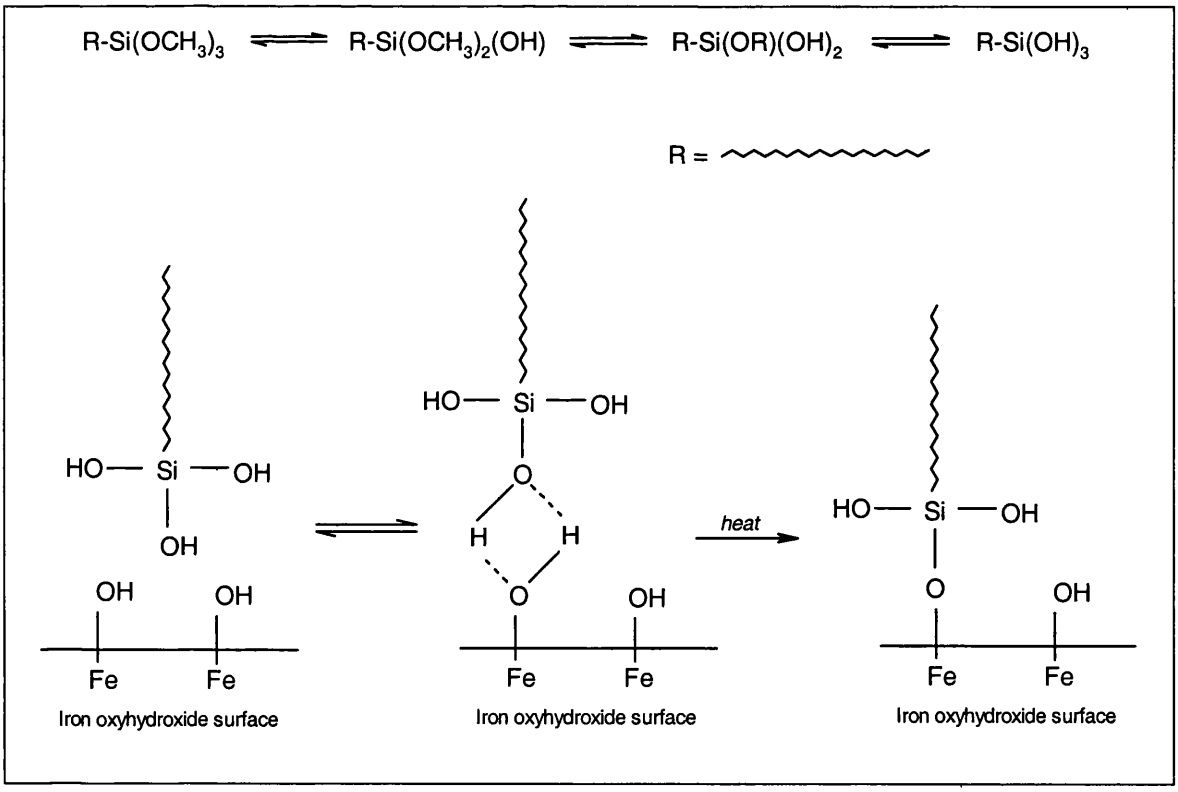

The second step of the reaction is the polymerisation of the silane molecules, now bonded to the iron corrosion product surfaces. With the addition of further water, all methoxy groups are hydrolysed, and a condensation reaction occurs between these hydroxy groups to form a siloxane network on the iron oxyhydroxide surface. This polymerisation can occur by two mechanisms. The first mechanism proceeds via the protonation of a silanol

group and the second mechanism, by the deprotonation of a silanol group (Fontaine *et al*, 1999). At pH's higher than 2.2 the second mechanism is thought to be the more likely (Fontaine *et al*, 1999). The two possible mechanisms are illustrated in figure 8.2.

Figure 8.2 Possible mechanisms of the condensation/polymerisation reaction between hydrolysed ODTMS molecules (Fontaine et al, 1999)

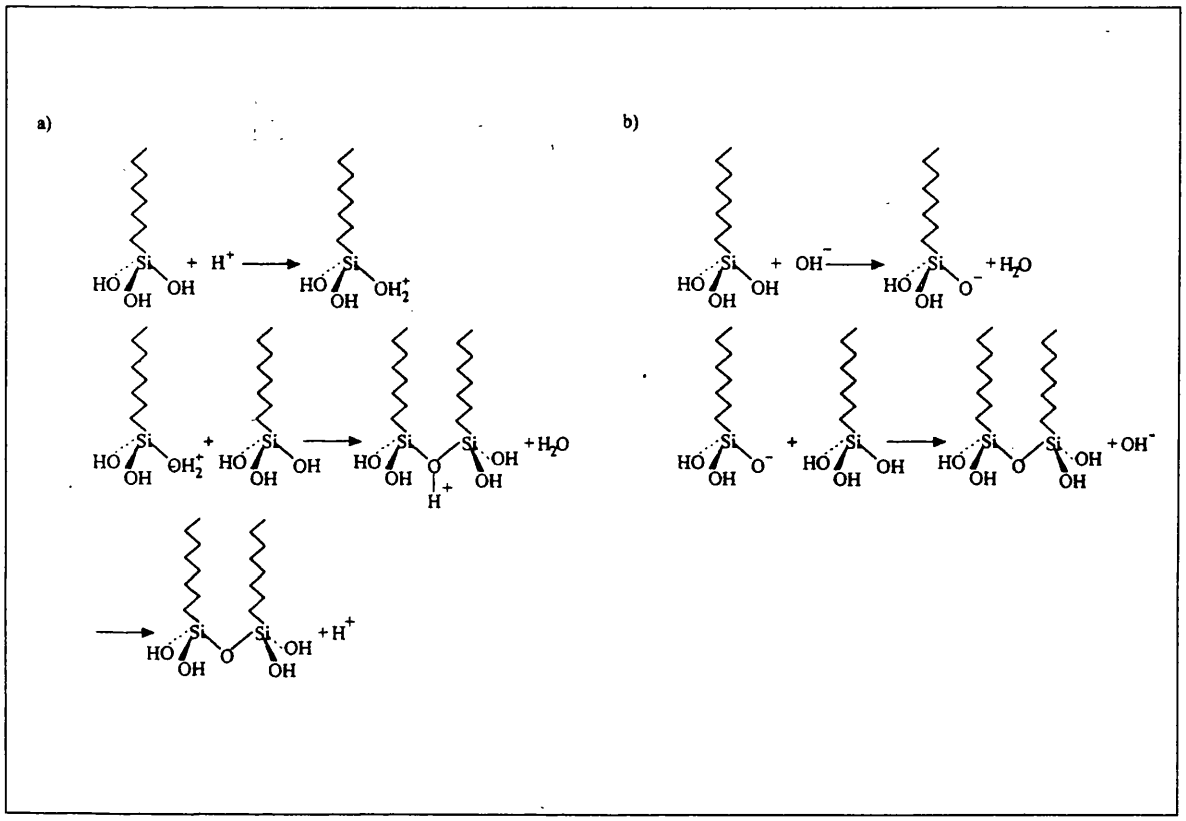

Figure 8.3a illustrates the polymerised silane on the iron oxyhydroxide surface, produced by the mechanism described. Obviously this description of a two step condensation, followed by polymerisation is an idealised model of the true situation. The conditions used in the treatment procedure were chosen to facilitate this mechanism. However, as soon as any hydrolysis occurs, there is the potential for polymerisation of ODTMS to occur. Therefore, some silane will be polymerised before reaction with the corrosion product surface and the coating formed will not be the uniform layer illustrated in figure 8.3a. Evidence is found by the detection of a vibration assigned to Si-OH in the FTIR spectra of the β-FeOOH sample treated with ODTMS. This illustrates that polymerisation is not total. Another possible conformation of the silane on the iron oxyhydroxide surface is shown in figure 8.3b.

Figure 8.3 Configurations of ODTMS on FeOOH

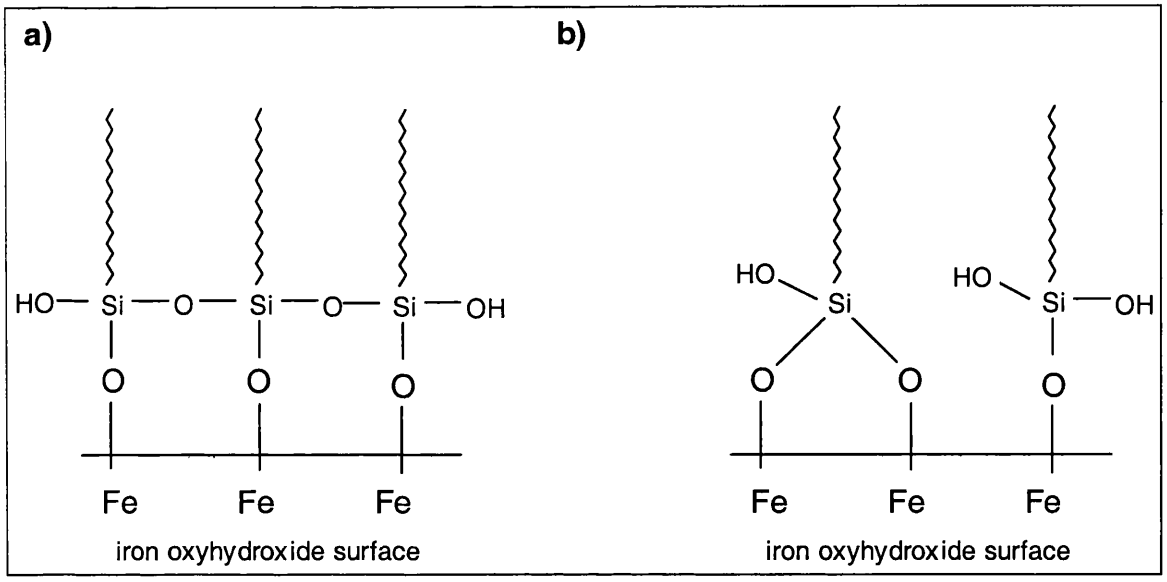

8.1.2 Mechanism of Interaction Between HFTMS and Corrosion Products

The mechanism for the reaction between HFTMS and the iron corrosion product substrate has been confirmed by the FTIR results to be identical to the mechanism described above for the reaction of ODTMS with iron oxyhydroxides. As with ODTMS, the FTIR data shows a loss of vibrations due to the $Si(OCH_3)_3$ head group and the addition of Si-O-Si vibrations, which confirms the reaction and polymerisation of the molecule. The main difference between these coatings is the nature of the hydrophobic chains that extend away from the surface, HFTMS containing fluorine rather than hydrogen.

In the formation of the silane film, it has been suggested that bilayers, and even trilayers may be present on the surface, rather than the monolayer suggested in the previous diagrams. Atomic force microscopy has indicated that HFTMS coupled to glass surfaces, consists of mainly bilayers (5.9nm) or trilayers (8.9nm) with only 4% of the modified surface consisting of monolayer or tetralayer coverage (Yoshino & Teranaka, 1997). These multilayers are formed via the same basic hydrolysis/condensation mechanism described for monolayers, however only half the silane molecules present are directly bonded to the surface. The other silane molecules are bonded to those molecules that are bonded to the substrate. Figure 8.4 illustrates the bonding in mono and bilayers for

comparison. It is possible that the polymer coating on the corrosion products produced in this work consists of bi or trilayers, however from this work there was no evidence to confirm or contradict this.

Figure 8.4 Models of polymerised HFTMS on FeOOH (Yoshino & Terenaka, 1997)

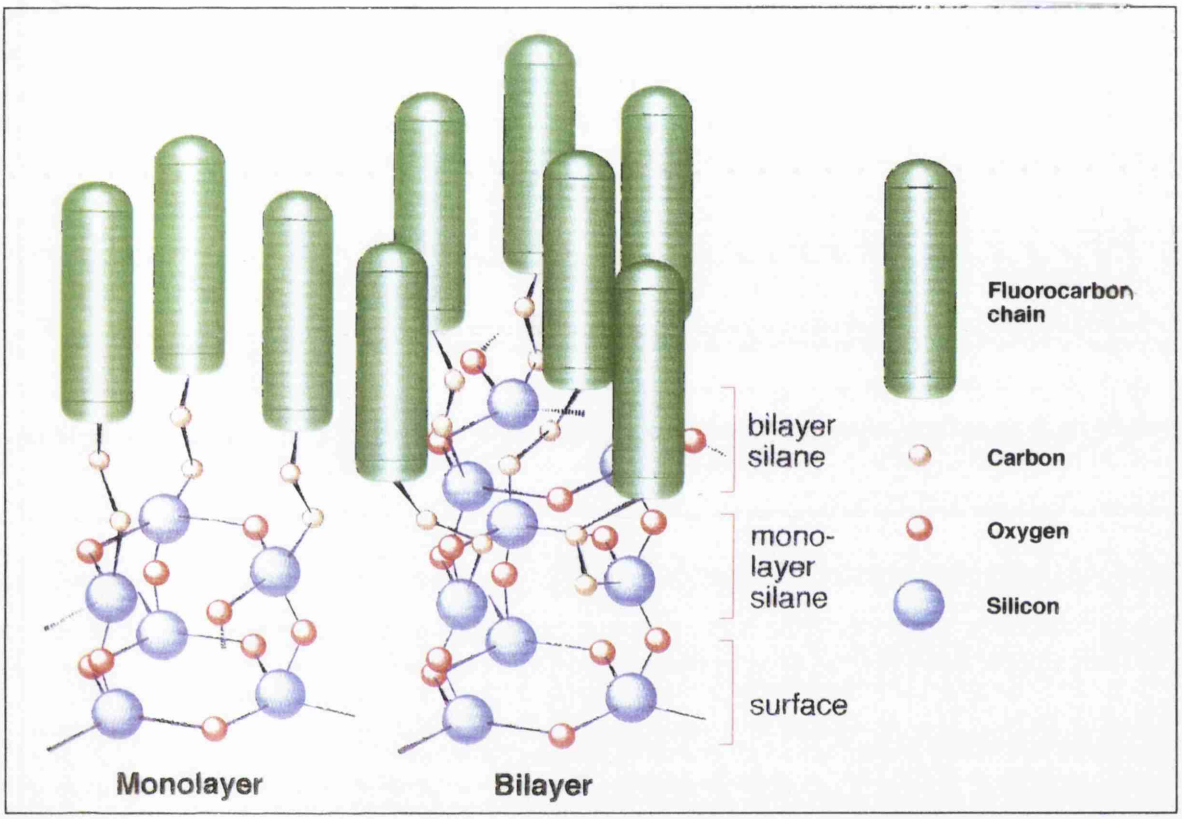

8.1.3 Mechanism of interaction between TTS and Corrosion Products

FTIR data showed the absence of vibrations from the OC_2H_5 group of TTS in the spectra from FeOOH samples treated with TTS. This inferred the presence of bonds between the TTS molecule and the FeOOH surface. Additional interactions between the carbonyl groups on the hydrocarbon chains of the TTS molecules and the iron oxyhydroxide surface were also inferred from the change in position of the C=O vibrations.

Given this evidence, a mechanism for the interaction between TTS and corrosion products can be suggested that involves the initial hydrogen bonding of TTS molecules to hydroxyl groups on the FeOOH surface. A hydrogen bond between a surface hydroxyl and the

carbonyl group of the TTS molecule will orientate and hold the TTS molecule in a position on the iron oxyhydroxide surface, thereby facilitating the formation of a covalent bond.

Figure 8.5 Mechanism of formation of bonds between TTS and FeOOH

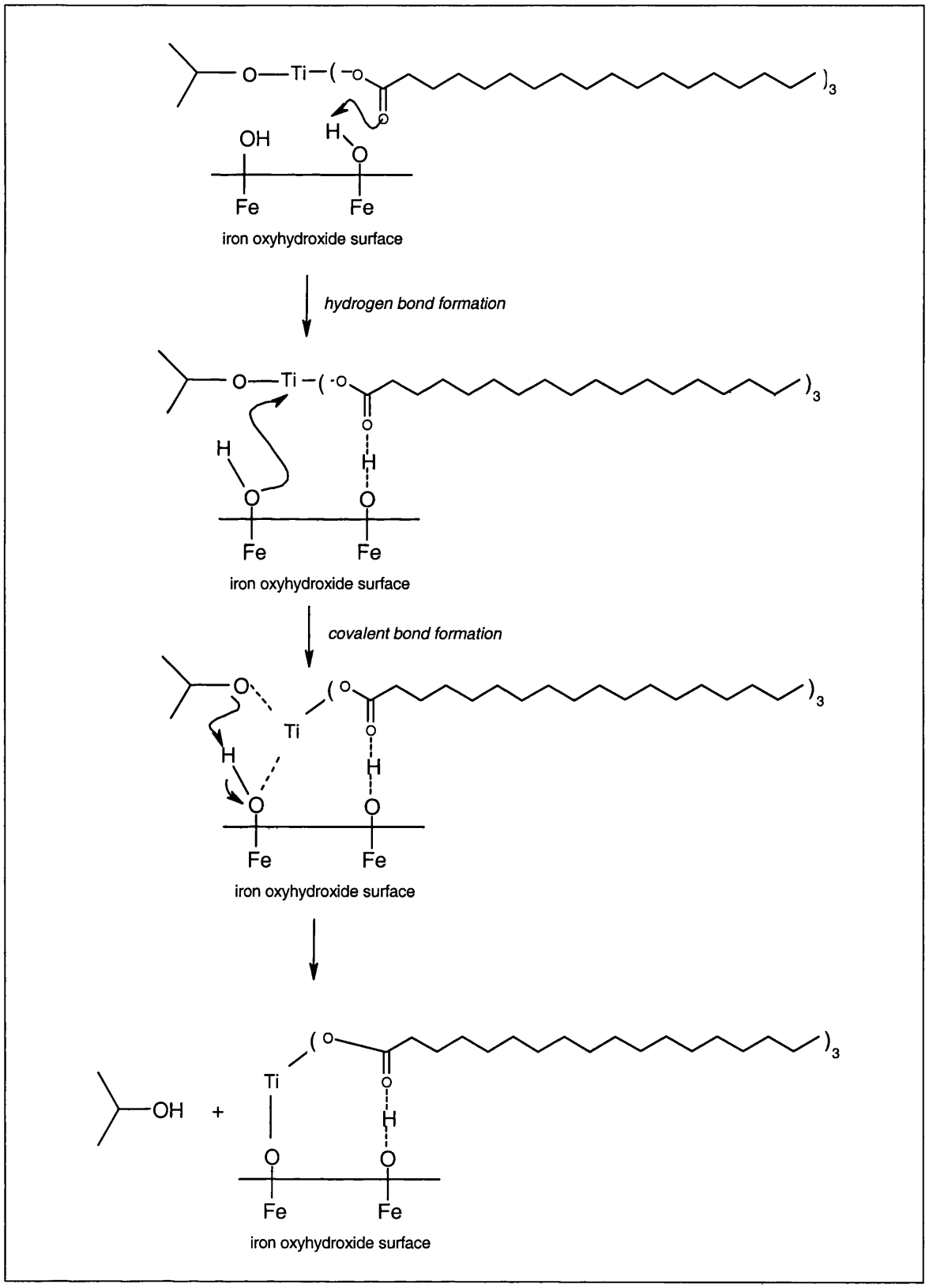

The formation of a covalent bond between the titanium atom and the oxygen atom of the hydroxyl group will occur via a substitution mechanism. This is likely to involve the formation of an intermediate species consisting of a partially formed bond between the Ti and O atom and a partially cleaved bond between the titanium and the oxygen of the OC_2H_5 leaving group. Deprotonation of the hydroxyl group will then occur, accompanied by protonation of the leaving group to form an ethanol molecule, C_2H_5OH. The process will be facilitated by heating the surface. This mechanism is illustrated in figure 8.5

The formation of these bonds will therefore lead to a new surface covered with the hydrophobic hydrocarbon chain. Each TTS molecule contributes three of these chains to make up this surface layer, as shown schematically in figure 8.7. There are however no bonding interactions between TTS molecules in contrast to the polymerisation that occurs with trialkoxysilanes.

Figure 8.6 TTS on the surface of FeOOH.

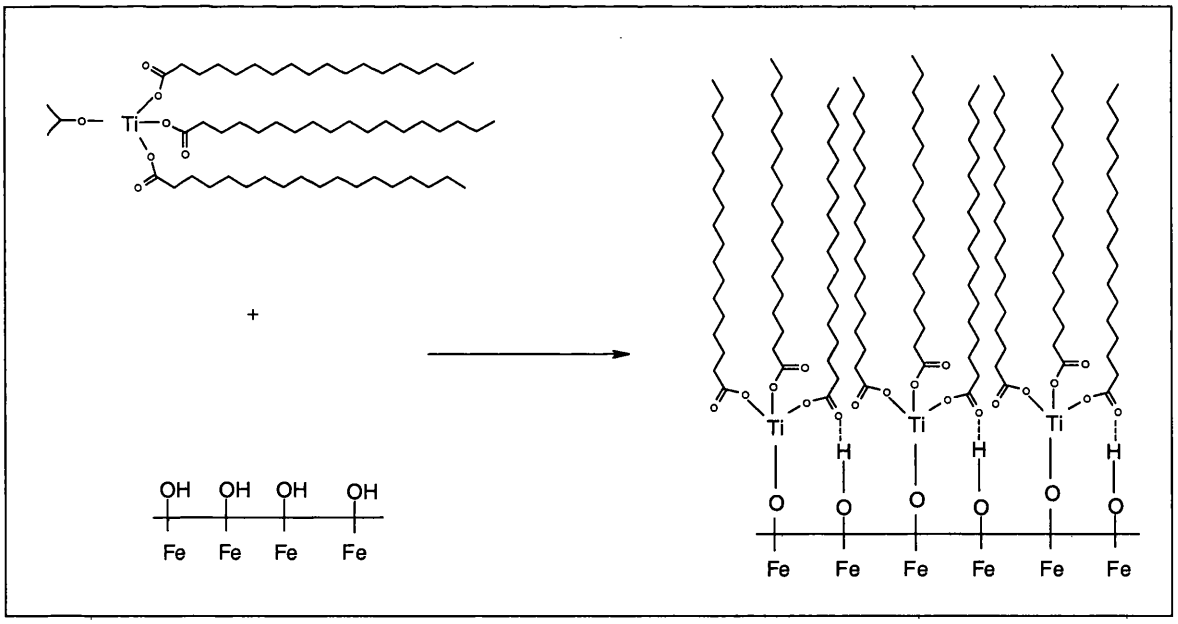

8.1.4 Mechanism of Interaction Between Long Chain Aliphatic Amines (ODA and DCA) and Corrosion Products.

The mechanism of interaction between corrosion product surfaces and the amines, ODA and DCA, tested in this work, can be deduced from the information gained in FTIR and XPS studies. FTIR spectra of FeOOH treated with ODA indicate the presence of primary

(RNH_2) and secondary (R_2NH) amine species on the FeOOH surface. The presence of cationic species, RNH_3^+ has also been confirmed from FTIR spectra and XPS spectra of corroded iron treated with DCA.

Figure 8.7 Mechanism for amine bonding to surface iron sites

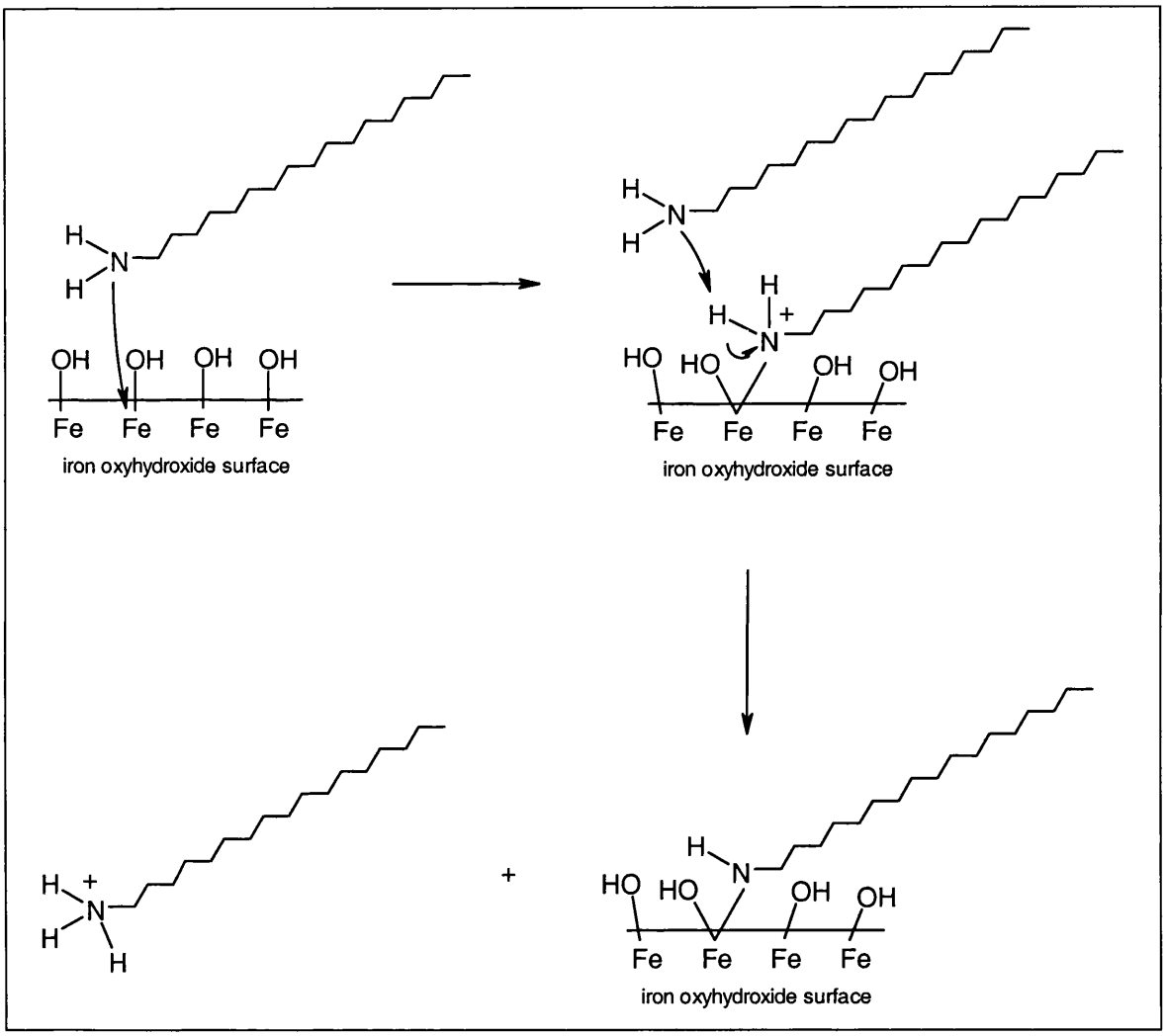

The presence of primary amines may indicate some amine molecules are physisorbed onto the FeOOH surface, however some chemical bonding is also indicated by the presence of other species. Several different mechanisms will account for the presence of these species, and it seems likely that amine molecules are present on the surface in different states (Braun *et al*, 1993). All mechanism involve bonding interactions of the amines nitrogen atom. The amine may form a covalent bond with an iron atom on the FeOOH surface. After deprotonation, this results in a secondary amine bonded to the surface and the

formation of a RNH_3^+ molecule that may take part in further bonding. This mechanism is illustrated in figure 8.7.

Interaction can also occur via a hydrogen bonding mechanism. RNH_3^+ species may hydrogen bond to surface oxide atoms, whilst RNH_2 molecules can hydrogen bond to surface hydroxyl groups. Both mechanisms will result in a tertiary ammonium cation. Two possible mechanisms are illustrated in figure 8.8, with the amine bonding to either a surface oxide or hydroxide group.

Figure 8.8 H-bonding of amines to iron oxyhydroxide surfaces via a) oxide or b) hydroxyl groups

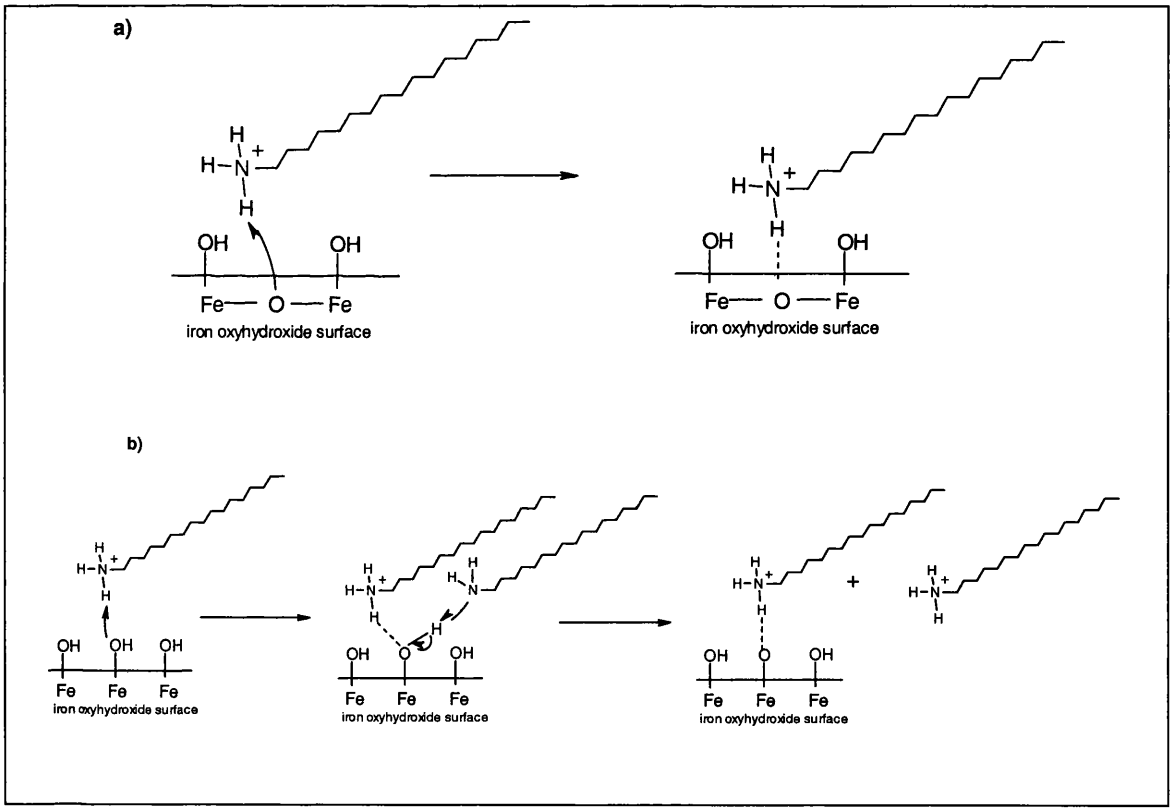

8.2 Evaluation of Inhibitors as Stabilisation Treatments for Archaeological Iron

The inhibitor treatments tested in this work can be evaluated in terms of the criteria for the selection of an inhibitor treatment set out in chapter two, section 2.4.2. These criteria were divided into two groups, those that relate only to the actual performance of the treatment in inhibiting corrosion, the physicochemical properties required and those that relate specifically to considerations relevant to archaeological conservation. Only the former physicochemical category will be discussed in this section.

The important properties that may facilitate efficient inhibition are, the ability to form strong, unhydrolysable bonds with the corrosion products surface, the formation of cross linkages between inhibitor molecules bonded to the surface and the formation of a dense closely packed layer of inhibitor molecules on this surface which should form a hydrophobic layer that stops the adsorption of water through the coating. Obviously the most important criteria is the actual ability of the coating to stop or diminish corrosion. The best inhibitor, in terms of chemical and physical properties therefore must be considered to be the one that performed best in the accelerated corrosion tests.

From FTIR data recorded there is evidence that all treatments tested do form bonds with the FeOOH, corrosion product surfaces. The mechanisms of these bonding interactions have been described in section 8.1. The resistance of these bonds against hydrolysis was observed using the simple floatation tests described in chapter five. These tests showed that the bonds formed between ODTMS, HFTMS and TTS were all resistant to hydrolysis during the 6 month testing period. However, bonds formed by ODA were easily hydrolysed. This may indicate that the majority of the ODA molecules are hydrogen bonded to the surface. These hydrogen bonds are easily broken, forming quaternary ammonium ions in solution. The ODA molecules are easily detached from the iron oxyhydroxide surface, and this will mean, that even if the treatment initially inhibits corrosion, this effect is likely to diminish with time. This is confirmed in the results of the electrochemical monitoring in chapter five. Although initially a good inhibitor, after 2 days its inhibiting ability starts to fall below that of the other treatments. ODA may not be an appropriate long term treatment.

The polymerisation, or cross linking of inhibitor molecules has been indicated from FTIR results to occur for the HFTMS and ODTMS treatments. Both these silanes have the ability to form siloxane networks on the surface of the corrosion products. Additional bonding interactions, such as polymerisation, was judged to assist in forming an unhydrolysable hydrophobic coating. In actual fact, the covering that seems to have provided the best inhibition, TTS, has no cross linking between adjacent molecules, however it does have additional hydrogen bonding interactions between its carbonyl groups and surface hydroxyl groups. Polymerisation of the surface coating has therefore not been shown to be a crucial factor in the efficiency of the treatments tested in this work.

The hydrophobic nature of the treated iron corrosion product surfaces was investigated by measuring how the amount of water adsorbed onto these surfaces varied with humidity. These water adsorption isotherms showed TTS, ODTMS and HFTMS all to provide good hydrophobic coatings that greatly reduced water adsorption. The hydrocarbon and fluorocarbon chains do act as hydrophobing agents as described in chapter two, section 2.4.3. ODA did not perform as well in these tests, presumably due to the hydrolysis that has been shown to occur which will remove some of the hydrophobic ODA layer. In all cases some water adsorption did occur. This shows that even the best treatments tested must have flaws in the coatings, or gaps within the close packed hydrocarbon tails which allow water to pass through.

It can be concluded from the accelerated corrosion tests on archaeological iron nails with a low chloride ion concentration (described in chapter four), that the TTS treatment has been shown to have the better corrosion inhibiting properties than the long chain aliphatic amines ODA and DCA. TTS and ODA were found to slightly inhibit the corrosion of coupons containing β-FeOOH. The difference in the performance of the inhibitors tested were much reduced in tests involving these corroded coupons as compared to differences detected in the experiments on archaeological iron nails. This suggests that when a high chloride concentration exists in the corrosion environment, the amount of water present is no longer the rate determining step in the corrosion process, Thus it is deduced that the more important factor is the catalytic effect of chloride ions, and this makes all the inhibiting coatings less effective. ODTMS was found to reduce corrosion only very slightly

on the high chloride concentration coupons it was tested on, again suggesting the diffusion of water is no longer the most important factor.

The greater efficiency of TTS as an inhibitor treatment may be connected to the presence of three hydrocarbon chains per molecule, whilst all the other treatments only possess one chain per molecule. If we assume an equal number of inhibitor molecules are bonded to each iron oxyhydroxide surface, we may conclude that there will be three times as many hydrocarbon chains on the surface. The density of the hydrophobic layer therefore seems to be a crucial factor in forming a successful coating.

The most puzzling result from the accelerated corrosion tests still remains the behaviour of HFTMS treated samples. Experiments on coupons showed that the HFTMS treatment actually accelerated the rate of corrosion considerably. Water adsorption isotherms showed that a hydrophobic layer, equivalent to that on TTS or ODTMS was present on iron oxyhydroxide surfaces treated with HFTMS. Floatation tests also showed that little detaching of these molecules occurred. In electrochemical monitoring experiments no acceleration of corrosion was detected in the potential of the HFTMS treated electrode.

The presence of fluorine in HFTMS is unlikely to cause an acceleration of corrosion. The carbon-fluorine bond is stronger than the carbon-hydrogen bond, for example the C-F bond in CF_4 has an energy of 484kJmol^{-1} whereas the C-H bond in CH_4 has an energy of 416kJmol^{-1} (Yoshino *et al*, 1997). Cleavage of the C-F bond is therefore highly unlikely. The larger size of the fluorine atom (0.72Å), in comparison to hydrogen (0.37Å) would also suggest that the carbon chain would be better protected against chemical attack, and that the polymer layer would be more dense and therefore a more efficient inhibitor. Results in this work have shown this not to be the case.

From the fact that the HFTMS treatment behaved in a similar manner to the ODTMS treatment in electrochemical testing (carried out in solution), both showing higher corrosion potentials than the untreated control sample, (therefore indicating corrosion had been inhibited to some extent), it is suggested here that the failure of the HFTMS treatment may be connected to the mechanism of atmospheric corrosion. It was suggested that the highly hydrophobic nature of the fluorocarbon surface prevented water adsorption

which in turn lead to an increase in atmospheric oxygen diffusion, the later in fact increasing the rate of corrosion. The addition of another corrosion inhibitor, pyridine, was hoped to block this increase in corrosion by adsorbing onto any gaps in the HFTMS coating, or possibly absorbing onto the metal surface below the corrosion layer. The addition of pyridine did decrease the rate of corrosion as compared to samples treated with HFTMS alone. However, the combined treatments, only reduced the corrosion rates to a similar level to that of the untreated control batch. This was not as low as the batch treated with ODTMS.

It is significant that results obtained for samples treated first with HFTMS and then pyridine and visa versa, showed identical corrosion rates in accelerated corrosion tests. This suggests that there are sufficient gaps and holes in the HFTMS coating formed, for pyridine to pass through this film, even though the surface has become hydrophobic as previous results have shown. The existence of these holes and gaps may be crucial in understanding the acceleration of corrosion that the HFTMS treatment seems to cause.

The integrity of a monolayer film is very difficult to investigate. Experiments on flat, clean glass surfaces using atomic force microscopy have managed to image such films (Banga *et al*, 1995, Rabinovich & Yoon, 1994, Flinn *et al*, 1994), but this would be impossible on an uneven surface such as is present on corroded iron. AFM data for the adsorption of silanes suggests that monolayers primarily form in patches or islands. As surface coverage increases the patches do not increase in size but rather become more numerous and eventually cover the entire surface (Flinn *et al*, 1994). Other evidence of film formation via domains for fluorocarbon and hydrocarbon silanes has been given by Rabinovich & Yoon (1994). It has also been shown that 'pin' holes exist in silane monolayers from several nanometers to 100 nanometers in diameter (Nakagawa *et al*, 1995).

Returning to the mechanisms for the formation of silane monolayer, and the competition between polymerisation and bonding to the iron oxyhydroxide surface, the above evidence suggests polymerisation is first occurring, followed by the adsorption of polymerised silane as islands onto the substrate. Small gaps between islands may be too small to be filled by polymerised silane and therefore become pin holes in the polymer film. The existence of holes may explain the failure of the HFTMS coating in inhibiting corrosion. XPS results

did not show HFTMS treated samples to have a particularly low surface coverage. Investigations into the statistical spread of corrosion rates in treated samples in corrosion tests suggested that failures of coatings were not uniform. This may suggest that only where flaws or 'pin' holes were present in the HFTMS films, did accelerated corrosion occur.

It is known that the rate of hydrolysis of fluorocarbon silanes is much greater than the rate of hydrolysis of hydrocarbon polymers (Banga *et al*, 1995). This is due to the greater electron withdrawing effect of CF_3 and CF_2 groups as compared to CH_3 and CH_2 groups. This would mean that the rate of polymerisation is also greater for fluorocarbon silanes. In fact, HFTMS is so reactive it was neccessary to store it in sealed glass ampoules under an inert atmosphere, and all reactions with it were carried out in an inert atmosphere. Moist air had to be eliminated to try and prevent polymerisation occurring before the silane makes contact with the iron oxyhydroxide surface. This increased reactivity (as compared to ODTMS) may result in increased polymerisation when in contact with the water adsorbed onto the FeOOH surface. The already polymerised HFTMS would then adsorb onto the FeOOH surface and thereby this may lead to the formation of more gaps and 'pin' holes than are present in monolayers of ODTMS.

The effect of pin holes and flaws within the HFTMS film may cause an acceleration of corrosion via the creation of a differential aeration cell. As corrosion proceeds the oxygen under the HFTMS coating will be depleted, but in uncoated areas oxygen will be replenished readily, so creating a differential in aeration. The aerated area of the metal surface will become the cathodic area and other regions will become anodic. This in turn will affect the pH of the anodic and cathodic regions, the cathodic region increasing in pH due to the production of OH^- ions. Hydrolysis of Fe^{2+} ions produced by corrosion will also decrease the pH of the anodic regions and may also set off a crevice or pitting corrosion mechanism. This will cause the accelerated corrosion of the anodic regions and in general accelerate the rate of corrosion (Jones, 1992). This is comparable to the mechanism of filiform corrosion which is known to occur under thin organic coatings covering steel when exposed to humid conditions. Filiform corrosion initiates at gaps or scratches in coatings and propagates as narrow streaks of corrosion with an actively corroding deaerated head followed by an inactive aerated tail of corrosion products.

Although no direct evidence for the acceleration of corrosion via this mechanism has been found it may explain the accelerated corrosion tests results. Perhaps the fact that fluorine atoms are larger than hydrogen atoms will actually lead to a decrease in oxygen diffusion through the covered areas of the HFTMS layer in comparison to the similar ODTMS coating, through which some oxygen can diffuse. This will therefore exacerbate the differential aeration that may occur if flaws are present in the film, and thus facilitate the acceleration of corrosion via this mechanism.

The difference in performance of the similar ODTMS and HFTMS coating is surprising, however it can be concluded that TTS is the most effective treatment of those tested in decreasing the rate of corrosion. The high density of hydrocarbon chains and the strength of its bonds to the FeOOH surface give it superior properties to other coatings such as ODA and ODTMS.

8.3 Evaluation of Inhibitor Coatings as Conservation Treatments

The actual performance of the inhibiting coatings tested is not the only important factor in assessing their performance. Not only must they inhibit corrosion but they must also satisfy other criteria relating to their suitability for use as conservation treatments. These criteria have been listed in chapter two, section 2.4.2. The ethics of conservation dictate that conservation treatments should not significantly change the colour or appearance of objects. For the conservation of metals there is also the issue of the temperature at which a treatment is carried out, as high temperatures may alter some tempered metallographic structures (Ehrenreich, 1987). Treatments should be reversible so that they may be removed by future conservators if found to be harmful or if improved treatments are discovered. They should also be easy to apply, non toxic and as cheap as possible.

Ideally, conservation treatments should be reversible so that any process or treatment can be reversed and removed in the future. Past experiences has shown conservators that treatments once thought beneficial can actual results in damage to an object in years to come. The reversibility of a treatment is therefore crucial so that conservators of the future may not be faced with some of the problems presented to conservators today such as objects damaged by irreversible past conservation treatments. This ideal situation does not however reflect reality. It is unrealistic to consider any conservation treatment as reversible. The act of removing an object from its burial environment in fact is itself an irreversible process. We have seen that once archaeological iron is removed from marine or land sites, irreversible deteriorating changes start to occur. Any cleaning process will lead to irreversible changes in the object as will all consolidation treatments (Cronyn, 1990, 86).

The more practical concept of minimal intervention is the approach taken by most conservators today. The United Kingdom Institute of Conservation of Historic and Artistic Works (UKIC) has set out guidelines that state the conservator should interfere minimally with the true nature of an artefact (Cronyn, 1990). This means that passive treatments involving the monitoring and controlling of environments are favoured over active interventions such as chemical treatments.

The primary aim of any conservation treatment must be to stabilise and therefore preserve an artefact. For this purpose, active treatment of otherwise unstable objects is within the ethics of conservation. The principle of minimum intervention must still be followed. The successful treatments tested in this work seem to fit well into this category. They are not reversible but the treatments that improve the stability of archaeological iron also change the object minimally, only a thin inhibitor film being present on the surface of the object.

Although corroded iron objects are already changed in colour from the original metal object, for the purpose of display in museums the brown or black appearance of the corroded surface is expected. Investigative cleaning is used to remove extraneous material from the surfaces of objects to reveal the original dimensions of the object, and if possible any original surface markings that may have been preserved. It is therefore important that any conservation treatment should not change the colour or appearance of the surface, or obscure any archaeological or archaeometallurgical evidence that may be present in the surface layers. All samples treated with inhibitor treatments were carefully examined for any changes in appearance the treatments may have caused. Visual inspection showed no change in the appearance or colour of nails or coupons treated with the TTS, HFTMS or ODTMS inhibitor treatments. Some samples treated with ODA became discoloured with a white surface layer. This change in appearance makes ODA an unacceptable conservation treatment.

Archaeometallurgists require any conservation procedure to retain the microstructure of the metal intact so that future examination of the structure will be possible. The microstructure of a metal is a crucial piece of evidence in the investigation of fabrication techniques and can thus yield much information on manufacturing processes and ancient technology. Information can be gained from metallographic studies, such as, if wrought iron has been cold worked and tempered, or if steel has been welded or case hardened. Changes in metallurgical structures can be caused by high temperatures and so the application of excessive heat during a conservation treatment must be considered as making a conservation procedure unacceptable. It has been shown that the treatment of iron at temperatures above 700°C will significantly alter the microstructure and hardness of an object. A temperature of 350°C has been found to be safe for all structures except martensitic or tempered martensitic steel (Archer & Barker, 1987). Martensitic steel is

produced when steel is heated to the temperature range 700-900°C and then rapidly cooled by plunging into water (quenching). Martensitic structures are known to start breaking down at temperatures approaching 100°C (Tylecote & Black, 1980). It would therefore not be safe to apply any conservation technique that requires temperatures of 100°C or more to martensitic steel or any objects of unknown structure that may contain martensitic steel.

Of the treatments tested in this work, HFTMS and ODTMS both required temperatures of 150°C to cure the coatings. These temperatures would not be appropriate for the conservation of martensitic steel but would not affect other archaeological iron. The TTS treatment required a temperature of 55°C and the ODA treatment was carried out at room temperature. Both these treatments would not affect the metallographic structure of any archaeological iron, making then appropriate to use on iron whose microstructure has not yet been investigated.

In evaluating a conservation treatment, the simplicity and practicality of a procedure is very important. Conservation laboratories often have large amounts of material for conservation and must constantly manage and prioritise time and resources. In this context, an ideal treatment would be simple and straightforward to carry out by any conservator, require simple laboratory equipment and be performed in a relatively short time scale in comparison to some other conservation treatments. The treatments tested in this work are simple to carry out, and can be completed in several days (which compares well to some washing techniques that may take weeks or months to complete). The ODTMS and HFTMS treatment are more complicated than the TTS and ODA treatments due to the fact that the reagents are moisture sensitive and so the treatments must be carried out in moisture-free environments using dry boxes and schlenk lines. These facilities may not be available in conservation laboratories and do complicate the treatment procedure. It is possible that the ODTMS treatment could be carried out in ambient conditions as this reagent is less moisture sensitive than HFTMS, however this would greatly shorten the shelf life of the reagent.

Health and safety criteria are obviously of vital importance to conservators. Many molecules found to inhibit corrosion are also found to be highly toxic, such as chromates,

arsenic (Jones, 1992, 502) and aromatic amines, many of which are carcinogenic (Lunn & Sansone, 1994). The toxicity data available for all treatments has been given in chapter two. All the treatments can be classified as having low to medium toxicity. Although detailed long term studies have not been carried out, from the general nature of the chemicals, it is not thought that any of the treatments pose a major health hazard when handled with care. As with many chemicals, they may cause skin or respiratory tract irritation and so should be used in accordance with general laboratory practises.

The costs of the treatments tested are given in table 8.1. The HFTMS treatments is the most expensive, as it is a recently synthesized molecule and is not widely available. The titanate TTS, is a product used in manufacturing industies, and is therefore sold in large quantities and is relatively cheap. The other treatments are also relatively cheap and can be purchased from large chemcial suppliers such as Sigma-Aldrich. The cost of these chemicals is unlikely to be prohibitive for most conservation laboratories. It must be remembered that only small quantities of inhibitor are used in each treatment and several objects can be treated with the same solution.

Table 8.1 Cost of inhibiting treatments

TREATMENT	COST
ODTMS	£28.10 per 25ml
HFTMS	$60 per 10ml
TTS	£36.68 per 1kg when 1 gallon purchased
ODA	£13.70 per 25g

It can therefore be concluded that as well as being the best treatment for inhibiting corrosion, TTS also fulfils all the criteria for a suitable conservation treatment. It improves the stability of archaeological iron without affecting the aesthetic, physical or metallographical integrity of an object and is a cheap and easily applied treatment. Previous studies have also shown that no damage or change in appearance occurs when other archaeological material, such as leather, bone, wood and textile is treated with TTS (Al Ahmed, 1992, 257). This would make TTS a suitable treatment for composite materials.

8.4 Evaluation of Polyaniline as a Stabilisation Treatments for Archaeological Iron

Results presented in chapter seven have shown that neither polyaniline or polyaniline doped with camphor sulphonic acid have a significant effect in inhibiting corrosion. The small inhibition observed for some of the polyaniline treatments was much less than that observed for the TTS treatment, evaluated to be the best tested inhibitor. The decrease in corrosion that was seen in some treatments can be attributed to the presence of the polymer as a barrier on the corrosion product surfaces. However, this barrier seems to be working in the same manner as any inactive polymer coating, such as PVAc's, and is not exhibiting the inhibiting effect attributed to it as a conductive polymer. Inactive polymer coatings have been shown to be fairly ineffective in conserving archaeological iron in the long term (Keene, 1984) as has been disscussed in section 1.6.5.

To try an explain the reason for the failure of polyaniline based coatings in inhibiting corrosion on archaeological iron it is necessary to reconsider the proposed mechanism of the inhibiting action. Linear voltammetry measurements presented in chapter seven confirmed literature results showing that when polyaniline coatings are applied to iron or steel they inhibit corrosion in acidic conditions (Deberry, 1985, Wrobleski *et al*, 1994). The mechanism of the inhibition is related to the electrochemical coupling of the polymer and metal. The polymer impresses a passive potential onto the metal as in anodic protection (Lu, 1995) and therefore corrosion of the metal is inhibited. For this type of inhibition to be effective, the polymer must be in electrical contact with the metal. The archaeological iron samples tested in this work and the majority of archaeological iron in need of stabilisation will be covered with a thick corrosion layer, and therefore any coating applied will not reach the underlying metal. The application of a vacuum when applying the coating did not improve accelerated corrosion test results and so it can be concluded that even this method will not provide electrical contact between the conducting polymer and the metal core of an object. For this reason conducting polymers are not applicable stabilisation treatments for archaeological iron.

Although further experiments have not been carried out, it is possible that conducting polymer corrosion inhibitors may be useful for conservation treatments on uncorroded

metal surfaces. PANI and PANI-CSA are however unsuitable for conservation due to their colour. The polymer coatings, although transparent, have a pale blue colour which is visible, even on the darkly coloured corroded samples tested. This colouration would be aesthetically unacceptable to conservators.

Research into conducting polymers is in its infancy. Commercially available polyaniline primers are still very expensive and are not yet widely used in industry. It may be possible that in the future colourless conducting coatings with inhibiting properties may be available and that these may be of use to conservators working on a selection of metals. This field of research should be closely followed so that any future advances may be fully utilised by conservators.

8.5 Surface Modification and Corrosion Inhibiting Coatings: The Right Approach for the Conservation of Archaeological Iron?

In this work selected surface modification techniques and inhibiting coatings have been assessed for their ability to inhibit the corrosion of archaeological iron. The TTS treatment was found to be the most appropriate for use as a conservation treatment. However none of the treatments tested had the ability to prevent all signs of corrosion when samples were exposed to a high humidity and elevated temperature environment.

It has also been noted that the amount of chloride present in corroded iron seems to have an effect on the difference in performance of the various treatments tested. Accelerated corrosion tests carried out on archaeological iron with relatively low chloride content showed the TTS treatment to be superior to the amine treatments tested. When the same treatments were tested on coupons with a higher chloride concentration, the differential between the performance of the TTS and ODA treatments was considerably reduced. This indicates that when corrosion occurs in high chloride ion environments, the amount of water that is able to pass through the corrosion product layers and reach the metal surface is a less significant factor in the corrosion process than in the case of samples with lower chloride concentration. In this type of environment therefore only a small amount of water is enough to allow corrosion to occur and the difference in hydrophobic properties of any coating applied is not the limiting or significant factor. This calls into question the ability of this type of hydrophobic barrier to prevent the breakout of corrosion caused by the presence of β-FeOOH in archaeological iron, and specifically iron from marine environments. Although the coupons produced had higher chloride levels than would be present in archaeological objects, they act as a model for the type of corrosion that may occur in certain regions of corrosion products. Even after desalination treatments, if areas of high chloride ion concentration build up in iron objects due to the presence of β-FeOOH, it is not at all certain that the presence of a hydrophobic barrier will prevent the corrosion that causes the spalling and flaking and eventual destruction of such objects.

This question can only be answered by long term testing of the TTS treatment in museum environments. Accelerated corrosion tests are ideal for comparing the effects of different

treatments, but it is impossible to directly extrapolate from these results the performance of treatments in a museum environment over a long time scale. Until long term testing is carried out, it can not be certain that the protection afforded to objects by the TTS treatment, gives a significant improvement in the survival rate of archaeological artefacts. Only this will make the treatment worthwhile for conservators. The only long term results we can so far use to assess this issue, is the treatment of several cast iron cannon shot from the Mary Rose, with TTS in 1992 (Al Ahmed, 1992). Two cannon shot were available for re-examination, seven years after the treatments were carried out. An untreated cannon shot was found to have totally disintegrated into many fragments. The cannon treated with TTS was found to be in a superior condition, being still in one piece. However many surface cracks were observed. It seems that the TTS treatment has significantly improved the long term survival rate of the cannon but signs of corrosion were starting to appear. This suggests that although the inhibitor treatment is worthwhile, a preliminary washing procedure to remove chloride ions is advisable to improve the performance of the treatment further. Obviously a much larger group of samples must be tested to make a more valid assessment.

The approach taken in this work was a response to the problems encountered in the use of other conservation techniques and the recent reassessments of the structure of the β-FeOOH corrosion product. Conservation techniques have focused on the desalination of archaeological iron as the presence of chloride ions has been found to be the cause of the rapid corrosion and deterioration of iron after excavation. It has previously been believed that chloride ions could be washed out of corrosion products and specifically could be removed from β-FeOOH by washing or ion exchange procedures (Al Ahmed, 1992). However, it seems clear from the analysis of the literature on the β-FeOOH structure that a proportion of chloride ions are structurally part of the corrosion products (in lattice or tunnel sites), and can not be washed away, or undergo ion exchange in a short time scale.

Some of the conservation methods found to be successful in stabilising archaeological iron circumvent this problem by destroying corrosion products in reduction processes such as hydrogen or plasma reduction. These methods reduce and breakdown corrosion products such as iron oxyhydroxides and thus release chloride ions (Gilberg & Seely, 1982, North & Owens, 1981, Sjøgren & Buchwald, 1991). Although they have been amongst the most

successful conservation methods, they do produce changes to either the physical appearance and structure or the metallurgical structure of the artefact treated.

It is for the above reasons that a non destructive conservation method, based on the application of a protective coating has been tested in this work. Subject to further long term testing, a combined method of desalination by soxhlet washing, followed by the application of a protective inhibitor treatment such as TTS, is the procedure that seems to best fit the practical and ethical criteria of conservators, archaeometallurgist and museum curators for the treatment of problematic archaeological iron.

8.6 CONCLUSION

The stabilisation of archaeological iron, particularly from marine environments, is still a considerable problem for conservators. The presence of chloride ions within iron corrosion products leads to the outbreak of corrosion at low relative humidity values, at which iron is often considered stable. A survey of conservation techniques employed show that some of the most successful methods involve the reduction and destruction of corrosion products to remove the harmful chloride ions, found specifically in the β-FeOOH corrosion product. The use of destructive techniques, such as the plasma reduction method, may lead to unacceptable changes in aesthetic, physical and metallurgical properties of an artefact (Bradley *et al*, 1997). Research into the structure of the chlorine containing corrosion product β-FeOOH, has lead to the conclusion that some chloride ions are structurally bound and can not be removed in a short time scale without the destruction of this corrosion product. A non destructive method to remove all harmful chloride ions is not at present available, and for this reason it was decided to investigate the use of corrosion inhibiting surface treatments as a method for stabilisation.

The hydrophilic nature of corroded surfaces is one factor that leads to the increased post excavation corrosion of objects that commonly occurs. Free hydroxyl groups found on the surfaces of all FeOOH phases (α,β,γ,δ and amorphous) act as adsorption sites for water and species such as SO_2 and oxides of nitrogen. Water and other pollutants will therefore be drawn to the metal surface below the corrosion products and cause increased cycles of corrosion.

The approach taken in this work was to change the surfaces of corrosion products by the addition of hydrophobic molecules. These molecules would bind to hydroxide groups or other sites on the corrosion product surfaces. The surface modification treatments contained long hydrophobic hydrocarbon (or fluorocarbon) chains that would stop the adsorption or condensation of water on the corrosion product surfaces. The adsorption of other pollutants which accelerate corrosion would also be prevented. Using this method it was hoped that the inhibitor treatments would stabilise archaeological iron.

The treatments chosen to test were a monoalkoxy titanate, isopropyl-triisostearoyl titanate (TTS), $CH_3.CH.CH_3OTi(OCO.C_{17}H_{35})_3$, a silane, octadecyltrimethoxysilane (ODTMS), $CH_3(CH_2)_{17}Si(OCH_3)_3$, a polyfluorinated silane, 1H, 1H, 2H, 2H-Henicosafluorododecyl-trimethoxysilane (HFTMS), $C_{10}F_{21}H_4Si(OCH_3)_3$ and the amines Decylamine (DCA), $C_{10}H_{21}NH_2$ and Octadecylamine, (ODA), $C_{18}H_{37}NH_2$. All these molecules have long hydrophobic chains that it was hypothesised would modify the surfaces of objects treated and lead to stabilisation.

XPS studies of corroded iron samples treated with the above inhibitors have shown a decrease in the amount of iron detected on the surface, indicating that the surfaces have been modified by the inhibitor treatments. FTIR spectra of the inhibitors adsorbed onto the α and β phases of iron oxyhydroxide have been used to suggest mechanisms for the reaction between FeOOH and the inhibitor molecules. The FTIR evidence indicates that covalent bonds are formed between TTS molecules and the iron oxyhydroxide surface. Evidence for polymerisation of both silanes tested is also apparent in the appearance of Si-O-Si vibrations. The presence of positively charged quaternary nitrogen atoms, as seen by vibrations assigned to $R_2NH_2^+$ groups has lead to the conclusion that at least some of the amine ODA is hydrogen bonded to hydroxyl groups on the corrosion product surface. A similar bonding mechanism is assumed for all long chain aliphatic amines and this could be seen in the XPS spectra of DCA where the presence of quaternary nitrogen atoms was also detected.

The inhibiting performance of each treatment was assessed by several methods. Water adsorption isotherms were recorded on α and β iron oxyhydroxide powders that had been modified by the inhibiting treatments tested. It was found that a similar performance was achieved for the TTS, ODTMS and HFTMS treatments, all significantly decreasing the amount of water that was adsorbed. The ODA treatment did not perform as effectively, and allowed considerably more water to be adsorbed into the iron oxyhydroxide. Floatation tests to assess the amount of debonding due to hydrolysis that occured for each treatment over a 6 month period of time, were also carried out. This test showed that the amine treatment immediately debonded from the corrosion product surface when placed in water, showing that the bonding interaction between the amine and the iron oxyhydroxide surface is easily hydrolysed. This indicates that amines would not make successful long

term surface modification treatments. Electrochemical monitoring of corroded iron electrodes treated with the modification treatments, also showed that all treatments had some effect in reducing the corrosion rate of iron.

Accelerated corrosion tests were performed to assess the actual inhibiting abilities of each treatment against atmospheric corrosion. High humidity and elevated temperature conditions were chosen to accelerate the corrosion process so that the effects of the treatments could be assessed in a period of weeks. Initial experiments were carried out on archaeological iron nails and further tests carried out on test coupons, specifically designed to mirror the type of corrosion occurring in archaeological iron.

A method of preparing coupons was devised so that a corrosion product layer would exist on each coupon. An initial method, method A, was devised by which iron coupons were corroded above 1M HCl at 40°C for one week in a desiccator. This method produced an adherent but complex and variable corrosion layer. A second method was devised, method B, which would lead to more standardised coupons. This would allow easier interpretation of accelerated corrosion test results, with quantifiable margins of error that would allow statistical analysis of results to be carried out. The corrosion layer was synthesised so that it would contain β-FeOOH, the corrosion product known to contain chloride ions and to be present in marine iron, or iron buried in environments with high concentrations of chloride ions. It is the presence of this iron oxyhydroxide that is a product of, or indicator of active corrosion occurring in archaeological iron. The most appropriate method was found to be the corrosion of the coupons over 1M HCl in a glass tank at 40°C for one week, followed by dipping each coupon in 1M HCl and drying in air. β-FeOOH is thought to be produced from the precipitation of β-$Fe_2(OH)_3Cl$ from the pore solution of the coupons corrosion products. This then aerially oxidates to β-FeOOH.

The TTS surface treatment was judged to be the most effective treatment, based on its ability to inhibit corrosion and its suitability for use as a conservation treatment. The success of the TTS treatment may be related to its higher density of hydrophobic chains, having three chains on each inhibitor molecule as compared to one chain on each of the other treatments. The treatment involves immersing the iron object in a solution of TTS in

toluene at 35°C for 12 hours. A 0.1M solution was found adequate to give a maximum surface coverage. Following the immersion the surface coating is cured at 45°C for 12 hours so that chemical bonds are formed between the TTS molecules and the surface hydroxyl groups on corrosion product surfaces. The treatment can be used to treat archaeological iron after desalination treatments such as soxhlet washing have been carried out.

The TTS treatment has been considered as suitable for the conservation of archaeological iron. Although not reversible, the treatment fits the ethic of minimal intervention. It is non destructive and only changes the object by the addition of a monomolecular surface layer. The treatment does not change the colour or appearance of an object and is cheap, non-toxic and simple to apply.

The polyfluorinated silane, HFTMS, was found to accelerate rather than inhibit corrosion. This result was unexpected as the HFTMS treatment has been shown from water adsorption isotherms and floatation tests to form a hydrophobic coating which is not easily hydrolysed and removed from the iron oxyhydroxide surface. The reason for the failure of this treatment is not fully understood. It is suggested that the high reactivity of the HFTMS molecule leads to extensive polymerisation before a surface layer has formed on the iron oxyhydroxide corrosion product. This leads to the presence of flaws and gaps within the coating which causes differential aeration cells to occur, accelerating the rate of corrosion.

Several forms of the conducting polymer corrosion inhibitor, polyaniline (PANI) were synthesised and tested as corrosion inhibiting coatings for archaeological iron. The undoped polymer, and polyaniline doped with camphor sulphonic acid were synthesised. The polymers were soluble in the solvent N-methyl pyridinone (NMP) and such solutions were used to coat archaeological iron nails and corroded coupons. Accelerated corrosion tests showed that the polymers did not inhibit corrosion. It is thought that these inhibitors must be in electrical contact with the metal surface to inhibit corrosion, and are therefore not suitable as conservation treatments for archaeological iron objects that are inevitably covered in corrosion products

In conclusion, the titanate, TTS was found to be successful in reducing the corrosion of archaeological iron nails and corroded coupons in accelerated corrosion tests. Some question still remains as to whether this treatment would significantly add to the long term stability of archaeological iron, and in particular iron from marine or high chloride environments. It is recommended that long term testing of the TTS titanate surface modification treatment, used on its own, and after desalinating washing procedures, should be carried out on archaeological objects in museum environments.

APPENDIX A

FTIR Data

Figure A1.1 FTIR spectrum of α-FeOOH treated with ODTMS

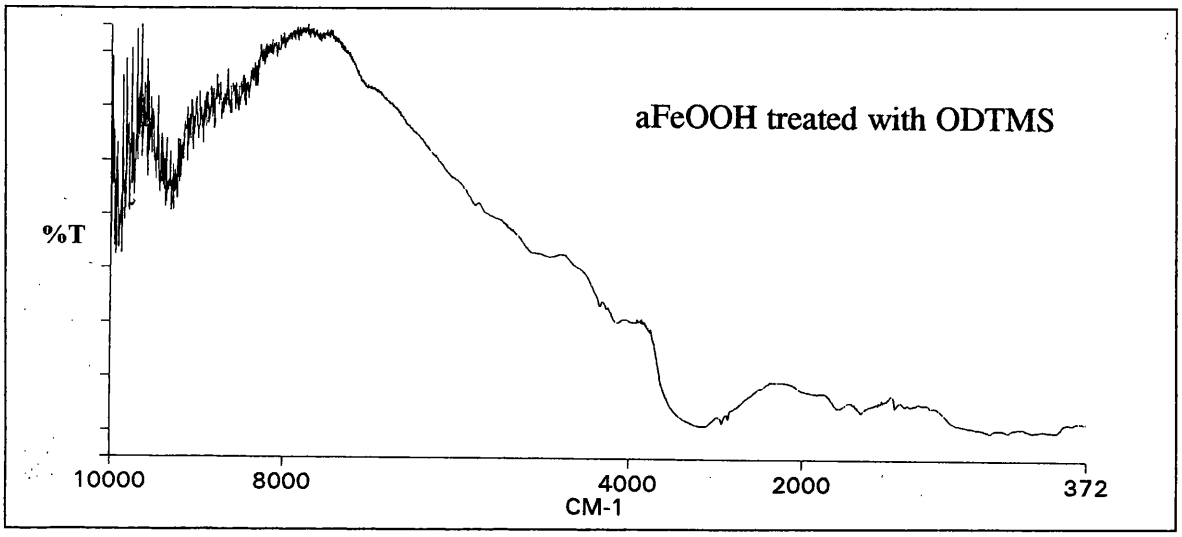

Figure A1.2 FTIR spectrum of α-FeOOH treated with ODTMS after the subtraction of α-FeOOH spectrum

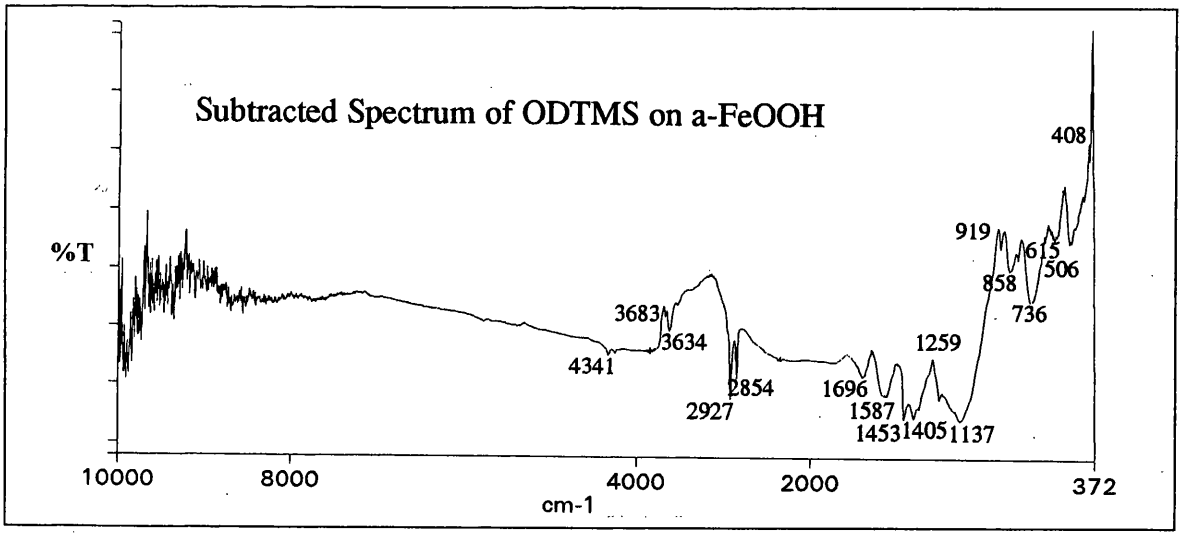

Figure A1.3 FTIR spectrum of ODTMS

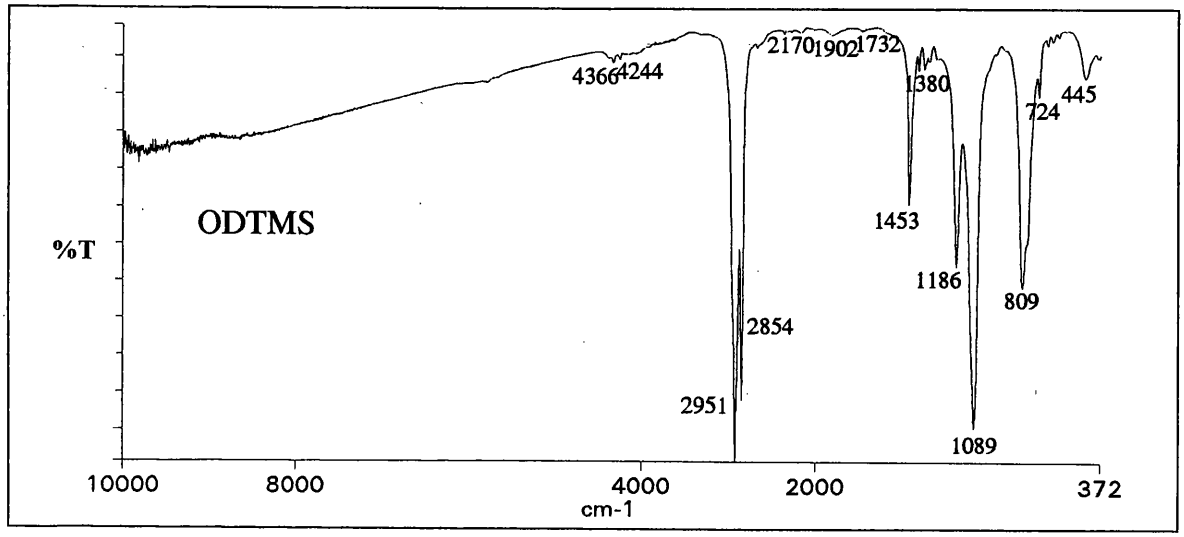

Figure A2.1 FTIR spectrum of β-FeOOH treated with ODTMS

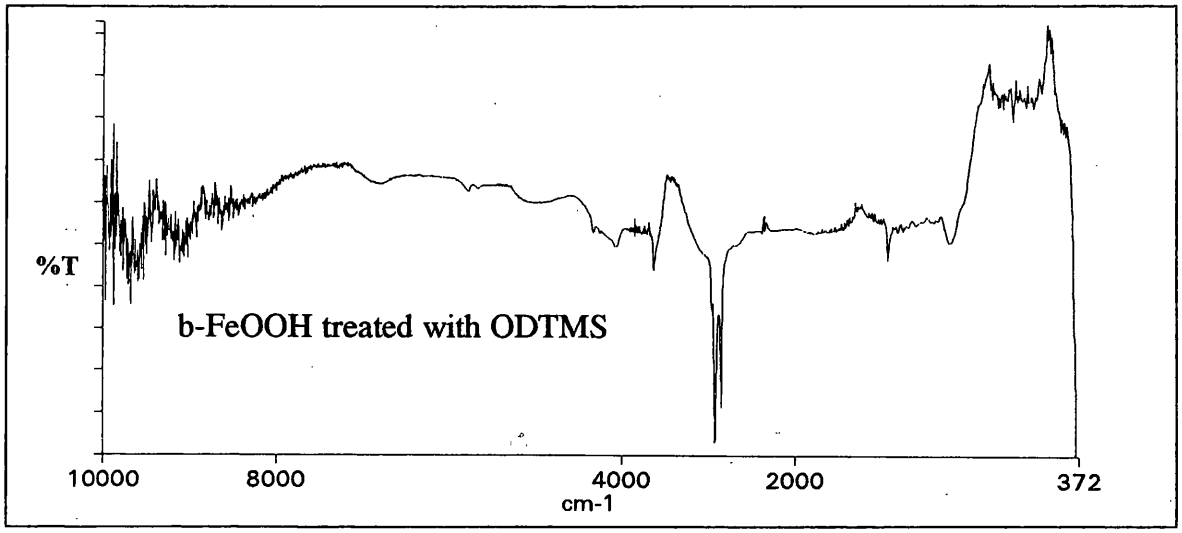

Figure A2.2 FTIR spectrum of β-FeOOH treated with ODTMS after the subtraction of β-FeOOH spectrum

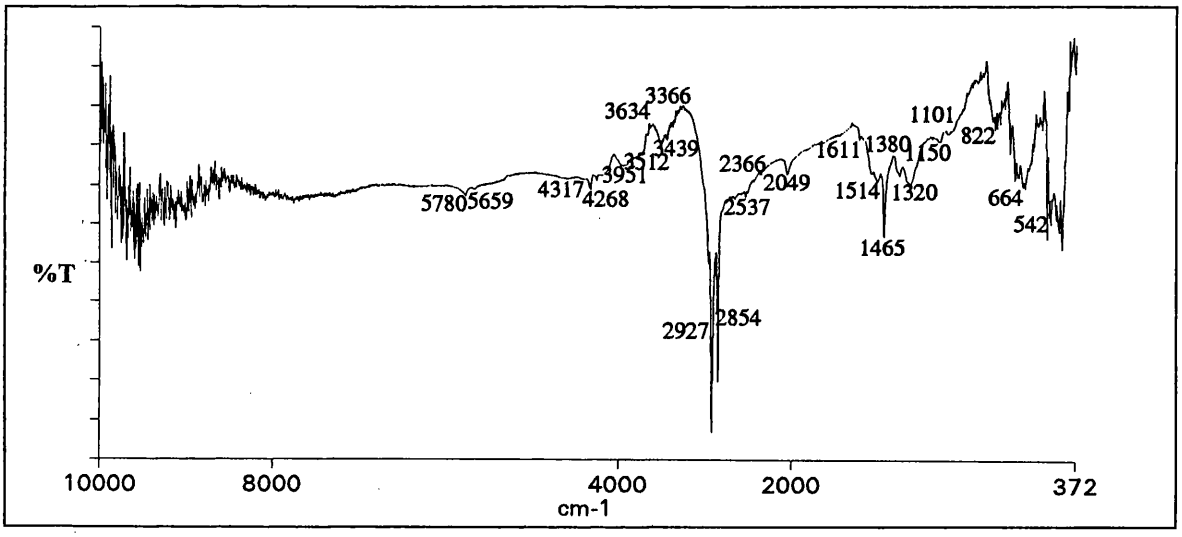

Figure A2.3 FTIR spectrum of ODTMS

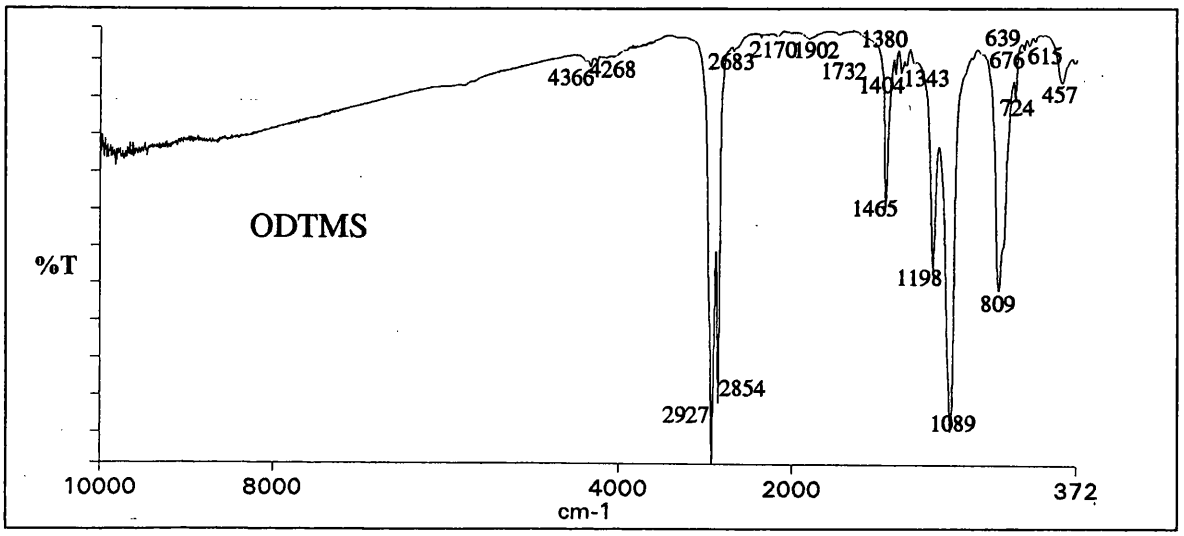

Figure A3.1 FTIR spectrum of α-FeOOH treated with HFTMS

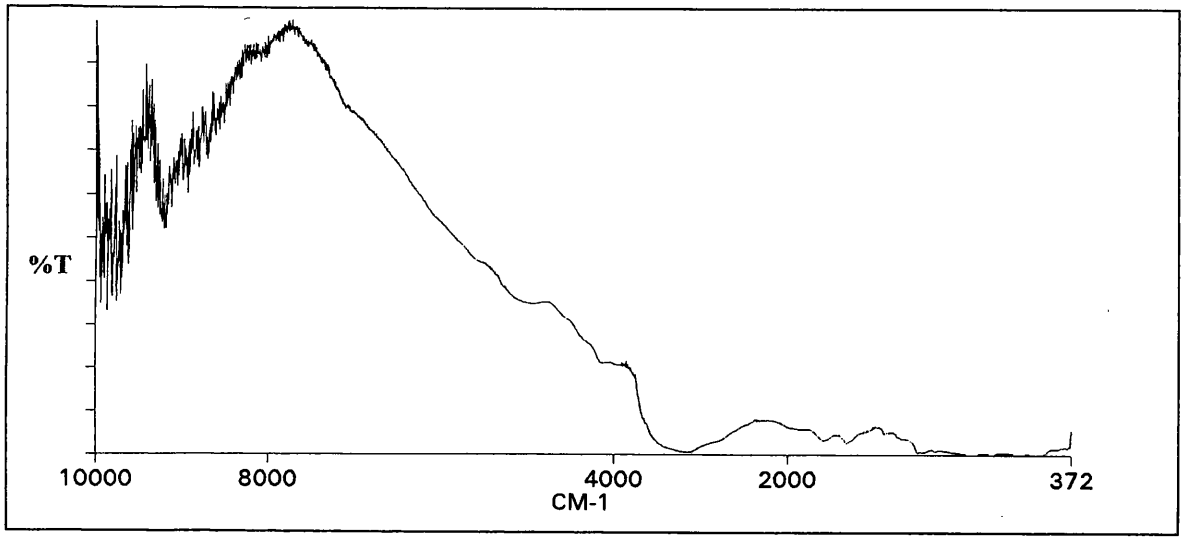

Figure A3.2 FTIR spectrum of α-FeOOH treated with HFTMS after the subtraction of α-FeOOH spectrum

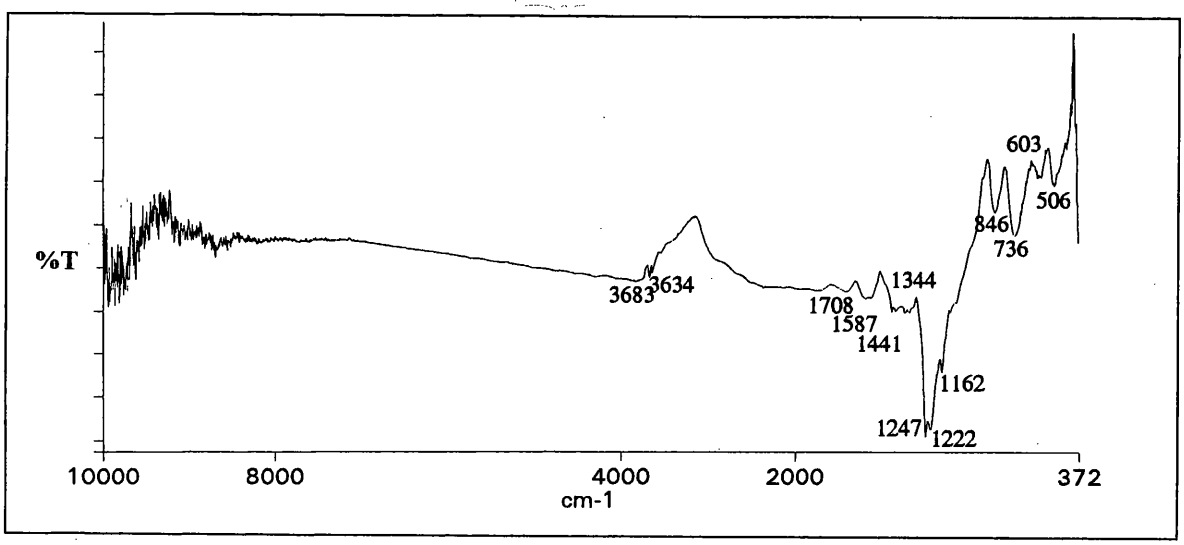

Figure A3.3 FTIR spectrum of HFTMS

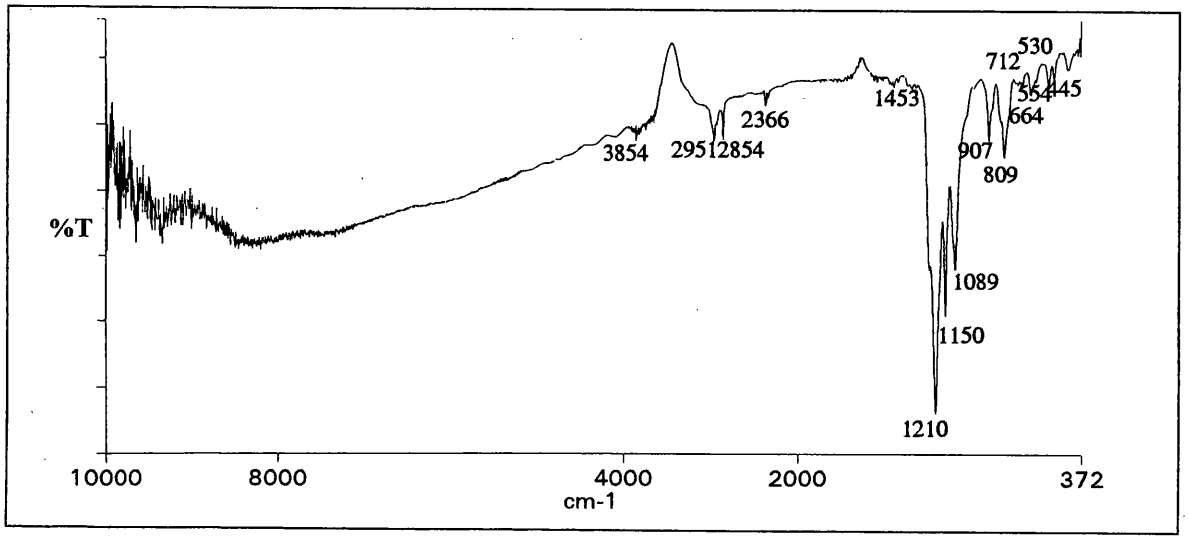

Figure A4.1 FTIR spectrum of β-FeOOH treated with HFTMS

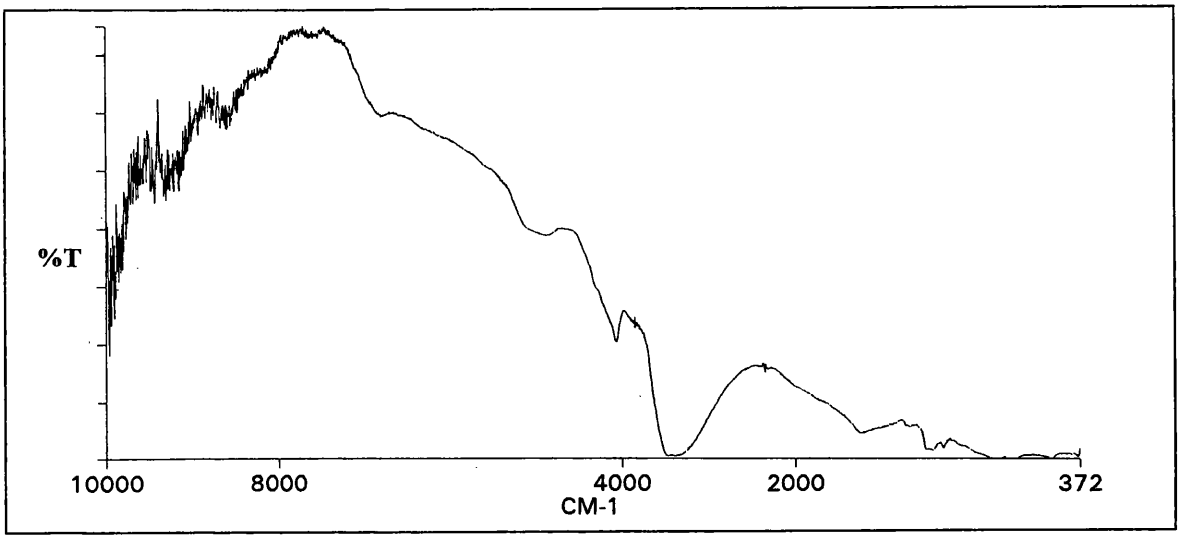

Figure A4.2 FTIR spectrum of β-FeOOH treated with HFTMS after the subtraction of β-FeOOH spectrum

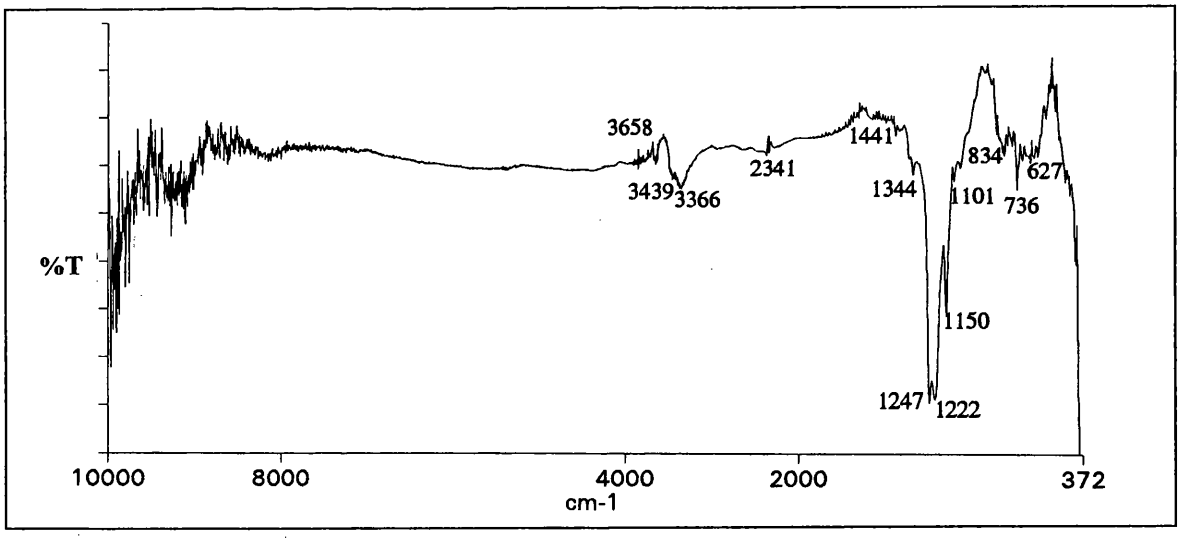

Figure A4.3 FTIR spectrum of HFTMS

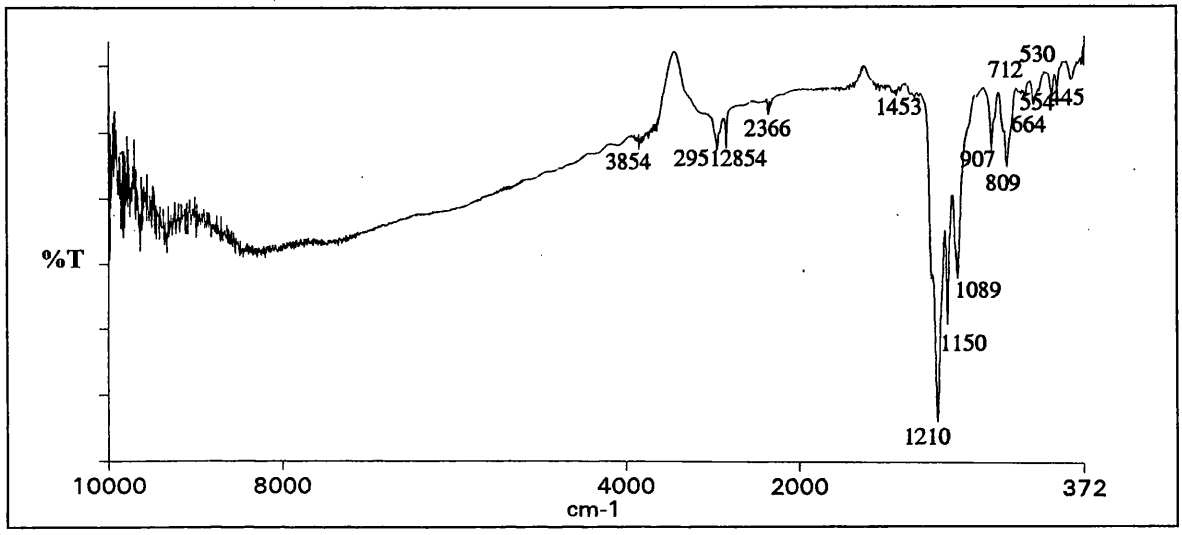

Figure A5.1 FTIR spectrum of α-FeOOH treated with TTS

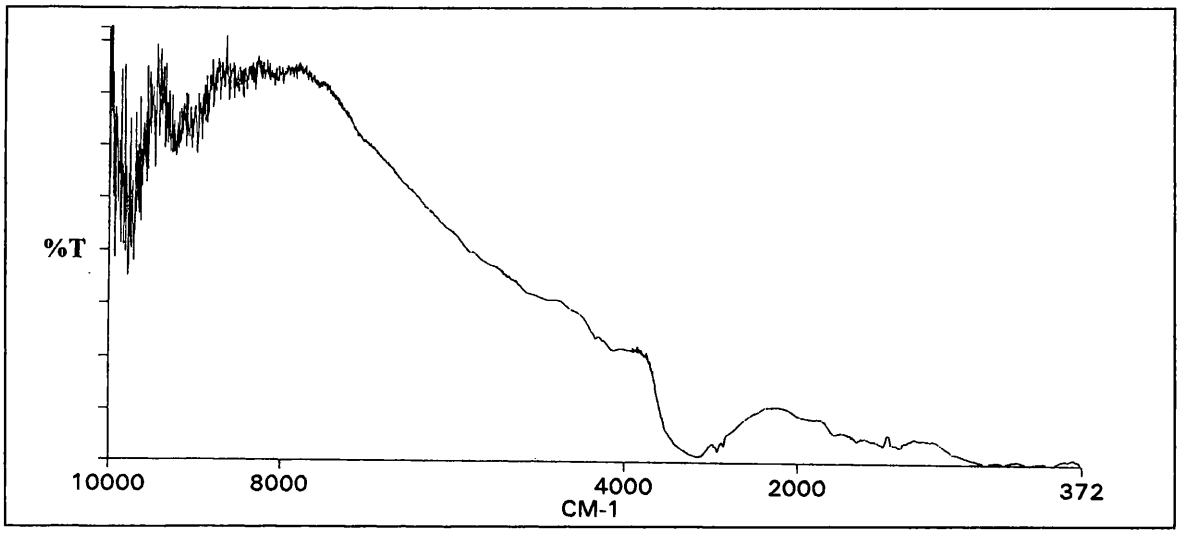

Figure A5.2 FTIR spectrum of α-FeOOH treated with TTS after the subtraction of α-FeOOH spectrum

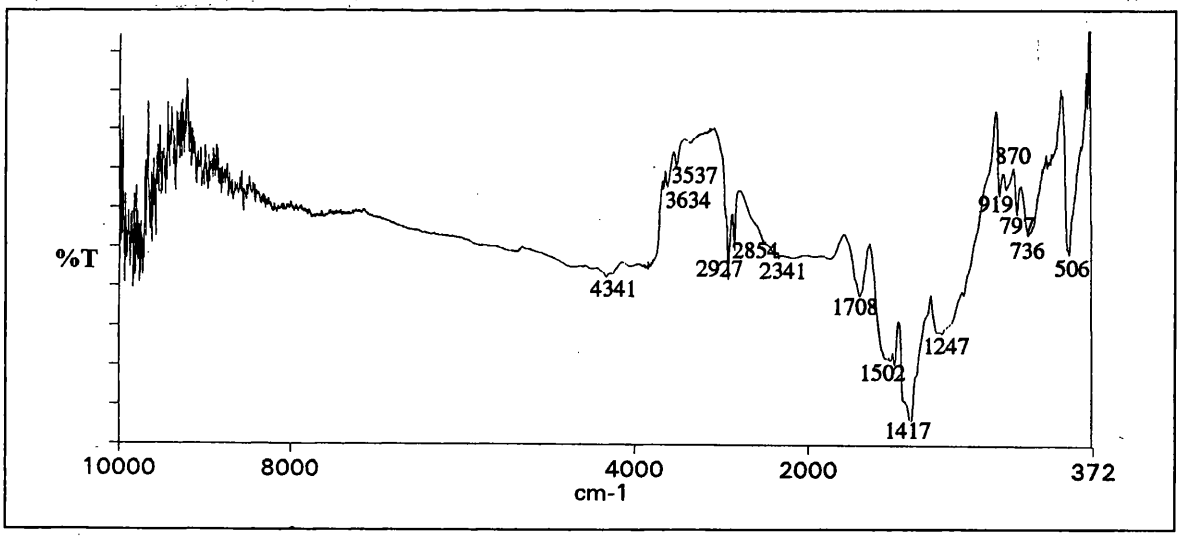

Figure A5.3 FTIR spectrum of TTS

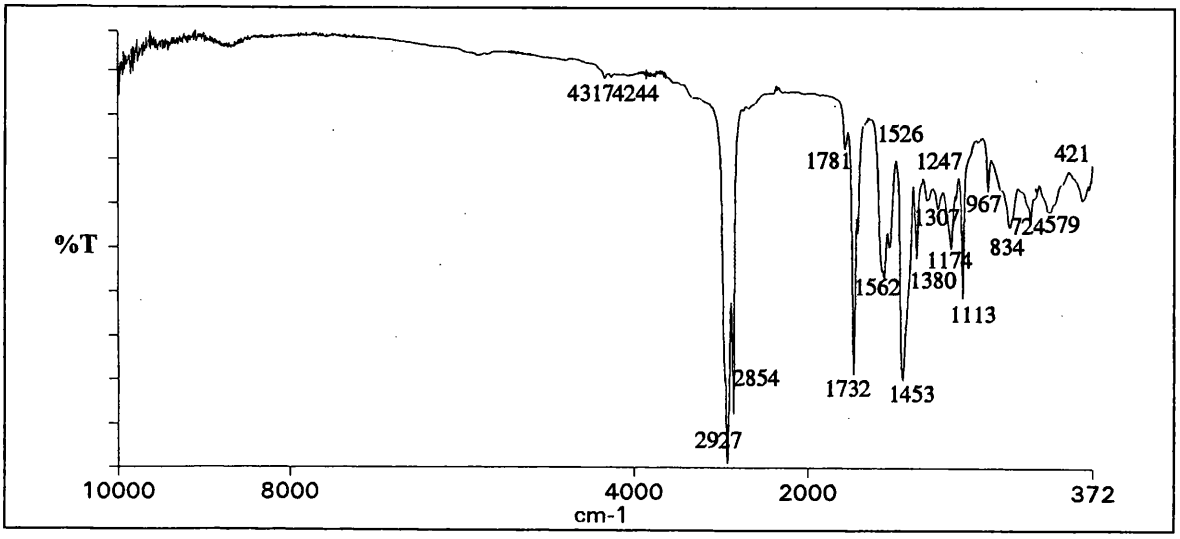

Figure A6.1 FTIR spectrum of β-FeOOH treated with TTS

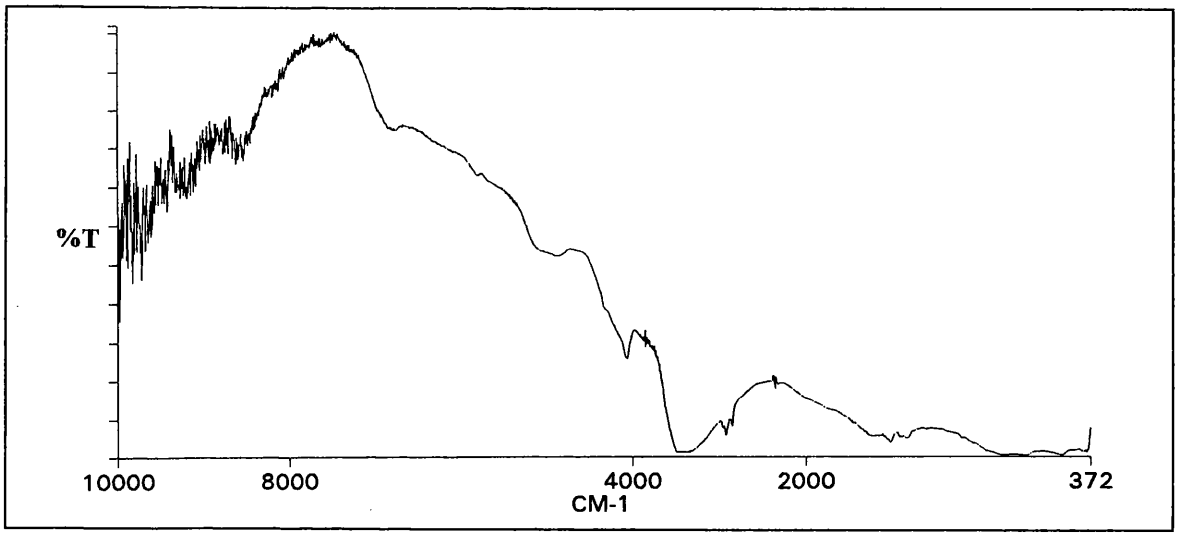

Figure A6.2 FTIR spectrum of β-FeOOH treated with TTS after the subtraction of β-FeOOH spectrum

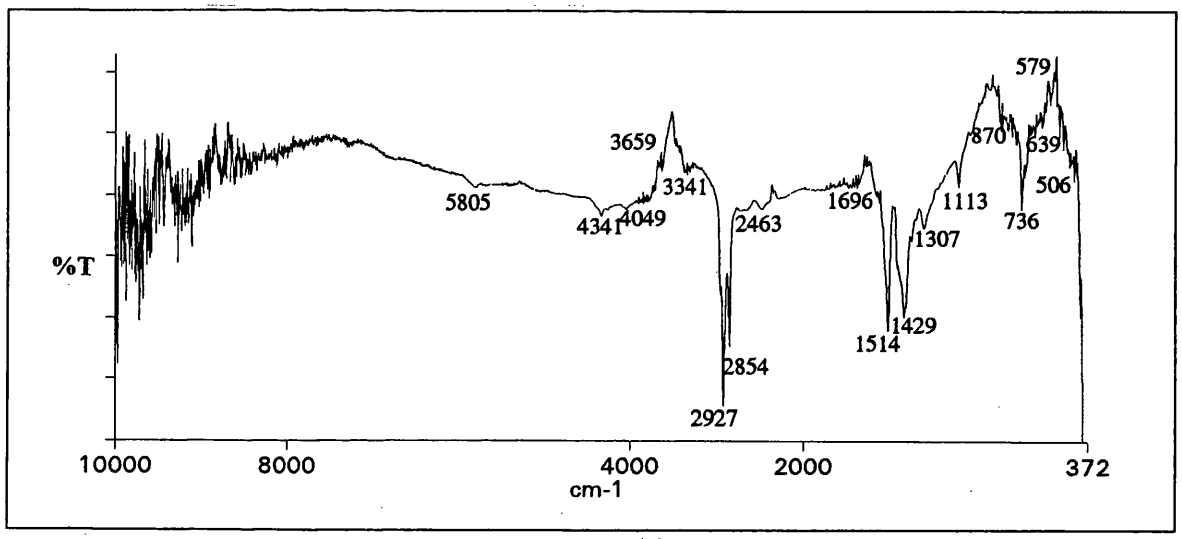

Figure A6.3 FTIR spectrum of TTS

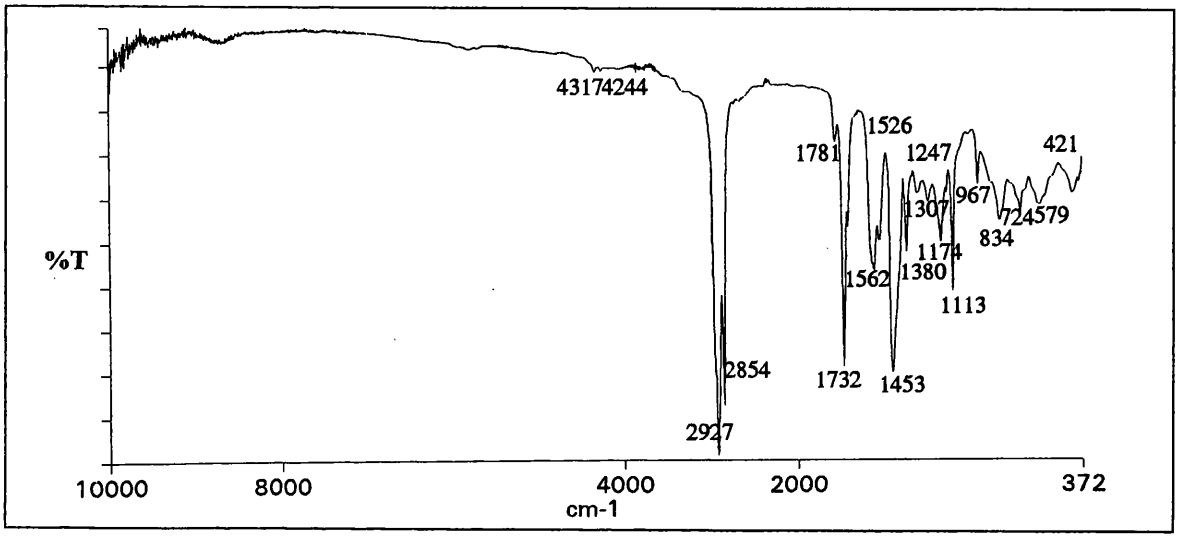

Figure A7.1 FTIR spectrum of α-FeOOH treated with ODA

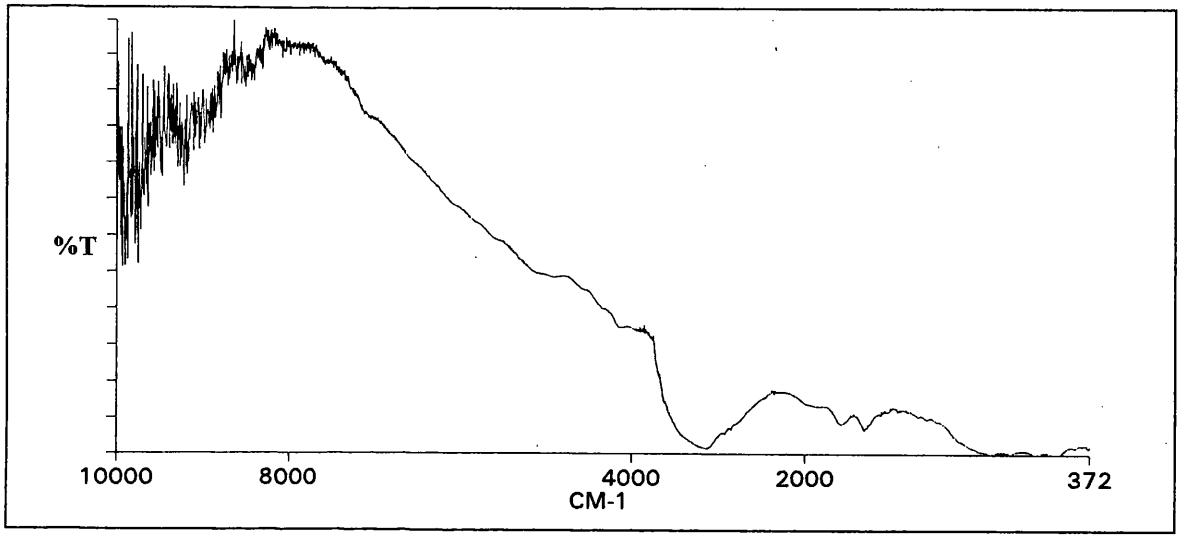

Figure A7.2 FTIR spectrum of α-FeOOH treated with ODA after the subtraction of α-FeOOH spectrum

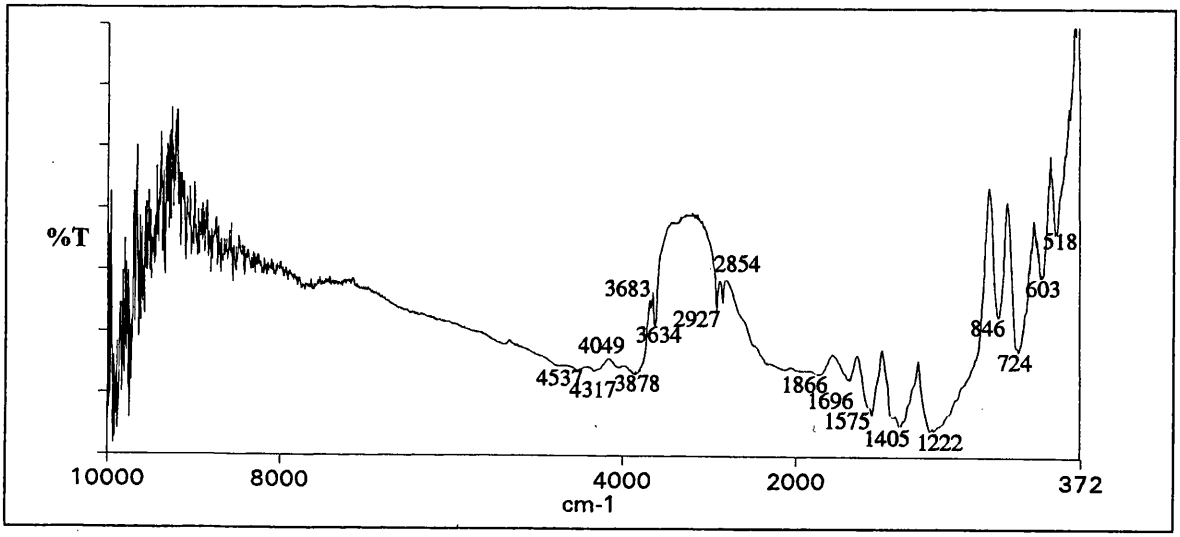

Figure A7.3 FTIR spectrum of ODA

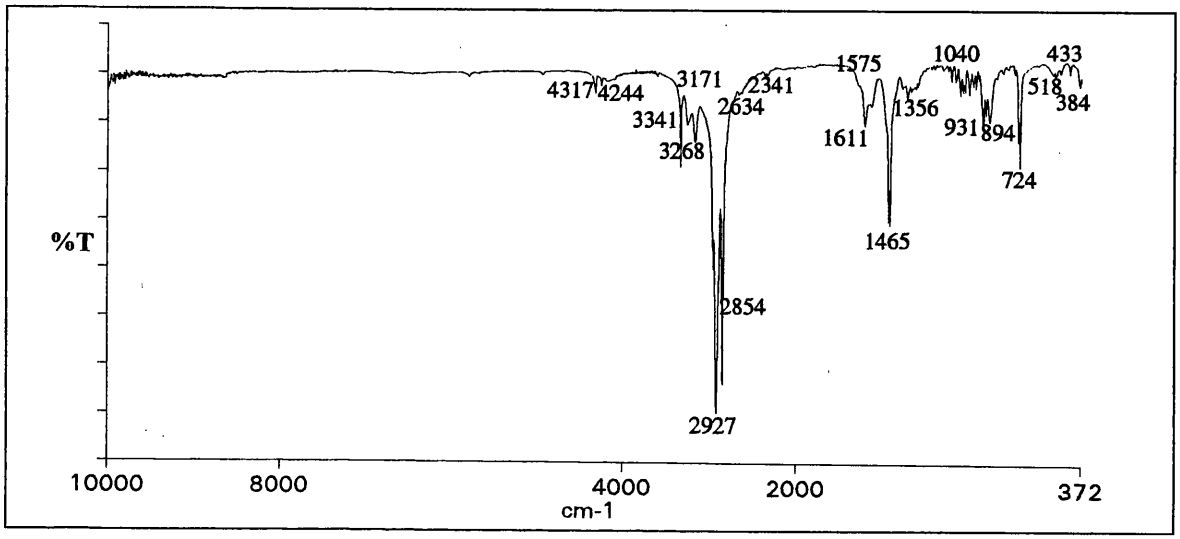

Figure A8.1 FTIR spectrum of β-FeOOH treated with ODA

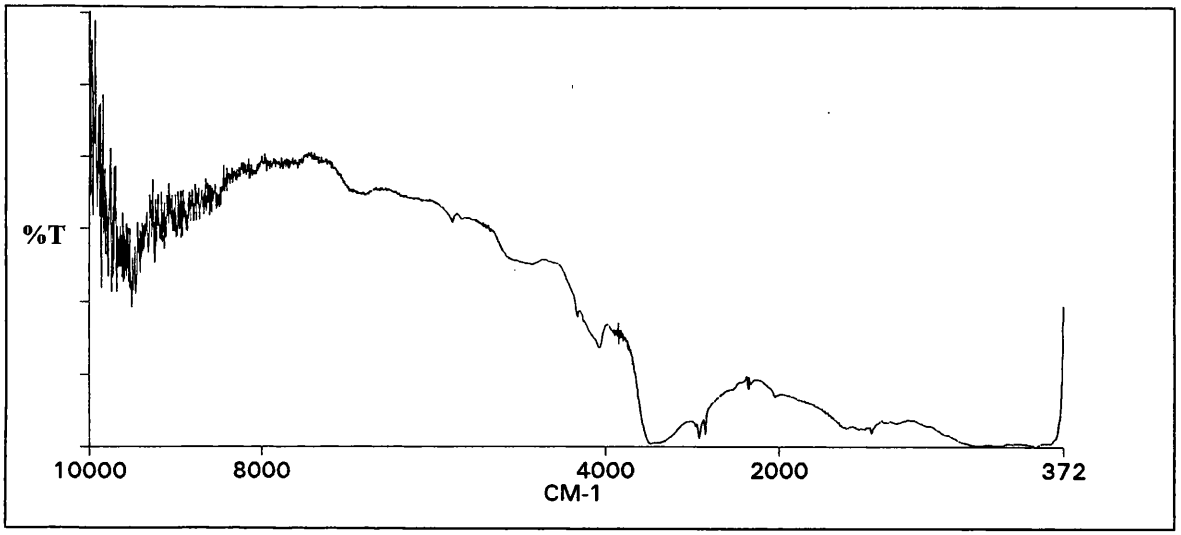

Figure A8.2 FTIR spectrum of β-FeOOH treated with ODA after the subtraction of β-FeOOH spectrum

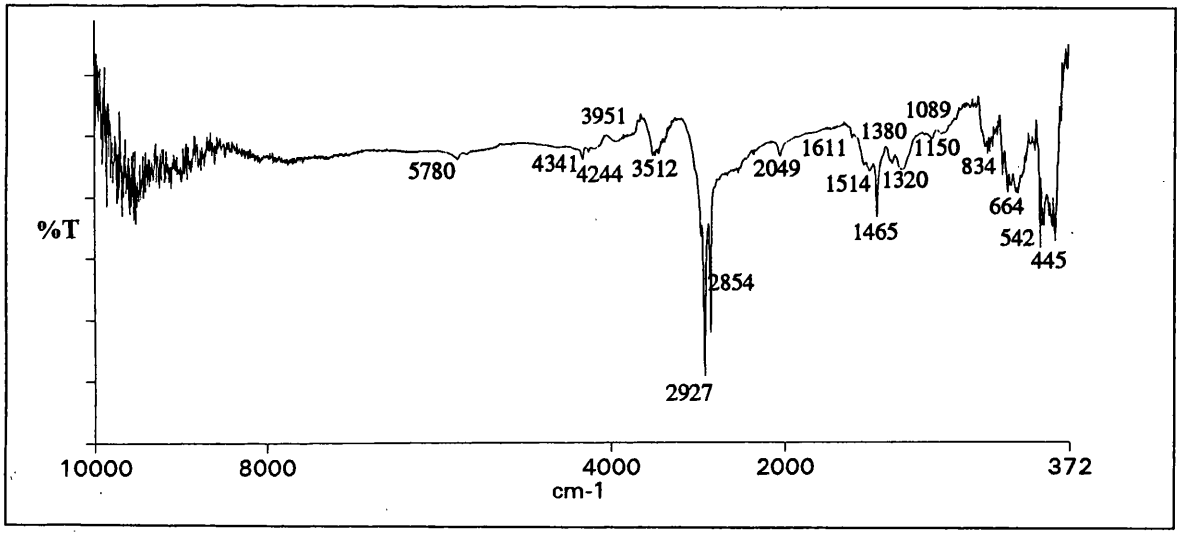

Figure A8.3 FTIR spectrum of ODA

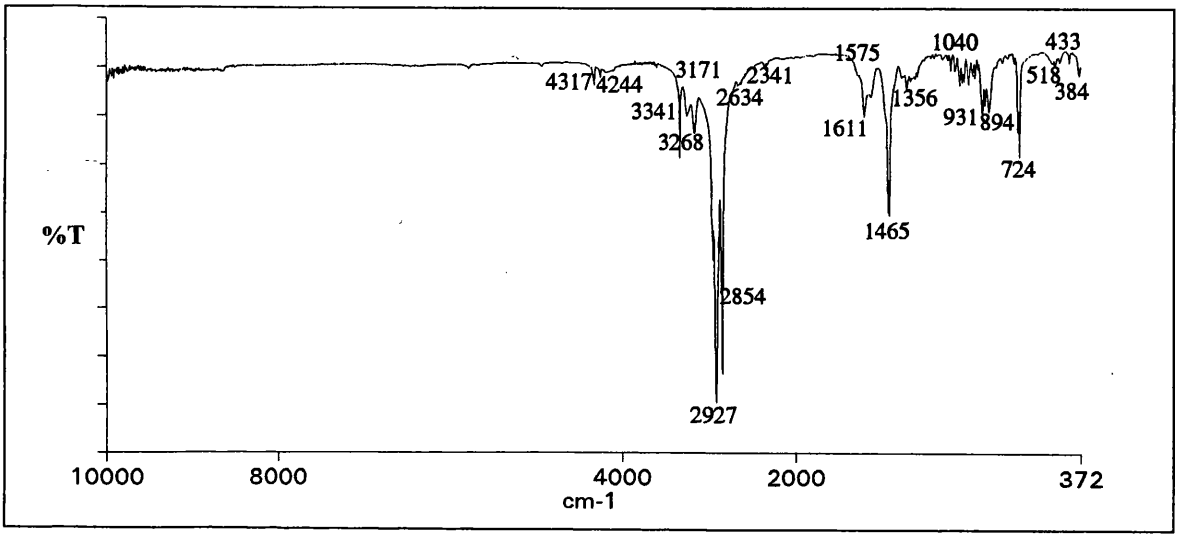

REFERENCES

AHMAD, N., and A.G. MACDIARMID, (1996). Inhibition of corrosion of steels with the exploitation of conducting polymers. *Synthetic Metals*, **78**: 103-110

AL AHMED, Z., (1992). *A new approach for the stabilisation of archaeological iron objects*. Unpublished PhD thesis, University of London.

AMBROSE, T., AND C. PAINE, (1993). *Museum basics*. London: ICOM in conjunction with Routledge.

ANDROPOV, L.I., V.M. LEDOVSKIKH and N.F. KULESHOVA, (1974). The influence of the structure of pyridine bases and diamines as inhibitors on the corrosion of iron in distilled water, translated from *Zashchita Metallov*, **9** (2): 166-170.

ANGELOPOULOS, M., G.E. ASTUNAS, S.P. ERMER, A. RAY, E.M. SCHERR, A.G. MACDIARMID, M. AKHTOR, Z. KISS and A.J. EPSTEIN, (1988). Polyaniline - solutions, films and oxidation state, *Molecular Crystals and Liquid Crystals*, **160**: 151-163

ANGUS, N.S., G.T. BROWN and H.F. CLEEVE, (1962). The iron nails from the Roman legionary fortress at Inchtuthil, Perthshire. *Journal of the Iron and Steel Institute,* **200** (2): 956-967.

ANRAKU, T., S. OLEKI, K. KANEKO and K. INOUYE, (1983). Abstract of the 47th symposium of the Chemical Society of Japan,**1U**: 15

AOKI, A., Y. HIRAO, S. HIRAI and H. KUBOTA, (1989). Stabilization of archaeological iron, in S. AOKI (ed), *Current problems in the conservation of metal antiquities, The 13th international symposium on the conservation and restoration of cultural property, Tokyo,*

October 4 - October 6, 1989. Tokyo: Tokyo National Research Institute of Cultural Properties.

ARCHER, P., and B.D. BARKER, (1987). Phase changes associated with the hydrogen redcution conservation process for ferrous artifacts, *Journal of the Historical Metals Society*, **21** (2): 86.

ARGO, J., (1981). On the nature of 'ferrous' corrosion products on marine iron, *Studies in Conservation,* **26**: 42.

ARGO, J., (1982). The treatment of corrosion with amines, *Conservation News*, **17**: 7.

ARGO, J., (1985). Amines and Iron Stabilisation, in S. KEENE (ed), *Corrosion inhibitors in conservation, the proceedings of a conference held by UKIC in association with the Museum of London*: Occasional papers, United Kingdom Institute for Conservation: no.4.

ARKLES, B., (1977). Tailoring surfaces with silanes. *Chemical Technology*, **7**.(12): 766-777

ARRHENIUS, O., L. BARKMAN, and E. SJÖSTRAND, (1973). Conservation of old rusty iron objects: reduction of rust with hydrogen gas. *National Swedish Maritime Museum and Swedish Corrosion Bulletin No. 61E*, Stockholm: Swedish Corrosion Institute.

ASTM, (1997), *Annual Book of ASTM standards, Vol 3.02, Wear and Errosion; Metal Corrosion, Metals Testing Methods and Analytical Procedures*. Philadelphia: American Society for Testing and Materials.

ATKINS, P., (1990). *Physical Chemistry*. Fourth edition. Oxford: Oxford University Press.

ATKINSON, R.J., A.M. POSENER and J.P. QUIRK, (1967). Adsorption of potential-determining ions at the ferric oxide-aqueous electrolyte interface. *Journal of Physical Chemistry*, **71**: 550.

ATKINSON, R.J., A.M. POSENER, and J.P. QUIRK, (1968). Crystal nucleation in Fe (III) solutions and hydroxide gels. *Journal of Inorganic and Nuclear Chemistry*, **30**: 2371.

BABOIAN, R., (1995). *Corrosion Tests and Standards, Application and Interpretation. Manual Series: MNL 20.* Philadelphia: American Society for Testing and Materials.

BALLHAUSEN, C.J., and H.B. GRAY, (1965). *Molecular orbital theory: an introductory lecture*. New York: Benjamin Inc.

BANERJEE, G., and S.N. MALHOTRA, (1992). Contribution to adsorption of aromatic amines on mild steel surface from HCl solutions by impedance, UV, and Raman spectroscopy. *Corrosion*, **48** (1): 10-15.

BANGA, R., J. YARWOOD, A.M. MORGAN, B. EVANS, and J. KELLS, (1995). FTIR and ATM studies of the kinetics and self-assembly of alkyltrichlorosilanes and (perfluoroalkyl) trichlorosilanes onto glass and silicon. *Langmuir*, **11**: 4393-4399.

BARKER, J.D., K. KENDELL, and C. O'SHEA, (1982). The hydrogen reduction process for the conservation of ferrous objects, in. R. W. CLARKE, and S.M. BLACKSHAW (eds), *Conservation of Iron. Greenwich, Proceedings of a symposium held at the National Maritime Museum, Greenwich on Friday, 4th July, 1980.* National Maritime Museum Monograph No. 53: 23-27. National Maritime Museum: Trustees of the National Maritime Museum.

BARSCH, U., and F. BECK, (1993). Electrodeposition of Polythiophene from Bisthiophene onto iron. *Synthetic Metals*, **55-57**: 1638-1643.

BASCOM, W.D., (1968). The Wettability of Fluoro- and Chlorocarbon Trialkoxysilane Films Adsorbed on Glass and Metal Surfaces. *Journal of Colloid and Interface Science*, **27** (4) :789-796.

BATRAKOV, V.V., I.G. GORICHEV, T.V. MARTYNOVA and A.V. GUTENEV, (1994). Regularities of Adsorption of Ions and Surfactants on metal corrosion products and salt deposits. *Protection of Metals*, **30** (1): 76-82.

BELLAMY, L.J., (1975). *The Infrared Spectra of Complex Molecules*. London: Chapman and Hall.

BERNAL, J.D., D.R. DASGUPTA and A.L. MACKAY, (1959). The oxides and hydroxides of iron and their structural inter-relationships. *Clay Mineralogical Bulletin*, **4**: 15.

BESSIÈRE, J., M. KHAYAR and A. ETAHIRIR, (1995). Impedance studies of the adsorption of hydrophobic and hydrophilic species on mineral pulps. *Analytica Chimica Acta*, **305**: 265-268.

BLECK, R.D., (1978). On the desalination of archaeological iron finds from the earth in anhydrous medium. *Conservation of iron objects found in a salty environment.* Warsaw: Historical Monuments Documentation Centre.

BRADLEY, S., H. NEWLEY, L. LEE, J. LANG, P. CRADDOCK, S. WATKINS, F. SHEARMAN and D. THICCKETT, (1997). Assessment of the plasma treatment for archaeological iron objects in the collections of the British Museum. *Conservation of metal objects in low-pressure hydrogen plasma, proceedings of the international symposium held at the Swiss national museum, Zurich, October 28th and October 29th 1996.* Revue Suisse d'Art et d'Archeologie, Band 54, Heft1. Zurich: Verlag Karl Schwegler.

BRASHER, D.M., (1962). Role of the anion in relation to metallic corrosion and inhibition. *Nature*, **193**: 868.

BRAUN, R.D., E.E. LOPEZ and D.P. VOLLMER, (1993). Low molecular weight straight-chain amines as corrosion inhibitors. *Corrosion Science*, **34** (8): 1251-1257.

BRESLE, A., (1974). A method and composition for reducing the rusting of particles of iron, steel or ferrous alloys. *British Patent No. 1,358,146.*

BRINCH MADSEN, H., (1985). Benzotriazole: a perspective, in. R. W. CLARKE, and S.M. BLACKSHAW (eds), *Conservation of Iron. Greenwich, Proceedings of a symposium held at the National Maritime Museum, Greenwich on Friday, 4th July, 1980.* National Maritime Museum Monograph No. 53: 23. National Maritime Museum: Trustees of the National Maritime Museum.

BRITT, D.W., and V. HLADY, (1999). Protonation, Hydrolysis, and Condensation of Mono- and Trifunctional Silanes at the Air/Water Interface. *Langmuir*, **15**: 1770-1776.

BROUSSEAU, J-L., S. VIDON, and R.M. LEBLANC, (1998). Investigation of the chemical nature of two-dimensional polymerized octadecyltrimethoxysilane Langmuir films by inelastic electron tunneling spectroscopy. *Journal of Chemical Physics*, **108** (17): 7391-7396.

BRUNAUER, S., S.W. DEMING, L.S. DEMING, and E. TELLER, (1940). On a theory of the van der waals adsorption of gases. *Journal of American Chemical Society*, **62**: 1723.

BRUNE, D., R. HELLBORG, H.J. WHITLOW and O. HUNDERI, (eds), (1997). *Surface Characterization, A User's Sourcebook.* Weinheim: Wiley-VCH.

BUCHWALD, V.F., and R.S. CLARKE, (1989). Corrosion of Fe-Ni alloys by Cl-containing akaganeite (β-FeOOH): The Antarctic meteorite case. *American mineralogist*, **74**: 656-667.

BUCHWALD, V.F., and C.B. KOCH, (1995). Hibbingite, A chloride rich corrosion product in meteorites and ancient iron objects. *Meteoritics*, **30** (5): 493.

CAHN, (1992). *Cahn D-200 Instruction Manual.* Cerritos.

CARPENTER, J., and I.D. MACLEOD, (1993). Conservation of Corroded Iron Cannon and the Influence of Degradation on Treatment Times, in J. BRIDGLAND (ed), *ICOM Committee for Conservation, 10th Triennial Meeting, Washington DC, USA, 22-27 August 1993.*

CARROL, M., K. TRAVIS, and J. NOGGLE, (1975). Structure-corrosion inhibition studies of polyfunctional metal chelating compounds. *Corrosion*, **31**: 123.

CARTER, V.E., (1982). *Corrosion Testing for Metal Finishing*, Oxford: Butterworth Scientific.

CHENG, J., M. FONE and M.W. ELLSWORTH, (1996). Solid state NMR study on the conformation and mobility of n-octadecyl chains in a silane coupling agent attached to the surface of colloidal silica. *Solid State Nuclear Magnetic Resonance*, **7**: 135-140.

CHILDS, C.W., B.A. GOODMAN, E. PATERSON, and F.W.D. WOODHAMS, (1980). The Nature of Iron in Akaganeite (β-FeOOH). *Australian Journal of Chemistry*, **33**: 15-26.

CHOVELON, J.M., L. EL AARCH, M. CHARBONNIER and M. ROMAND, (1995). Silanization of Stainless Steel Surfaces: Influence of Application Parameters. *Journal of Adhesion*, **50**: 43-58.

CHRISTIE, A.B., (1989). X-ray photoelectron spectroscopy, in, WALLS, J.M. (ed) *Methods of Surface Analysis*. Cambridge: Cambridge University Press: 127-168

CLARK, N.S., and P.G. HALL, (1991). Adsorption of water vapour by iron oxides. *Langmuir*, **7**: 672.

CORNELL, R.M., and S. MANN, (1983). A high-resolution electron microscopy examination of domain boundaries in crystals of synthetic geothite. *Journal of the Chemical Society, Faraday Transactions 1*, **79**: 2679.

CORVO, F., A.R. MENDOZA, M. AUTIE and N. BETANCOURT, (1997). Role of water adsorption and salt content in atmospheric corrosion products of steel. *Corrosion Science*, **39** (4): 815-820.

COULSON, C.B., R.I. DAVIES, and D.A. LEWIS, (1960). Polyphenols in plant humus and soil. *Journal of Soil Science*, **11**: 20.

COYNE, G.S., (1997). *The Laboratory Companion. A practical guide to materials, equipment and technique*. New York: John Wiley & Sons.

CRONYN, J.M., (1990). *The Elements of Archaeological Conservation*. London, Routledge.

CROW, D.R., (1994). *Principles and applications of electrochemistry*. 4th edition. London: Blackie Academic & Professional.

CULLER, S.R., H. ISHIDA and J.L. KOENIG, (1986). FT-IR Characterization of the Reaction of the Silane/Matrix Resin Interphase of Composite Materials. *Journal of Colloid and Interface Science*, **109** (1): 1-10.

DANIELS, V.D., (1981). Plasma reaction of silver tarnish on daguerreotypes. *Studies In Conservation*, **26**: 45.

DANIELS, V.D., L. HOLLAND, and M.W. PASCOE, (1979). Gas plasma reactions for the conservation of antiquities. *Studies In Conservation*, **24**: 85.

DAY, P., (1983). Low-dimensional solids. *Chemistry in Britain*, **April**: 308-312.

DEBERRY, D.W., (1985). Modification of the Electrochemical and Corrosion Behavior of Stainless Steels with an Electroactive Coating. *Journal of the Electrochemical Society*, **132** (5): 1022.

DEBERRY, D.W., and A.V. VIEHBECK, (1984). Properties of Active/Passive metals modified by electroactive coatings, in MCCAFFERTY, E., C.R. CLAYTON and J. OUDAR (eds) *Fundamental aspects of protection by surface modification*: 308-326. London: The Electrochemical Society softbound proceedings series.

DEMJEN, Z., B. PUKANSZKY, E. FOLDES and J. NAGY, (1997). Interaction of Silane Coupling Agent with $CaCO_3$. *Journal of Colloid and Interface Science*, **190**: 427-436.

DERNOVAYA, L.I., A.E. CHALYCH and Y.A. ELTEKOV, (1993). Adsorption properties of surface iron oxide modified with stearic acid and octadecylamine. *Pure & Applied Chemistry,* **65** (10): 2201-2204.

DESAI, M.N., G.H. THANKI, and M.H. GANHI, (1963). Thiourea and its derivatives as corrosion inhibitors. *Anti-corrosion manual.* London: Corrosion prevention and control: 12.

DOUSMA, J.A., T.J.VAN HOVEN and P.L. DE BRUYN, (1978). The Influence of Chloride Ions on the Formation of Iron (III) Oxyhhydroxide. *Inorganic and Nuclear Chemistry*, **40**: 1089-1093.

DUNCAN, S.J., (1986). Chloride removal from iron; a new technique. *Conservation News*, **31**: 21.

EHRENREICH, R.M., and D.K. STRAHAN, (1987). The effect of boiling on the quenched steel structure of Martensite, in J. BLACK (ed), *Recent Advances in the Conservation and Analysis of Artifacts.* London: Summer School Press, Institute of Archaeology, University College London: 125.

EICHHORN, P., (1975). Eisenonservierung und Restaurierung am Wuttembergischen Landesmusuem. *Arbeitsblatter*, **8** (1): 74.

ELDKAER, N., and K. NOBE, (1976). Effect of Tolytriazole on iron corrosion and the hydrogen evolution reaction in H_2SO_4. *Corrosion*, **32** (6): 238.

ELLIS, R.G., R. GIOVANOLI, and W. STUMM, (1976). Anion exchange properties of β-FeOOH. *Chimia*, **30**: 194.

EPSTEIN, A.J., J.M. GINDER, F. ZUO, R.W. BIGELOW, H.S WOO, D.B. TANNER, A.F. RICHTER, H-S. HUANG and A.G. MACDIARMID (1987). Insulator-to-Metal Translation in Polyaniline. *Synthetic Metals*, **18**:303

EVANS, U.R., (1951). Stress corrosion: Its relation to other types of corrosion. *Corrosion*, **7** (6): 238-244.

EVANS, U.R., (1960). *The corrosion and oxidation of metals*. London: Arnold.

EVANS, U.R., (1969). Mechanism of rusting. *Corrosion Science*, **9**: 813.

EVANS, U.R., and C.J.A. TAYLOR, (1972). Mechanism of Atmospheric rusting. *Corrosion Science*, **12**: 227.

EWING, F.G., (1935). The crystal structure of Lepidocrocite. *Journal of Physical Chemistry*, **3**: 420.

FABEH, E.W., and J. TRIER, (1978). Methods for treating marine iron, in Preprints of *ICOM Committee for Conservation, 5th Triennial Meeting, Zagreb, 1-8 October 1978.* Paris: International Council of Museums.

FALTERMEIER, R., (1995). *The evaluation of corrosion inhibitors for application to copper and copper alloy archaeological atefacts*. Unpublished PhD thesis, University of London.

FEITKNECHT, W., and G. KELLER, (1950). Die dunkelgrunen hydroxyverbind ungen des Eisen. *Zeitschrift fur anorgaische Chemie*, **262**: 61.

FENN, J.D., and K. FOLEY, (1975). Passivation of iron, In D. LEIGH (ed), *Conservation In Archaeology and the Applied Arts: preprints of the contributions to the Stockholm Congress 2-6 June 1975*. London: The International Institute for Conservation of Historic and Artistic Works.

FIELDING, H.C., (1979). Organofluorine Surfactants and Textile Chemicals. Organofluorinbe Chemicals and their Industrial Applications. In R.E. BANKS (ed), *Fluorocarbons and their derivatives*, 2nd Edition. London: Macdonald & Co.

FLINN, D.H., D.A. GUZONAS and R-H YOON, (1994). Characterization of Silica Surfaces hydrophobized by octadecyltrichlorosilane. *Colloids and Surfaces. A: Physicochemical and Engineering Aspects*, **87**: 163-176.

FOCKE, W.W., G.E. WNEK and Y. WEI, (1987). Influence of oxidation-state, pH and counterion on the conductivity of Polyaniline. *Journal of Physical Chemistry*, **91** (22): 5813-5818.

FOLEY, R.T., (1970). Role of the Chloride Ion in Iron Corrosion. *Corrosion*, **26** (2): 58-70.

FOLEY, R.T., (1977). Measures for preventing corrosion of metals, in B. FLOYD BROWN (ed) *Corrosion and metal artefact: a dialogue between conservators and archaeologists and corrosion scientists*, NBS special publication 479: 67.Washington DC: National Bureau of Standards.

FONTANA, M.G., (1987). *Corrosion Engineering*. 3rd Edition. New York: McGraw-Hill Book Company.

FUJII, S., and K. ARAMAKI,. (1960). Amine-type corrosion inhibitors and their chemical structures,. *1st European Symposium of Corrosion Inhibition, Ferrara, Italy*. 215-227.

GAINES, G.L., (1982). Langmuir-Blodgett films of long-chain amines. *Nature*, **298**: 298.

GALBRAITH, S., S.T. Talbraith, T. Baird and J.R. FRYER, (1979). Structural changes in β-FeOOH caused by radiation damage. *Acta Crystallogripha*, **A35**: 197-200.

GALLAGHER, K.J., (1970). The atomic structure of tubular subcrystals of β-Iron (III) oxide hydroxide. *Nature*, **226**: 29.

GALLAGHER, K.J, and PHILLIPS, D.N, (1969). Hydrogen exchange studies and proton transfer in β-iron (III) Oxyhydroxide. *Chimia*, **23**: 465.

GANAIRIS, H., (1998). *Personal. communication.*

GANGULY, P., D.V. PARANJAPE and M. SASTRY, (1993). Novel structure of Langmuir-Blodgett films of chloroplatinic acid using n-octadecylamine: evidence for interdigitation of hydrocarbon chains. *Journal of American Chemistry Society*, **115**: 793-794.

GENIN. J-M.R.., P.REFAIT, A.A. OLOWE, M. ABDELMOULA, I. FALL and S.H. DRISSI (1998a). Identification of Green Rust compounds in the aqueous corrosion processes of steels; the case of Microbially Induced Corrosion and use of 78K CEMS. *Hyperfine Interactions*, **112** (1-4): 47-50.

GENIN, J.-M.R., P. REFAIT, L. SIMON and S.H. DRISSI, (1998b). Preparation and Eh-pH diagrams of Fe(II)-Fe(III) green rust compounds; hyperfine interaction characteristics and stoichiometry of hydroxy-chloride, -sulphate and -carbonate. *Hyperfine Interactions*, **111**: 313-318.

GILBERG, M.R., and. N.J. SEELY, (1982a). Liquid ammonia as a solvent and reagent in conservation. *Studies In Conservation*, **27**: 38.

GILBERG, M.R., and. N.J. SEELY, (1982b). The alkaline sulphite reduction process for archaeological iron. *Studies In Conservation*, **27**: 180.

GOLDEN, D.C., D.W. MING and M.E. ZOLENSKY, (1995). Chemistry and mineralogy of oxidation products on the surface of the Hoba nickel-iron meteorite. *Meteoritics*, **30**: 418-422.

GONZALEZ-CALBET, J.M., and M.A. ALARIO-FRANCO, (1981). Microporosidad Estructural de la Akaganeita Sintetica. *Anales de Quimica*, **77**: 19.

GONZALEZ-CALBET, J.M., M.A. ALARIO-FRANCO. and. M. GAYOSO-ANDRADE, (1981). The porous structure of synthetic akaganeite. *Journal of Inorganic Nuclear Chemistry*, **43**: 257-264.

GREGG, S.J., and K.S.W. SING, (1967). *Adsorption, surface area and porosity*. London: Academic Press.

HAMILTON, D.L., (1976). *Conservation of metal objects from underwater sites, A study in methods*. Texas Memorial Museum and Texas Antiquities Committee, Misc. Paper No. 4, Publication No. 1: 21. Austin: Texas Memorial Museum.

HANDA, A., J. KOBAYASHI, Y. UJIHIRA, (1985). Formation and analysis of corrosion products deposited on steel under HCl atmosphere by means of conversion electron Mossbauer spectroscopy at room temperature and 80K. *Applied Surface Science*, **20** (4): 581-593..

HARNETT, D.L,. and J.L. MURPHY, (1975). *Introductory Statistical Analysis*. Reading, Massachusetts: Addison-Wesley.

HARWOOD, L.M., a.nd C.J. MOODY. (1989). *Experimental Organic Chemistry*. Oxford: Blackwell Scientific.

HEEGER, A.J., (1993). Polyaniline with surfactant counterions - conducting polymer materials which are processible in the conducting form. *Synthetic Metals*, **57** (1): 3471-3482

HERTL, W., (1968). Mechanism of gaseous siloxane reaction with silica. *Journal of physical chemistry*, **72** (4): 1248.

HJELM-HANSEN, N., J. VAN LANSCHOT, C.D. SZALKAY and S. TURGOOSE, (1993). Electrochemical assessment and monitoring of stabilisation of heavily corroded archaeological iron artefacts. *Corrosion Science*, **35** (1-4): 767.

HOAR, T.P., (1967). The production and breakdown of the passivity of metals. *Corrosion Science*, **7**: 341.

HOFER, L.J. E, W.C. PEEBLES and W.E. DIETER, (1946). X-ray diffraction and magnetic studies of unreduced feric oxide fischer-Tropsch catalysis. *Journal of the American Chemistry Society*, **68**: 1953-1956.

HOLM, N.G., (1985). New Evidence for a Tubular Structure of β-Iron (III) oxide hydroxide - Akaganeite. *Origins of Life*, **15**: 131-139.

HORR, T.J., P.S. ARORA, J. RALSTON and R.ST.C. SMART, (1995). XPS film thickness and adsorption studies of alkyltrimethylammnoium bromides and organosilanes on silica surfaces. *Colloids and Surfaces. A: Physicochemical and Engineering Aspects*, **102**: 181-190.

HREBICIK, M., G. BUDINOVA, T. GODARSKA, D. VLACIL, S.B. VOGENSEH and K. VOLKA, (1997). Diffuse-reflectance infrared Fourier transform spectroscopy: new technique of sample preparation. *Journal of Molecular Structure*, **410-411**: 527-530.

INOUYE, K., K. SHIBATA, S. OZEIK and K. KANEKO (1986). Ferromagnetic iron oxides from synthetic β-FeOOH by vacuum thermal decomposition. *Journal of the Electrochemical Society*, **131**: 2435.

ISHIDA, H. and J.L. KOENIG, (1978a). Fourier Transform Infrared Spectroscopic Study of the Silane Coupling Agent/Porous Silica Interface. *Journal of Colloid and Interface Science*, **64** (3): 555-563.

ISHIDA, H. and J.L. KOENIG, (1978b). Vibrational Assignments of Organosilanetriols. I. Vinylsilanetriols and Vinylsilanetriol-d_3 in Aqueous Solutions. *Applied Spectroscopy*, **32** (5): 462-469.

ISHIKAWA, T., and K. INOUYE, (1975). Role of chlorine in β-FeOOH on its thermal change and reactivity to sulphur dioxide. *Bulletin of the Chemical Society of Japan*, **48** (5): 1580.

ISHIKAWA, T., S. NITTA and S. KONDO, (1986). Fourier-transform Infrared spectroscopy of colloidal α-, β-, and γ-ferric oxyhydroxides. *Journal of the Chemical Society, Faraday Transaction 1*, **82**: 2401.

ISRAELACHVILI, J., (1991). *Intermolecular and Surface Forces*. London, Academic Press.

IWASHITA, N., E. PSOMIADOU and Y. SAWADA, (1998). Effect of coupling treatment of carbon fiber surface on mechanical properties of carbon fiber reinforced carbon composites. *Composites Part A*, **29A**: 965-972.

JAKOBSEN, T., (1988). Iron corrosion theories and the conservation of archaeological iron objects in the 19th centuary with an emphasis on scandinavian and german sources, in V. DANIELS (ed), *Early Advances in Conservation*, British Museum Occasional Paper No 85. London: British Museum.

JAÑCZUK, B., E. CHIBOWSKI, T. BIALOPIOTROWICZ, L. HOLYSZ and A. KLISZCZ, (1990). Influence of dodecylamine chloride on the surface free energy of kaolinite. *Clays and Clay Minerals*, **38** (1): 53-56.

JOHNSTON, J.M., and N.E. LOGAN, (1979). A precise iron-57 Mossbauer spectroscopic study of iron (III) in the octahedral and channel sites of akaganeite (β-iron hydroxide oxide). *Journal of the Chemistry Society, Dalton Transactions* **13**: 13-16

JONES, D.A., (1992). *Principles and Prevention of Corrosion*. New York: Macmillan Publishing Company.

KANEKO, K., and K. INOUYE, (1973). Electrical conductivity of a-ferric oxides. *Journal of the Chemical Society of Japan*, **48** (1): 1075.

KANEKO, K., and K. INOUYE, (1974). Electrical properties of ferric oxyhydroxides. *Bulletin of the Chemical Society of Japan*, **47** (5): 1139.

KANEKO, K., and K. INOUYE, (1975). The semiconductive property of gamma-ferric oxyhydroxide. *Journal of the Electrochemical Society: Solid State Science and Technology*, **122** (3): 451.

KANEKO, K., M. SERIZAWA, T. ISHIKAVA and K. INOUYE, (1975). Dielectric behaviour of water molecules adsorbed on FeOOH. *Bulletin of the Chemical Society of Japan*, **48**: 1764.

KANEKO, K., and K. INOUYE, (1977). The electrical conductivity of iron (III) hydroxide oxides (FeOOH) with chemisorped sulphur dioxide. *Journal of the Chemical Society of Japan*, **52** (1): 162.

KANEKO, K., and K. INOUYE, (1984). Fast chemisorption of NO and SO_2 on FeOOH crystals. *Polyhedron*, **3** (2): 223.

KANEKO, K., and K. INOUYE, (1987). The growth of FeOOH microcrystals and chemisorption rate of NO. *Journal of Chemical Technology and Biotechnology*, **37**: 11.

KANEKO, K., (1989a). Surface chemistry of FeOOH microcrystals, in S. AOKI (ed), *Current problems in the conservation of metal antiquities, The 13th international symposium on the conservation and restoration of cultural property, Tokyo, October 4 - October 6, 1989*. Tokyo: Tokyo National Research Institute of Cultural Properties.

KANEKO, K., N. INOUE and T. ISHIKAWA, (1989b). Electrical and photoadsorptive properties of valence-controlled α-FeOOH. *Journal of Physical Chemistry*, **93**: 1988.

KANEKO, K., and K. INOUE, (1976). Electrical conductivity as a defect property of γ-FeOOH. *Journal of the Chemical Society, Faraday Transactions 1*, **72**: 1258.

KANEKO, K., and K. INOUE, (1979). Adsorption of water on FeOOH as studies by electrical conductivity measurements. *Bulletin of the Chemical Society of Japan*, **52**: 315.

KANUNGO, S.B., (1994). Adsorption of Cationd on Hydrous Oxides of Iron. *Journal of Colloid and Interface Science*, **162**: 86-92.

KASS, R.L., and J.L. KARDOS, (1971). The interaction of alkoxy silane coupling agents with silica surfaces. *Polymer Engineering and Science*, **11** (1): 11.

KASSIANIDOU, V., (1994). *The use of Organo-Titanates for the Conservation of Archaeological Iron*, Unpublished report, Institute of Archaeology, University College London.

KATHIRGAMANATHAN, P., (1991). Some Applications of Conducting Polymers. in A.H. FAWCETT (ed), *High Value Polymers, the proceedings of the marco group of the Royal Society of Chemisty, Belfast, 1990*, Special Publication No 87, The Royal Society of Chemistry.

KAUZMANN, W., (1959). Some factors in the interpretation of protein denaturation. *Advances in Protein Chemistry*, **14**: 1-63.

KEENE, S., (1984). The performance of coatings and consolidants used for archaeological iron,. in N.S. BROMMELLE (ed), *Adhesives and Consolidants, Pre-prints of the contributions to the Paris Congress, 2-8 September 1984*. London: International Institute of Conservation of Historic and Artistic Works.

KEENE, S., (1994). Real-time survival rates for treatments of archaeological iron, in D.A. SCOTT, J. PADANY and B.B. CONSIDONE (eds), *Ancient and Historic Metals; Conservation and scientific research. Proceedings of a symposium organized by the J. Paul Getty Museum and Getty Conservation Institute, November 1991*: 249-263: Getty Conservation Institute

KEENE, S., and C. ORTON, (1985). Stability of treated archaeological iron: an assessment. *Studies In Conservation*, **30**: 136.

KELLER, G., (1948). *Uber Hydroxide und basische Slaze des Zwertigen Eisen und deren dunkelgrunen Oxidationsprodukte*, Unpublished Phd thesis, Universtat Bern.

KELLER, P.,(1970). Eigenschaften Von (Cl, F OH) $2Fe_8$ $(O, OH)_{16}$ und Akaganeit. *Neues jahruch Mineralogie*, **113**: 29.

KELLER, W., O. KRATKY and H. NOWOTNY, (1936). *Comptes. Rendus. Acadamie d'. Science Paris.* **202**: 1171-1173.

KEMP, W., (1987). *Organic Spectroscopy*, 2nd edition. Basingstoke: Macmillan.

KIRLAND, J.J., J.L. GLAJCH AND R.D. FARLEE, (1989). Synthesis and characterisation of highly stable bonded phases for high performance liquid chromatography cplumn packings. *Analytical Chemistry* **61** (1): 2.

KIYAMA, M., (1969). Commentary experiments on the formation of Fe_3O_4 precipitate from aqueous solution. *Bulletin of the Institute of Chemical Research, Kyoto University*, **47**: 607.

KNAACK, D.F., and D. BROOKS, (1973). Corrosion inhibitors, in C.C. NATHAN (ed), Corrosion Inhibitors: 221. Houston: National Association of Corrosion Engineers.

KNIGHT, B., (1982). Why do some iron objects break up in store, in. R. W. CLARKE, and S.M. BLACKSHAW (eds), *Conservation of Iron. Greenwich, Proceedings of a symposium held at the National Maritime Museum, Greenwich on Friday, 4th July, 1980.* National Maritime Museum Monograph No. 53: 50. National Maritime Museum: Trustees of the National Maritime Museum.

KOENIG, J.K., (1985). FTIR Studies of Interfaces. Silane, Surfaces and Interfaces, in D.S. LEYDEN (ed), *Chemically Modified Surfaces, Silanes Surfaces and Interfaces, Proceedings of the Silanes, Surfaces, and Interfaces Symposium, Snowmass, Colorado, June 19-21:* 43-57. New York: Gordon & Breach.

KURTH, D.G., and T. BEIN, (1993). Surface Reactions on Thin Layers of Silane Coupling Agents. *Langmuir*, **9**: 2965-2973.

KURTH, D.G., and T. BEIN, (1995). Optical Effects in Reflectance-Absorption IR Spectroscopy of Thin Films of Silane Coupling Agents on Metallic Surfaces. *Langmuir*, **11**: 578-584.

LAMBERT, J.B., and. C.D. MCLAUGHLIN, (1976). X-ray photoelectron spectroscopy: A new analytical method for the examination of archaeological artifacts. *Archaeometry*, **18** (2): 169-180.

LEE, L, (1968). Wettability and conformation of reactive polysiloxanes. *Journal of Colloid and Interface Science,* **27**: 51.

LEE, M.C.H., (1987). Effects of polymer filler adhesion on the properties of polychloroprene elastomers filled with surface treated filler. *Journal of applied polymer science,* **33** (7):2479-2492.

LENGA, R.E., (1988). *Sigma-Aldrich library of chemical safety data*, 2nd edition. Milwaukee: Sigma-Aldrich Corp.

LETHBY, H., (1862). *Journal of Chemical Society.*

LEYDEN, D.E., R.S. SHREEDHARA MURTHY, J.P. BLITZ, J.B. ATWATER and A. RACHETTI, (1988). Reflectance FTIR Investigations of the Reactions of Silanes on Silica Surfaces. *Mikrochim Acta,* **11**: 53-56.

LI, Z., R.F. GIESE, C.J. VAN OSS, J. YVON and J. CASES, (1993). The surface thermodynamic properties of talc treated with octadecylamine. *Journal of Colloid and Interface Science*, **156**: 279-284.

LIAO, H., and T.W. COYLE, (1995). Effects of Organotitanate Additions on the Dispersion of Aluminium Nitride in Nonpolar Solvents. *Journal of American Ceramic Society*, **78** (5): 1291-1296.

LINDEN, M., J.P. SLOTTE and J.B. ROSENHOLM, (1996). Two dimensional Gelation: Octadecyltrimethoxysilane at the air/water interface. *Langmuir*, **12**: 4449-4454.

LU, W-K., R.L. ELSENBAUMER and B. WESSLING, (1995). Corrosion Protectrion of mild steel by coatings containing polyaniline. *Synthetic Metals,* **71**: 2163.

LUMSDON, D.G., and L.J. EVANS, (1994). Surface complexation model parameters for Goethite (α-FeOOH). *Journal of Colloid and Interface Science,* **164**: 119.

LUMSDEN, J.B., and Z. SZKARSKA-SMIALOWSKA, (1978). The properties of films formed on iron exposed to inhibitive solutions. *Corrosion.*, **34** (169).

LUNN, G., and E.B. SANSONE, (1994*). Destruction of hazardous chemicals in the laboratory*. New York, John Wiley & Sons.

MACCAFFERTY, E., V. PRAVDIC and. A.C. ZETTELMOYER, (1969). Dielectric behaviour of adsorbed water films on the α-Fe_2O_3 surface. *Journal of the Chemical Society, Faraday Transaction I*, **66**: 1720-1731.

MACDAIRMID, A.G., J.C. CHIANG, M. HALPERN, W.S. HUANG, S.L. MU, N.L.D. SOMASIRI, W.Q. WU and S.I. YOUNGER, (1985). Polyaniline - Interconversion of metallic and insulating forms. *Molecular Crystals and Liquid Crystals*, **121** (1-4): 173-180.

MACDIARMID, A.G., J.C. CHIANG, A.F. RICHTER, N.L.D. SOMASIRI, and A.J. EPSTEIN, (1987). Polyaniline: Synthesis and Characterization of the Emeraldine Oxidation State by Elemental Analysis, in L.D. ALCACER (ed), *Conducting Polymers*, 105. Reidel Publishing Company.

MACKAY, A.L., (1960). β-Ferric oxyhydroxide. *Mineralogical Magazine*, **32**: 545.

MACLEOD, I.D., (1981). Shipwrecks and Applied Electrochemistry. *Journal of Electroanalitical. Chemistry*, **118**: 291-303.

MACLEOD, I.D., (1988). Conservation of corroded concreated iron, *in Proceedings of conference 28*, Australian Corrosion Association, **I**, 2-6: 1-9. Perth: Australian Corrosion Association.

MACLEOD, I.D., (1989). The electrochemistry and conservation of iron in seawater. *Chemistry in Archaeology,* **56** (7): 227.

MACLEOD, I.D., (1995). In situ corrosion studies on the Duart Point wreck. *International Journal of National Archaeology*, **24** (1): 53-59.

MAEDA, Y., Y. MATSUO, S. SUGIHARA, N. MOMOSHIMA and Y. TAKASHIMA, (1992). Mossbauer studies of first-stage corrosion products on iron powder and corrosion products on highly corroded nails. *Corrosion Science*, **33** (10): 1557-1567.

MALIK, H., (1995). Influence of C_{16} quaternary amine on surface films and polarization resistance of mild steel in carbon dioxide-saturated 5% sodium chloride. *Corrosion*, **51** (4): 321-328.

MATIJEVIC, E., and P. SCHEINER, (1978). Ferric Hydrous Oxide Sols. III. Preparation of Uniform Particles by Hydrolysis of Fe (III)-Chlroide, -Nitrate, and -Perchlorate Solutions. *Journal of Colloid and Interface Science*, **63** (3): 509-524.

MATSUMOTO, A., and K. KANEKO, (1989). Infrared study on SO_2 chemisorption activity of crystallite-size controlled γ-FeOOH. *Colloids and Surfaces*, **37**: 81.

MICALE, F.J., D. KIERNAN, and A.C. ZETTLEMOYER, (1985). Characterisation of the surface properties of iron oxides. *Journal of Colloid and Interface Science*, **105** (2): 570.

MICALE F.J., and. P. PENDLETON, (1988). Vapour adsorption by hematite after thermal and chemical surface modification. *Journal of Colloid and Interface Science*, **125** (1): 359-361.

MILLER, J.D. and H. ISHIDA, (1986). Identification of Covalent Bonds between substituted silanes and Inorganic Surfaces, in D.S. Leyden (ed), *Chemically Modified Surfaces, Silanes Surfaces and Interfaces, Proceedings of the Silanes, Surfaces, and Interfaces Symposium, Snowmass, Colorado, June 19-21.* New York: Gordon & Breach.

MISAWA, T., T. KUYNO, W. SUETAKA, and S. SHIMODAIRA, (1971). The mechanism of atmospheric rusting anf the effect of Cu and P on the rust formation of low alloy steel. *Corrosion Science*, **11**: 35.

MISAWA, T., K. HASHIMOTO and S. SHIMODAIRA, (1974). The mechanism of formation of iron oxide and oxyhydroxides in aqueous solutions at room temperature. *Corrosion Science*, **14**: 131.

MISAWA, T., W. SUETAKA, and S. SHIMODAIRA, (1969). Infrared Absorption Spectra and Oxidation of Iron (II) Hydroxide and Green Rust I. *Bulletin of the Chemical Society of Japan*, **42**: 339-3340.

MONCRIEFF, A., (1976). The treatment of deteriorating stone with silicone resins. *Studies in Conservation*, **21**: 179-191.

MONKMAN, A.P, and P. ADAMS, (1991). Structural Characterisation of Polyaniline Free Standing Films. *Synthetic Metals*, **41-43**: 891.

MONTE, S.J., and. G. SUGERMAN, (1981). *United States and Japanese Application of Titanate Coupling Agent in Polyolefins.* New Jersey: Kenrich Petrochemicals. Inc.

MONTE, S.J., and. G. SUGERMAN, (1985). Titanate Coupling Agents - 1985. Urethane Applications. *Journal of Cellular Plastics,* **November-December**: 385-398.

MONTE, S.J., and G. SUGERMAN, (1988a). Corrosion resistant one hundered percent solids, Environmentally sound coatings. *Water-Borne and Higher Solids Symposium*, New Orleans, LA, 5.

MONTE, S.J., and G. SUGERMAN, (1988b). The usage of organometallic reagents as catalysts and adhesion promoters in reinforced composites. *Second international conference on composite interfaces,* Case Western Reserve University, Cleveland, Ohio.

MORRISON, W.H., (1984). Aqueous adsorption of anions onto oxides at pH levels above the point of Zero charge. *Journal of Colloid and Interface Science*, **100** (1): 121-127.

MURALIDHORAN, S., P. CHANDRAKUMARI, K. MADHAVAN, T. VASUDEVAN and S. VENKATAKRISHNA IYER, (1994). n-Octadecylamine as the inhibitor for the corrosion of mild steel in acidic solutions. *Anti-Corrosion Methods and Materials*, **41** (6): 4-8.

NAKAGAWA, T., K. OGAWA and T. KURUMIZAWA, (1994). Atomic force microscope images of monolayers from alkyltrichlorosilane on mica surfaces and studies on an anchoring mechaism of alkyltrichlorosilane molecules to the surface. *Langmuir* **10** (2): 525-529.

NAONO, H., and R. FUJIWARA, (1980). Micropore formation due to thermal decomposition of acicular microcrystals of α-FeOOH. *Journal of Colloid and Interface Science*, **87**: 317.

NAONO, H., and K. NAKAI, (1989). Thermal-decomposition of gamma FeOOH fine oarticles. *Journal of Colloid and Interface Science*, **128** (1): 146-156.

NEEDHAM, G.F., R.D. WILLET and H.F. FRANZEN, (1984). Phase transitions in crystalline model of bilayers. 1. differential scanning calorimetric and x-ray studies of $(C_{12}H_{25}NH_3)_2MCl_4$ and $(C_{14}H_{29}NH_3)_2MCl_4$ salts ($M=Mn^{2+}$, Cd^{2+}, Cu^{2+}). *Journal of Physical. Chemistry*, **88**: 674-680.

NEWEY, C., R. BOFF, V. DANIELS, M. PASCOE and N. TENNANT, (1996). *Adhesives and Coatings. Science for Conservators; Book 3.* London: Routledge, for the Conservation Unit of the Museums & Galleries Commission.

NOMURA, K., M. TASAKA, and Y. UJIHIRA, (1987). Conversion Electron Mossbauer Spectrmetric Study of Corrosion Products of Iron Immersed in Sodium Chloride Solution. *Corrosion*, **44** (3): 131-135.

NORTH, N.A., and C. PEARSON, (1975). Investigations into methods for conserving iron relics recovered from the sea, in D. LEIGH (ed), *Conservation In Archaeology and the Applied Arts: preprints of the contributions to the Stockholm Congress 2-6 June 1975.* 189. London: The International Institute for Conservation of Historic and Artistic Works.

NORTH, N.A., (1976). Formation of coral concretions on marine iron. *The International Journal of Nautical and Underwater Exploration*, **5** (3): 253-258.

NORTH, N.A., M. OWENS, and C. PEARSON, (1976). Thermal stability of cast and wrought marine iron. *Studies In Conservation*, **21**: 192.

NORTH, N.A., and C. PEARSON, (1977). Thermal decomposition of FeOCl and marine cast iron corrosion products. *Studies In Conservation*, **22**: 146.

NORTH, N.A., and C. PEARSON, (1978). Washing Methods for Chloride Removal from Marine Iron Artefacts. *Studies in Conservation*, **23**: 174-186.

NORTH, N.A., and M. OWENS, (1981). Design and operation of a furnace for H_2 reduction of marine iron. *The International Journal of Nautical Archaeology and Underwater Exploration*, **10** (2): 95-100.

NORTH, N.A., (1982). Corrosion products on marine iron. *Studies In Conservation*, **27**: 75.

NORTH, N.A., and I.D. MACLEOD, (1987). Corrosion of metals. in C. PEARSON (ed), *Conservation of Marine Archaeological Objects*, 68-98. London: Butterwoths:.

NOSEK, E.M., (1978). *Conservation of Iron Objects Found in Salty Environments.* Warsaw: Historic Monuments Documentation Centre.

ODDY, W.A., (1987). A new method for the conservation of iron: Ionophoresis in a non-aqueous electrolyte, in S. AOKI (ed), *Current problems in the conservation of metal antiquities, The 13th international symposium on the conservation and restoration of cultural property, Tokyo, October 4 - October 6, 1989.* Tokyo: Tokyo National Research Institute of Cultural Properties.

OELKRUG, D., M. FRITZ and H. STAUCH, (1992). Topology of iron surfaces in the early stages of electrochemical corrosion. *Journal of the Electrochemical Society*, **139** (9): 2419.

OHYABU, M., and Y. UJIHIRA, (1981). Study of the Chemical States of Chlorine and Fluorine in Akaganeite. *Journal of Nuclear Chemistry*, **43** (12): 3125-3129.

OKABAYASHI, H., I. SHIMIZU, E. NISHIO and C.J. O'CONNOR, (1997). Diffuse reflectance infrared Fourier transform spectral study of the interaction of 3-aminopropyltriethoxysilane on silica gel. Behavior of amino groups on the surface. *Colloid and Polymer Science*, **275**: 744-753.

OOSTERHOUT, G.W., (1960). Morphology of synthetic submicroscopic crystals of α and γ-FeOOH and of γ-Fe_2O_3 prepared from FeOOH. *Acta Crystallographica*, **13**: 932.

ORGAN, R.M., and P. SHORER, (1962-3). An improved method of consolidating fragile iron objects. *The Museums Journal*, **62**: 109-113.

OSWALD, N., (1997). In Search of the Lost Surface: 10 years of active hydrogen research. An attempt to convert destructive critisim into improvements of the plasma method, in

I.D. MACLEOD, S.L. PENNEC, L. ROBBIOLA (eds), *International Conference on Metals Conservation, Semur en Auxois, France 25-28 Sept. 1995*. London: James and James.

PARFITT, R.L., and .R.S.C. SMART, (1977). Infrared spectra from binuclear bridging complexes of sulphate adsorbed on goethite (α-FeOOH)). *Journal of the Chemical Society, Faraday Transaction I*, **73**: 796.

PATERSON, E., and J.M. TAIT, (1971). Nitrogen adsorption on synthetic Akaganeite and its structural implications. *Clay Mineral*, **12**: 345.

PATERSON, R., and H. RAHMAN, (1983). The ion exchange properties of crystalline inorganic oxide-hydroxide. I. β-FeOOH: A variable capacity anion exchanger. *Journal of Colloid and Interface Science*, **94** (1): 60-69

PATERSON, R., and H. RAHMAN, (1984). The ion exchange properties of crystalline inorganic oxide-hydroxide. III. The ion exchange properties of α-FeOOH. *Journal of Colloid and Interface Science*, **98**: 494.

PATERSON, R., and A.M. SMITH, (1988). The ion exchange properties of crystalline inorganic oxide-hydroxide. Exclusion of Iodide and Bromide from β-FeOOH by an anion sieve mechanism. *Journal of Colloid and Interface Science*, **124**: 581.

PATSCHEIDER, J., and S. VEPREK, (1986). Application of low-pressure hydrogen plasma to the conservation of ancient iron artefacts. *Studies In Conservation*, **31**: 29-37.

PEARSON, C., (1977). On-site conservation requirements for marine archaeological excavations. *International Journal of Nautical Archaeology*, **6**: (1) 37-41.

PEARSON, C., (1987). *Conservation of Marine Archaeological Objects*. London: Butterworths.

PEARSON, G., (1968). Hard and soft acids and bases, HSAB, part 1, Fundamental priciples.. *Journal of Chemical Education*, **45** (9): 581-587.

PESEK, J.J., and. M.T. MATYSKA. (1997). Methods for the Modification and Charaterization of Oxide Surfaces. *Interface Science*, **5**: 103-117.

PHILIPS, M., (1994). Polymer stops the rot under space shuttle. *New Scientist*, **29th October**, 24.

PIERS, A., and C.H. ROCHESTER, (1995). IR Studies of Adhesion Promoters. *Journal of the Chemistry Society, Farraday Transactions*, **91** (2): 359-365.

PING, Z., H. NEUGEBAUER, and A. NECKEL, (1996). FTIR ATR Spectroelectrochemical Investigations of Polyaniline with Perrhenate as a New Doping System. *Electrochimica Acta*, **41** (5): 767-772.

PING, Z., (1996). In Situ FTIR attenuated total reflection spectroscopy investigations on the base-acid transitions of polyaniline. *Journal of the Chemical Society, Faraday Transactions*, **92** (17): 3063.

PLENDERLEITH, H.J., and A.E.A. WERNER, (1971). *The conservation of antiquities and works of art*, 2nd edition. London: Oxford University Press.

PLUEDDEMAN, E.P., (1974). Mechanism of adhesion through silane coupling agents, in E.P. PLUEDDEMANN (ed), *Interfaces in polymer matrix composites, Composite Materials, Volume 6, Chapter 6.* New York: Academic Press.

PLUEDDEMANN, E.P., (1982). *Silane Coupling Agents.* New York, Plenum Press.

POHJAKALLIO, M., G. SUNDHOLM, P. TALONEN, C. LOPEZ and E. VIEIL, (1995). Characterization of the redox processes of poly(thiophene-3-methanol) by voltammetry, in situ optical beam deflection and Fourier transformation IR techniques. *Journal of Electroanalytical Chemistry*, **396**: 339.

POST, J. E. and. V.F. BUCHWALD, (1991). Crystal Structure Refinement of akaganeite. *American Mineralogist*, **76**: 272 - 277.

POURBAIX, M.J.N, (1966). *Atlas of electrochemical equilibria in aqueous solutions*, Pergamon Press: New York.

POURBAIX, M.J.N., (1977). Electrochemical corrosion of iron., in B. FLOYD BROWN (ed) *Corrosion and metal artefact: a dialogue between conservators and archaeologists and corrosion scientists*, NBS special publication 479: Washington DC: National Bureau of Standards.

PRZYLUSKI, J., (1991). *Conducting Polymers: electrochemistry*. Vaduz, Liechtenstein: Sci-Tech Publications.

RABINOVICH, Y.I., R-H. YOON, (1994). Use of Atomic Force Microscope for the Measurement of Hydrophobic Forces between Silanated Silica Plate and Glass Sphere. *Langmuir*, **10**: 1903-1909.

RANNEY, M.W., S.E BERGER and J.G. MARSDEN, (1974). Silane coupling agents in particulate mineral filled composites, in E.P. PLUEDDEMANN (ed), *Interfaces in polymer matrix composites, Composite Materials, Volume 6, Chapter 5*. New York: Academic Press.

RATNER, M.A., and D.F SHRIVER, (1988). Ion-transport in solvent free polymers. *Chemistry Reviews*, **88** (1): 109-124.

REFAIT, P., R. OUAHMAN, C. FORRIERES and J-M.R. GENIN, (1992). The Role of Cl- ions in the oxidation of iron artifacts from chlorinated archaeological environments. *Hyperfine Interactions*, **70**: 997-1000.

REFAIT, P., and J-M.R. GENIN, (1993). The oxidation of ferrous hydroxide in chloride-containing aqueous media and pourbaix diagrams of green rust one. *Corrosion Science*, **34** (5): 797-819.

REFAIT, P., S.H. DRISSI, J. PYTKIEWICZ and J-M.R. GENIN, (1997). The Anionic species competition in iron aqueous corrosion: reole of varrious green rust compounds. *Corrosion Science*, **39** (9): 1699-1710.

REFAIT, P., and. J.-M.R. GENIN, (1997). The Mechanisms of oxidation of ferrous hydroxyxhloride β-$Fe_2(OH)_3Cl$ in Aqueous Solution: The formation of Akaganeite vs Goethite. *Corrosion Science*, **39** (3): 539-553.

REN, S. and D. BARKY, (1992). Electrochemically Prepared Poly(3-methylthiophene) Films for Passivation of 430 Stainless Steel. *Journal of Electrochemistry Society*, **139** (4): 1021.

REZEL D., and J.M.R. GENIN, (1990). The substitution of chloride ions to OH^- ions in the akaganeite beta ferric oxyhydroxide studied by Mossbauer effect. *Hyperfine Interactions*, **57**: 2067-2076

RINUY, A., and F. SCHWEIZER, (1982). Application of alkaline sulphite treatment to archaeological iron: A comparative study of different desalination methods, in. R. W. CLARKE, and S.M. BLACKSHAW (eds), *Conservation of Iron. Greenwich, Proceedings of a symposium held at the National Maritime Museum, Greenwich on Friday, 4th July, 1980.* National Maritime Museum Monograph No. 53: 23. National Maritime Museum: Trustees of the National Maritime Museum.

ROSENFELD, I.L., and. I.K. MARSHAKOV, (1964). Mechanism of crevice corrosion. *Corrosion* **20**: 115t-125t.

ROSS, T. K., and R.A. FRANCIS, (1978). The Treatment Of Rusted Steel With Mimosa Tannin. *Corrosion Science,* **18**: 351-361.

ROSTOKER, W., and B. BRONSON, (1990). *Pre-Industrial Iron, Its technology and Ethnology*. Archeomaterials monograph ; no. 1. Philadelphia, Pensylvania.

ROTH, S., and H. BLEIER, (1987). Solitons in Polyaniline. *Advances in Physics*, **36**: 385.

ROZENFELD, I.L, (1981). New data on the mechanism of metals protection with inhibitors. *Corrosion*, **37**: 371.

SAINI-EIDUKAT, B., H. KUCHA, and H. KEPPLER, (1994). Hibbingite, γ-$Fe_2(OH)_3Cl$, a new mineral from the Duluth Complex, Minnesota, with implications for the oxidation of Fe-bearing compounds and the transport of metals. *American Mineralogist*, **79**: 555-561.

SÁNCHEZ DEL JUNCO, A., D.A. MORENO, C. RANNINGER, J.J. ORTEGA-CALVO and C. SÁIZ-JIMÉNEZ,(1992). Microbial induced corrosion of metallic antiquities and works of art: A critical review. *International Biodeterioration and Biodegradation*, **29**: 367.

SARICIFTCI, N.S., M. BARTONEK, H. KUZMANY, H. NEUGEBAUER and A. NECKEL, (1989). Analysis of various doping mechanisms in Polyaniline by Opitical, FTIR and Raman Spectroscopy. *Synthetic Metals*, **29**: E193-E202.

SASTRI, V.S., (1998). *Corrosion Inhibitors, Principles and Applications*, London: John Wiley.

SASTRI, V.S. and P.R. ROTERGE, (1990). Corrosion inhibition in sour media,in *Innovation and technology transfer for corrosion control, Proceedings of the 11th International Corrosion Congress, April 1990, Florence, Italy*. **3**: 55-62. Associazione Italiana di Metallurgia.

SATHIYANARAYANAN, S., S.K. DHAWAN, D.C. TRIVEDI and K. BALAKRISHNAN, (1992). Soluble conducting Poly Ethoxy aniline as an inhibitor for iron in HCl. *Corrosion Science*, **33** (12): 1831.

SATHIYANARAYANAN, S., K. BALAKRISHNAN, S.K. DHAWAN and D.C. TRIVEDI, (1994). Prevention of Corrosion of Iron in Acidic Media Using Poly(o-Methoxy-Aniline). *Electrochimica Acta*, **39** (6): 831.

SAWADA, H., and M. NAKAYAMA, (1991). Synthesis of Fluorine-containing Organosilicon Oligomers. *Journal of the Chemistry Society, Chemical Communications*: 677-678.

SCHEIFLER, L.G., (1985). Vapour Phase Inhibitors, in S. KEENE (ed), *Corrosion inhibitors in conservation, the proceedings of a conference held by UKIC in association with the Museum of London*: Occasional papers, United Kingdom Institute for Conservation: no.4.

SCHWERTMANN, U., and. R.M. CORNELL, (1991). *Iron Oxides in the Laboratory, Preparation and Characterisation.* Weinheim: VCH.

SCOTT, D.A., and N.J. SEELEY, (1987). The washing of fragile iron artefacts. *Studies In Conservation*, **32**: 73.

SCOTT, D.A., (1991). *Metallography and Microstructure of Anciet and Historic Metals*, The Getty Conservation Institute in association with Archetype Books.

SCULLY, J.C., (1975). *The Fundamentals of Corrosion*, 2nd edition. Oxford: Pergamon,

SEKINE, I., K. KOHARA, T. SUGIYAMA and M. YUASA, (1992). Syntheses of Polymerized Films on Mild Steels by Electro-oxidation and Electroreduction and Their Corrosion Resistance. *Journal of Electrochemical Society*, **139** (11): 3090.

SELWYN, L.S., and J.A. LOGAN, (1993). Stability of treated iron: a comparison of treatment methods, in J. BRIDGLAND (ed), *ICOM Committee for Conservation, 10th Triennial Meeting, Washington DC, USA, 22-27 August 1993.*

SHAW, D.J., (1992). *Introduction to Colloid and Surface Chemistry*, Oxford: Butterworth-Heinemann.

SHIRLEY, D.A., (1972). High resolution x-ray photoemission spectrum of the valence bands of gold. *Physical Review B*, **5**: 4709.

SHIER, L.L.,(1964). Tannins to control corrosion. *New Scientist* **403**: 332.

SHEIR, L.L., R.A. JARMAN and G.T. BURSTEIN, (1994). *Corrosion.* Oxford: Butterworth-Heinemann.

SHRIVER, D.F., P.W. ATKINS and C.H. LANGFORD, (1990). *Inorganic Chemistry*, Oxford: Oxford University Press.

SIMON, L., P. REFAIT and J-M.R. GENIN, (1998). Transformation of Fe(II)-Fe(III) hydroxysulphite into hydroxysulphate Green Rusts. *Hyperfine Interactions*, **112** (1-4): 217-220.

SJOBLOM, J., G. STAKKESTAD, and H. EBELTOFT, (1995). Hydrolysis and Condensation of Alkylmethoxysilanes, Studied by Means of the Langmuir-Blodgett Technique and Electron Spectroscopy for Chemical Analysis. *Langmuir*, **11**: 2652-2660.

SJOGREN, A., and V.F. BUCHWALD, (1991). Hydrogen Plasma Reactions in a DC. mode for the conservation of iron meteorites and antiques. *Studies In Conservation*, **36**: 161-171.

SKERRY, B.S., (1985). How corrosion inhibitors work, in S. KEENE (ed), *Corrosion inhibitors in conservation, the proceedings of a conference held by UKIC in association with the Museum of London*: Occasional papers, United Kingdom Institute for Conservation: no.4.

SKERRY, B.S., and C.H. SIMPSON, (1993). Accelerated Test Method for Assessing Corrosion and Weathering of Paints for Atmospheric Corrosion Control. *Corrosion*, **49** (8): 663-674.

SOCRATES, G., (1994). *Infrared Characteristic Group Frequencies*. London: John Wiley and Sons.

SPRINGER, G., (1989). Chlorine-bearing and other unknown minerals in the Strathcona deep copper zone, Sudbury district, Ontario. *Canadian Mineralogist*, **27**: 311-313.

STAFSTROM, S., J.L. BREDAS, A.J. EPSTEIN, H.S. WOO, D.B. TANNER, W.S HUANG and A.G. MACDIARMID, (1987). Polaron lattice in highly conducting polyaniline - theoretical and optical studies. *Physical Review Letters*, **59** (13):1464-1467

STAMBOLOV, T., (1978). Corrosion Inhibitors, in preprints of *ICOM Committee for Conservation, 5th Triennial Meeting, Zagreb, 1-8 October 1978*. Paris: International Council of Museums.

STAMBOLOV, T., (1979). Introduction To The Conservation Of Ferrous And Non-Ferrous Metals, in E.A. SLATER and N.H. TENNANT, (eds), *The Conservation and Restoration of Metals, symposium held in Edinburgh, 30-31 March, 1979*, Endinburgh: Proceedings of the Scotish Society for Conservation and Restoration.

SUGERMAN, M. and S.J. MONTE, (1978). in R.B. SEYMOUR (ed) *Additives for Plastics*. New York: Academic Press: 169.

SUGERMAN, M. and S.J. MONTE, (1983). *Adhesion Aspects of Polymer Coatings*. New York: Plenum Press.

SUGERMAN, M. and S.J. MONTE, (1985*). Ken -react reference manual-Titanate and Zirconate coupling agents*. New Jersey: Kenrich Petrochemicals.

SWIFT, E.A., A.J. PAUL and J.C. VICKERMAN, (1993). Investigation of the surface activity of corrosion inhibitors by XPS and Time-of-Flight SIMS. *Surface and Interface Analysis*, **20**: 27-35

TAKADA, T., (1969). Magnetic properties of several iron compounds studies by the Mossbauer effect. *Bulletin of the Institute of Chemical Research, Kyoto University*, **47**: 298.

TANFORD, C., (1980). *The Hydrophobic Effect*. New York: Wiley.

TATLOW, J.C., (1979). Aspects of Organofluorine Chemistry. Organofluorine chemicals and their industrial applications, in R.E. BANKS (ed), *Fluorocarbons and their derivatives*, 2nd Edition. London: Macdonald & Co.

TAYLOR, D.M., S.K. GUPTA and P. DYNAROWICZ, (1996). Characterisation of monolayers and LB films of octadecyltialkoxysilanes. *Thin Solid Films*, **284-285**: 80-84.

THOMSON, G., (1997). *The Museum Environment*, Oxford, Butterworth-Heinemann.

TURGOOSE, S., (1983). in R. JANAWAY and B. SCOTT (eds), *Evidence Preserved in Corrosion Products: New Fields in Artifact Studies. Proceedings of a joint conference between UKIC Arcgaeology Section and the Council for British Archaeology Science Committee, Leeds, UKIC.* Occasional papers;no.8. London: United Kingdom Institute for Conservation.

TURGOOSE, S., (1985a). Corrosion inhibitors for conservation, in S. KEENE (ed), *Corrosion inhibitors in conservation, the proceedings of a conference held by UKIC in association with the Museum of London*: Occasional papers, United Kingdom Institute for Conservation: no.4.

TURGOOSE, S., (1985b). The corrosion of archaeological iron during burial and treatment. *Studies In Conservation*, **30**: 13.

TURGOOSE, S., (1989). Structure, composition and deterioration of unearthed iron objects. in S. AOKI (ed), *Current problems in the conservation of metal antiquities, The 13th international symposium on the conservation and restoration of cultural property, Tokyo, October 4 - October 6, 1989.* Tokyo: Tokyo National Research Institute of Cultural Properties.

TURGOOSE, S., (1982). The nature of surviving iron objects, in. R. W. CLARKE, and S.M. BLACKSHAW (eds), *Conservation of Iron. Greenwich, Proceedings of a symposium held at the National Maritime Museum, Greenwich on Friday, 4th July, 1980.* National Maritime Museum Monograph No. 53. National Maritime Museum: Trustees of the National Maritime Museum.

TURNER, S.J., (1985). Surface treatment for local history collections, in S. KEENE (ed), *Corrosion inhibitors in conservation, the proceedings of a conference held by UKIC in*

association with the Museum of London: Occasional papers, United Kingdom Institute for Conservation: no.4.

TYLECOTE, R.F., and J.W. BLACK, (1980). The effect of hydrogen reduction on the properties of ferrous materials. *Studies In Conservation*, **25**: 87.

URBAN, M.W., (1993). *Vibrational spectroscopy of molecules and macromolecules on surfaces*, New York: John Wiley & Sons.

VAN OOIJ, W.J., and. T.CHILD, (1998). Protecting metals with silane coupling agents. *Chemical Technology*, **28** (2): 26-35

VEPREK, S., J.T. ELMER, C. ECKMANN and M. JURCIK-RAJMAN, (1987). Restoration and conservation of Archaeological artifacts by means of a New Plasma-Chemical Method. *Journal of the Electrochemical Society*, **134** (10): 2398-2405.

VEPREK, S., (1989). A new method for the restoration of archaeological metallic artefacts by means of low pressure plasma treatment: The development and the present status, in S. AOKI (ed), *Current problems in the conservation of metal antiquities, The 13th international symposium on the conservation and restoration of cultural property, Tokyo, October 4 - October 6, 1989*. Tokyo: Tokyo National Research Institute of Cultural Properties.

VIDON, S., LEBLANC, R.M, (1998). Langmuir study of octadecyltrimethoxysilane behavior at the air-water interface. *Journal of Physical Chemistry B*, **102**: 1279-1286.

WAGNER, C.D., L.E. DAVIS, M.V. ZELLER, J.A. TAYLOR, R.M. RAYMOND and L.H. GALE, (1981). Empirical atomic sensitivity factors for quantitative analysis by electron spectroscopy for chemical analysis. *Surface and Interface Analysis* **3** (5): 211.

WAGNER, C., and W. TRAUD, (1938). *Journal of Electrochemistry*, **44**: 391.

WALKER, R., (1982). The Corrosion and Preservation of Iron Antiques. *Journal of Chemcial Education*, **59** (11): 943-947.

WALKER, R., (1982). The role of corrosion inhibitors in the conservation of iron, in R. W. CLARKE, and S.M. BLACKSHAW (eds), *Conservation of Iron. Greenwich, Proceedings of a symposium held at the National Maritime Museum, Greenwich on Friday, 4th July, 1980.* National Maritime Museum Monograph No. 53: 23. National Maritime Museum: Trustees of the National Maritime Museum.

WALKER, R., (1996). Stabilisation of marine iron artefacts. *British Corrosion Journal*, **31** (1): 69-71.

WANG, L., X. JING, and F. WANG, (1991). Light-Assisted Oxidative Doping of Polyanilines. *Synthetic Metals*, **41-43**: 685-690.

WASSERMAN, S.R., and L. SODERHOLM, (1998). Effects of Surface Modification on the Interlayer chemistry of Iron in a Smectite Clay. *Chemistry of Materials*, **10**: 559-566.

WATKINSON, D., (1979). Lithium hydroxide: An interim report, in E.A. SLATER and N.H. TENNANT, (eds), *The Conservation and Restoration of Metals, symposium held in Edinburgh, 30-31 March, 1979*, Endinburgh: Proceedings of the Scotish Society for Conservation and Restoration.

WATKINSON, D., (1982a). An assessment of lithium hydroxide and sodium hydroxide treatments for archaeological iron work, in R. W. CLARKE, and S.M. BLACKSHAW (eds), *Conservation of Iron. Greenwich, Proceedings of a symposium held at the National Maritime Museum, Greenwich on Friday, 4th July, 1980.* National Maritime Museum Monograph No. 53: 23. National Maritime Museum: Trustees of the National Maritime Museum.

WATKINSON, D., (1982b). Degree of mineralization: Its significance for the stability and treatment of excavated iron work. *Studies In Conservation*, **28**: 85.

WATSON, J.H.L., R.R. CARDELL, and W. HELLER, (1962). The internal structure of colloidal crystals of β-FeOOH and remarks on their assembles inschiller layers. *Journal of Physical Chemistry*, **66**: 1757.

WEBER, H., (1975). Stone renovation and consolidation using silicones and silic esters, in R. Rossi-Manaesi (ed), *The conservation of stone I. Proceedings of the International Symposium, June 1975, Bologne, Italy*: 375-385. Bologna: Centro per la conservazione della sculture all'aperto.

WEI, Y., J. WANG, X. JIA and J-M. YEH, (1995). Polyaniline as corrosion protection coatings on cold rolled steel. *Polymer*, **36** (23): 4535.

WERTIME, T.A., and J.A. MUHLY, (1980). *The Coming of the Age of Iron.* New Haven: Yale University Press.

WESSLING, B., (1994). Passivation of Metals by Coating with Polyaniline:Corrosion Potential Shift and Morphological Changes. *Advanced Materials*, **6** (3): 226.

WESSLING, B., and J. POSDORFER, (1999). Corrosion prevention with an organic metal (polyaniline): corrosion test results. *Electrochimica Acta*, **44**: 2139-2147.

WIHR, R., (1975). Electrolytic desalination of archaeological iron, in D. LEIGH (ed), *Conservation In Archaeology and the Applied Arts: preprints of the contributions to the Stockholm Congress 2-6 June 1975.* 189. London: The International Institute for Conservation of Historic and Artistic Works.

WILLET, R.D., and B.G. GERSTEIN, (1973,). Critical point exponents and magnetic susceptibilities of some two-dimensionally layered Fe^{2+} salts,. *Physics Letters*, **44A** (2): 153-154.

WILLIAMS, D.E., (1997). *Personal communication.*

WROBLESKI, D.A., and. B.C. BENICEWICZ, (1994). Corrosion Resistant Coatings from Conducting Polymers. *Polymer Preprints*, **35**: 265.

YAMASHIKA, J., and T. KUROSAWA, (1960). *Journal of the Physical Society of Japan*, **15**: 802.

YATES, D.E., and T.W. HEALY, (1975). Mechanism of anion adsorption of the ferric and chromic oxide/water interfaces. *Journal of Colloid and Interface Science*, **52** (2): 222.

YOSHINO, N., Y. YAMAMOTO, K. HAMANO and T. KAWASE, (1993a). Syntheses and Reactions of Metal Organics. XVIII. Syntheses of (1H,1H,2H,2H-Polyfluorododecyl)trimethoxysilane and Surface Modification of Glass Plate. *Bulletin of the Chemical Society of Japan*, **66**: 1754-1758.

YOSHINO, N., Y. YAMAMOTO, and T. TERANAKA, (1993b). Surface modification of Denture to Provide Contamination-Free Ability by Using Silane Coupling Agent Containing Fluorocarbon Chain. *Chemistry Letters*: 821-824.

YOSHINO, N., H. NAKASEKO, Y. YAMAMOTO, (1994a). Syntheses and Reactions of Metal Organics, XX. Syntheses of silane-coupling agents having end-branck fluorocarbon chain and surface modification of glass. *Reactive Polymers*, **23**: 157-163.

YOSHINO, N., (1994b). Atomic Force Microscopy of Glass Surface Modified with Silane Coupling Agent Containing Fluorocarbon Chain. *Chemistry Letters*: 735-736.

YOSHINO, N., A. SASAKI and T. SETO, (1995). Synthesis of a silane coupling agent containing a 4-(perfluoroalkyl)phenyl group and its application to the surface modification of glass. *Journal of Fluorine Chemistry*, **71**: 21-29.

YOSHINO, N., Y. KONDO, and T. YAMAUCHI, (1996). Syntheses and reaction of metal organics. XXI. Syntheses of (1H, 1H, 2H, 2H-polyfluoroalkyl) triisocyanate silanes and surface modification of glass. *Journal of Fluorine Chemistry*, **79**: 87-91.

YOSHINO, N., (1997). *Personal communication.*

YOSHINO, N., AND T. TERANAKA, (1997). Synthesis of Silane Coupling Agents Containing Fluorocarbon chain and applications to dentistry: Plaque-controlling surface modifiers. *Journal of Biomaterials Science*, **8** (8): 623-653.

YOSHIOKA, H., (1949). A syudy on corrosion of iron by electron diffraction. *Journal of the Physical Society of Japan*, **4**: 270.

ZETTLEMOYER, A.C., R.D. LYENGAR, and P. SCHEIDT, (1966). Heat of immersion and water sorption studies on bore and silica-coated rutile surfaces. *Journal of Colloid and Interface Science*, **22**: 172.

ZIPPERLING-KESSLER, (1996). *http://www.zipperling.de/products/PAni.*

ZUCCHI, F., G. MORIGI and V. BERTOLASI, (1977). Beta iron oxide hydroxide formation in localized active corrosion of iron artefacts. In B. FLOYD BROWN (ed) *Corrosion and metal artefact: a dialogue between conservators and archaeologists and corrosion scientists*, NBS special publication 479: 103.Washington,DC: National Bureau of Standards.